

Copyright
by
Doo-Hee Lee
2021

**The Dissertation Committee for Doo-Hee Lee Certifies that this is the approved
version of the following Dissertation:**

**Chemically Triggered Transformable Polymers and Supramolecular
Materials for Detection of Nerve Agents**

Committee:

Eric V. Anslyn, Supervisor

Brent L. Iverson

Hung-Wen Liu

Brian A. Korgel

Nathaniel A. Lynd

**Chemically Triggered Transformable Polymers and Supramolecular
Materials for Detection of Nerve Agents**

by

Doo-Hee Lee

Dissertation

Presented to the Faculty of the Graduate School of

The University of Texas at Austin

in Partial Fulfillment

of the Requirements

for the Degree of

Doctor of Philosophy

The University of Texas at Austin

August 2021

Dedication

For God. I give glory to God who is always with me and who is all I am. And for my parents and family, who have given me strength and shelter.

Acknowledgements

First of all, I am grateful to Professor Eric Anslyn, my advisor. Thank you for guiding and leading my research during the four years of my doctoral life. In particular, I sincerely admire your gentle nature and attitude as a scientist in your search for truth. Following your advice, I will never give up my ideas, never stop working, and never give in to the peer-review system.

I would like to acknowledge to the precious people I met in the lab. I thank Dr. Jongdoo Lim who gave advice not only on research but also on life in general, Matt Minus, my workout mate and best friend, Stephanie Valenzuela, my chemistry/English/culture teacher and Mickey's friend, Sarah Moor, Mickey's mentor and my friend next to me, James Howard, always kind Hollywood top star James Howard, Jaime Coronado, a dad with a cute daughter Jaime Coronado, Shawn Sun and Inhong Hwang, my collaborators, Sam Dahlhauser, very smart guy, Hyun Meen Park, my little friend, Caroline Hinson, my neighboring hood, Brenden Herrera, Rogelio Escamilla, Logan Bachman and Baylie Burke, my kind seniors, Qifan Xiao, Lingyu, Emily Babcock, Le Zhang, Chris Wight and Liz Gratton, my good friends, Phuoc Ngo, a K-Pop lover, Bipin Pandey, hard-working first year, Adrian Rylski and Daniel Diaz, the 3rd year, Ram Edupuganti, Joe, CJ and Jimmy, great postdocs.

I would also like to thank the competent and kind coordinator Betsy Hamblen and the support of the ROK Army. My work would not have been done without everyone's help including those whom I did not mention.

Abstract

Chemically Triggered Transformable Polymers and Supramolecular Materials for Detection of Nerve Agents

Doo-Hee Lee, Ph.D.

The University of Texas at Austin, 2021

Supervisor: Eric V. Anslyn

Polymers can be designed to transform their structure in response to a changing environment. However, it is challenging to efficiently morph or transform the static and persistent macromolecular structures. In this study, synthetic routes of chemically triggered transforming polymers have been developed based on click and declick chemistry. Linear polymers, a cross-linked polymer, and a hydrogel were synthesized through a copper(I)-catalyzed alkyne-azide cycloaddition reaction. On the basis of these subconstructs, amphiphilic linear polymers, deformed cross-linked polymers, and recombined hydrogels were prepared via amine-thiol or thiol-thiol exchanges using a newly developed Meldrum's acid-derived conjugate acceptor under mild conditions. Furthermore, all the polymers could be degraded into small molecules with a reducing agent, dithiothreitol. Going one step further, declicking reactions were designed to selectively respond to a nerve agent surrogate. The morphological changes of these next-generation polymers were investigated using a self-propagating cascade reaction and applied to develop a novel nerve agent detecting system. Nerve agents are highly hazardous chemical compounds that have been used in terrorism as well as in wars. They

contain an organophosphorus functional group and trigger a powerful activation of the parasympathetic nerve through phosphorylation of the hydroxy groups in the body, causing fatal injuries to humans. To avoid these threats, it is important to detect and eliminate them. Thus, a self-degradable hydrogel was utilized to detect a nerve agent, tabun, via a nucleophilic attack of a cyanide anion that is the leaving group of tabun and a thiol-sulfide redox reaction. Additionally, the hydrogel was able to be employed as a membrane. It could be used as a barrier between two liquids, and the degradation of the membrane can be controlled by varying the thickness of the membrane and the concentration of the target material to allow the liquid to pass through. Additionally, a bis-pyridinium calix[4]pyrrole was employed as a receptor which can remediate and detect nerve agents through hydrogen bonding interactions and anion binding, respectively. The receptor induced a hydrolysis of nerve agents and detected nerve agents using their leaving groups simultaneously.

Table of Contents

List of Tables	xii
List of Figures	xiii
List of Schemes.....	xxxiv
Chapter 1: Nerve Agents and Methods of Detecting them using Polymer Morphology Changes, Self-Propagating Cascade Reactions and Supramolecular Receptors.....	1
1.1 Introduction.....	1
1.2 Nerve Agents: History and the Mechanism of Action.....	2
1.2.1 Historical Background	2
1.2.2 Mechanism of Action for Nerve Agents in Body	3
1.2.3 Classification of Nerve Agents	11
1.3 Polymer Morphology Changes	13
1.3.1 Transformable and Degradable Polymers.....	13
1.3.2 Perturbation of Gel Network for Detection of Nerve Agents	16
1.3.3 Hydrogel Sensors for Detection of Nerve Agents	17
1.4 Self-Propagating Cascade Reactions	21
1.4.1 Features of Self-Propagating Cascades.....	21
1.4.2 A Conjugate Acceptor and A Self-Propagating Cascade Sensor for VX.....	22
1.4.3 A Cascade for the Detection of Fluoride-Containing Nerve Agents ...	25
1.5 Supramolecular Sensors and Catalysts	27
1.5.1 Metal-Complex Sensors for Detection of Nerve Agents	27
1.5.2 Organic Based Sensors for Detection of Nerve Agents.....	29

1.5.3 Catalysts for Nerve Agent Remediation	33
1.6 Summary	37
1.7 References.....	38
Chapter 2: Chemically Triggered Synthesis, Remodeling, and Degradation of Soft Materials	43
2.1 Introduction.....	44
2.2 Results and Discussion	46
2.2.1 New conjugate acceptor (CA) and clicking-declicking reactions	46
2.2.2 Polymer design, analysis and transformation. An overview	55
2.2.3 Dimerized PEG transformation to aggregated structures	59
2.2.4 Hydrophobic polymer transformations to lightly cross-linked and amphiphilic co-polymers	64
2.2.5 Lightly cross-linked polymer transformations to cross-linked polymer	70
2.2.6 Hydrogel transformations to mono- and double networking hydrogels.....	73
2.2.7 Macromolecular degradation into small molecules	78
2.3 Conclusion	99
2.4 Experimental Section.....	100
2.4.1 Methods and Instruments.....	100
2.4.2 Materials	101
2.4.3 Synthesis	102
2.5 References.....	110
Chapter 3: A Self-Degradable Hydrogel Sensor for a Nerve Agent Tabun Mimic through a Self-Propagating Cascade.....	114
3.1 Introduction.....	115

3.2 Design Criteria.....	116
3.3 Results and Discussion	121
3.3.1 Preliminary Test.....	121
3.3.2 Optimized Conditions and Rate Constant for the Thiol Trigger	126
3.3.3 Titration Studies at pH 10 and 7.3	132
3.3.4 Selectivity Test	135
3.3.5 Membrane Degradation	139
3.4 Conclusion	144
3.5 Experimental Section.....	145
3.5.1 Methods and Instruments.....	145
3.5.2 Materials	146
2.4.3 Synthesis	148
3.6 References.....	166
Chapter 4: A Bis-Pyridinium Calix[4]pyrrole Derivative for Remediation and Detection of Nerve Agents.....	170
4.1 Introduction.....	171
4.2 Results and Discussion	174
4.2.1 Synthesis of the Receptor 1	174
4.2.2 ¹ H NMR Studies of Receptors with Nerve Agent Simulants	175
4.2.3 Association Constants between 1 and Nerve Agents Leaving Groups.....	180
4.2.4 Hydrolysis Rates of Nerve Agent Simulants with the Receptors	183
4.2.5 Detection of Nerve Agent Simulants	190
4.3 Conclusion	193

4.4 Experimental Section.....	194
4.4.1 Methods and Instruments.....	194
4.4.2 Materials	195
4.4.3 Synthesis	195
4.4.4 Additional Figures	200
4.5 References.....	204
Bibliography	207

List of Tables

Table 1.1	Changes in hydrolysis rates of the nerve agent mimics, DCP and DCNP, in acetone/water (80:20 v/v) in the presence of one of the organocatalysts. Data are presented as the rate of improvement in hydrolysis rate compared to the hydrolysis of the mimics in the absence of catalyst.	36
Table 2.1	Original polymers and transformed polymers via various amine derivatives.	59
Table 2.2	GPC data for the topological polymers.	67
Table 3.1	Experiment results to find optimized conditions to obtain 5 from LC/MS data. The numbers in the table are the ratio (%) among the four products above. Between 0.5 and 1 hour, the yield of 5 did not significantly change. Due to the negligible yield difference between 0.5 and 1 hour, the 0.5-hour reaction time was adopted due to the relative speed to obtaining results.	127
Table 4.1	The 2 nd order hydrolysis rate constants of DCNP and DFP with 1 or 2 or receptor-free in 1% H ₂ O in CH ₃ CN.	183

List of Figures

Figure 1.1	Autonomic nervous system.....	5
Figure 1.2	G-series nerve agents.	11
Figure 1.3	V-series nerve agents.	12
Figure 1.4	A-series nerve agents (Novichok). R ¹ = alkyl, alkoxy, alkylamino or fluorine; R ² = C or N; R ³ = alkyl, alkoxy or alkylamino; R ⁴ = alkyl or alkylamino; X = halogen (F, Cl, Br) or pseudohalogen (CN).	13
Figure 1.5	Commonly used acidic degradable linkers and their degradation products.....	15
Figure 1.6	Suggested probes 1-4 and nerve agent analytes.....	16
Figure 1.7	(a) Polyacrylamide hydrogels (b) a proposed fluorescence quenching mechanism.	18
Figure 1.8	(a) Two lanthanide complexes. (b) a proposed chelate ring between a V-type nerve agent and lanthanide ion.....	29
Figure 1.9	Hydrogen-bond donating host receptors 17-20	30
Figure 1.10	The complex between 20 and soman based on a DFT calculation.	31
Figure 1.11	A fluorescent probe (left) and proposed sensing mechanism with DMMP (right).	32
Figure 1.12	The proposed structures of the complex formed between probes and anions (F ⁻ , CN ⁻).....	33
Figure 1.13	Catalysts 18-20 and 23 used for hydrolysis of nerve agents and indicator 24	34
Figure 2.1	¹ H NMR for compound 3 in CDCl ₃	47
Figure 2.2	¹³ C NMR for compound 3 in CDCl ₃	48

Figure 2.3	High Resolution Mass Spectra (HRMS) for compound 3 . HRMS (ES+) m/z calc. for [M + Na] ⁺ , 403.1008; found, 403.0996.	48
Figure 2.4	UV-Vis absorbance time-kinetics between conjugate acceptor 3 (100 μM) and reagents (100 μM). (A) Dithiothreitol (DTT); (B) β-Mercaptoethanol (BME); (C) Ethanedithiol (EDT); (D) Cysteine (Cys); (E) Cysteamine (CYA); (F) Time-kinetics curves for all the reagents. Spectra were obtained every 20 mins till 1000 mins in PBS buffer (20% acetonitrile as co-solvent).	50
Figure. 2.5	LC-MS data to track reaction between 3 and amine derivatives (benzyl amine and 1,3,5-triaminomethylbenzene). The reactions were run in chloroform with (A) 3 : 8 = 1 : 1 for 5 mins and (B) 3 : 9 = 3.3 : 1 for 5 mins. The solutions were then diluted with methanol for LC-MS.	53
Figure 2.6	LC-MS data to track decoupling of compound 11 in the presence of DTT. The reactions were run in acetonitrile and HEPES buffer (1:1) for 24 hours. The solutions were then diluted with acetonitrile for LC-MS sampling.	54
Figure 2.7	¹ H NMR for linear polymer.	60
Figure 2.8	ESI LC/MS retention time for starting material (poly(ethylene glycol) methyl ether azide) and polymeric product 12 with retention time at 11 mins and 12 mins, respectively.	60

Figure 2.9 UV-Vis absorbance time kinetics, GPC, and rheometry for the polymer remodeling. (A) **12** (0.25 mg/mL) to **16** using amine terminated polystyrene **24** (1.0 mg/mL); (B) **13** (0.4 mg/mL) to **17** using 1,3,5-triaminomethylbenzene **9** (20 μ M); (C) **13** (0.2 mg/mL) to **18** using PEG diamine **26** (0.2 mg/mL); (D) **14** (0.14 mg/mL) to **19** using **9** (41 μ M) before adding hydrogen peroxide. The time kinetics were run in chloroform every 20 mins for (A); every 10 mins for (B) and (D); every 30 mins for (C); (E) GPC for **12**, **16**, **23** and **24** in chloroform; (F) DLS for **16** in water; (G) GPC for **13** and **18** in chloroform; (H) GPC for **13** and **17** in DMF (containing 0.01 M LiBr); (I) GPC for lightly cross-linked polymer **14** in chloroform; (J) Storage modulus G' and loss modulus G'' for cross-linked polymer **19**; (K) Storage modulus G' and loss modulus G'' for swelled hydrogel **15**, **20**, **21** and **22** in HEPES buffer.....61

Figure 2.10 ^1H NMR for amphiphilic polymer **16** in CDCl_362

Figure 2.11 UV-Vis absorbance of linear polymer **16** in chloroform.63

Figure 2.12 Size distribution by intensity of amphiphilic polymer **16** in water.....63

Figure 2.13 Relationship between correlation coefficient and correlation delay time for the amphiphilic polymer **16** in water.....64

Figure 2.14 ^1H NMR for linear polymer **13** in CDCl_365

Figure 2.15 ^1H NMR spectrum titration for **13** (14 mg/mL) with **9** in CDCl_366

Figure 2.16 ^1H NMR spectrum for **17** in DMSO.67

Figure 2.17 LC-MS data for **1** before and after adding H_2O_2 . To a solution of **1** (10mg, 0.04 mmol) in THF/DMF (50/50 = v/v), hydrogen peroxide (10 μ L, 30% aqueous solution) was added. After 2 hours, it was monitored.68

Figure 2.18 Proton NMR spectrum for 18 in CDCl ₃	69
Figure 2.19 ¹ H NMR for hyperbranched polymer 14 in CDCl ₃	71
Figure 2.20 ¹ H NMR spectrum titration for 14 with 9 in CDCl ₃	72
Figure 2.21 Macroscopic transformation of 14 to crosslinked gel network 19	72
Figure 2.22 GPC, ¹ H NMR spectroscopy, and LC-MS for the polymer degradation. (A) GPC of 12 and 16 before and after degradation; (B) Mass spectra for tricyclic product 4 observed in LC-MS; (C) Masses for 33 and 35 observed in LC-MS, resulted from decomposition of 13 , 17 and 18 ; (D) ¹ H NMR for the thiol-terminated PEG product 32 released from 12 ; (E) ¹ H NMR for the four-arm PEG thiol 29 degraded from hydrogel 15 ; (F) Mass spectra for 34 released from 14 and 19 in LC-MS.	74
Figure 2.23 After swollen in HEPES buffer (pH 7.3), 15 was treated with excess DTT (> 10 eq. of conjugate acceptor) for three hours in HEPES buffer and the hydrogel became sol liquid with release of quantitative four-arm PEG thiol 29 . The resulting suspension was placed on dialysis tubing (1.0 kDa molecular weight cut-off) and suspended in deionized water for 24 hours to remove the small molecules. After dry under lyophilizer, solid four-arm PEG thiol was obtained. Next, after addition of hydrogen peroxide (20 mM) to the aqueous solution of four-arm PEG thiol (180 mg/mL), free thiols cross-linked together via disulfide bonds to offer hydrogel 20	75

- Figure 2.24** After swollen in HEPES buffer (pH 7.3), **15** was mixed with four-arm poly(ethylene glycol) amines **30** ($M_n = 2,000$, 1 : 1 ratio of amine : conjugate acceptor **1**) for six hours and the hydrogel became sol with release of quantitative terminal thiols. Next, addition of hydrogen peroxide (20 mM) cross-linked free thiols together via disulfide bonds to offer hydrogel **21**.....76
- Figure 2.25** After swollen in HEPES buffer (pH 7.3), **15** was mixed with four-arm poly(ethylene glycol) thiol **31** ($M_n = 5,000$, 1 : 1 ratio of free thiol : conjugate acceptor) for six hours and the hydrogel firstly became sol state with release of quantitative terminal thiols. Next, addition of hydrogen peroxide cross-linked free thiols together via disulfide bonds to offer hydrogel **22**.77
- Figure 2.26** 20 mg **12** and 6.0 mg DTT were added into HEPES buffer (pH = 7.3) and the mixture was stirred under room temperature for three hours. The resulting suspension was placed on dialysis tubing (1.0 kDa molecular weight cut-off) and suspended in deionized water for 40 hours (change the solvent every ten hours) to remove the small molecules. After dry under lyophilizer, solid PEG-SH **32** was obtained.79
- Figure 2.27** 20 mg **16** and 20 mg DTT were added into HEPES buffer (pH = 7.3, 50% acetonitrile as co-solvent) and the mixture was stirred under room temperature for 36 hours. The resulting suspension was placed on dialysis tubing (1.0 kDa molecular weight cut-off) and suspended in deionized water for 40 hours (change the solvent every ten hours) to remove the small molecules.....80

- Figure 2.28** Degradation of **13** (5 mg) in the presence of DTT (20 mM) in HEPES buffer (pH = 7.3, 50% acetonitrile as co-solvent). Vial A is control sample without DTT; vial B is sample with DTT. After overnight shaking, solid in vial B was dissolved to form the yellow suspension. LC-MS tracked the main products: **4** and **33** in different retention times. Also the azide molecule **35** was observed due to insufficient CuAAC click reaction.....82
- Figure 2.29** Degradation of **18** in the presence of DTT in HEPES buffer (pH = 7.3, 50% acetonitrile as co-solvent). After 48 hours shaking, solid in vial was dissolved to form the yellow suspension. LC-MS tracked the main products: **4** and **33, 35** in different retention times. Azide molecule was observed due to insufficient reaction.84
- Figure 2.30** Degradation of **17** in the presence of DTT in HEPES buffer (pH = 7.3, 50% acetonitrile as co-solvent). After 48 hours shaking, solid was dissolved to form the yellow suspension. LC-MS tracked the main products: **4** and **33, 35** in different retention times.86
- Figure 2.31** Degradation of **14** in the presence of DTT under HEPES buffer (pH 7.3, 50 % acetonitrile as cosolvent). After overnight shaking, solid in vial was dissolved to form the yellow suspension. LC-MS tracked the main products: **4** and **34** in different retention times. Also the azide molecules **36, 37** were observed due to insufficient click reaction.....88

Figure 2.32 Degradation of 19 in the presence of DTT in HEPES buffer (pH = 7.3, 25% acetonitrile/25% methanol as co-solvent). Inset photos were Gel samples before and after DTT decoupling. LC-MS tracked the main product 4 and 34 . Also the azide molecule 36 and 37 was observed due to insufficient reaction.	91
Figure 2.33 Degradation of hydrogel 15 in the presence of DTT under HEPES buffer (pH 7.3). Vial 1 is control sample without DTT; vial 2 is sample with DTT. After 20 mins shaking, hydrogel in vial 2 was dissolved to form the yellow suspension.	93
Figure 2.34 Monitoring hydrogel degradation by rheometer. (A) Time-based kinetics for degradation of hydrogel 15 in the presence of DTT; (B) TCEP-induced disulfide reduction for hydrogel 20 degradation; (C) Two cross-linked networks: disulfide bond and amine/thiol conjugate acceptor linked in hydrogel 21 were degraded by TCEP and DTT, respectively; (D) Two cross-linked networks: a bis-vinylogous thiol-ester such as 1 and disulfide bond linking hydrogel 22 were degraded by ethanolamine and TCEP, respectively. Storage modulus and loss modulus for hydrogels 20 , 21 and 22 were scanned before and after degradation.	94
Figure 2.35 Changes of storage modulus and loss modulus of hydrogel 15 before and after degradation. Hydrogel 15 was processed in the presence of DTT for 10 mins.	95

- Figure 2.36** Reversibility of hydrogel **20** degradation and reformation in the presence of TCEP and H₂O₂. After adding TCEP, hydrogel **20** decomposed into four-arm PEG thiol **29** and then dialysis tubing to remove TCEP/oxidized TCEP. Next, hydrogen peroxide reversed the sol into hydrogel through thiol oxidation.95
- Figure 2.37** Degradation of conjugate acceptor and disulfide-linked hydrogel **21** in the presence of TCEP and DTT. TCEP firstly reduced the disulfide bonds while DTT subsequently cleaved the conjugate acceptors to release the tricyclic product, **29** and **30**.97
- Figure 2.38** Degradation of bis-vinylogous thiol ester and disulfide-linked hydrogel **22** in the presence of ethanolamine and TCEP. Ethanolamine decoupled the conjugate linker and then TCEP reduce the disulfide bond rapidly.98

Figure 3.1 Kinetics experiments for the preliminary test results of **Scheme 3.3**.
Butanethiol was exploited as the thiol trigger and it was conducted in pH 10 (borax/sodium hydroxide buffer). **3** was synthesized with Meldrum’s acid derivative 5 μmol and four-arm PEG azides 2.5 μmol . Rhodamine 6-G was added during the synthesis of **3**. There were four samples **3** + 2-hydroxyethyl disulfide (BMEox) 5 μmol + butane thiol 0.5 μmol (0.1 equivalent), **3** + BMEox 5 μmol + butane thiol 1.5 μmol (0.3 equivalent), **3** + BMEox 5 μmol and only **3**. (a) Absorbance spectra at 525 nm. (b) Fluorescence intensity at 555 nm. It was obtained by excitation at 470 nm. (c) Photograph showing changes of **3** from a hydrogel to a solution. (d) Optical changes of the first sample (**3** + BMEox 5 μmol + butane thiol 0.5 μmol (0.1 equivalent)) with extracted solution. (e) Optical changes of the third sample (**3** + BMEox 5 μmol) with extracted solution.....123

Figure 3.2 Absorption data of the preliminary test. (**Figure 3.1a**) (a) **3** + BMEox + butane thiol 0.1 equivalent, (b) **3** + BMEox + butane thiol 0.3 equivalent, (c) **3** + BMEox, (d) **3** were added in 5 ml of pH 10 buffer.124

Figure 3.3 Fluorescence data of the preliminary test ($\lambda_{\text{ex}} = 470 \text{ nm}$). (**Figure 3.1b**) (a) **3** + BMEox + butane thiol 0.1 equivalent, (b) **3** + BMEox + butane thiol 0.3 equivalent, (c) **3** + BMEox, (d) **3** were added in 5 ml of pH 10 buffer.....124

Figure 3.4 A titration study at physiological pH (phosphate-buffered saline (PBS)). After reacting **4** (1.5 μmol), **DCNP** (0, 0.25, 0.5, and 1.5 μmol), and triethylamine (3 μmol) in acetonitrile for 30 minutes, the resulting mixture was added to 5 ml PBS buffer in the presence of **BME-ox** (5 μmol) and **3** with **R6G**. The reactions were then shaken. (a) Photos of the four samples with different amount of **DCNP**. (b) Absorption data for the time dependent release of **R6G** from the degradation of **3** at 525 nm. (c) Absorption spectra of kinetic data with 0.25 μmol of **DCNP**. The spectra were changed according to the numbers and arrows.....125

Figure 3.5 (a) Time kinetic studies with absorption changes of **DCNP** and **6** in acetonitrile in the presence of 2 equivalent of triethyl amine. (b) Time kinetic results for a concentration of **6** based on the absorption data spectra. 1, 2, 3, and 4 equivalents **DCNP** were added separately into acetonitrile in the presence of **6** (5 mM), and triethyl amine (10 mM). (c) First order rate constant was calculated from (b). Y-axis is $-kt$, so the slope is regarded as $-k$. (d) Second order rate constant was calculated with concentration of **DCNP** and the first order rate constant (c).129

Figure 3.6 ^1H NMR kinetic studies between **DCNP** and **6**. There are 24 NMR results each and they were taken every 5 minutes for 2 hours. (a) 2 equivalents **DCNP** (20 mM) was added into acetonitrile-d in the presence of **6** (10 mM), and triethyl amine (20 mM). The disappearance of **a** was monitored over time. (b) 5 equivalents **DCNP** (50 mM) was added into acetonitrile-d in the presence of **6** (10 mM), and triethyl amine (20 mM).130

Figure 3.7 (a) Time kinetic studies with absorption changes of cyanide and **7** in acetonitrile. Cyanide was prepared from the mixture of potassium cyanide and 18-crown-6. (b) Time kinetic results for a concentration of **7** based on the absorption data spectra. 1, 2, 3, and 4 equivalents cyanide were added separately into acetonitrile in the presence of **7** (50 μM). (c) First order rate constant was calculated from (b). Y-axis is $-kt$, so the slope is regarded as $-k$. (d) Second order rate constant was calculated with concentration of cyanide and the first order rate constant (c).....131

Figure 3.8 Kinetics titration study at pH 10 buffer (borax/sodium hydroxide buffer). After reacting **4** (5 μmol), DCNP (0, 0.25, 0.5, and 1.5 μmol), and triethylamine (10 μmol) in acetonitrile for 30 minutes, the resulting mixture was added to the pH 10 buffer 5 mL in the presence of 2-hydroxyethyl disulfide (5 μmol) and **3**. (a) Photos of the four samples with varying amounts of DCNP without Rhodamine 6G. The equivalent (eq.) is the ratio between the conjugate acceptor in **3** and DCNP: 0, 0.05, 0.1, and 0.3 (left to right). (b) Absorption data of time dependent titration for degradation of **3** with Rhodamine 6G. Absorption (525 nm) was measured by extracting 100 μL of each solution at intervals of 10 minutes for a total of 90 minutes.133

Figure 3.9 Selectivity test. Absorption data of time dependent titration for **3** degradation with DCNP (a tabun mimic), DFP (a sarin and soman mimic), and Demeton-S-methyl (a VX mimic) in physiological pH (Phosphate-buffered saline). After reacting **4** (5 μmol), triethylamine (10 μmol), and (a) DCNP 0.5 μmol (0.1 equivalent); (b) DFP 5 μmol (1 equivalent); (c) DSM 5 μmol (1 equivalent) in acetonitrile for 30 minutes, the result mixture was added to the PBS 5 mL in the presence of 2-hydroxyethyl disulfide (5 μmol) and **3** with Rhodamine 6G (5 μmol). Absorption was measured by extracting 100 μL of the solution at intervals of 20 minutes for 240 minutes. (d) shows absorbance spectra of (a), (b), and (c) at 525 nm.137

Figure 3.10 LC-MS data of the reaction **4** (10 mM) and triethylamine (20 mM) with (a) DCNP (10 mM); (b) DFP (10 mM); (c) DSM (10 mM) in acetonitrile for 90 minutes.138

Figure 3.11 Membrane degradation test of **3**. There were four different weights and thicknesses of gels created with **3** which were synthesized with 5 μmol , 7 μmol , 9 μmol , and 11 μmol of the Meldrum's acid linker in the gel. (a) Thickness of **3**: 1.7 mm, 2.2 mm, 2.6 mm, and 3.2 mm. (b) A photo for the four samples before connecting the top vial. (c) Visualization for the kinetic samples designated 1, 2, 3, and 4 (left to right). Four different sets were made of **3** containing 5 μmol , 7 μmol , 9 μmol , and 11 μmol of the conjugate acceptor for samples 1, 2, 3, and 4, respectively. Each sample was made in a 1 dram vial, however, the reactants and solvent varied to make alter the thickness of the membrane. The conditions for each sample shown above was: 1. Meldrum's acid linker (1.90 mg, 5 μmol , 1 equiv.), four-arm PEG azides (25 mg, 2.5 μmol , 0.5 equiv.), tert-butanol (50 μL), Milli-Q water (50 μL), sodium ascorbate (0.5 mg, 2.5 μmol , 0.5 equiv.), and copper sulfate (0.5 mg, 2 μmol , 0.40 equiv.), 2. Meldrum's acid linker (2.66 mg, 7 μmol , 1 equiv.), four-arm PEG azides (35 mg, 3.5 μmol , 0.5 equiv.), tert-butanol (70 μL), Milli-Q water (70 μL), sodium ascorbate (0.7 mg, 3.5 μmol , 0.5 equiv.), and copper sulfate (0.7 mg, 2.8 μmol , 0.4 equiv.), 3. Meldrum's acid linker (3.42 mg, 9 μmol , 1 equiv.), four-arm PEG azides (45 mg, 4.5 μmol , 0.5 equiv.), tert-butanol (90 μL), Milli-Q water (90 μL), sodium ascorbate (0.9 mg, 4.5 μmol , 0.5 equiv.), and copper sulfate (0.9 mg, 3.6 μmol , 0.4 equiv.), and 4. Meldrum's acid linker (4.18 mg, 11 μmol , 1 equiv.), four-arm PEG azides (55 mg, 5.5 μmol , 0.5 equiv.), tert-butanol (110 μL), Milli-Q water (110 μL), sodium ascorbate (1.1 mg, 5.5 μmol , 0.5 equiv.), and copper sulfate (1.1 mg, 4.4 μmol , 0.4 equiv.).....141

Figure 3.12 Experiment showing the alteration in degree of dispersion of nanocrystals due to a change in pH induced by membrane decomposition. (a) Representation of the **ITO NCs** with the ligands functionalized on the **NC** surface. Acidic conditions cause the ligands to be stripped from the **NCs** causing **NC** degradation and aggregation. (b) Top is a picture before the membrane degradation, and the bottom is a picture after degradation. The top vial contained a pH 10 aqueous solution (4 mL) containing dispersed colloidal **NCs**, and the bottom was pH 3 water (1 mL). (c) and (d) are STEM images before and after, respectively, the membrane degradation. Both scalebars are 250 nm.143

Figure 3.13 ¹H NMR spectrum of **4** (CDCl₃).....151

Figure 3.14 ¹³C NMR spectrum of **4** (CDCl₃).....151

Figure 3.15 High resolution mass data of **4**.....152

Figure 3.16 ¹H NMR spectrum of **6** (CD₃CN).....153

Figure 3.17 ¹H NMR spectrum of diethyl (4-(methylthio)phenyl) phosphate (CD₃CN).153

Figure 3.18 ¹³C NMR spectrum of diethyl (4-(methylthio)phenyl) phosphate (CD₃CN).154

Figure 3.19 High resolution mass data of diethyl (4-(methylthio)phenyl) phosphate. ...154

Figure 3.20 ¹H NMR spectrum of 4-methoxybenzenethiol (CD₃CN).155

Figure 3.21 ¹H NMR spectrum of **7** (CDCl₃).....156

Figure 3.22 ¹³C NMR spectrum of **7** (CDCl₃).....156

Figure 3.23 High resolution mass data of **7**.....157

Figure 3.24	The benzyl-ligand purity conformation via LC-MS. (a) The UV-trace at both 240 and 214 nms over a 12 minutes (LCMS Trace: 5% to 95% MeOH gradient) displays only one peak. (b) The MSD-TIC (+) of the single peak shown in (a) displaying the mass of the desired ligand.	160
Figure 3.25	The LCMS-trace of the benzyl-ligand prior to HPLC purification. (a) The crude UV-trace of the benzyl-ligand at 240 and 214 nm. (b) The identities of known impurities.	160
Figure 3.26	The Aldehyde-ligand purity conformation via LC-MS. (a) The UV-trace at both 240 and 214 nms over a 12 minutes (LCMS Trace: 5% to 95% MeOH gradient) displays only one peak. (b) The MSD-TIC (+) of the single peak shown in (a) displaying the mass of the desired ligand.	161
Figure 3.27	The LCMS-trace of the Aldehyde-ligand prior to HPLC purification. (a) The crude UV-trace of the Aldehyde-ligand at 240 and 214 nm. (b) The identities of known impurities.	162
Figure 3.28	¹ H NMR spectrum of NCs.	163
Figure 3.29	Absorbance data of NCs and triethylamine (TEA).	164
Figure 3.30	(a) and (b) are STEM images before (a) and after (b) the membrane degradation. Both scalebars are 100 nm.	165
Figure 4.1	Receptors 1 and 2 used for nerve agent remediation and detection, G-series nerve agents and their simulants.	172

Figure 4.2	¹ H NMR spectra of receptors for pyrrole protons in acetonitrile-[d ₃]. (a) Initial free compound 1 (bottom) and 1 with the addition of 1 equivalent of DCNP (top). (b) Initial free compound 1 (bottom) and 1 with the addition of 1 equivalent of DFP (top). (c) Initial free compound 2 (bottom) and 2 with the addition of 1 equivalent of DCNP (top). (d) Initial free compound 2 (bottom) and 2 with the addition of 1 equivalent of DFP (top). (e) Initial free compound 1 (bottom) and 1 with the addition of 1 equivalent of TBACN (top). (f) Initial free compound 1 (bottom) and 1 with the addition of 1 equivalent of TBAF.	176
Figure 4.3	Job plot obtained from ¹ H NMR titration of 1 with (a) DCNP and (b) DFP in CD ₃ CN for which [1]+[DCNP] = 5 mM and [1]+[DFP] = 5 mM each.	177
Figure 4.4	(a) ¹ H NMR studies between DCNP and 1 . DCNP (0 equiv. (bottom) to 4 equiv. (top)) was gradually added to the solution of CD ₃ CN in the presence of 1 (6 mM). (b) Association constants of 1 with DCNP calculated with (a).	178
Figure 4.5	(a) ¹ H NMR studies between DFP and 1 . DFP (0 equiv. (bottom) to 4 equiv. (top)) was gradually added to the solution of CD ₃ CN in the presence of 1 (6 mM). (b) Association constants of 1 with DFP calculated with (a).	179
Figure 4.6	(a) Fluorescence emission spectra ($\lambda_{\text{ex}} = 372 \text{ nm}$) of 1 (20 μM) upon addition of TBACN (0-50 equivalents) along with the arrow in CH ₃ CN. (b) Association constant of 1 with TBACN calculated with (a) at 416 nm.	180

- Figure 4.7** (a) Fluorescence emission spectra ($\lambda_{\text{ex}} = 372 \text{ nm}$) of **1** ($20 \mu\text{M}$) upon addition of TBAF (0-50 equivalents) along with the arrow in CH_3CN .
 (b) Association constants of **1** with TBAF calculated with the result of (a) at 416 nm181
- Figure 4.8** Fluorescence emission spectra ($\lambda_{\text{ex}} = 372 \text{ nm}$) changes of **1** ($20 \mu\text{M}$) upon addition of various anions (100 equiv.) in CH_3CN . The anions were F^- , Cl^- , Br^- , I^- , OAc^- , OBz^- , NO_3^- , NO_2^- , SO_4^{2-} , HSO_4^- , $\text{H}_2\text{PO}_4^{2-}$, CN^- , HCO_3^- from TBA salts.182
- Figure 4.9** Time kinetic studies with fluorescence intensity changes of DCNP (a) $100 \mu\text{M}$; (b) $200 \mu\text{M}$; (c) $300 \mu\text{M}$; (d) $400 \mu\text{M}$ in acetonitrile (99%) and water (1%). Each time fluorescence was measured, the amount of released cyanide anion after hydrolysis was measured by the change in fluorescence intensity of **1** ($100 \mu\text{M}$). (e) First order rate constant was calculated from (a)-(d). Each slope represented the first order rate constant. (f) The second order rate constant was calculated from the concentration of DCNP and the first order rate constant (e). Finally, the second order rate constant was calculated to be $0.687 \text{ M}^{-1} \cdot \text{min}^{-1}$184

Figure 4.10 Time kinetic studies with fluorescence intensity changes of DFP (a) 100 μM ; (b) 200 μM ; (c) 300 μM ; (d) 400 μM in acetonitrile (99%) and water (1%). Each time fluorescence was measured, the amount of released fluoride anion after hydrolysis was measured by the change in fluorescence intensity of **1** (100 μM). (e) First order rate constant was calculated from (a)-(d). Each slope represented the first order rate constant. (f) The second order rate constant was calculated from the concentration of DFP and the first order rate constant (e). Finally, the second order rate constant was calculated to be $0.525 \text{ M}^{-1} \cdot \text{min}^{-1}$185

Figure 4.11 Time kinetic studies with fluorescence intensity changes of **1** (100 μM) and DCNP (a) 1; (b) 2; (c) 3; (d) 4 equivalents compared to **1** in acetonitrile (99%) and water (1%). (e) First order rate constant was calculated from (a)-(d). The slope was the first order rate constant, respectively. (f) The second order rate constant was calculated from the concentration of DCNP and the first order rate constant (e). Finally, the second order rate constant was determined to be $2.795 \text{ M}^{-1} \cdot \text{min}^{-1}$186

Figure 4.12 Time kinetic studies with fluorescence intensity changes of **1** (100 μM) and DFP (a) 1; (b) 2; (c) 3; (d) 4 equivalents compared to **1** in acetonitrile (99%) and water (1%). (e) First order rate constant was calculated from (a)-(d). The slope was the first order rate constant, respectively. (f) The second order rate constant was calculated from the concentration of DFP and the first order rate constant (e). Finally, the second order rate constant was determined to be $2.536 \text{ M}^{-1} \cdot \text{min}^{-1}$187

Figure 4.13 Time kinetic studies with fluorescence intensity changes of **2** (100 μM) and DCNP (a) 1; (b) 2; (c) 3; (d) 4 equivalents compared to **2** in acetonitrile (99%) and water (1%). Each time fluorescence was measured, the amount of released cyanide anion after hydrolysis was measured by the fluorescence intensity changes of **1** (100 μM). (e) First order rate constant was calculated from (a)-(d). The slope was the first order rate constant, respectively. (f) The second order rate constant was calculated from the concentration of DCNP and the first order rate constant (e). Finally, the second order rate constant was $0.942 \text{ M}^{-1} \cdot \text{min}^{-1}$.
 1188

Figure 4.14 Time kinetic studies with fluorescence intensity changes of **2** (100 μM) and DFP (a) 1; (b) 2; (c) 3; (d) 4 equivalents compared to **2** in acetonitrile (99%) and water (1%). Each time fluorescence was measured, the amount of released fluoride anion after hydrolysis was measured by the fluorescence intensity changes of **1** (100 μM). (e) First order rate constant was calculated from (a)-(d). The slope was the first order rate constant, respectively. (f) The second order rate constant was calculated from the concentration of DFP and the first order rate constant (e). Finally, the second order rate constant was $0.759 \text{ M}^{-1} \cdot \text{min}^{-1}$.
 1189

Figure 4.15 Fluorescence emission spectra of 1 (20 μ M) were obtained upon addition of 0-20 equivalents of a mixture of DCNP/EtOH/ DBU (1/1/1) in CH ₃ CN (λ_{ex} = 372 nm). The wavelength range was (a) 385-600 nm and (b) 416 nm, respectively. The inset of (b) is for calculating the limit of detection (LOD). The slope of the calibration curve was 336,145,733.9 and the standard deviation of the response of the curve (σ) was 189.0506. The LOD was calculated by the equation of $3.3 \times \sigma \div slope$, so the LOD was 1.86×10^{-6}	191
Figure 4.16 Fluorescence emission spectra of 1 (20 μ M) were obtained upon addition of 0-20 equivalents of a mixture of DFP/EtOH/ DBU (1/1/1) in CH ₃ CN (λ_{ex} = 372 nm). The wavelength range was (a) 382-600 nm and (b) 416 nm, respectively. The inset of (b) is for calculating the limit of detection (LOD). The slope of the calibration curve was 755,694,222.3 and the standard deviation of the response of the curve (σ) was 515.1028. The LOD was calculated by the equation of $3.3 \times \sigma \div slope$, so the LOD was 2.25×10^{-6}	192
Figure 4.17 ¹ H NMR spectrum of 4 recorded in DMSO- <i>d</i> ₆ at 298 K.	196
Figure 4.18 ¹³ C NMR spectrum of 4 recorded in DMSO- <i>d</i> ₆ at 298 K.	197
Figure 4.19 High resolution mass data of 4	197
Figure 4.20 ¹ H NMR spectrum of 1 recorded in DMSO- <i>d</i> ₆ at 298 K.	198
Figure 4.21 ¹³ C NMR spectrum of 1 recorded in CD ₃ CN at 298 K.	199
Figure 4.22 High resolution mass data of 1	199
Figure 4.23 ¹ H NMR studies between DCNP and 2 . DCNP (0 equivalent (bottom) to 5 equivalent (top)) was gradually added to the solution of CD ₃ CN in the presence of 2 (6 mM).	200

Figure 4.24 ¹ H NMR studies between DFP and 2 . DFP (0 equivalent (bottom) to 4 equivalent (top)) was gradually added to the solution of CD ₃ CN in the presence of 2 (6 mM).....	201
Figure 4.25 ¹ H NMR studies between TBACN and 1 . TBACN (0 equivalent (bottom) to 2 equivalent (top)) was gradually added to the solution of CD ₃ CN in the presence of 1 (6 mM).	202
Figure 4.26 ¹ H NMR studies between TBAF and 1 . TBAF (0 equivalent (bottom) to 1.5 equivalent (top)) was gradually added to the solution of CD ₃ CN in the presence of 1 (6 mM).....	203

List of Schemes

Scheme 1.1	Degradation of acetylcholine by acetylcholinesterase in a normal state.	7
Scheme 1.2	Inhibition of acetylcholinesterase activity by a nerve agent.	8
Scheme 1.3	Mechanism of 2-PAM.	10
Scheme 1.4	Diene displacement reactions between the Diels-Alder adduct of furan and hydroxyethyl maleimide and anthracene derivative.	14
Scheme 1.5	Synthesis of probe 4.	17
Scheme 1.6	Homopolymers and their precursors., as DCP (100 equiv.) was added, the color of the compound was changed from colorless to either green or red, depending on the R group.	19
Scheme 1.7	Rapid color change (from colorless to green) of a random double copolymer in detection of DCP or TFA vapors.	20
Scheme 1.8	Molecular structure of a random triple copolymer hydrogel and its response to TFA.	20
Scheme 1.9	Click and chemically triggered declicks reactions.	22
Scheme 1.10	The proposed scheme for the self-propagating cascade protocol for the detection of the thiol trigger.	24
Scheme 1.11	Thiol released in 20% acetonitrile in a pH 12.0 buffer solution at 60 °C.	25
Scheme 1.12	Detection of fluoride via an auto-inductive cascade with ratiometric changes of optical properties.	26
Scheme 1.13	Proposed scheme of a nerve agent mimic detection.	28

Scheme 1.14	The proposed scheme of hydrolysis cycle of a nerve agent mimic. The developed catalysts were employed for the reaction between DCNP and water.	37
Scheme 2.1	A general schematic of the coupling-decoupling reactions exploited herein. The addition of an amine to 1 or 3 leads to formation of 2 through thiol release. Next, thiols can be scrambled using structures such as 1 or 2 with varying R-groups. The addition of various reagents release thiols and amines in aqueous conditions and can create species 4 , and the generalized structures 5 , 6 , and 7 , each with distinctive UV-Vis λ_{max} values. (4 : 250 nm, 5 : 290 nm, 6 : 330 – 350 nm, and 7 : 280 – 300 nm).	46
Scheme 2.2	Synthesis of the conjugate acceptor 3	47
Scheme 2.3	The reactions between 3 and amine derivatives.	51
Scheme 2.4	Schematic representation of the polymer synthesis and topological changes achieved via click-declick chemistry and disulfide-thiol scrambling. Dimerized PEG (12) and hydrophobic linear polymer (13), lightly cross-linked polymer (14), and hydrogel (15) were synthesized via CuAAC. New amphiphilic linear polymer (16), lightly cross-linked (17), random copolymer (18), cross-linked polymer (19) and hydrogels (20 , 21 , 22) were created via amine scrambling using the conjugate acceptor core of 3 , and/or thiol-disulfide reactions. Note: Given the potential hazards of poly(azide) compounds, the reactions were carried out in the fume hood, treated carefully, stored and used in safe places. ²⁹	56

Scheme 2.5	Synthesis of the initial set of subunits. Reagents and conditions: a. CuSO ₄ ·5H ₂ O, sodium ascorbate, tert-butanol:H ₂ O = 1:1 (vol), 20 °C; b. CuI, tris(benzyltriazolylmethyl)-amine (TBTA), sodium ascorbate, THF:DMF:H ₂ O = 2:2:1 (vol), 20 °C; c. CuI, TBTA, sodium ascorbate, THF:DMF:H ₂ O = 1:1:1 (vol), 20 °C; d. CuSO ₄ ·5H ₂ O, sodium ascorbate, tert-butanol:H ₂ O = 1:1 (vol), 20 °C.....	57
Scheme 2.6	Schematic depiction of polymer degradation induced in the presence of DTT or tris(2-carboxyethyl)phosphine (TCEP)/ethanolamine in neutral HEPES buffer. The degradation process was triggered either by the cyclization between a bis-vinylogous derivatives of 3 with DTT, or disulfide cleavage by reduction with TCEP, or ethanolamine-induced decoupling of structures such as 1 , respectively.	91
Scheme 3.1	A thiol auto-inductive cascade in the previous work.....	117
Scheme 3.2	Selected tabun mimic and synthesized hydrogel.	119
Scheme 3.3	Detection of a tabun mimic via a self-propagating cascade with perturbation of gel formation.	120
Scheme 3.4	A hydrogel self-propagating cascade into a solution via degradation in preliminary test.	122
Scheme 3.5	Model studies for rate constant. (a) Model reaction to release cyanide. (b) Model reaction for cyanide capture and thiol release.	128
Scheme 3.6	Nerve agents and their mimics. DCNP (diethylcyanophosphonate) is a simulant of a tabun, and both DFP (diisopropylfluorophosphate) and DCP (diethylchlorophosphate) are surrogates of a sarin and a soman. DSM (demeton-S-methyl) is employed as a mimic of VX.	136

Scheme 4.1	The proposed scheme for remediation and detection of a nerve agent simulant, incorporating 1 and DFP.	173
Scheme 4.2	Scheme of synthesis of 1	174
Scheme 4.3	Synthesis of receptor 1	195

Chapter 1: Nerve Agents and Methods of Detecting them using Polymer Morphology Changes, Self-Propagating Cascade Reactions and Supramolecular Receptors

1.1 INTRODUCTION

Chemical weapons used for military or terrorism purposes are classified as a class of weapons of mass destruction. Chemical warfare agents (CWAs), the main material of chemical weapons, are toxic chemicals that have chemical effects on living things, resulting in temporary paralysis, permanent damage, or death. CWAs are considered inhumane weapons because they inflict horrendous suffering on the victims along with the indiscriminate slaughter of lives and, thus, have been designated as prohibited substances by the Organisation for the Prohibition of Chemical Weapons (OPCW). However, CWAs are still used because of their ease of manufacture, low price, and efficiency in killing. Some countries still have large quantities of chemical weapons and use them for tactical purposes, especially since their use for military purposes can create favorable conditions for operations by killing personnel and contaminating certain equipment and areas, making them unusable.

Improvements in detection and decontamination capabilities are needed to limit the use of dangerous chemical toxic materials, eliminate threats, and reduce their effectiveness. Therefore, many studies have been conducted and reported to detect CWAs and eliminate toxic substances. In this chapter, the history, types, and chemical operation principle of nerve agents, the most representative CWAs, were introduced. Methods using polymer transformation and supramolecular receptors were dealt with to detect nerve agents. In addition, studies on polymers that cause conformational changes by

chemical triggers or external stimuli have been introduced, and literature on the detoxification of nerve agents using supramolecular receptors has been presented.

1.2 NERVE AGENTS: HISTORY AND THE MECHANISM OF ACTION

1.2.1 Historical Background

The first use of chemical weapons in a modern sense was the release of chlorine gas by German forces on the Allied line in Ypres, Belgium in 1915. Chemical weapons were exploited during World War I in the form of tear gas, mustard gas, chlorine gas, and phosgene.¹ After the end of World War I, many countries signed the Geneva Protocol in 1925 that they would no longer use chemical weapons, but the research, development, and use of CWAs have continued.

There are several types of CWAs, such as nerve agents, blister agents, blood agents, pulmonary agents, riot control agents, and vomiting agents. Among them, nerve agents are the most studied, developed, and employed.

In the nerve agents' history, the G-series nerve agents were invented from 1930s to 1940s by the Nazi German scientists, including Gerhard Schrader. In the 1980s Iran-Iraq war, Iraq used tabun (GA) against Iran and Kurdish forces. The Aum Shinrikyo Group, a Japanese religious group, sprayed sarin gas (GB) on ordinary civilians on the Tokyo subway in 1995, from which 14 people died and around 6,252 people were injured.² GB was also exploited in the Syria civil war that broke out in 2013.

Developed in the 1950s in many countries, including the Soviet Union and the United Kingdom, V-series nerve agents have persistent toxicity. These were exploited by Aum Shinrikyo in 1995 to attack three people, one of whom died. VX was also used to assassinate North Korea's political affiliate in 2017.

In Russia in 1995, a banker died three days later after the exposure to a Novichok agent, which is an A-series nerve agent developed in Russia from 1970s. It was also used to eliminate the Russian military officer family in the UK in 2018,²⁻⁴

Nerve agents, which were originally developed for military purposes during wars, are not only limited to soldiers, but also have been indiscriminately used against civilians recently, raising interest in them.

1.2.2 Mechanism of Action for Nerve Agents in Body

Nerve agents contain extremely toxic organo-phosphorus group in their chemical structure. They paralyze the nervous system and interfere with vital biological activities by inhibiting the function of acetylcholinesterase. As shown in **Figure 1.1**, the nervous system is largely divided into the central nervous system and the peripheral nervous system. The peripheral nervous system is further divided into the somatic nervous system and the autonomic nervous system. Here, the autonomic nervous system is a nervous system that autonomously regulates body functions without being directly affected by the brain and is mainly responsible for life-sustaining activities such as digestion, circulation, respiration, and any functions related to homeostasis. The hypothalamus of the diencephalon, the center of homeostasis, detects changes in the internal environment and releases adrenaline when the sympathetic nerve needs to be stimulated and acetylcholine when the parasympathetic nerve needs to be stimulated. These secreted neurotransmitters transmit this stimulus to each receptor.⁵ The sympathetic nervous system works antagonistically with the parasympathetic nervous system, helping to maintain our body homeostasis. The sympathetic nervous system controls the physiological phenomena necessary to maintain the health of our body in a short period of time to cope with emergencies. On the other hand, the parasympathetic nervous system reduces respiration

and heart rate during stressful times, relieving tension in the body and increasing digestion. When exposed to nerve agents, nerve agents block the breakdown of acetylcholine, so that acetylcholine continues to accumulate in the body, which, in return, causes parasympathetic nerve to stimulate. As a result, symptoms such as pupillary constriction, salivation, runny nose, urination, dyspnea, sweating, and muscle cramps may appear.

Depending on the route of penetration into the body by the Nerve agents, the time for the effect to appear may vary. Inhalation of Nerve agents through the respiratory system produces symptoms between 2 and 5 minutes, and death occurs within 15 minutes when a lethal dose is inhaled. If the eyes are exposed, the symptoms are expressed within 2-3 minutes. When exposed to the skin, in small amounts, there are no other symptoms than local sweating or convulsions, and even if a lethal dose is absorbed within 1-2 minutes, death is delayed to 1-2 hours. Nerve agents are cumulative, so repeated exposure, even in dilute concentrations, may cause symptoms.⁶

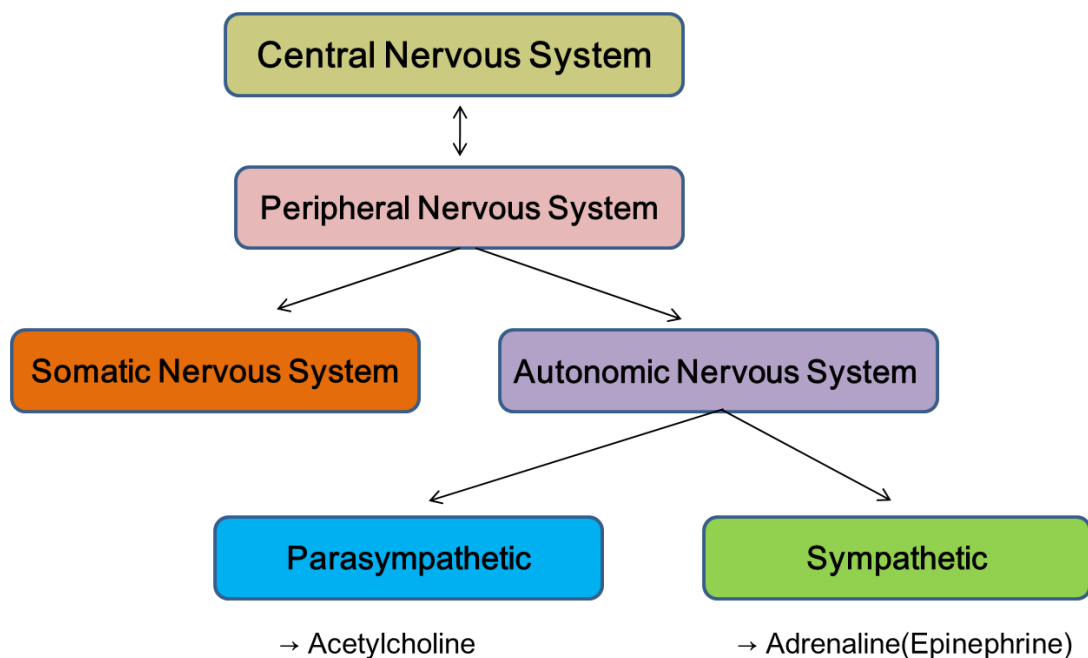
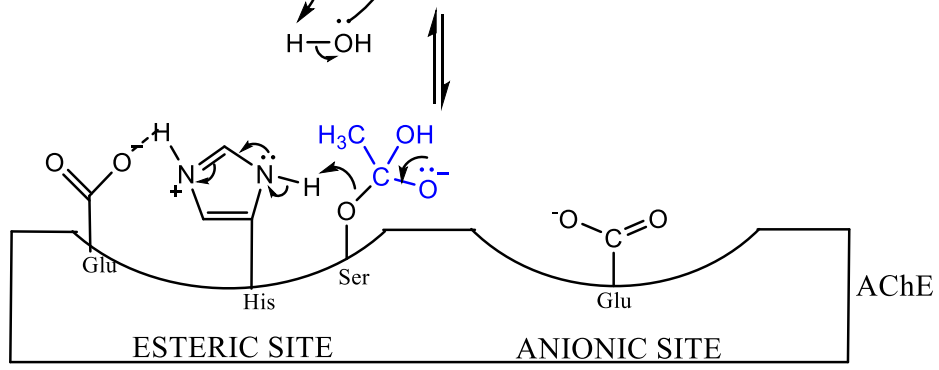
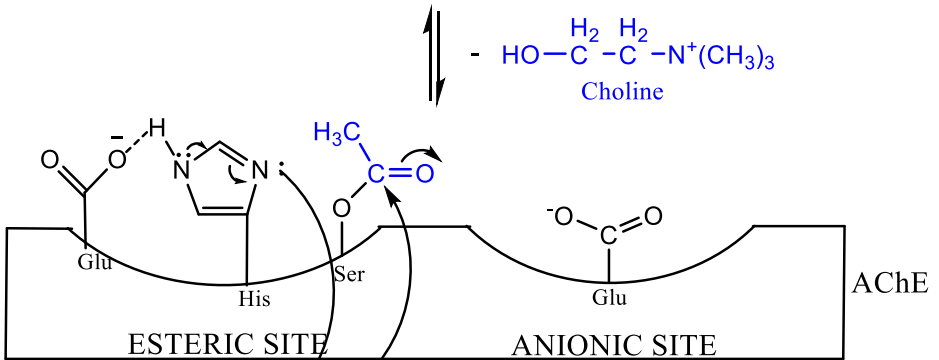
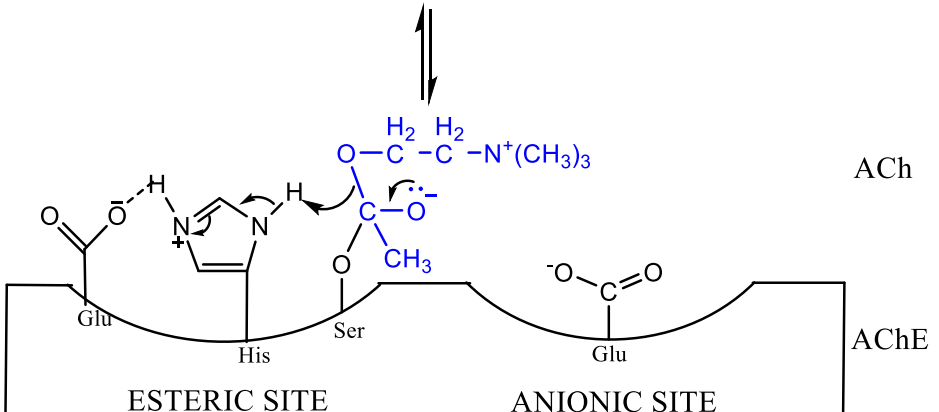
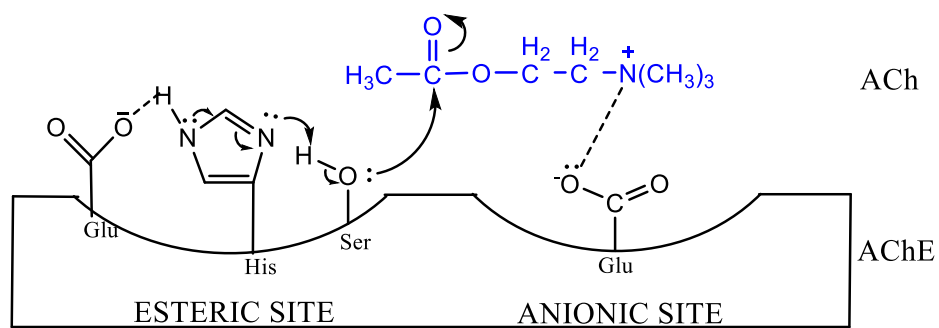
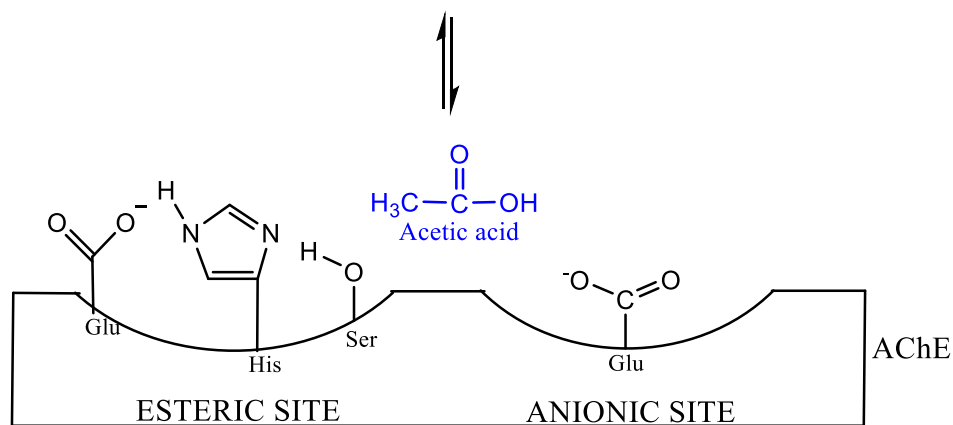


Figure 1.1 Autonomic nervous system.

Acetylcholine (ACh) is degraded in two steps by an enzyme called acetylcholinesterase (AChE). AChE acts as a catalyst and is loosely bound to the post-synaptic cell membrane. The active site of AChE consists of an esteric site and an anionic site, and among several amino acids in the esteric site, the hydroxy group of serine plays a decisive role in degrading acetylcholine by nucleophilic attack on the carbonyl carbon of ACh. Glutamate in the anionic site facilitates the nucleophilic attack of serine on ACh through weak binding to the cationic nitrogen in ACh.

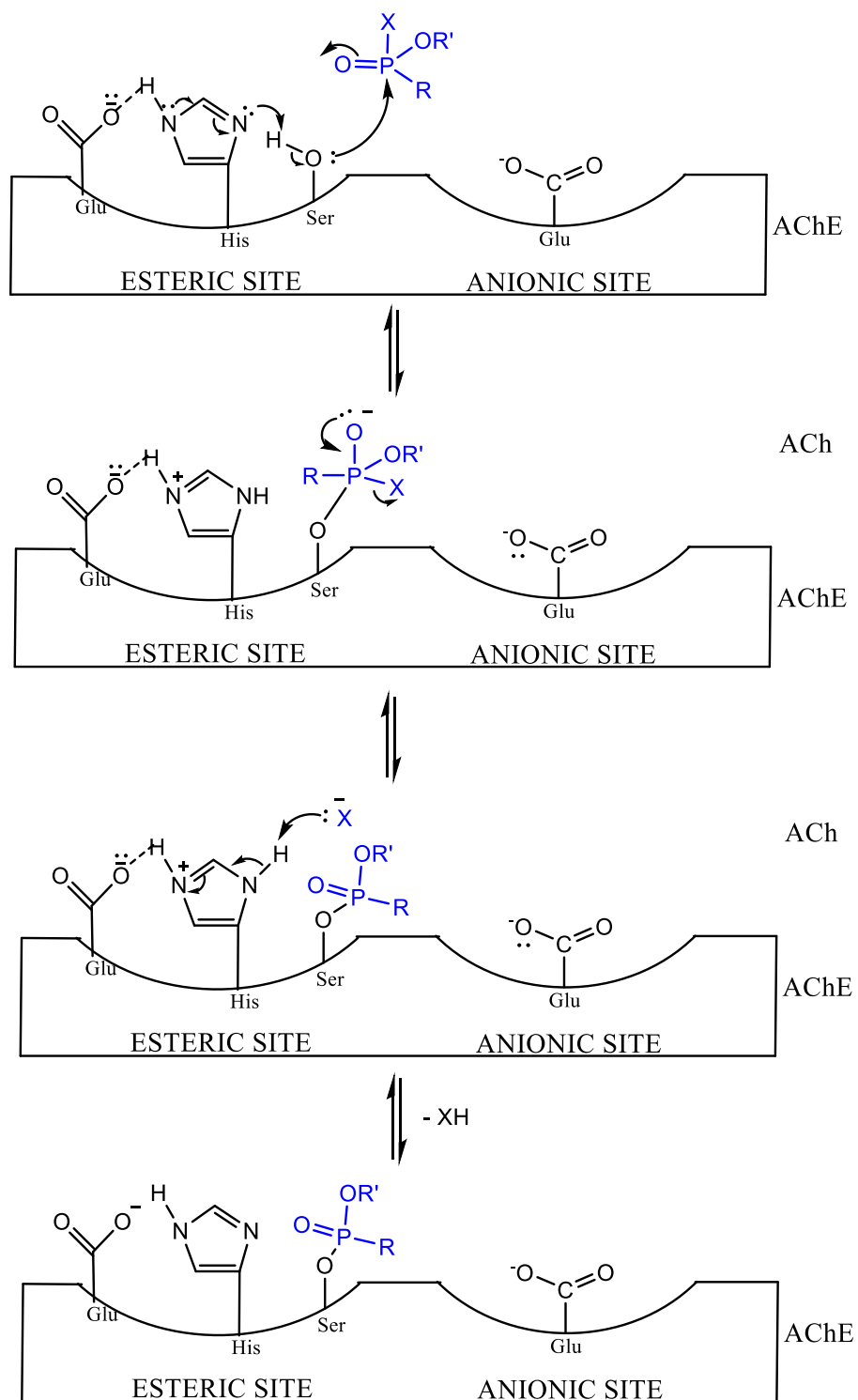
In the first step, acetylation occurs by serine at the active site to release choline, and in the second step, hydrolysis occurs to produce acetic acid (acetate). That is, ACh is decomposed into choline and acetic acid by AChE (**Scheme 1.1**). One AChE enzyme can decompose 15,000 ACh molecules per second under appropriate conditions. If this enzyme is present in large quantities, ACh gets reduced rapidly in cholinergic synapse.⁶⁻⁸





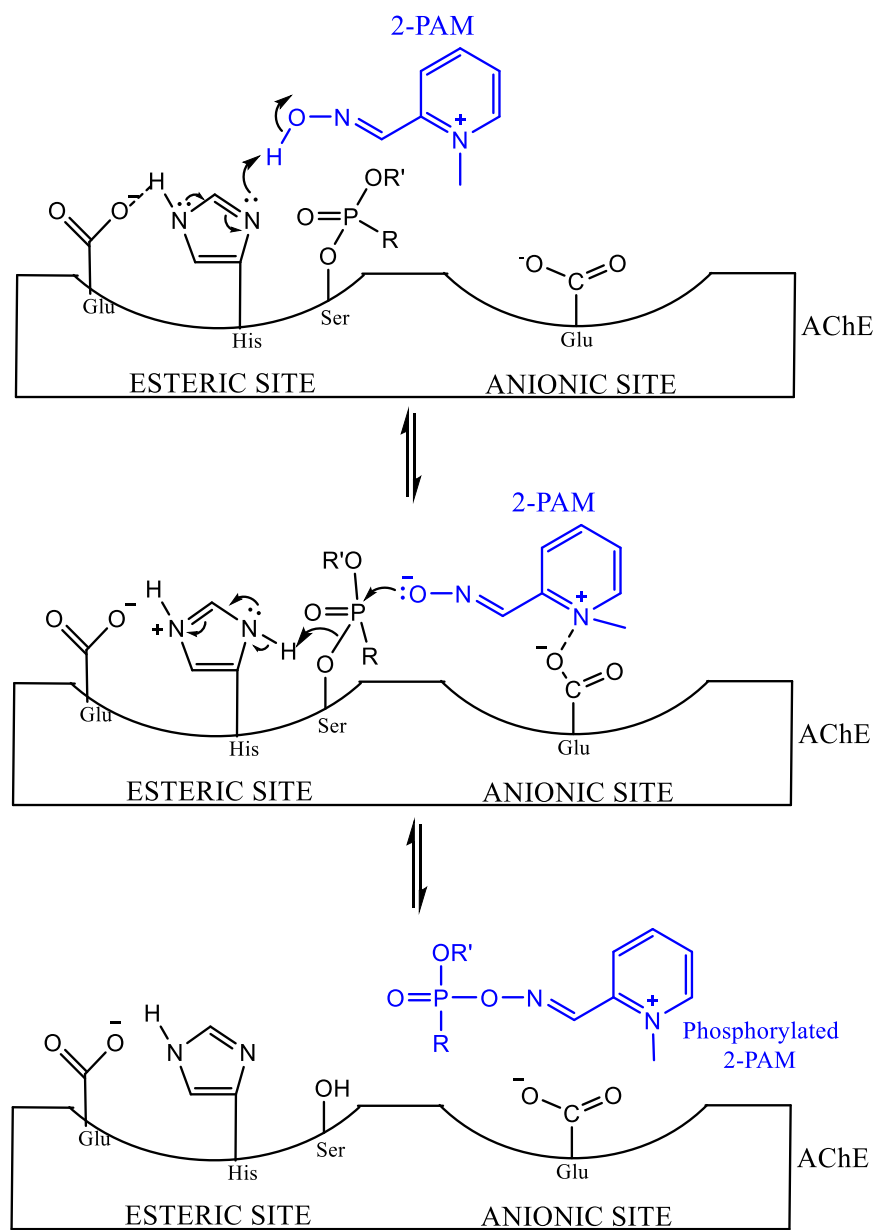
Scheme 1.1 Degradation of acetylcholine by acetylcholinesterase in a normal state.

The mechanism of the reaction between a nerve agent and AChE in the body is introduced in **Scheme 1.2**. Similar to the process by which AChE degrades ACh, a nerve agent subjected to nucleophilic attack by AChE serine forms a covalent bond with serine and inhibits AChE activity. In this case, similar to the carbonyl carbon (C=O) of ACh, the phosphorus center (P=O) of the nerve agent is electrophilic, making it more prone to nucleophilic attacks by the hydroxy group of serine. The difference from ACh is that the nerve agent has a leaving group, so it can better bind to serine with the leaving group easily removed. Also, when the phosphorylated enzyme is hydrolyzed by water, the nerve agent may undergo dealkylation of not the serine but another OR' group (aging). As a result, serine of AChE irreversibly binds to the oxophilic phosphorus center of the nerve agent and the activity of the enzyme is inhibited.⁸⁻¹⁰



Scheme 1.2 Inhibition of acetylcholinesterase activity by a nerve agent.

2-Pyridine aldoxime methyl chloride (2-PAM) is the most representative among therapeutic agents for reactivating AChE whose activity is inhibited by the nerve agents. 2-PAM is an FDA-approved treatment for the nerve agents and pesticides in the United States. The mechanism of action of 2-PAM is that the oxime group of 2-PAM breaks the bond between serine and a nerve agent by nucleophilic attack on the phosphorus center of the nerve agent (**Scheme 1.3**). Thus, a compound in which 2-PAM and the nerve agent are combined is formed and AChE becomes reactive again. Further research is needed to elucidate whether 2-PAM is in an oxime form or an oximate form, a deprotonated form of oxime, in the process of attacking the nerve agent.^{11,12} There is an opinion that the oxime of 2-PAM with a pK_a of 7.51 – 7.74 attacks the nerve agent in the neutral state.^{13,14} Also, there is another study that 2-PAM becomes oximate then attacks under the influence of amino acids such as glutamate and histidine, just like when serine binds to ACh. In any case, the action of 2-PAM can remove the nerve agent and reactivate AChE. However, if the nerve agent bound to serine is aged (dealkylated), removal of the nerve agent is limited even if 2-PAM is administered. Therefore, it is necessary to inject 2-PAM into the body as soon as possible after the exposure to nerve agents.



Scheme 1.3 Mechanism of 2-PAM.

1.2.3 Classification of Nerve Agents

Nerve agents can be classified into three classes: G-series, V-series, and A-series. They are divided by the degree of toxicity, the persistence according to the boiling point of the substance, the time and country of development, etc.

In G-series nerve agents, the 'G' stands for Germany since those agents were developed in Germany. They are volatile liquids (at 25°C GA: 576-610 mg/m³, GB: 16,400-22,000 mg/m³, GD: 3,060-3,900 mg/m³, GF: 59 mg/m³), so regarded as less persistent (GA: T_{1/2} = 24-36 hours, GB: 2-24 hours, GD: relatively persistent).^{15,16} Lethal dose 50% (LD₅₀) is the amount at which 50% of a group of subjects taking the substance will die. LD₅₀ of G-series agents is 1000 mg/person (GA), 1700 mg/person (GB), 350 mg/person (GD), and 30 mg/person (GF), respectively. Lethal concentration 50% (LCt₅₀) is a measure of the lethal dose of vapor or aerosol material, at which 50% of the exposed population dies. LCt₅₀ of G-agents is 100-400 mg×min/m⁻³ (GA), 50-100 mg×min/m⁻³ (GB), and 25-70 mg×min/m⁻³ (GD), respectively.³ G-series nerve agents can be permeated into the body through the eyes or abrasive skin and ingesting them is highly dangerous. They pose less percutaneous menace than V-series agents.

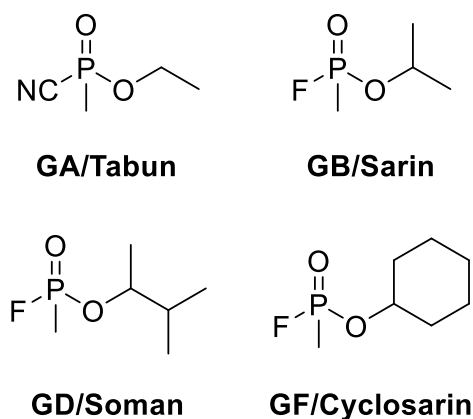


Figure 1.2 G-series nerve agents.

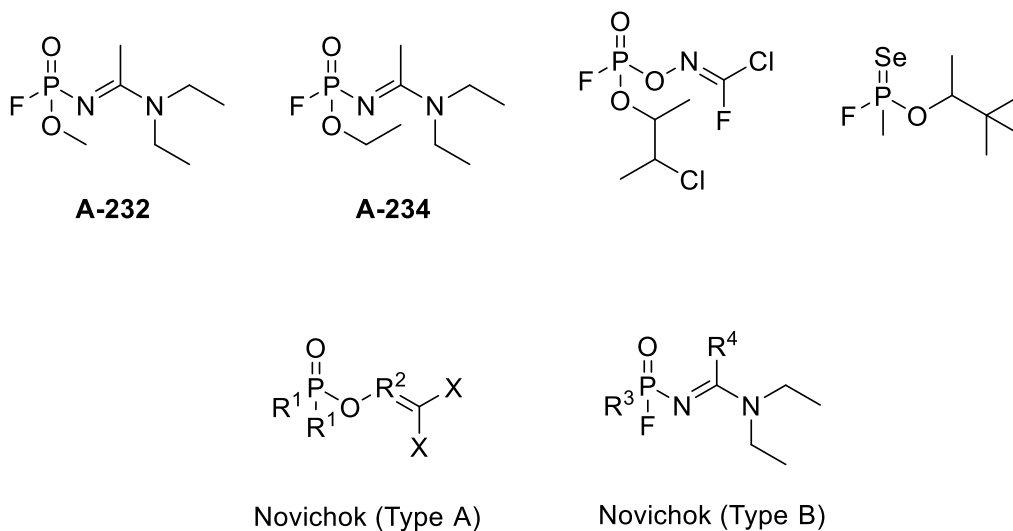


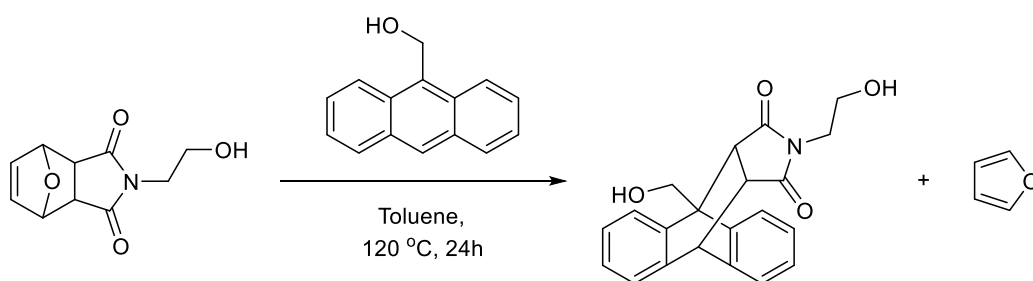
Figure 1.4 A-series nerve agents (Novichok). R^1 = alkyl, alkoxy, alkylamino or fluorine; R^2 = C or N; R^3 = alkyl, alkoxy or alkylamino; R^4 = alkyl or alkylamino; X = halogen (F, Cl, Br) or pseudohalogen (CN).

1.3 POLYMER MORPHOLOGY CHANGES

1.3.1 Transformable and Degradable Polymers

Polymers have been prevalent in our lives. Generally, polymers are very light in weight with significant degrees of strength. In most cases, polymer architecture and its properties have been considered a constant, static feature. However, in some areas, such as biology and medicine, it is necessary to transform polymers. Also, degradable polymers are an important field of research in polymer science and have been used in a wide range of applications spanning from microelectronics to environmental protection.^{18,19} To overcome these disadvantages, stimuli-responsive materials or chemically triggered transformable polymers have been studied in various applications such as biology, medicine, and manufacturing. These materials are capable of adapting their structure, constitution and reactivity upon receiving an external signal.²⁰⁻²²

In the exploration of polymer morphologies, the Sumerlin group reported stimuli-induced transformations of polymers.²³ A linear amphiphilic block copolymer and a segmented hyperbranched polymer that contain furan-maleimide moiety were topologically transformed into polymers of different shapes through retro Diels-Alder and Diels-Alder reactions (**Scheme 1.4**). They found that the anthracene-bound form was more thermally stable than the epoxy-isoindole. Thus, utilizing diene displacement reaction, the initial polymers could undergo “metamorphosis” into comb, star or hydrophobic block copolymer architectures.



Scheme 1.4 Diene displacement reactions between the Diels-Alder adduct of furan and hydroxyethyl maleimide and anthracene derivative.

There are various stimuli-responsive nanoparticles that can be converted into micelles, nanogels, or core-shell particles. Changes of those nanoparticles are able to be induced via self-assembly, surface modification, and chemical triggers with certain functional groups by external stimuli. In the case of some block copolymers, they can form micelle or variable layers depending on the solvent, and when external stimulation is applied to the system, aggregate morphology varies. This allows the formation of appropriate micelle to inhibit the formation of a macroscopic polyelectrolyte complex.²⁴ Nanogels of kinds that perform similarly to hydrogels can be utilized as oxidation-

reduction- or temperature-sensitive nanoparticles. For instance, heat-sensitive copolymers which contain poly(*N*-isopropylacrylamide) and polysaccharide can dissolve in cold water and turn into nanogels by heat.²⁵ Another example of nanoparticles is a pH-sensitive polymer shell, which controls the reversible aggregation and dispersion of nanoparticles, which can be coupled with changes in pH due to a combination of complex biocatalytic reactions.²⁶

To prepare drug delivery systems, pH sensitive degradable polymers are chosen. Those polymers are stable under neutral conditions, but they can be degraded at mild acidic pH. The widely used acid-sensitive linkers are orthoester, acetal/ketal, imine, hydrazone and cis-aconityl groups (**Figure 1.5**).²⁷ The initial polymer bonds undergo hydrolysis or cleavage due to their electrophilicity or protonation under marginally acidic conditions.

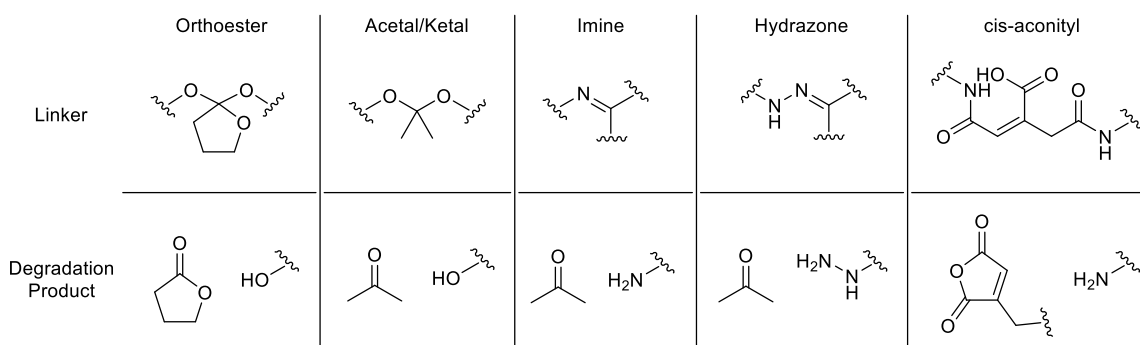


Figure 1.5 Commonly used acidic degradable linkers and their degradation products.

1.3.2 Perturbation of Gel Network for Detection of Nerve Agents

Not many studies have been conducted on detection of nerve agents using polymer gel network. There is a study reported by the Gale group in 2013, which was about detecting GD nerve agent, using a probe of supramolecular gel formation. They developed four probes, and the probes form gel network under certain solvents due to amphiphilic characters (**Figure 1.6**).²⁸

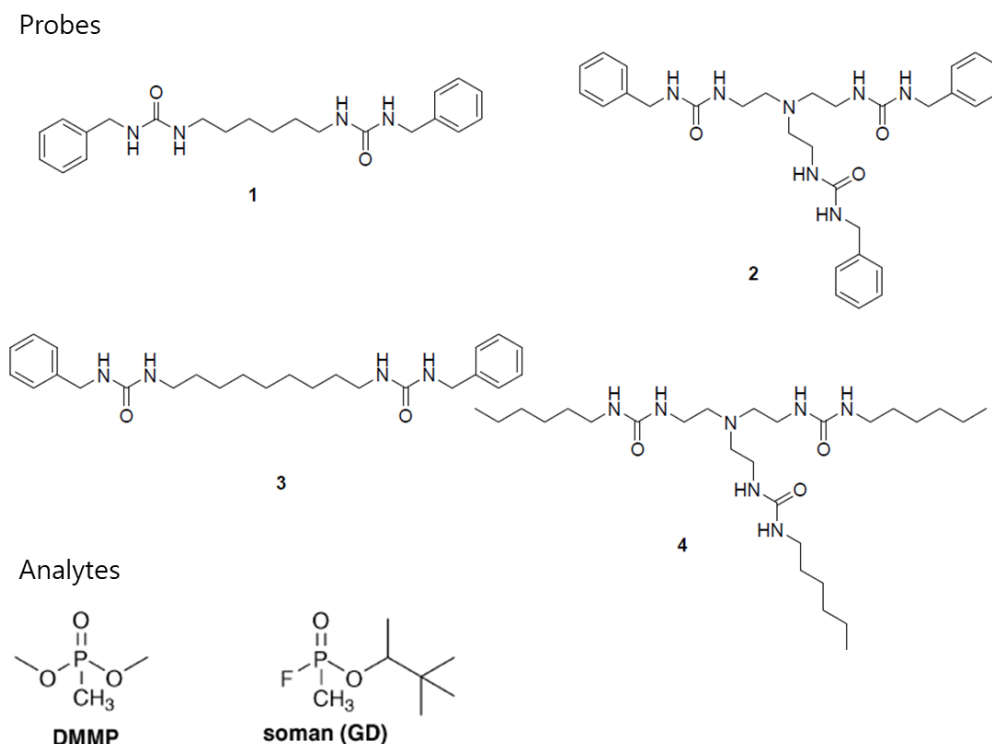
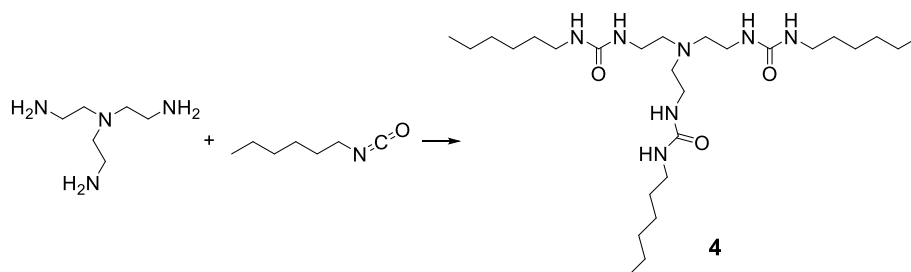


Figure 1.6 Suggested probes 1-4 and nerve agent analytes.

Among four probes, **4** is the most sensitive. **4** is synthesized with an amine moiety and an isocyanate moiety in toluene (**Scheme 1.5**). However, if the target material, GD or DMMP which is a nerve agent surrogate, is added to either side and the reaction

proceeds, the gel formation will either be delayed or not take place at all. Using these sensing methods, they could detect nerve agent targets.



Scheme 1.5 Synthesis of probe 4.

1.3.3 Hydrogel Sensors for Detection of Nerve Agents

There are studies for detection of nerve agents using hydrogels. However, most hydrogel sensors use changes in fluorescence or color rather than changes in hydrogels themselves. To the best of my knowledge, no transformable or degradable hydrogel sensors for detection of nerve agents have been reported.

The Whitaker group introduced a coumarin-based fluorescent sensor for detection of a nerve agent surrogate, using a series of hydrogels.²⁹ The structure of the hydrogel is as shown in **Figure 1.7a**, and it is embedded with 6,7-dihydroxycoumarin. This sensor is a “turn-off” sensor, and they demonstrate that the photophysical property of fluorescence is changed by hydrogen bonds between 6,7-dihydroxycoumarin and 2 equivalents diethylchlorophosphate (DCP) (**Figure 1.7b**).

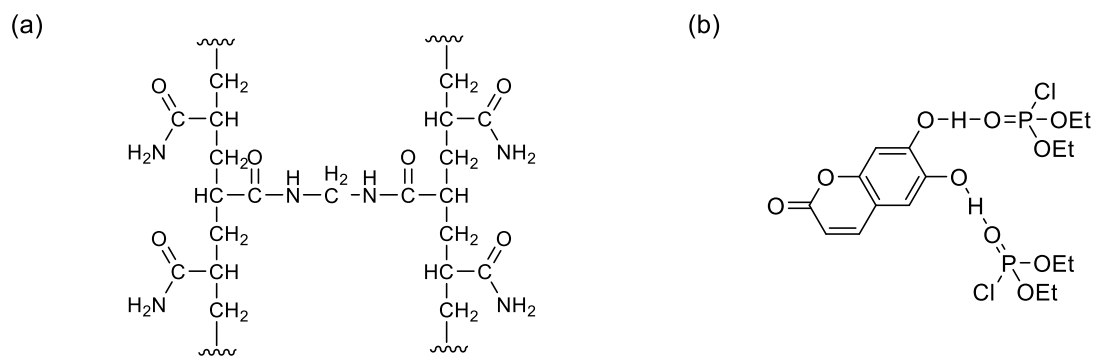
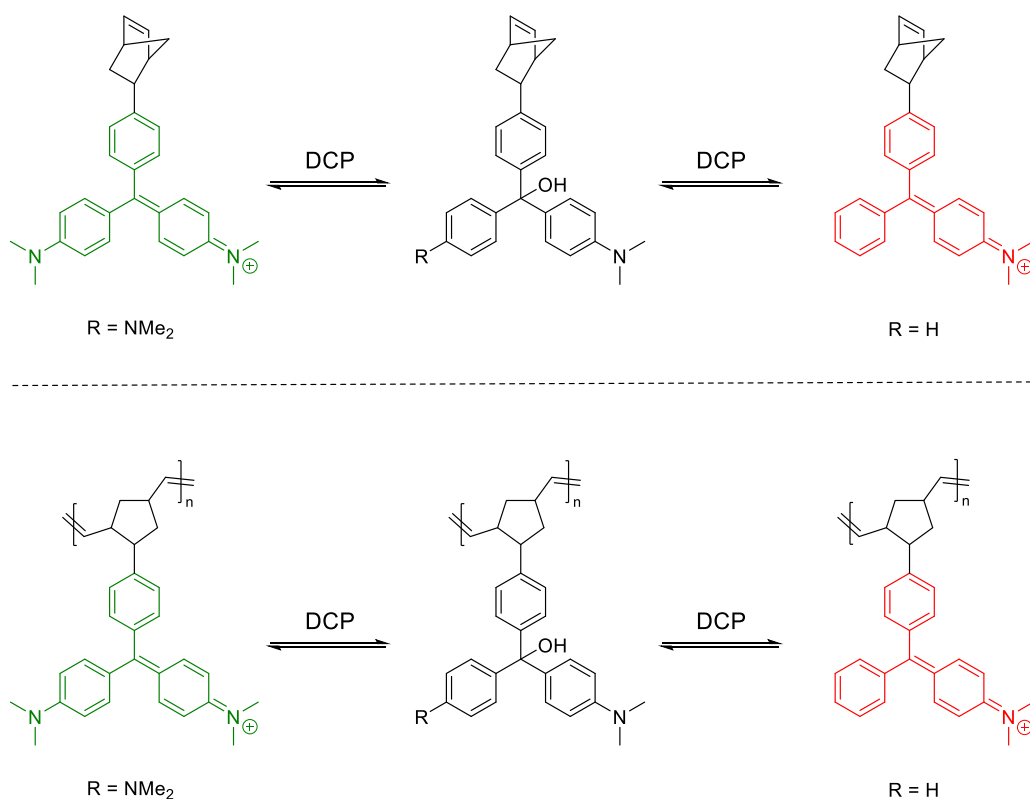


Figure 1.7 (a) Polyacrylamide hydrogels (b) a proposed fluorescence quenching mechanism.

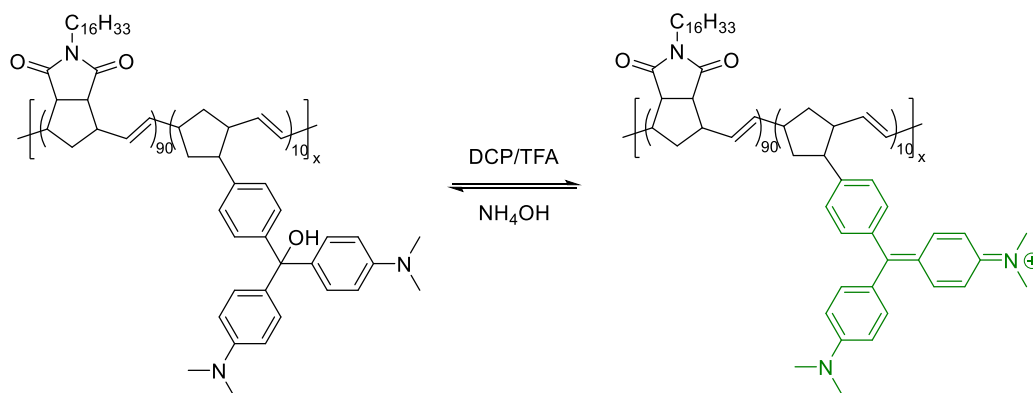
Their smart hydrogel-film-based fluorescent “turn-off” sensor was able to detect nerve agents instantly and selectively in real time. The fluorescence changes could also be observed with the naked eye, using a UV hand lamp.

The Swager group reported colorimetric stimuli-responsive hydrogels for detection of nerve agent simulants in 2015.³⁰ The color of the precursors could be altered when DCP was added. Hydroxyl moiety underwent a nucleophilic attack on DCP, resulting in phosphorylation, and DCP attached to an amino group was released. In this process, an immediate color change occurred due to the ionized amino group. Through ring-opening metathesis polymerization, homopolymers were obtained, and their chromogenic response was similar to the monomers (**Scheme 1.6**).



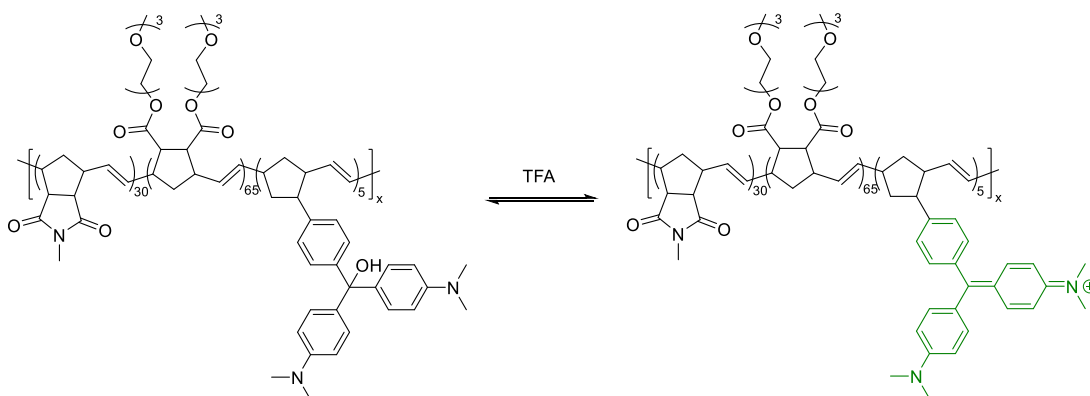
Scheme 1.6 Homopolymers and their precursors., as DCP (100 equiv.) was added, the color of the compound was changed from colorless to either green or red, depending on the R group.

Using these sensing features, they were able to synthesize a variety of random double or triple copolymers with three types of monomers. Among them, the polymers in **Scheme 1.7** were applied onto the cotton tips, and the color of the cotton tips were converted to green quickly when they were exposed to DCP. Also, the color of the cotton tips could easily return to its original state after being exposed to an aqueous ammonium hydroxide vapor.



Scheme 1.7 Rapid color change (from colorless to green) of a random double copolymer in detection of DCP or TFA vapors.

One of the random triple copolymers was formed through the hydrogel network (**Scheme 1.8**). Interestingly, the volume of the swollen hydrogel became smaller and its color changed to dark green when exposed to trifluoroacetic acid (TFA) vapors. This was evidence that it could be employed as a mechanical and volumetric sensor to TFA. After dealt with sodium hydroxide or tetrabutylammonium hydroxide, it returned to its initial swollen state and color. In the case of the analyte, DCP, only the color was altered from yellowish to green.



Scheme 1.8 Molecular structure of a random triple copolymer hydrogel and its response to TFA.

In summary, the Swager group developed chromogenic stimuli-responsive polymer sensors for detection of nerve agent mimics. They were able to rapidly detect the target molecules in ppb level. After detecting nerve agent mimics, the polymers could be regenerated by hydroxide compounds such as NH_4OH , NaOH , or TBAOH . Also, some hydrogels of the various polymers responded mechanically and volumetrically upon exposure to TFA vapors. They expected that these mechanical methods could be applied to the detection of nerve agents.

1.4 SELF-PROPAGATING CASCADE REACTIONS

1.4.1 Features of Self-Propagating Cascades

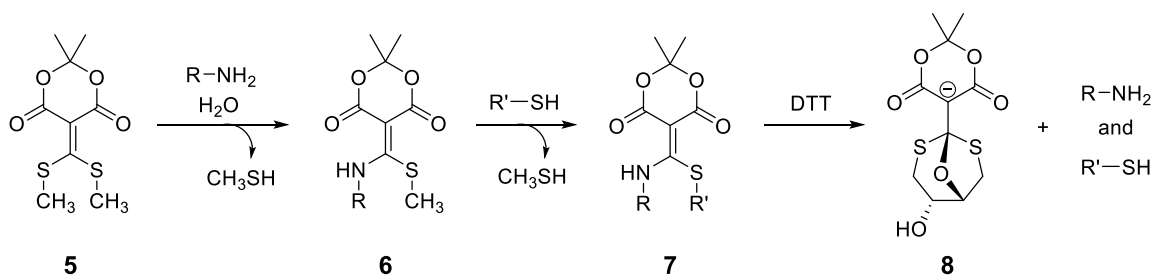
A self-propagating cascade is a chain or a cyclic chemical reaction that amplifies the signal by reacting the target substance that is automatically induced by the trigger.³¹ Its biggest advantage is sensitivity. Amplification of signals through self-propagation provides the possibility to conduct sensitive analytical studies by reducing the detection limit of target analytes.

There are four key parts in the signal amplification reagent. The first is the ability to respond to a specific target signal called a "trigger". This is an analyte or an active reagent that initiates the signal amplification reaction. The second fragment has the ability to release pendant molecules when the target signal activates the trigger. This core feature is termed a "dendritic adapter". This core functionality is linked to the third and fourth major parts termed reagents and reporters, respectively. The reagents and the reporter are both activated when detached from the core functionality and inactivated when attached to the amplification reagent. The released reagents become the "active reagents" and react

with triggers on other copies of the signal amplification reagent. Typically, the analyte and the active reagents are the same substances.

1.4.2 A Conjugate Acceptor and A Self-Propagating Cascade Sensor for VX

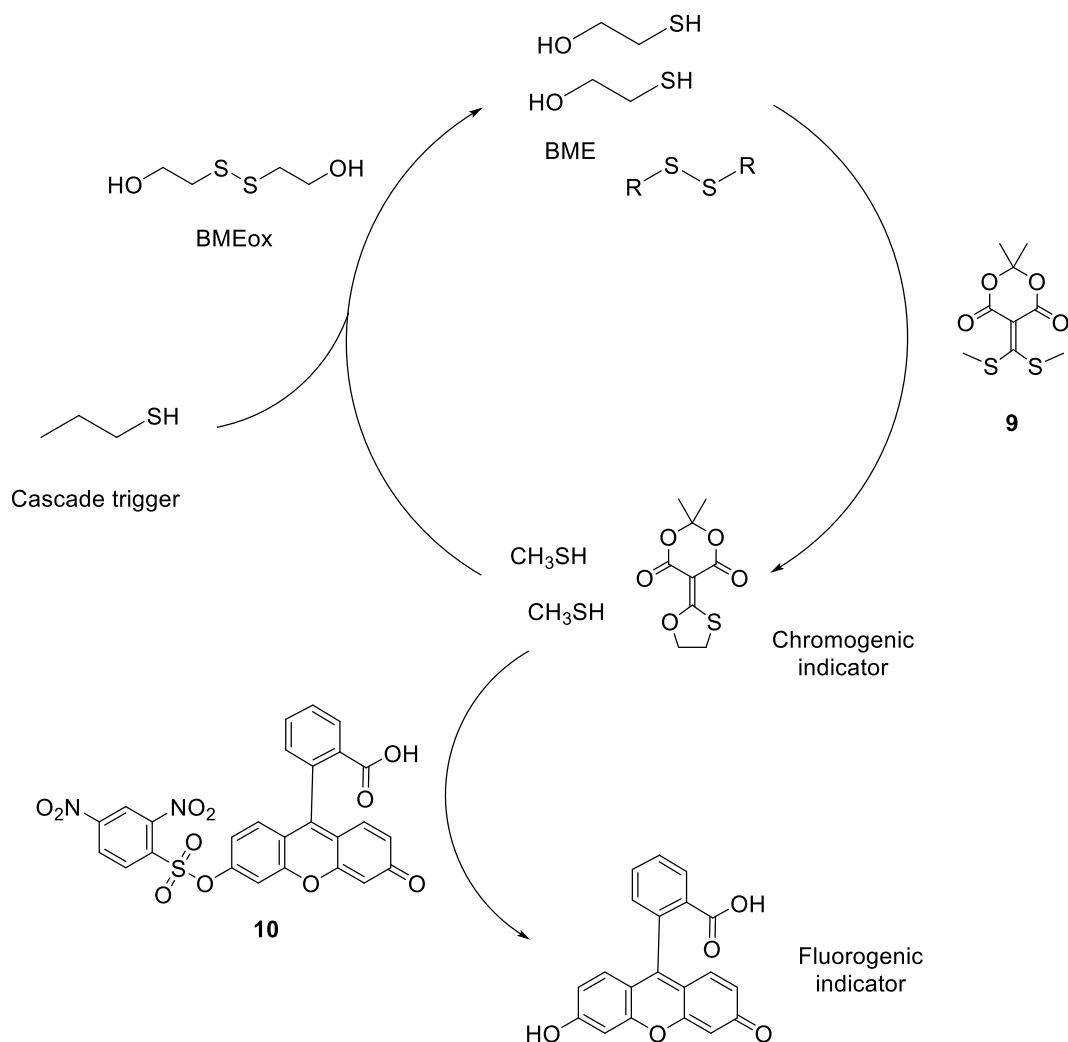
The click-declick reactions using a conjugate acceptor Meldrum's acid derivative were reported by the Anslyn group.^{32,33} In **Scheme 1.9**, Conjugate acceptor **5** would undergo a single reaction with an amine in a protic media to replace one methanethiol, then the reaction stops. The second amine cannot react in a protic media. In water at neutral pH, an amine is insufficiently nucleophilic to perform a second addition because it exists predominately as its conjugate acid. On the other hand, a thiol is still nucleophilic, so compound **7** can be formed and methanethiol is removed with evolution of N₂. At this point, the first amine has been clicked with the desired thiol. From **5** to **7**, this is the “click” reaction that was defined in the Anslyn group as clicking the amine with the thiol. The great virtue of the structure **7** is that it can be readily declicked by releasing the original amine and the original thiol to generate the product **8**. The last step is the “declick” reaction. The overall goal is to conjugate an amine and a thiol to conjugate acceptor.



Scheme 1.9 Click and chemically triggered declicks reactions.

Next study was also reported by the Anslyn group.³⁴ In **Scheme 1.10**, the auto-inductive cascade is initiated by a thiol-disulfide exchange between 2-hydroxyethyl disulfide (BMEox) and a thiol trigger. Then, a rapid reaction between **9** and beta-mercaptoethanol (BME) generates two thiols again, which then cleave the BMEox again, until **9** is entirely decoupled. The analyte was V-series nerve agents which have thiol groups, but the preliminary test was conducted with butanethiol as a cascade trigger. The solvent was pH 10 buffer (borax/sodium hydroxide buffer), and 20% acetonitrile was employed as a co-solvent.

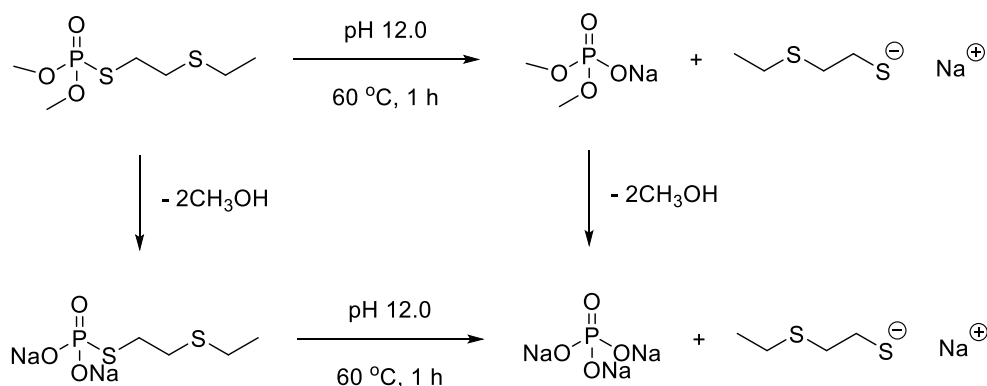
In the absorbance test, only the amount of butanethiol was controlled, and **9** and BMEox were kept constant. As a result, as the amount of the trigger increased, the absorbance decreased rapidly. It means that the more triggers were added, the faster the reaction worked. The results were similar to the result of fluorescence titration tests, using fluorophore **10**. However, a decrease in absorbance was also observed in the sample without butanethiol, which is postulated to be due to the fact that this experiment was performed at pH 10.



Scheme 1.10 The proposed scheme for the self-propagating cascade protocol for the detection of the thiol trigger.

They applied this cascade system to detect a VX Nerve agent surrogate, demeton-S-methyl (DSM), using it as an effective cascade trigger. Under normal conditions, the thiol group of DSM was not released, so they added a step to separate the thiol group (**Scheme 1.11**). Although this process was carried out in harsh conditions (high temperature and strong basic pH) and took a relatively long time, it is meaningful in that

it is a study that can detect trace amounts of potent V-series nerve agents through signal amplification.

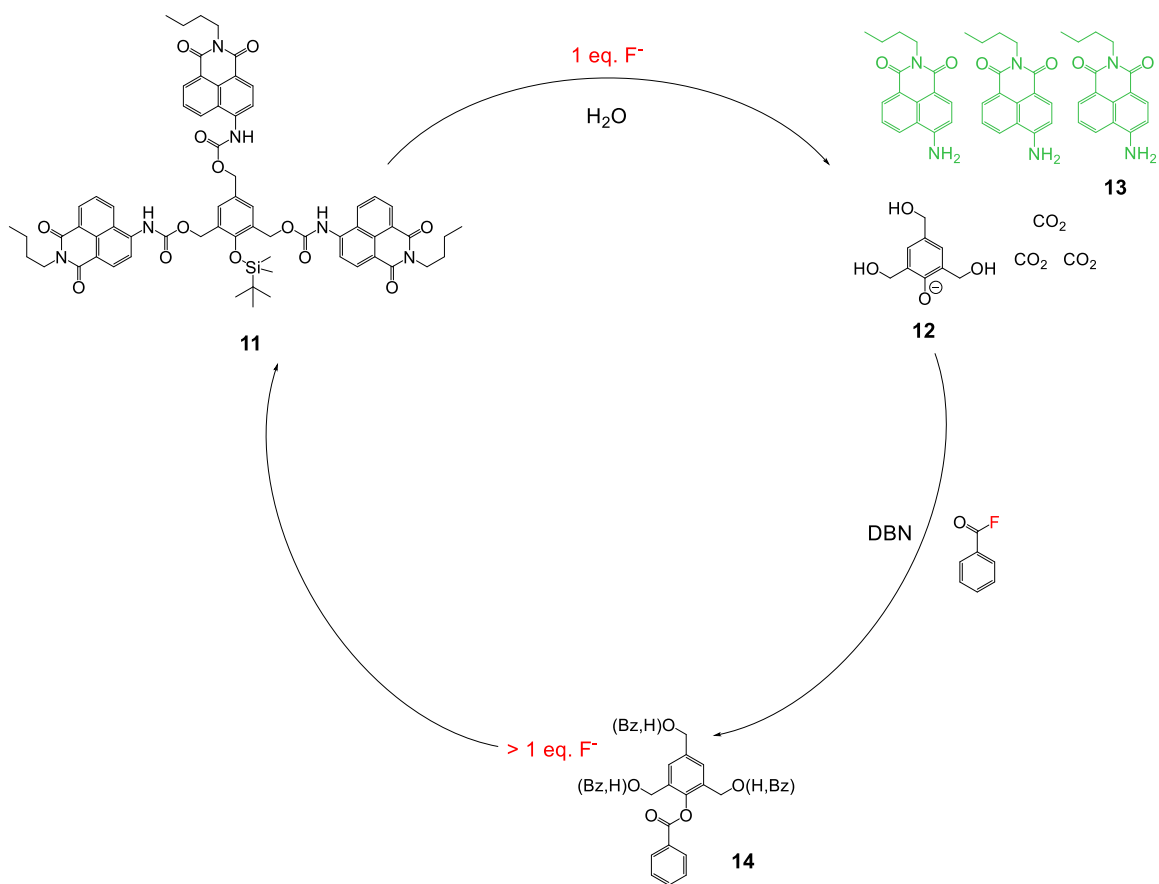


Scheme 1.11 Thiol released in 20% acetonitrile in a pH 12.0 buffer solution at 60 °C.

1.4.3 A Cascade for the Detection of Fluoride-Containing Nerve Agents

The Anslyn group published a study to detect trace amounts of a target molecule, fluoride, by signal amplification through an auto-inductive cascade.³⁵ They adopted a method of amplifying the cycle of the cascade by regenerating fluoride within the cascade when they first detect the fluoride. They developed a protocol that can detect the presence or absence of an analyte, using the change in photophysical properties as the quenched fluorophores are released and turned on. Inspired by the study of the Levacher group, which introduced the combination of benzoyl fluoride (BF) and EtOH as a potential source of HF, it was expected that phenoxide **2**, a product of **1** and fluoride, would react with BF to produce fluoride.³⁶ At this time, 1,5-diazabicyclo(4.3.0)non-5-ene (DBN) was added as a catalyst to help the reaction between **2** and BF, and up to 4 fluorides were released and acted as a retrigger for the propagating cascade (**Scheme**

1.12). As a solvent, methyl tert-butyl ether (MTBE), which had the best fluorescence increase efficiency, was employed.



Scheme 1.12 Detection of fluoride via an auto-inductive cascade with ratiometric changes of optical properties.

The sensing mechanism is as follows. When fluoride deprotects the silyl group of **11**, phenoxide is formed. The oxide releases three of each CO_2 and fluorophores to form quinomethide intermediates. Simplified **12** reproduces up to 4 fluorides through reaction with BF_3 in the presence of DBN, and this F^- again initiates a reaction with **11**, and the cascade cycle is repeated until the remaining **11** is gone.

They confirmed this hypothesis by examining the ratiometric changes of absorbance and fluorescence with time and concentration of the analyte. They also showed the possibility of using this protocol as a sensor to detect nerve agents by producing similar results with fluoride generated by the reaction of phosphoryl fluoride nerve agents with oxime.

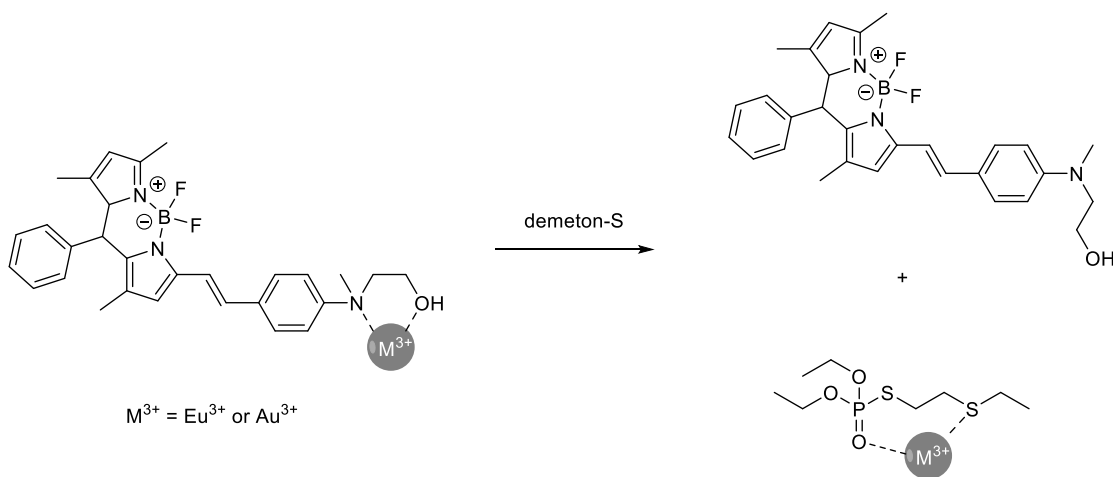
1.5 SUPRAMOLECULAR SENSORS AND CATALYSTS

1.5.1 Metal-Complex Sensors for Detection of Nerve Agents

There have been several published studies of nerve agent detection, using coordination with metal ions. The studies have developed metal coordination-based supramolecular sensors that can detect nerve agents by using the electron-rich parts of V-series nerve agents such as nitrogen and oxygen (O=P bond) to which certain metals can directly bind. In the absence of V-series nerve agents, the developed supramolecular compound forms a complex with the metal ion. However, the addition of the nerve agent makes the photophysical properties of the probe change, as the metal is coordinated more strongly with the nerve agent, breaking the metal-probe complex. In other words, the luminescence of the metal-probe complex is changed by the V-series nerve agent.

There was a study that used the complex of BODIPY dye and metal ion to detect V-series nerve agents (**Scheme 1.13**).³⁷ The concept is that the metal of the probe-metal complex strongly binds to a nerve agent mimic called demeton-S. This causes the complex to be broken, so intramolecular charge transfer (ICT) quenching occurs due to the change of aniline, an electronic donating group, and the fluorescence of the probe becomes turned-off.

When the aniline group was complexed with Eu^{3+} , it was confirmed that the aromatic peak underwent downfield shift in ^1H NMR. It was also proved that ICT was blocked due to Eu^{3+} . In addition, it was substantiated that the metal ions affect the probe by increasing the fluorescence intensity of the probe by adding Eu^{3+} or Au^{3+} . The fluorescence mechanism was demonstrated with these two experiments. The effective sensitivity and selectivity tests of the V-type nerve agent mimic were performed through a UV-vis absorption spectroscopy, and the results support their hypothesis.



Scheme 1.13 Proposed scheme of a nerve agent detection.

A study was reported in 2014 that when a V-series nerve agent was added to the lanthanide-ligand complex (**Figure 1.8a**), which had luminescence at a certain wavelength, bidentate complexation between the nerve agent and lanthanide ion was formed as shown in **Figure 1.8b**. The sensitizing ligand was also shown to be displaced and the luminescence intensity decreased.³⁸

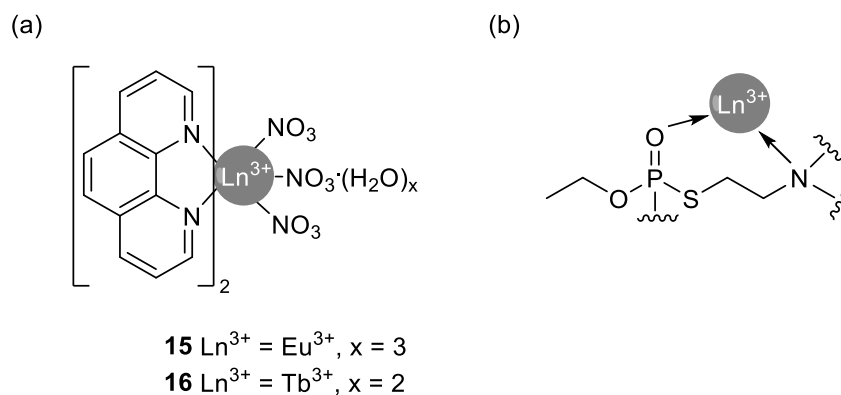


Figure 1.8 (a) Two lanthanide complexes. (b) a proposed chelate ring between a V-type nerve agent and lanthanide ion.

Herein, two things are presented as evidence of detecting V-type nerve agents. First, adding VX or VG resulted in a decrease in luminescence intensity. Next, changes in phenanthroline were adopted as evidence. As the amount of a V-nerve agent added to the solution in the presence of the lanthanide-ligands complex increased, the UV-vis absorbance of phenanthroline gradually shifted to the lower wavelength (hypsochromic shift), and the absorption band spectrum became the same as that of free phenanthrene (262 nm).

1.5.2 Organic Based Sensors for Detection of Nerve Agents

Hydrogen bonding is usually employed for supramolecular sensors for detection of nerve agents, which consist only of metal-free organic materials. Although hydrogen bonding is weak compared to coordination with metal, it has shown some meaningful results in detecting nerve agents. The following three studies have been published on organic-based supramolecular sensors for nerve agents or their leaving groups.

The first is a study reported by the Gale group.³⁹ In this study, four receptors were developed to detect soman, and only proton NMR was used to prove the change of

receptors due to interaction with soman (**Figure 1.9**). The four receptors commonly contain one urea and two indole groups, and it was confirmed that the protons attached to them undergo downfield shift because of the interaction with oxygen of soman (O=P). Since soman can undergo hydrolysis in aqueous environments, all experiments were carried out in organic solvent conditions consisting of acetonitrile-d₃ (95-98%) and DMSO-d₆ (2-5%) to prevent this.

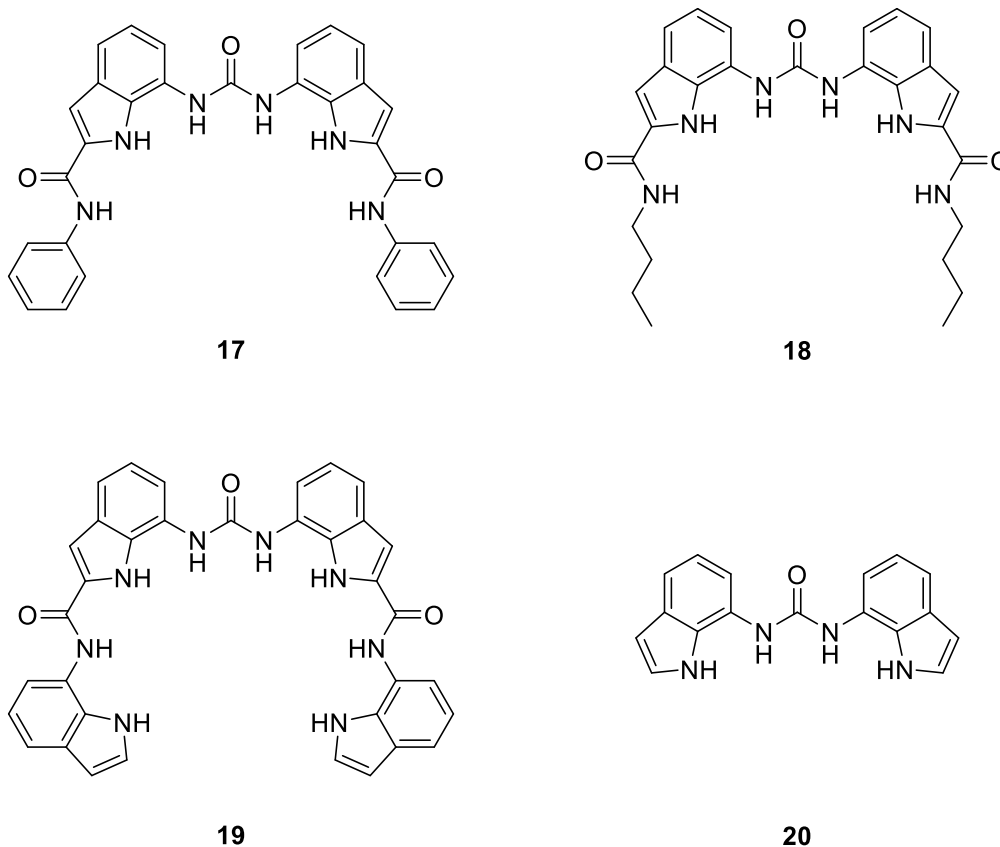


Figure 1.9 Hydrogen-bond donating host receptors **17-20**.

They also confirmed that receptor **18** formed a 1:1 complex with soman through the Job plot analysis. Through DFT calculation, it was expected that receptor **20** and

soman would bind to each other as shown in **Figure 1.10**. The calculated model showed that among the four hydrogens of receptor **20**, three would form hydrogen bonds with the oxygen of O=P and one would form a hydrogen bond with the fluoride, but no hydrogen bond between the fluoride and NH was observed in the experimental data.

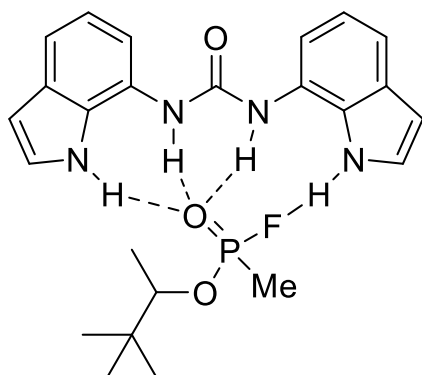


Figure 1.10 The complex between **20** and soman based on a DFT calculation.

This study was limited in that the soman recognition study was performed solely relying on ^1H NMR without optical changes and did not clearly reveal the interaction between receptors and soman. However, this was the first recognition study, using hydrogen bonding of the developed receptors and nerve agents.

The next study is about a supramolecular fluorescent sensor based on naphthalimide derivatives.⁴⁰ In this study, when two ethanolamines attached to the fluorophore naphthalimide meet DMMP, one of nerve agent mimics, multitopic hydrogen bonds are formed. Then, the emission intensity of the fluorophore increases, which is the concept of recognizing the nerve agent mimic (**Figure 1.11**).

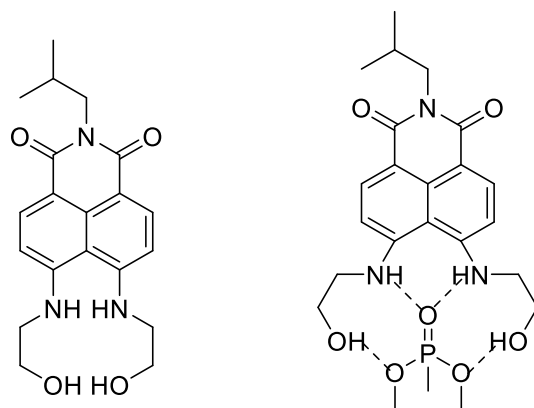


Figure 1.11 A fluorescent probe (left) and proposed sensing mechanism with DMMP (right).

They demonstrated multitopic hydrogen bonds using the proton NMR peaks of the hydroxy and amine groups of ethanolamine which were shifted with changes in the concentration of DMMP. In addition, their hypothesis was verified through the increase of fluorescence along with the increase of DMMP concentration and the paper strip application studies.

The third study did not directly detect nerve agents or their mimics, but the developed supramolecular sensors could selectively detect fluoride and cyanide, which are the main leaving groups of G-series nerve agents.⁴¹ The NH of the thiourea group included in the sensor is shown to change the absorbance of the probes by forming hydrogen bonds with anions. As shown in **Figure 1.12**, the sensor has two thiourea groups, so that one probe and two anions form a complex with a 1:2 stoichiometric ratio.

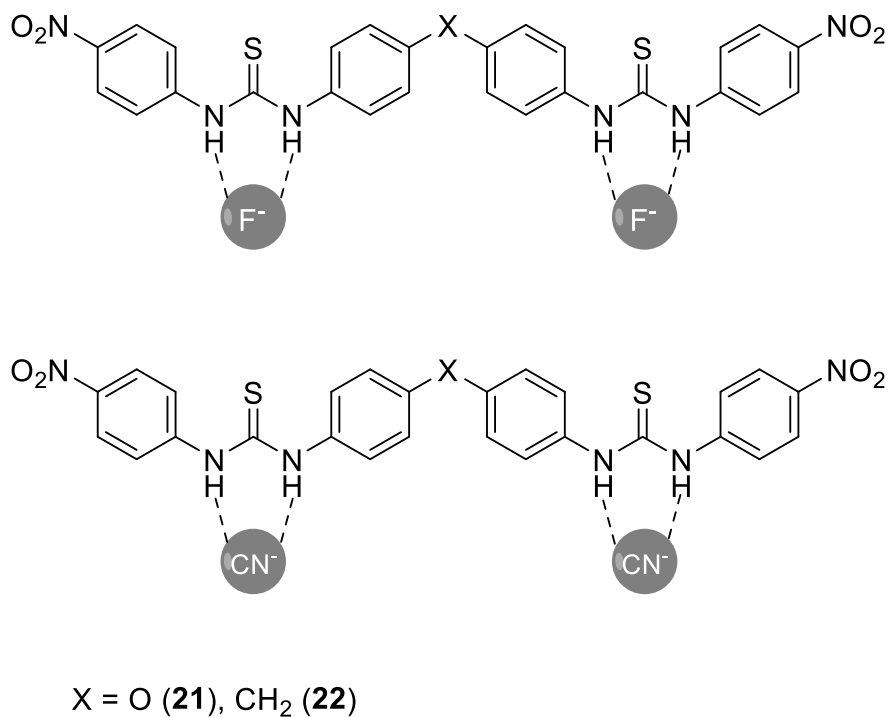


Figure 1.12 The proposed structures of the complex formed between probes and anions (F⁻, CN⁻).

They proved the initial state of the sensors with X-ray crystallography. In the case of sensor **21**, where X was O, N-H of thiourea and S of another molecule **21** formed intermolecular hydrogen bonds (N-H···S) before the guest entered. In sensor **22**, it was confirmed that not only the same N-H···S bond as in **21** is present, but also C-H···O intermolecular interactions exist between the proton of the central aromatic ring and the oxygen of the nitro group. And they conducted chromogenic response studies on various anions, and only F⁻ and CN⁻ resulted in the significant changes in color.

1.5.3 Catalysts for Nerve Agent Remediation

This study is reported by the Gale group about catalysts for nerve agent remediation using neutral 1,3-diindolylureas.⁴² The catalysts were from the work of the

Gale group themselves, mentioned in the previous chapter 1.5.2.³⁹ The most commonly used method to remove the toxicity of nerve agents is to hydrolyze the nerve agent to remove the leaving group and to reduce the electrophilicity of the phosphorus center. The four catalysts presented in this study were determined to speed up remediation by increasing the hydrolysis rate of nerve agents in an aqueous environment. To confirm this, they observed the shift change in ¹H NMR and the pH change using the indicator **24** (Figure 1.13).

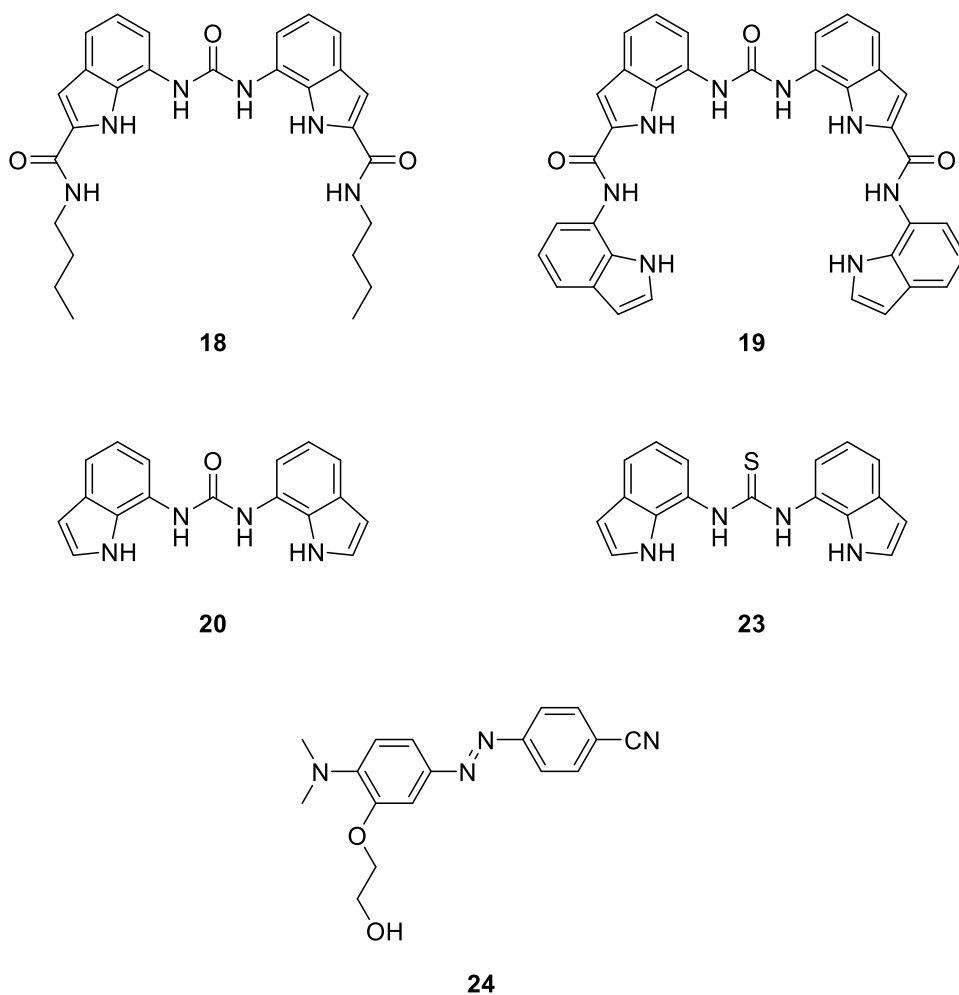


Figure 1.13 Catalysts **18-20** and **23** used for hydrolysis of nerve agents and indicator **24**.

First, the complex stoichiometry and association constant values between the catalysts **18-20** or **23** and DCNP were obtained by confirming the shift of proton NMR. Catalysts **18** and **19** formed a complex with DCNP in a 1:2 ratio, and catalysts **20** and **23** in a 1:1 ratio. In the case of binding constant, **18** and **20** were much higher than **19** and **23**, and the values were $881\pm 90\text{ M}^{-1}$, $4.4\pm 0.3\text{ M}^{-1}$, $1743\pm 35\text{ M}^{-1}$, and $10.1\pm 0.9\text{ M}^{-1}$ from **18**, **19**, **20**, and **23**, respectively. The reason for this was interpreted that **18** and **20** have a larger number of binding sites available for hydrogen bonds than **19** or **23**. The reason **20** was greater than **18** is because **20** has more H-N group than **18**. And it was postulated that **23** was greater than **19** because the protons of the thiourea group are more acidic than the urea group.

Next, the hydrolysis rate of DCP and DCNP, which are nerve agent mimics, was studied using indicator **24** in co-solvent of water/acetone (20:80, v/v) in the presence of the catalyst. When the nerve agent mimics are hydrolyzed and produced enough protons, the color of the solution containing indicator **24** can be changed from yellow to colorless. They observed the color change of the solution with the naked eye, measured the time for the solution to become transparent, and obtained the data in **Table 1.1**. Each of these values is a calculation of how quickly the color changed compared to the sample without the catalyst. In their opinion, these data clearly showed that the catalysts increased the hydrolysis rate of nerve agent mimics. The reason why the hydrolysis rate of DCP was faster than that of DCNP was that the chloride of DCP was a better leaving group than the cyanide of DCNP. In addition, they believed the data reinforced results of the previous NMR study, which showed that **1** and **3**, which had higher association constants than **2** and **4**, also had a faster hydrolysis rate. They explained the result that the hydrolysis rate of **3**, which had higher binding constant among **18** and **20**, was slower

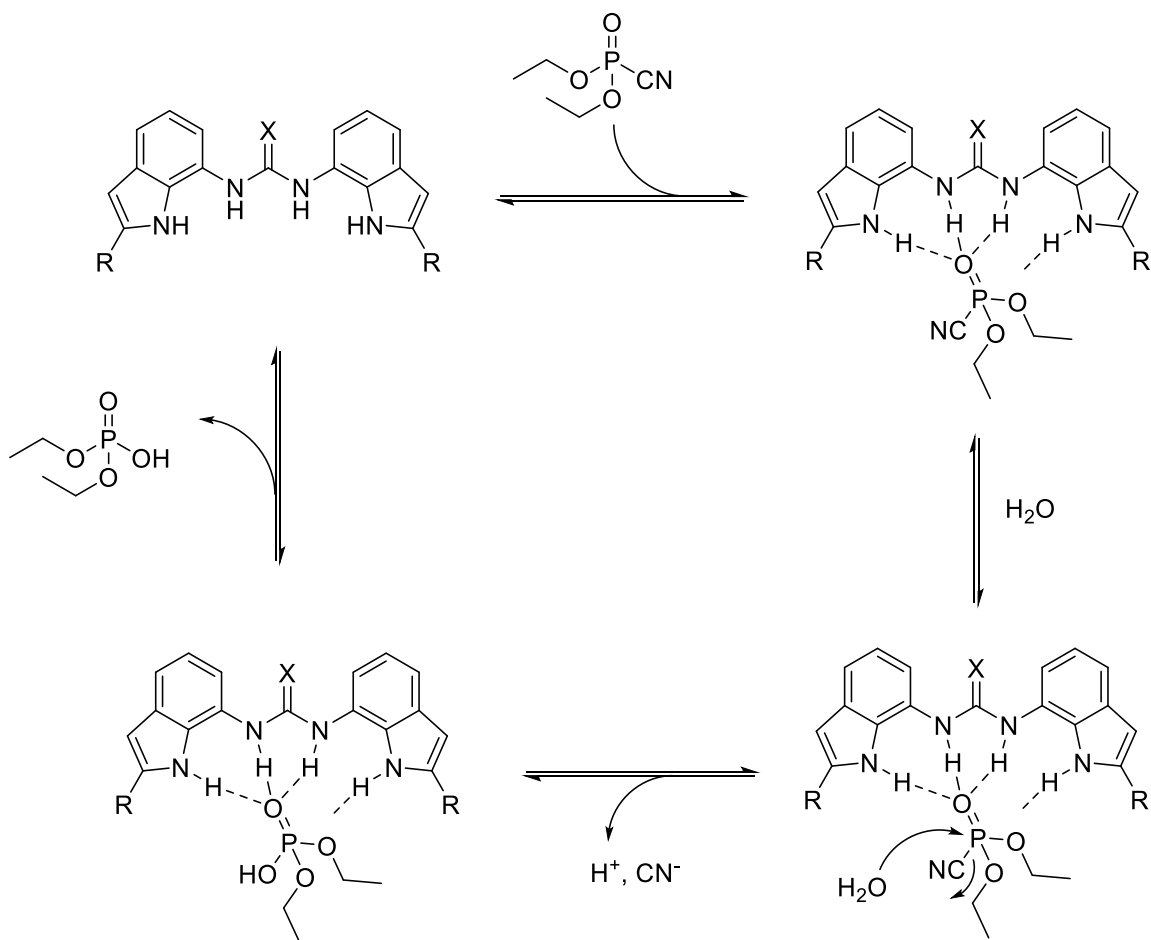
than that of **18** as follows. The catalytic effect of **20**, which was less hydrophobic compared to **18**, was reduced due to an increase in affinity with the nerve agent mimics, which had a decreased hydrophobic character after hydrolysis.

Catalysts	DCP	DCNP	DCP	DCNP
	0.001 equiv. ^[a]	0.001 equiv. ^[a]	0.005 equiv. ^[a]	0.005 equiv. ^[a]
18	44.6±0.4%	17±2%	30±1%	6.3±0.2%
19	13±1%	6.4±0.3%	14.8±0.2%	6.3±0.4%
20	27±2%	19.5±0.6%	29.5±0.5%	6.4±0.2%
23	9.8±0.5%	6.7±0.3%	12.7±0.2%	11.3±0.4%

[a] Equivalents of catalyst relative to the amount of mimic.

Table 1.1 Changes in hydrolysis rates of the nerve agent mimics, DCP and DCNP, in acetone/water (80:20 v/v) in the presence of one of the organocatalysts. Data are presented as the rate of improvement in hydrolysis rate compared to the hydrolysis of the mimics in the absence of catalyst.

Lastly, they presented **Scheme 1.14** and stated that the developed catalysts formed complexes with nerve agent mimics and they enhanced the electrophilicity of the phosphorus center, thereby facilitating the nucleophilic attack by water and hydrolysis of nerve agent mimics. This study suggests a method that helps to rapidly remediate nerve agents with small amounts of catalysts. It is also meaningful that the study was conducted with supramolecular receptors made of only organic compounds.



Scheme 1.14 The proposed scheme of hydrolysis cycle of a nerve agent mimic. The developed catalysts were employed for the reaction between DCNP and water.

1.6 SUMMARY

This chapter has described the history of nerve agents, their chemical activities *in vivo*, and how to detect them. It is not only important to detect the highly dangerous toxic substance, nerve agents, rapidly and selectively, but it is also essential to detect them accurately. Various studies have been conducted to detect and detoxify chemical warfare agents, including the use of chromogenic or fluorogenic methods, electrochemical

methods, and metal-organic frameworks as well as the modification of polymer forms, signal amplification, and the use of supramolecular sensors and catalysts. Cross-validation using various methods is believed to contribute to improving the accuracy in the detection of chemical warfare agents. Therefore, it is expected that more diverse and active research for detection of chemical warfare agents will be carried out.

1.7 REFERENCES

1. Trumpener, U., The Road to Ypres: The Beginnings of Gas Warfare in World War I. *J. Mod. Hist.* **1975**, *47*, 460-480.
2. Wiener, S. W.; Hoffman, R. S., Nerve Agents: A Comprehensive Review. *J. Intensive Care Med.* **2004**, *19*, 22-37.
3. Kaszeta, D., *Toxic: A History of Nerve Agents, from Nazi Germany to Putin's Russia*; C. Hurst & Co.: London, 2020.
4. Hayoun, M. A.; Smith, M. E.; Ausman, C.; Yarrarapu, S. N. S.; Swoboda, H. D., Toxicology, V-Series Nerve Agents. *In StatPearls [Internet]*; StatPearls Publishg: Treasure Island, FL, 2021.
5. McCorry, L. K., Physiology of the Autonomic Nervous System. *Am. J. Pharm. Educ.* **2007**, *71* (4), 78.
6. Lee, S.; Yang, I.; Lee, N.; Jeong, W.; Kye, Y.; Kim, S.; Kim, S., *Military Chemistry*; Bongmyeong: Seoul, 2004.
7. Nachmansohn, D.; Wilson, I. B., The Enzymic Hydrolysis and Synthesis of Acetylcholine. In *Advances in Enzymology and Related Subjects of Biochemistry Volume XII*; Nord, F. F., Ed.; Interscience Publishers, Inc.: New York, 1951; pp 259-340.
8. Colović, M B.; Kristić, D. Z.; Lazarević-Pašti, T. D.; Bondžić, A. M.; Vasić, V. M., Acetylcholinesterase Inhibitors: Pharmacology and Toxicology. *Curr. Neuropharmacol.* **2013**, *11*, 315-335.
9. Quinn, D. M.; Topczewski, J.; Yasapala, N.; Lodge, A., Why is Aged Acetylcholinesterase So Difficult to Reactivate?. *Molecules* **2017**, *22* (9), 1464.

10. Hirsch, A.; Hauke, F., Post-Graphene 2D Chemistry: The Emerging Field of Molybdenum Disulfide and Black Phosphorus Functionalization. *Angew. Chem. Int. Ed.* **2018**, *57*, 4338-4354.
11. Delfino, R. T.; Ribeiro, T. S.; Figueroa-Villar, J. D., Organophosphorus Compounds as Chemical Warfare Agents: A Review. *J. Braz. Chem. Soc.* **2009**, *20* (3), 407-428.
12. Silva, G. R.; Borges Jr., I.; Figueroa-Villar, J. D., DFT Conformational Studies of the HI-6 Molecule. *Int. J. Quantum Chem.* **2005**, *105*, 260-269.
13. Musil, K.; Florianova, V.; Bucek, P.; Dohnal, V.; Kuca, K.; Musilek, K., Development and Validation of a FIA/UV–Vis Method for pK_a Determination of Oxime Based Acetylcholinesterase Reactivators. *J. Pharm. Biomed. Anal.* **2016**, *117*, 240-246.
14. Castro, A. T.; Figueroa-Villar, J. D., Molecular Structure, Conformational Analysis and Charge Distribution of Pralidoxime: Ab Initio and DFT Studies. *Int. J. Quantum Chem.* **2002**, *89*, 135-146.
15. Sidell, F. R., Nerve Agents. In *Textbook of Military Medicine: Medical Aspects of Chemical and Biological Warfare*; Sidell, F. R.; Takafuji, T. E.; Franz, D. R., Eds.; Office of the Surgeon General, U.S. Army: Falls Church, VA, 1997; pp 129-179.
16. Ellison, D. H., *Handbook of Chemical and Biological Warfare Agents*; CRC Press: Boca Raton, FL, 2000; pp 220-239.
17. Chai, P. R.; Hayes, B. D.; Erickson, T. B.; Boyer, E. W. Novichok Agents: A Historical, Current, and Toxicological Perspective. *Toxicol. Commun.* **2018**, *2*, 45-48.
18. Delplace, V.; Nicolas, J., Degradable Vinyl Polymers for Biomedical Applications. *Nat. Chem.* **2015**, *7* (10), 771-784.
19. Lamb, J. B.; Willis, B. L.; Fiorenza, E. A.; Couch, C. S.; Howard, R.; Rader, D. N.; True, J. D.; Kelly, L. A.; Ahmad, A.; Jompa, J., Plastic Waste Associated with Disease on Coral Reefs. *Science* **2018**, *359* (6374), 460-462.
20. Auilar, M. R.; Roman, J. S., *Smart Polymers and their Applications*, Elsevier, Cambridge, UK, 2014, pp. 1-11.
21. Stuart, M. A. C.; Huck, W. T. S.; Genzer, J.; Muller, M.; Ober, C.; Stamm, M.; Sukhorukov, G. B.; Szleifer, I.; Tsukruk, V. V.; Urban, M.; Winnik, F.; Zauscher,

- S.; Luzinov, I.; Minko, S., Emerging Applications of Stimuli-Responsive Polymer Materials. *Nat. Mater.* **2010**, *9*, 101-113.
22. Blum, A. P.; Kammeyer, J. K.; Rush, A. M.; Callmann, C. E.; Hahn, M. E.; Gianneschi, N. C., Stimuli-Responsive Nanomaterials for Biomedical Applications. *J. Am. Chem. Soc.* **2015**, *137*, 2140-2154.
 23. Sun, H.; Kabb, C. P.; Dai, Y.; Hill, M. R.; Ghiviriga, I.; Bapat, A. P.; Sumerlin B. S., Macromolecular Metamorphosis via Stimulus-Induced Transformations of Polymer Architecture. *Nat. Chem.* **2017**, *9*, 817-823.
 24. Blanazs, A.; Armes, S. P.; Ryan, A. J., Self-Assembled Block Copolymer Aggregates: From Micelles to Vesicles and their Biological Applications. *Macromol. Rapid Commun.* **2009**, *30*, 267-277.
 25. Morimoto, N.; Qiu, X. P.; Winnik, F. M.; Akiyoshi, K., Dual Stimuli-Responsive Nanogels by Self-Assembly of Polysaccharides Lightly Grafted with Thiol-Terminated Poly(*N*-isopropylacrylamide) Chains. *Macromolecules* **2008**, *41*, 5985-5987.
 26. Motornov, M.; Zhou, J.; Pita, M.; Gopishetty, V.; Tokarev, I.; Katz, E.; Minko, S., "Chemical Transformers" from Nanoparticle Ensembles Operated with Logic. *Nano Lett.* **2008**, *8*, 2993-2997.
 27. Binauld, S.; Stenzel M. H., Acid-Degradable Polymers for Drug Delivery: A Decade of Innovation. *Chem. Commun.* **2013**, *49*, 2082-2102.
 28. Hiscock, J. R.; Piana, F.; Sambrook, M. R.; Wells, N. J.; Clark, A. J.; Vincent, J. C.; Busschaert, N.; Browna, R. C. D.; Gale, P. A., Detection of Nerve Agent via Perturbation of Supramolecular Gel Formation. *Chem. Commun.* **2013**, *49*, 9119-9121.
 29. Whitaker, C. M.; Derouin, E. E.; O'connor, M. B.; Whita-ker, C. K.; Whitaker, J. A.; Snyder, J. J.; Kaufmann, N. R.; Gilliard, A. N.; Reitmayer, A. K. Smart Hydrogel Sensor for Detection of Organophosphorus Chemical Warfare Nerve Agents. *Journal of Macromolecular Science, Part A* **2017**, *54*, 40-46.
 30. Belger, C.; Weis, J. G.; Egap, E.; Swager, T. M. Colorimetric Stimuli-Responsive Hydrogel Polymers for the Detection of Nerve Agent Surrogates. *Macromolecules* **2015**, *48*, 7990-7994.

31. Sun, X.; Shabat, D.; Phillips, S. T.; Anslyn E. V., Self-Propagating Amplification Reactions for Molecular Detection and Signal Amplification: Advantages, Pitfalls, and Challenges. *J. Phys. Org. Chem.* **2018**, *31*, e3827.
32. Diehl, K. L.; Kolesnichenko, I. V.; Robotham, S. A.; Bachman, J. L.; Zhong, Y.; Brodbelt, J. S.; Anslyn, E. V., Click and Chemically Triggered Declick Reactions through Reversible Amine and Thiol Coupling via a Conjugate Acceptor. *Nat. Chem.* **2016**, *8* (10), 968-973.
33. Meadows, M. K.; Sun, X.; Kolesnichenko, I. V.; Hinson, C. M.; Johnson, K. A.; Anslyn, E. V., Mechanistic Studies of a “Declick” Reaction. *Chem. Sci.* **2019**, *10*, 8817-8824.
34. Sun, X.; Anslyn, E. V., An Auto-Inductive Cascade for the Optical Sensing of Thiols in Aqueous Media: Application in the Detection of a VX Nerve Agent Mimic. *Angew. Chem. Int. Ed.* **2017**, *129* (32), 9650-9654.
35. Sun, X.; Dahlhauser, S. D.; Anslyn, E. V., New Autoinductive Cascade for the Optical Sensing of Fluoride: Application in the Detection of Phosphoryl Fluoride Nerve Agents. *J. Am. Chem. Soc.* **2017**, *139* (13), 4635-4638.
36. Poisson, T.; Dalla, V.; Marsais, F.; Dupas, G.; Oudeyer, S.; Levacher, V., Organocatalytic Enantioselective Protonation of Silyl Enolates Mediated by Cinchona Alkaloids and a Latent Source of HF. *Angew. Chem. Int. Ed.* **2007**, *46*, 7090-7093.
37. Barba-Bon, A.; Costero, A. M.; Gil, S.; Sancenón F.; Martínez-Máñez, R., Chromo-Fluorogenic BODIPY-Complexes for Selective Detection of V-Type Nerve Agent Surrogates. *Chem. Commun.* **2014**, *50*, 13289-13291.
38. Dennison, G. H.; Sambrook, M. R.; Johnston, M. R., VX and VG Chemical Warfare Agents Bidentate Complexation with Lanthanide Ions. *Chem. Commun.* **2014**, *50*, 195-197.
39. Sambrook, M. R.; Hiscock, J. R.; Cook, A.; Green, A. C.; Holden, I.; Vincent, J. C.; Gale, P. A., Hydrogen Bond-Mediated Recognition of the Chemical Warfare Agent Soman (GD). *Chem. Commun.* **2012**, *48*, 5605-6507.
40. Puglisi, R.; Pappalardo, A.; Gulino, A.; Sfrassetto, G. T., Multitopic Supramolecular Detection of Chemical Warfare Agents by Fluorescent Sensors. *ACS Omega* **2019**, *4*, 7550-7555.
41. Kumar, V.; Kaushik, M. P.; Srivastava, A. K.; Pratap, A.; Thiruvankatam, V.; Row, T. N. G., Thiourea Based Novel Chromogenic Sensor for Selective

- Detection of Fluoride and Cyanide Anions in Organic and Aqueous Media. *Anal. Chim. Acta* **2010**, *663*, 77-84.
42. Barba-bon, A.; Costero, A. M.; Parra, M.; Gil, S.; Martínez-Máñez, R.; Sancenón, F.; Gale, P. A.; Hiscock, J. R., Neutral 1,3-Diindolylureas for Nerve Agent Remediation. *Chem. Eur. J.* **2013**, *19*, 1586-1590.

Chapter 2: Chemically Triggered Synthesis, Remodeling, and Degradation of Soft Materials¹

Polymer topology dictates dynamic and mechanical properties of materials. For most polymers, topology is a static characteristic. In this article, we present a strategy to chemically trigger dynamic topology changes in polymers in response to specific chemical stimulus. Starting with a dimerized PEG and hydrophobic linear materials, a lightly cross-linked polymer, and a cross-linked hydrogel, transformations into an amphiphilic linear polymer, lightly cross-linked and linear random copolymers, a cross-linked polymer, and three different hydrogel matrixes, were achieved via two controllable cross-linking reactions: reversible conjugate additions and thiol-disulfide exchange. Significantly, all the polymers, before or after morphological changes, can be triggered to degrade into thiol- or amine-terminated small molecules. The controllable transformations of polymeric morphologies and their degradation heralds a new generation of smart materials.

¹This chapter was adapted with permission from the published article: Sun, X.; Chwatko, M.; Lee, D.-H.; Bachman, J. L.; Reuther, J. F.; Lynd, N. A.; Anslyn, E. V. Chemically Triggered Synthesis, Remodeling, and Degradation of Soft Materials. *J. Am. Chem. Soc.* **2020**, *142*, 3913–3922. Copyright (2020) American Chemistry Society.

2.1 INTRODUCTION

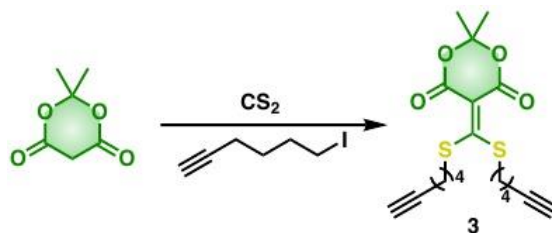
Stimuli-responsive polymers that are capable of adapting their structure, constitution, and reactivity on receiving an external stimulus have been emerging in various fields of study, such as biology, medicine, and manufacturing.¹⁻⁴ Currently, the control of their properties has been limited to single chemical functional group interchanges, and very limited structural/morphological changes. Similarly, degradable polymers are an important goal within polymer science, and have been used in a wide range of applications spanning medicine and drug delivery, to microelectronics and environmental protection.⁵ In 2018, Lamb *et al.* reported that a billion plastic items are entangled on coral reefs across the Asia-Pacific.⁶ Thus, it is increasingly critical that plastics and other polymers be triggered to degrade at will.⁷

The physical properties of polymers are strongly dependent on several features: their molecular weight distribution, tacticity, topology, chemical functionality, and density of cross-linking.⁸ It is rare that these features can be triggered to change by altering the bonding patterns within the backbone structure, as well as changing cross-linking group functionality, and thereby manipulate material properties. To realize transformations of macromolecular topology, exploiting the reversibility and orthogonality of dynamic covalent chemistry is useful because these reactions enable independent control over differing functional groups in a single chemical system.⁹⁻¹² As alluded to above, if the orthogonal interactions can be manipulated under physiological conditions (*i.e.* in neutral aqueous media), they could lead to new therapeutic materials platforms. Further, if the molecular architecture can be morphed under mild conditions, and with the ability to disassemble the soft materials into small molecules on demand, controllable material properties and triggered biodegradation are within reach. Each of these features is described herein.

In the pursuit of such materials, Sumerlin reported that macromolecular metamorphosis via reversible Diels-Alder transformations of polymer architectures can be achieved in organic media at high temperature over the period of few days.¹³⁻¹⁴ This exploration of topological interchange was an important step-forward because a single system could be converted to several macromolecular architectures depending upon reaction conditions. However, the use of elevated temperatures, organic solvents, and the lack of polymer degradation following transformation, limits the applications that can be envisioned.

“Click chemistry” is a term used to describe reactions that are high yielding, wide in scope, and create byproducts that can be easily removed.¹⁵⁻¹⁷ The Cu(I)-catalyzed Azide/Alkyne Cycloaddition (CuAAC) 'click' reaction has been used extensively in the field of polymer science.¹⁸⁻²⁰ Recently, our group reported an alternative click strategy, and an associated chemically-triggered “declick”, which involves the coupling of amines and thiols via conjugate acceptor **1** that functions in both aqueous and organic media.²¹⁻²² (**Scheme 2.1**). The two thioethers in **1** can be released using various reagents,²³ and amine/thiol conjugates such as **2** could be declicked with dithiothreitol (DTT). Noticeably, decoupling of conjugate acceptor **1** releases two equivalents of thiol which can facilitate thiol-disulfide exchange reactions.²³⁻²⁵ Thus, we envisioned the use of structures such as **1** to couple and decouple amines/thiols in polymers,²⁶ as well as facilitate disulfide dynamic exchange, as two reversible covalent bonding interactions for independent control of polymer morphology. With these reactions in mind, we pursued linear polymers and cross-linked networks creation, along with chemically-triggered metamorphosis and degradation. The dramatic topological manipulations reported herein, and associated changes in physical properties, induced by chemically-triggered transformations, represent a promising approach to generate tunable ‘smart’ materials.

or disulfide exchange to chemically trigger morphological changes of the polymer/gel and subsequently “declick” degradation.



Scheme 2.2 Synthesis of the conjugate acceptor **3**.

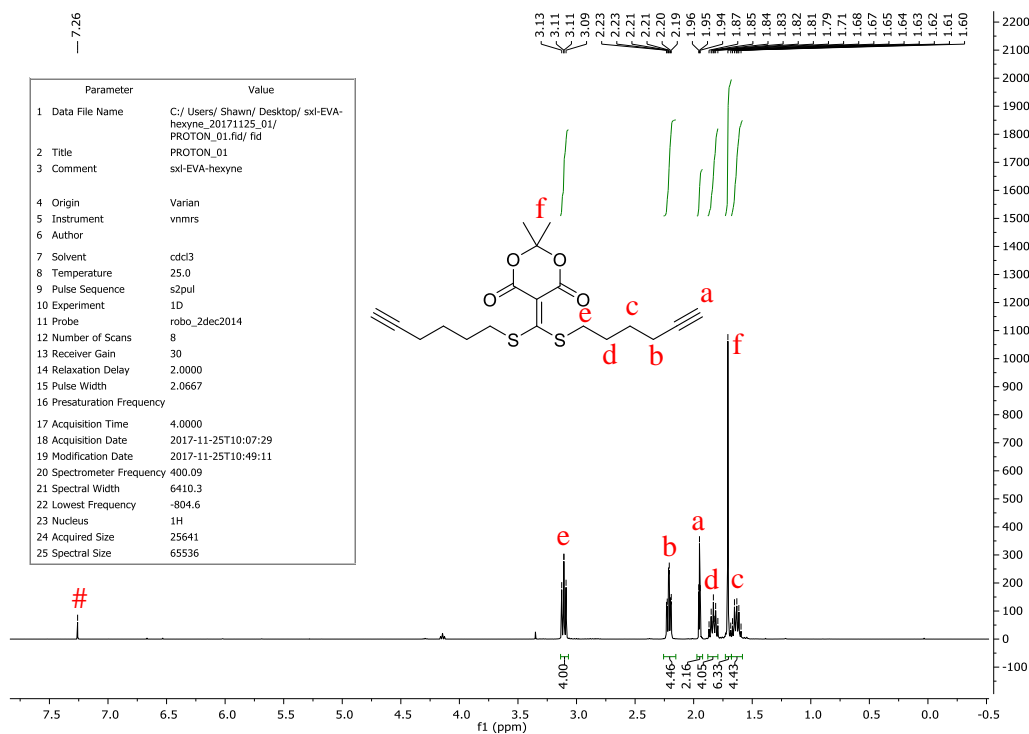


Figure 2.1 ^1H NMR for compound **3** in CDCl_3 .

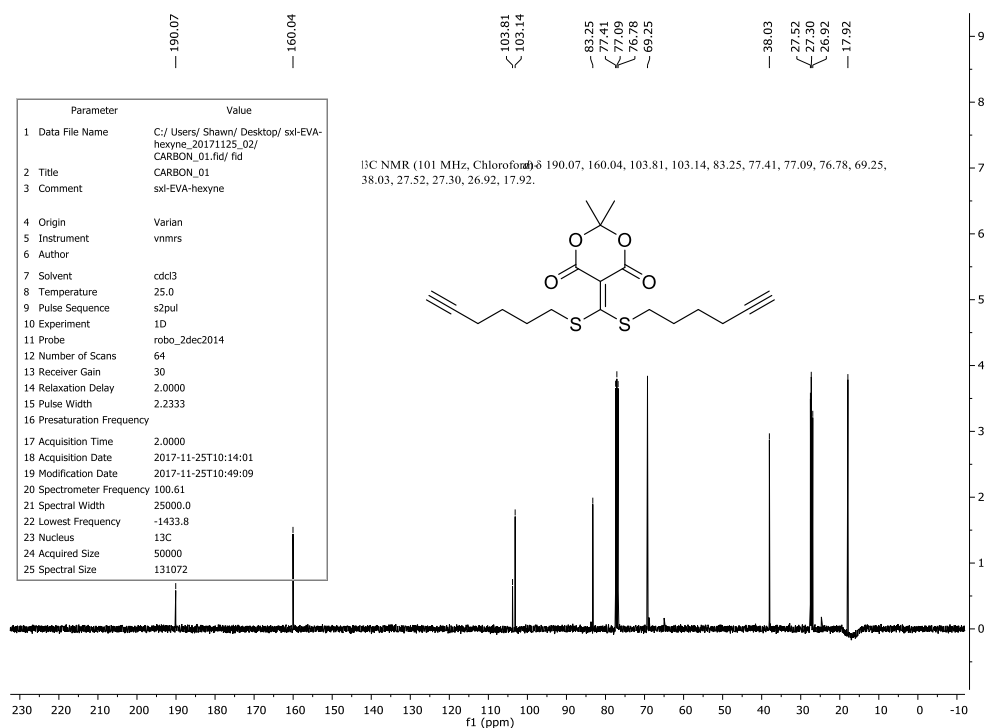


Figure 2.2 ¹³C NMR for compound 3 in CDCl₃.

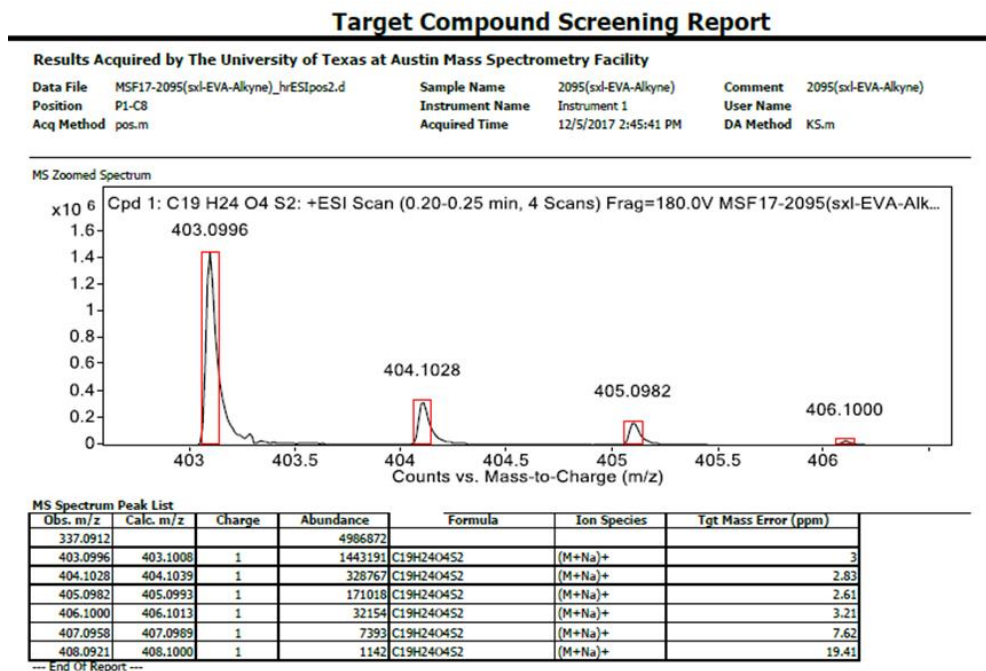


Figure 2.3 High Resolution Mass Spectra (HRMS) for compound 3. HRMS (ES⁺) m/z calc. for [M + Na]⁺, 403.1008; found, 403.0996.

To generate characteristic spectroscopic signals that would allow us to monitor the transformations of the polymers and gels, we analyzed the spectral differences of the chromophores involved in the clicking and declicking reactions of **1** with small molecules via UV-Vis spectrophotometry. The vinyllogous thio-, oxo-, and amino-derivatives shown in Scheme 1 all have distinct absorbance spectra. For example, the reaction of **3** in phosphate-buffered saline (PBS) with DTT, β -mercaptoethanol (BME), ethanedithiol (EDT), cysteine (Cys) and cysteamine (CYA), gave distinguishable UV-Vis absorbance spectra. The λ_{\max} for **3** was at 350 nm, while reagent-induced declicking led to blue-shifted spectra and different λ_{\max} values depending on the structure of the cyclized products: DTT (250 nm, a tricyclic product, **4**),²⁸ BME (290 nm, **5**), EDT (330 nm, **6**), Cys or CYA (280 nm, **7**) (**Figure 2.4**). The relative speed of decoupling was DTT > BME > EDT ~ CYA > Cys. Thus, the chemical group interchanges involved in the polymer/network topological changes could be monitored by simple UV-Vis absorbance spectroscopy, and the rate of decoupling could be controlled, if desired. As described below, the λ_{\max} values allowed us to follow the extent of chemical functional group interchange.

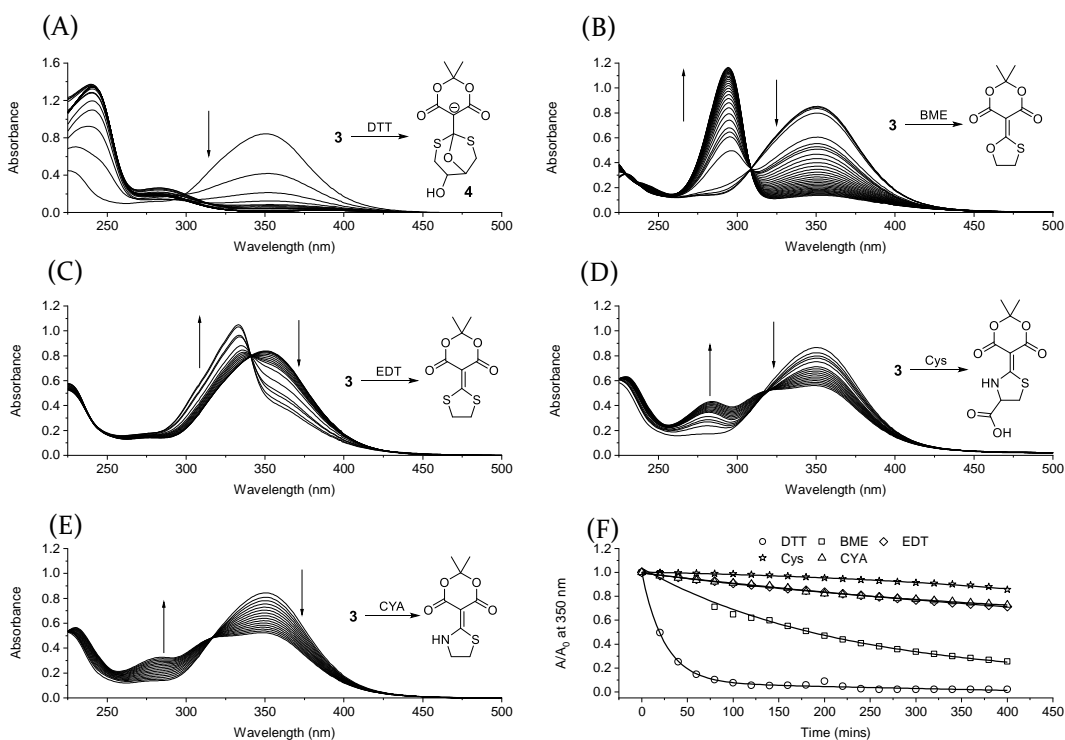
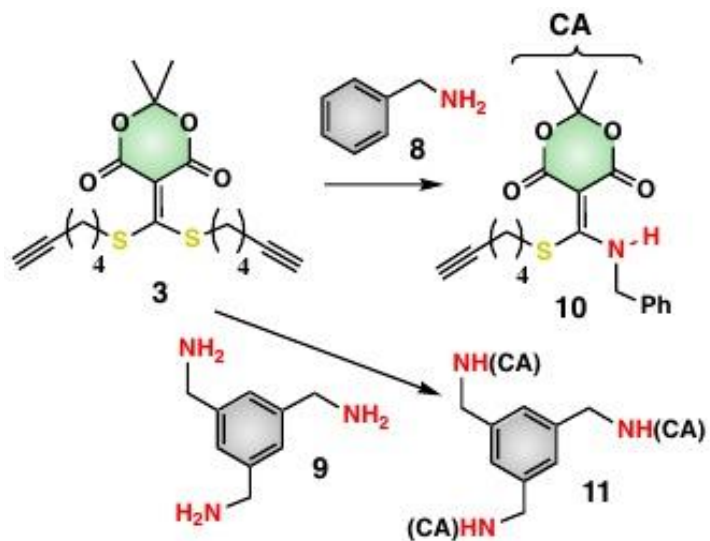


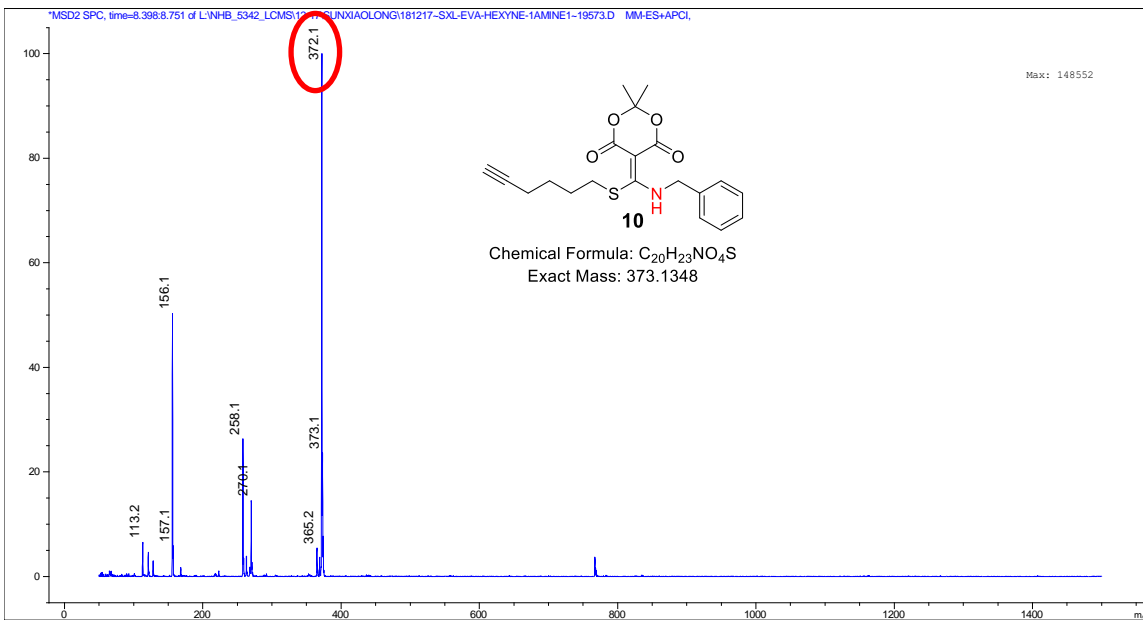
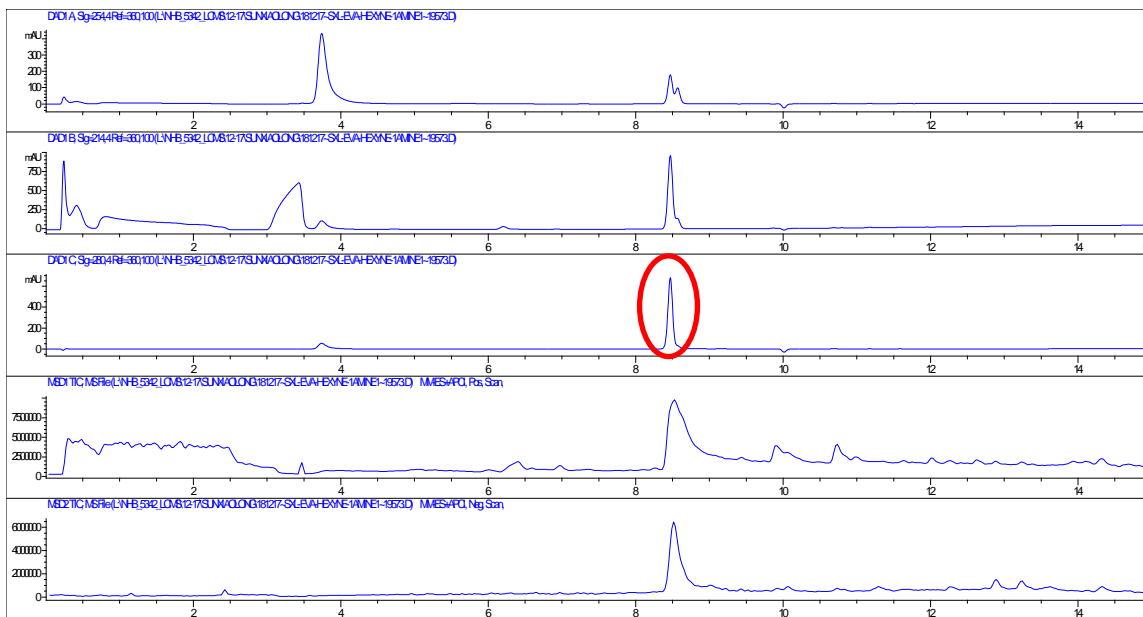
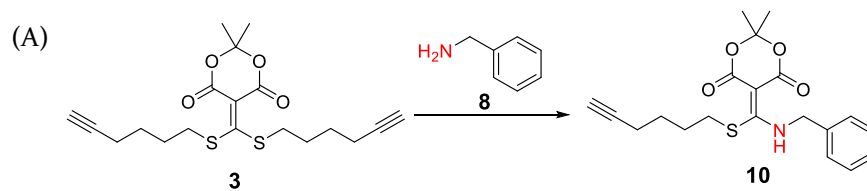
Figure 2.4 UV-Vis absorbance time-kinetics between conjugate acceptor **3** (100 μ M) and reagents (100 μ M). (A) Dithiothreitol (**DTT**); (B) β -Mercaptoethanol (**BME**); (C) Ethanedithiol (**EDT**); (D) Cysteine (**Cys**); (E) Cysteamine (**CYA**); (F) Time-kinetics curves for all the reagents. Spectra were obtained every 20 mins till 1000 mins in PBS buffer (20% acetonitrile as co-solvent).

Next, LC-MS was employed to monitor the reactions between **3** and small molecular amines, such as benzyl amine (**8**) and 1,3,5-triaminomethylbenzene (**9**), to confirm the expected mono-thiol displacements. After five minutes, LC-MS peaks corresponding to complete product formation (**10** and **11**, CA = conjugate acceptor derived from **3**) were identified for both amines (**Scheme 2.3**, **Figure 2.5**). Further, upon addition of a declicking trigger (DTT), the LC-MS peak corresponding to **10** and **11** vanished and a peak indicative of the tricyclic product **4** was observed (**Figure 2.6**),

confirming that **3** retained similar chemical properties to **1** in the context of click and declick reactions.



Scheme 2.3 The reactions between **3** and amine derivatives.



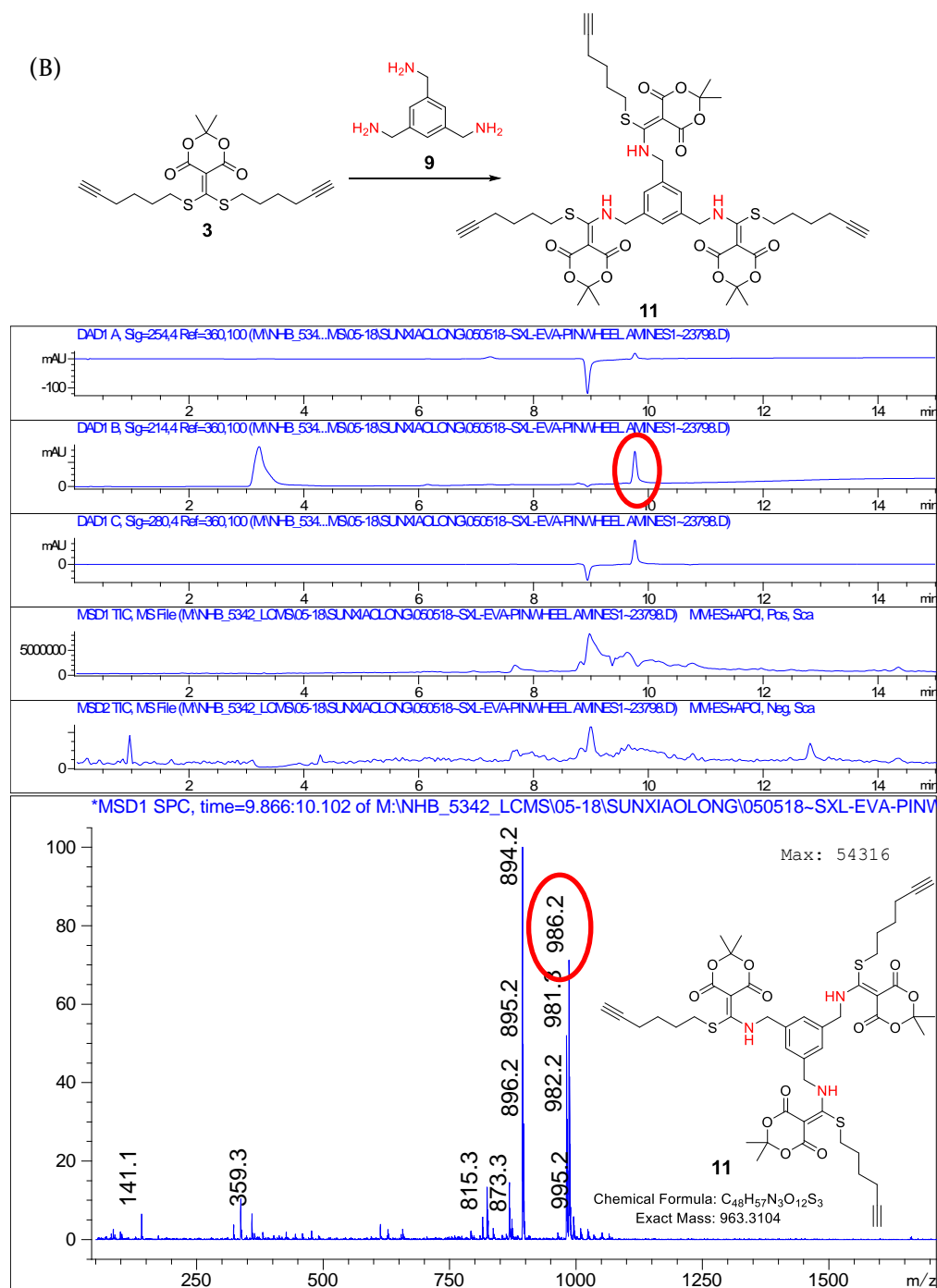


Figure 2.5 LC-MS data to track reaction between **3** and amine derivatives (benzyl amine and 1,3,5-triaminomethylbenzene). The reactions were run in chloroform with (A) **3** : **8** = 1 : 1 for 5 mins and (B) **3** : **9** = 3.3 : 1 for 5 mins. The solutions were then diluted with methanol for LC-MS.

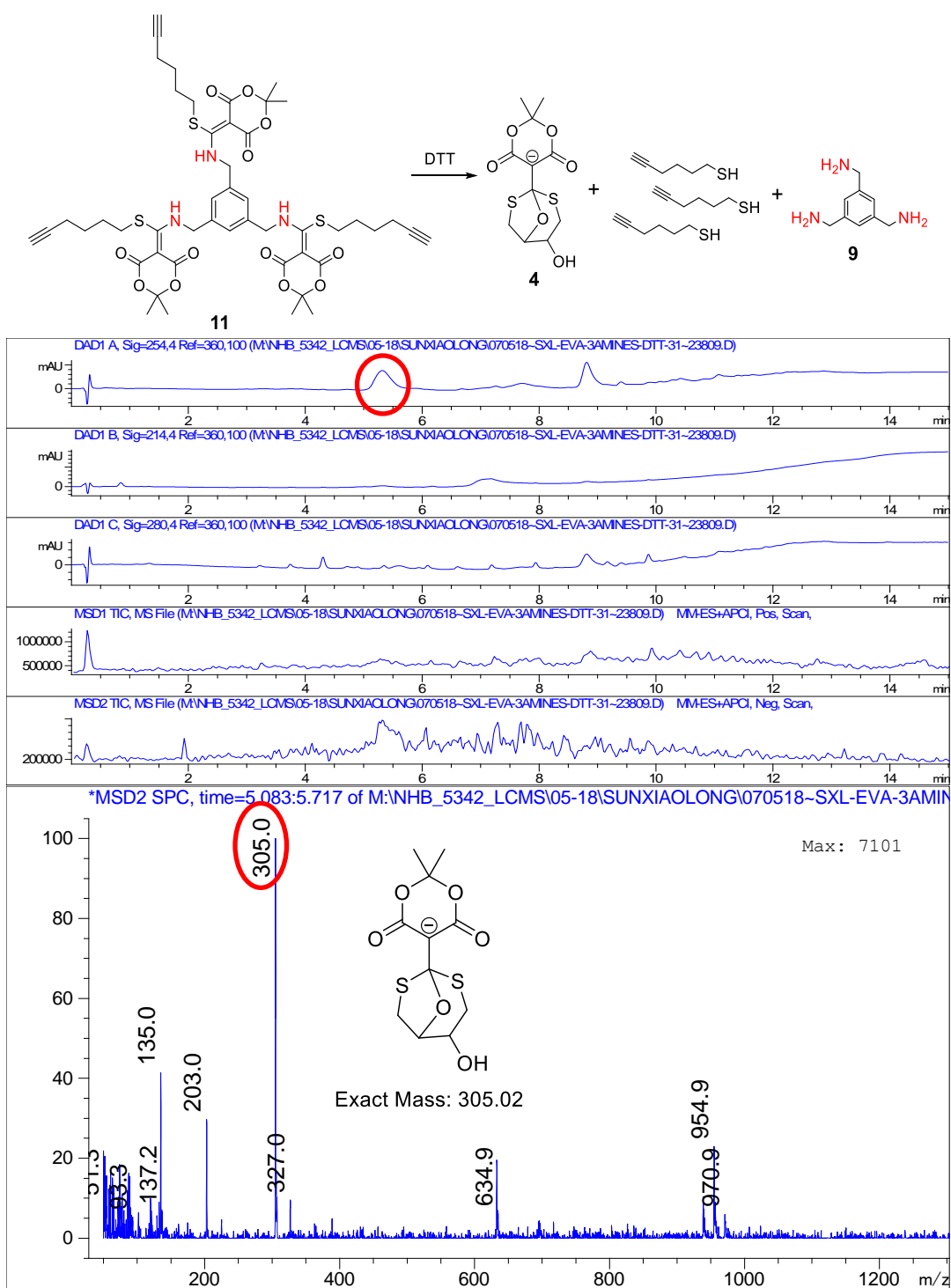
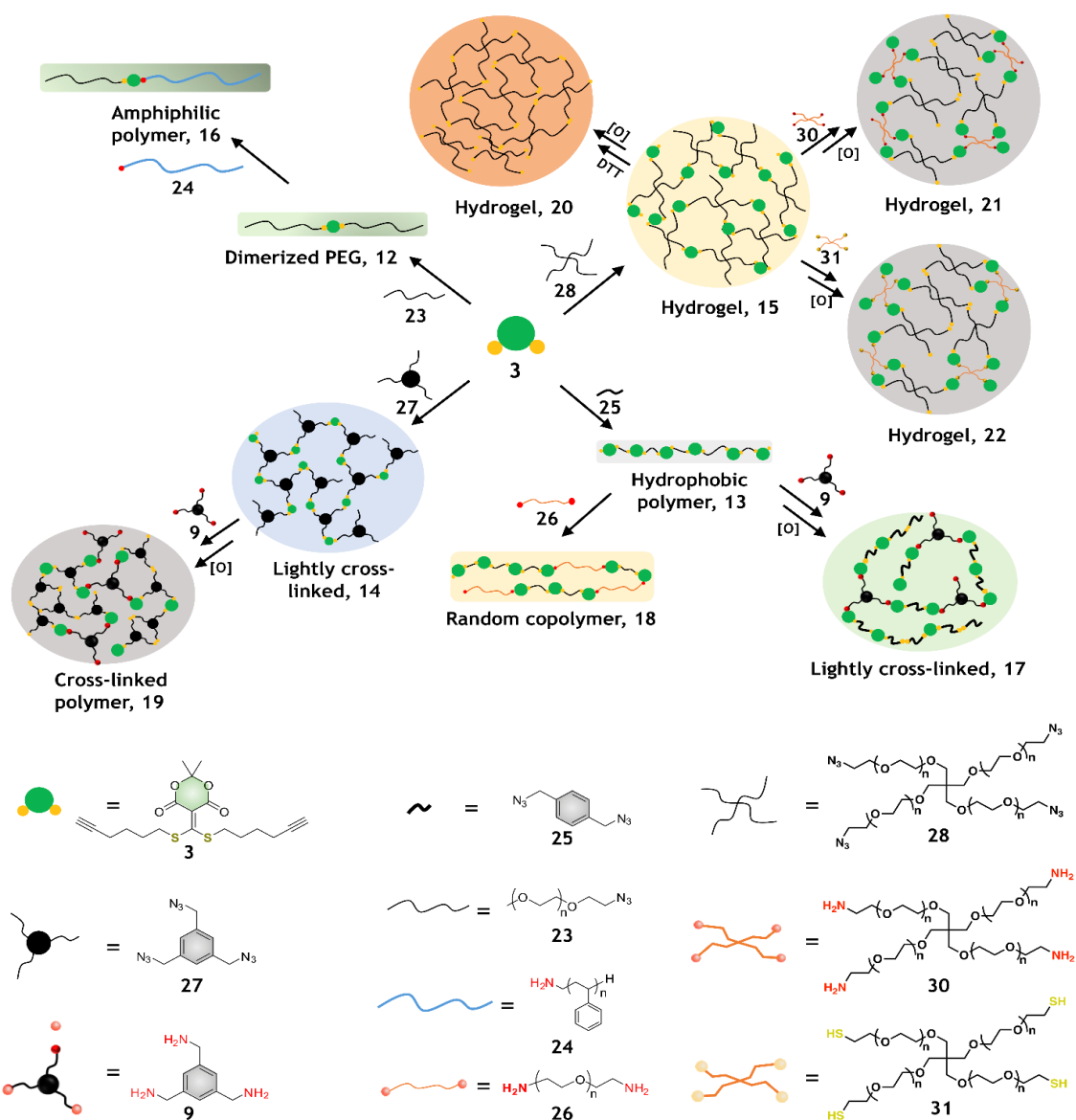


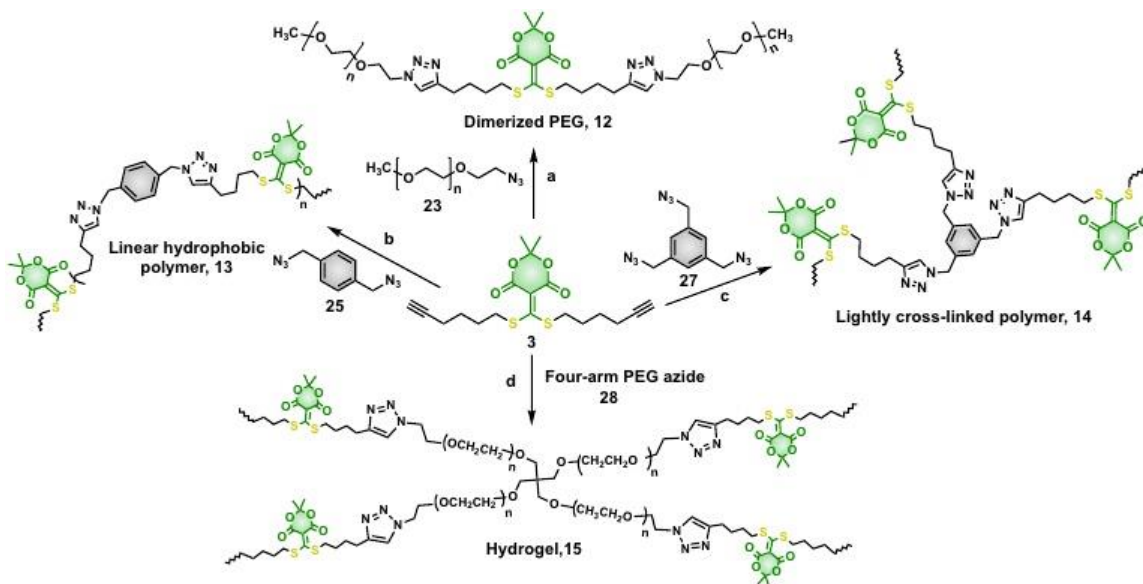
Figure 2.6 LC-MS data to track decoupling of compound **11** in the presence of DTT. The reactions were run in acetonitrile and HEPES buffer (1:1) for 24 hours. The solutions were then diluted with acetonitrile for LC-MS sampling.

2.2.2 Polymer design, analysis and transformation. An overview

To start, we created four polymer types by using standard CuAAC reactions: dimerized PEG **12**, linear hydrophobic **13**, hyper-branched **14**, and a cross-linked hydrogel **15** (**Schemes 2.4** and **2.5**). There were several reasons to choose these four architectures as our starting point. Linear polymers such as polyethylene, nylons, and polyesters possess high densities, high tensile strengths, and high melting points.³⁰ Lightly cross-linked polymers have been widely applied in many applications, such as light emitting materials, biomaterials, and composites.³¹ Hydrogels are commonly used scaffolds in tissue engineering, drug delivery, as well as sensing.³²⁻³³ Important for our triggered morphology changes, these four starting polymeric architectures contain repeating core conjugate-acceptors analogous to **1** and **3**. These acceptors could undergo reactions with amine-terminated polymers or branched monomers via the click reaction that releases a thiol. In turn, the released thiols can be used in oxidation/reduction reactions through disulfide exchange. Thus, starting with structures **12-15**, an amphiphilic linear **16**, a lightly cross-linked homopolymer **17**, a random copolymer **18**, a cross-linked polymer **19**, and hydrogels **20**, **21**, **22** were generated by amine scrambling and thiol disulfide formation (**Scheme 2.4**, and **Table 2.1**). Furthermore, all the polymeric architectures — before or after morphological changes — were degraded into small molecules or homopolymers induced by declick triggers, hence presaging potential applications such as plastic remediation, drug delivery, tissue engineering, or microelectronics.^{2, 5}

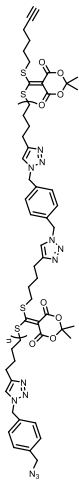
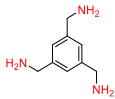
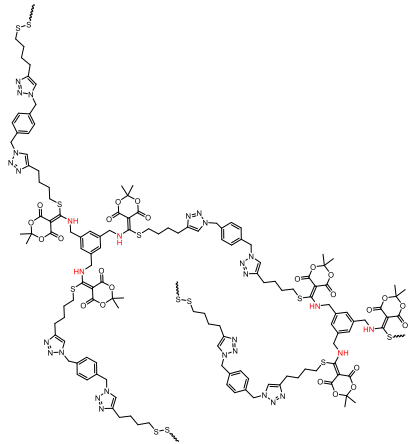
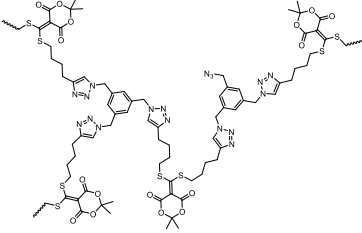
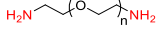
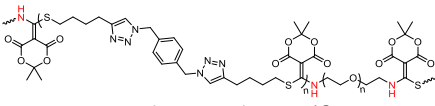
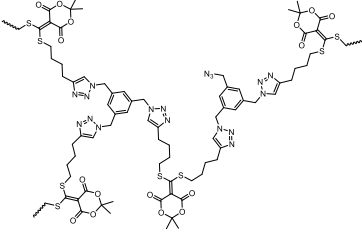
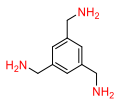
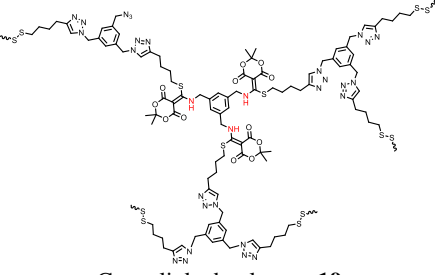
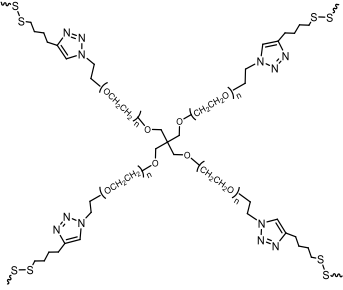


Scheme 2.4 Schematic representation of the polymer synthesis and topological changes achieved via click-declick chemistry and disulfide-thiol scrambling. Dimerized PEG (**12**) and hydrophobic linear polymer (**13**), lightly cross-linked polymer (**14**), and hydrogel (**15**) were synthesized via CuAAC. New amphiphilic linear polymer (**16**), lightly cross-linked (**17**), random copolymer (**18**), cross-linked polymer (**19**) and hydrogels (**20**, **21**, **22**) were created via amine scrambling using the conjugate acceptor core of **3**, and/or thiol-disulfide reactions. Note: Given the potential hazards of poly(azide) compounds, the reactions were carried out in the fume hood, treated carefully, stored and used in safe places.²⁹



Scheme 2.5 Synthesis of the initial set of subunits. Reagents and conditions: a. $\text{CuSO}_4 \cdot 5\text{H}_2\text{O}$, sodium ascorbate, tert-butanol: H_2O = 1:1 (vol), 20 °C; b. CuI , tris(benzyltriazolylmethyl)-amine (TBTA), sodium ascorbate, THF: DMF : H_2O = 2:2:1 (vol), 20 °C; c. CuI , TBTA, sodium ascorbate, THF: DMF : H_2O = 1:1:1 (vol), 20 °C; d. $\text{CuSO}_4 \cdot 5\text{H}_2\text{O}$, sodium ascorbate, tert-butanol: H_2O = 1:1 (vol), 20 °C.

Original structures	Amine derivatives	Transformed structures
<p>Linear hydrophilic polymer, 12</p>	<p>Amine-terminated polystyrene, 24</p>	<p>Amphiphilic block copolymer, 16</p>

 <p>Linear hydrophobic polymer, 13</p>	 <p>1,3,5-Triaminomethylbenzene, 9</p>	 <p>Hyperbranched polymer, 17</p>
 <p>Hyperbranched polymer, 14</p>	 <p>Polyethylene glycol diamine, 26</p>	 <p>Random copolymer, 18</p>
 <p>Hyperbranched polymer, 14</p>	 <p>1,3,5-Triaminomethylbenzene, 9</p>	 <p>Cross-linked polymer, 19</p>
	<p>DTT/[O]</p>	 <p>20</p>

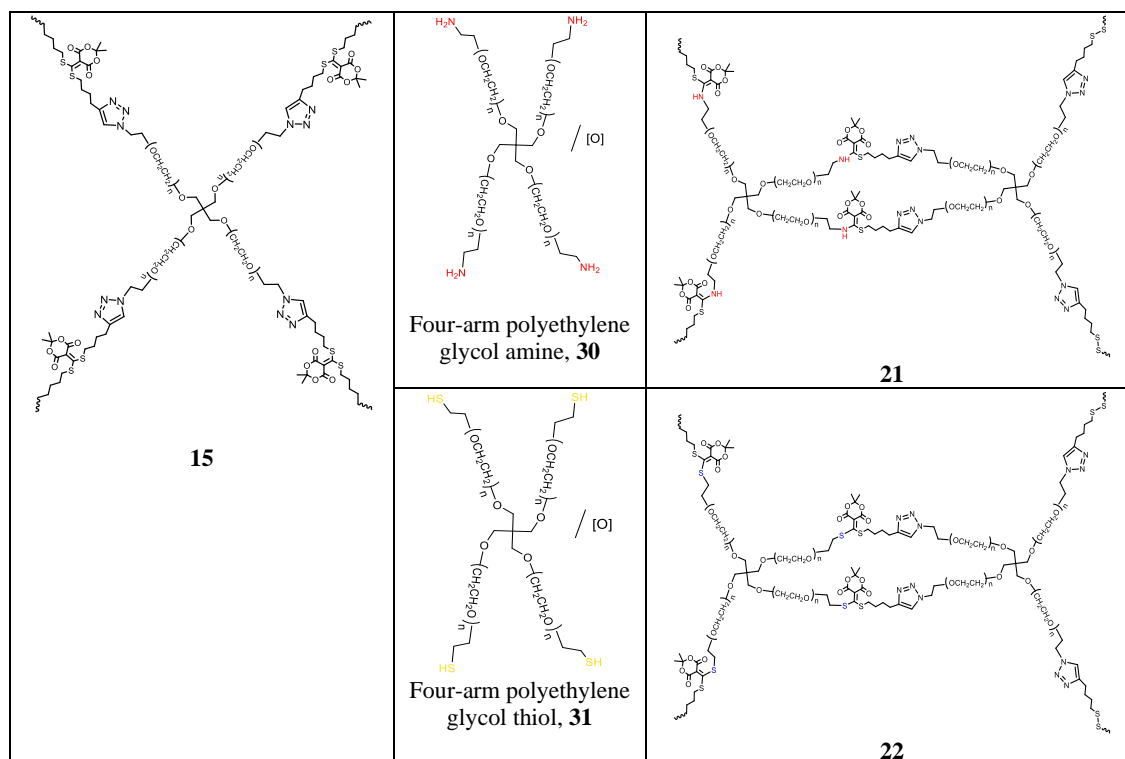


Table 2.1 Original polymers and transformed polymers via various amine derivatives.

2.2.3 Dimerized PEG transformation to aggregated structures

The dimerized PEG **12** was formed by CuAAC of poly(ethylene glycol) methyl ether azide (**23**, M_n ca. 1,000 g mol⁻¹) and **3** in a *tert*-butanol/water mixture (**Scheme 5**). Proton NMR spectroscopy (**Figure 2.7**) displayed the formation of triazole moieties and LC-MS spectrum (**Figure 2.8**) showed the product with mass/charge ratio (m/z) = 2565.40 for [**12**+H]⁺, and 1327.24 for [**12**+2H]²⁺. Next, gel permeation chromatography (GPC) displayed a shift to a lower elution time for **12** compared to **23** (**Figure 2.9E**), indicating the successful click of **23** with **3**.

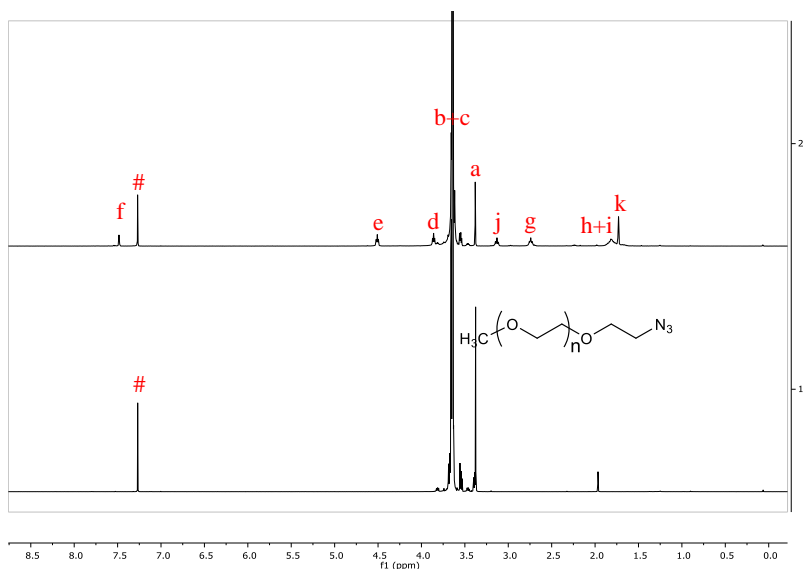


Figure 2.7 ^1H NMR for linear polymer.

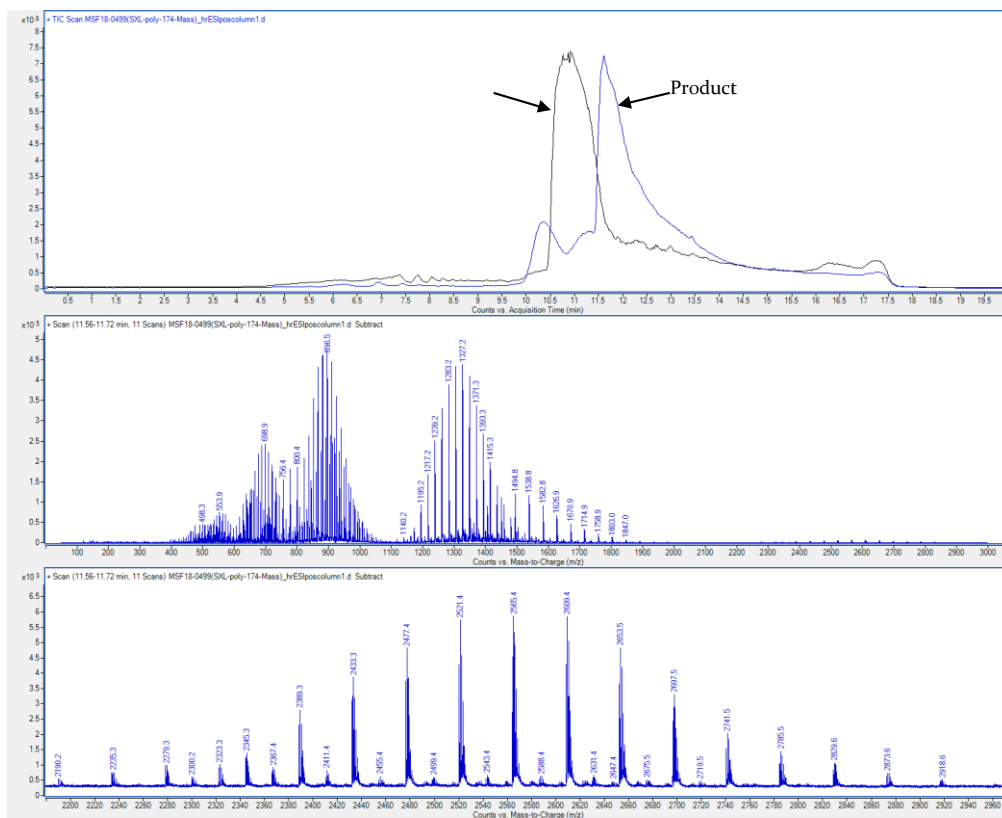


Figure 2.8 ESI LC/MS retention time for starting material (poly(ethylene glycol) methyl ether azide) and polymeric product **12** with retention time at 11 mins and 12 mins, respectively.

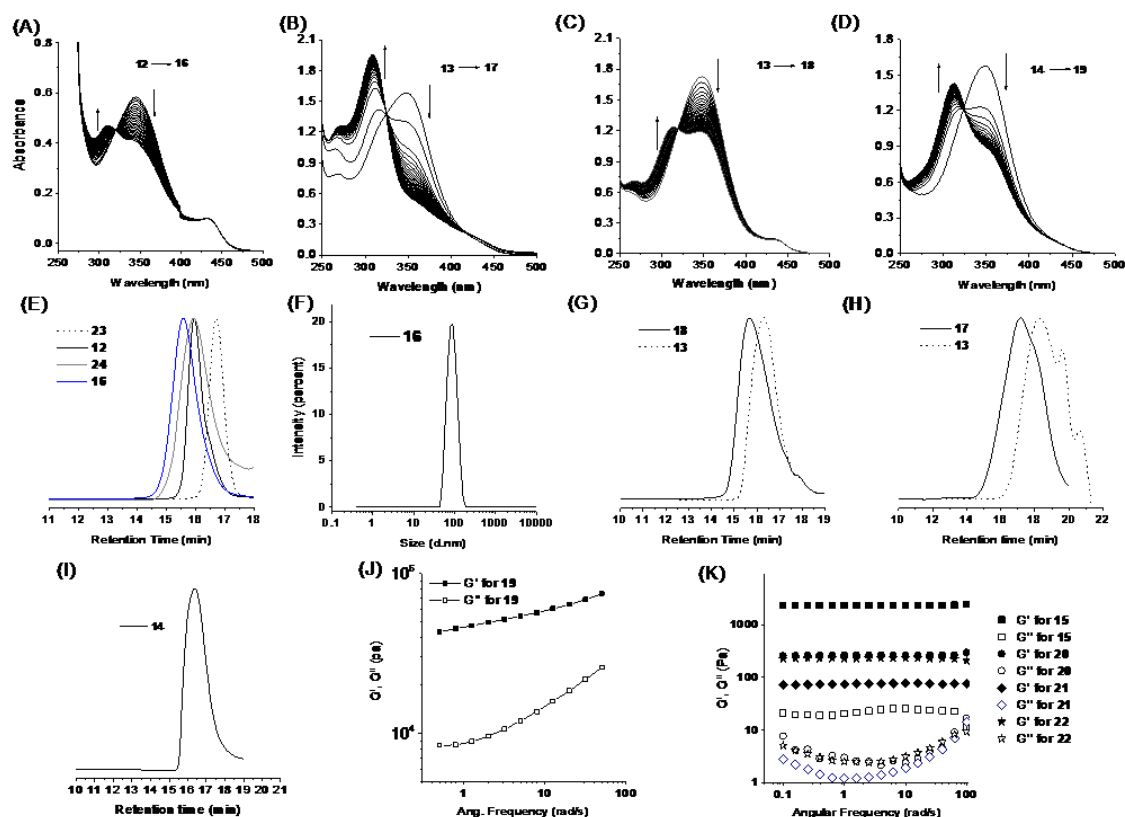


Figure 2.9 UV-Vis absorbance time kinetics, GPC, and rheometry for the polymer remodeling. (A) **12** (0.25 mg/mL) to **16** using amine terminated polystyrene **24** (1.0 mg/mL); (B) **13** (0.4 mg/mL) to **17** using 1,3,5-triaminomethylbenzene **9** (20 μ M); (C) **13** (0.2 mg/mL) to **18** using PEG diamine **26** (0.2 mg/mL); (D) **14** (0.14 mg/mL) to **19** using **9** (41 μ M) before adding hydrogen peroxide. The time kinetics were run in chloroform every 20 mins for (A); every 10 mins for (B) and (D); every 30 mins for (C); (E) GPC for **12**, **16**, **23** and **24** in chloroform; (F) DLS for **16** in water; (G) GPC for **13** and **18** in chloroform; (H) GPC for **13** and **17** in DMF (containing 0.01 M LiBr); (I) GPC for lightly cross-linked polymer **14** in chloroform; (J) Storage modulus G' and loss modulus G'' for cross-linked polymer **19**; (K) Storage modulus G' and loss modulus G'' for swelled hydrogel **15**, **20**, **21** and **22** in HEPES buffer.

To transform **12** to an amphiphilic polymer, amine-terminated polystyrene **24** (M_n ca. 5,000 g mol⁻¹) was utilized to scramble one thiol of **12** to generate **16** (Scheme 2.4 and Figure 2.10). To monitor the transformation, UV-Vis absorbance was used, which revealed a blue-shifted ratiometric signal corresponding to product formation. Specifically, the shift in absorbance of the bis-vinylous thiol ester, as found in structure **1** (as in **6**) (λ_{\max} = 330 - 350 nm), relative to an amine/thiol version of the conjugate acceptor, as found in structure **2** (as in **7**) (λ_{\max} = 310 nm), indicated the formation of polymeric product **16** (Figure 2.9A and 2.11). In GPC analysis, **16** displayed a lower retention time and higher molecular weight (M_n = 5,800 g mol⁻¹) with $D = 1.3$ (Figure 2.9E). Subsequently, **16** was investigated using DLS to evaluate the size and amphiphilic properties (Figure 2.9F, 2.12 and 2.13). The correlation in size determined by DLS in aqueous solution (ca. 90 nm) suggests that **16** existed in assemblies.³⁴⁻³⁶ Thus, a hydrophilic freely aqueous soluble compound was triggered to generate aggregation in-situ by an exchange of a single block unit.

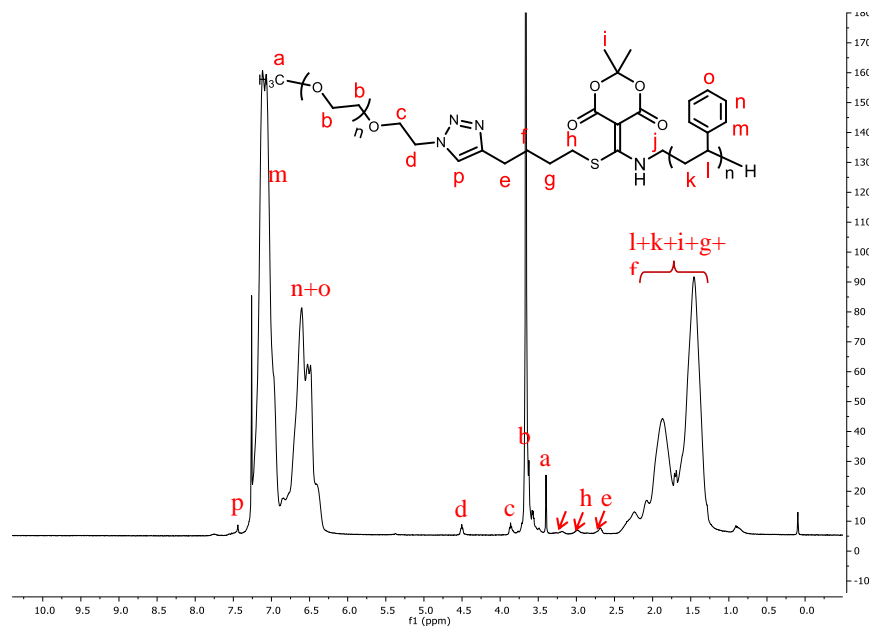


Figure 2.10 ¹H NMR for amphiphilic polymer **16** in CDCl₃.

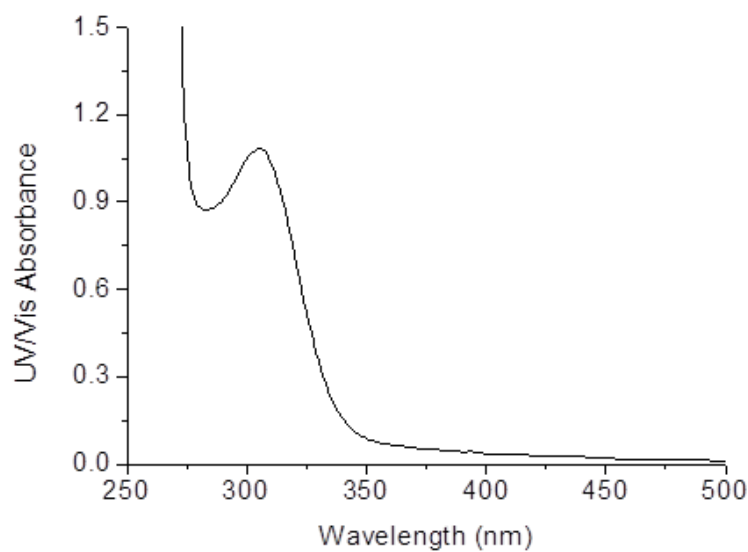


Figure 2.11 UV-Vis absorbance of linear polymer **16** in chloroform.

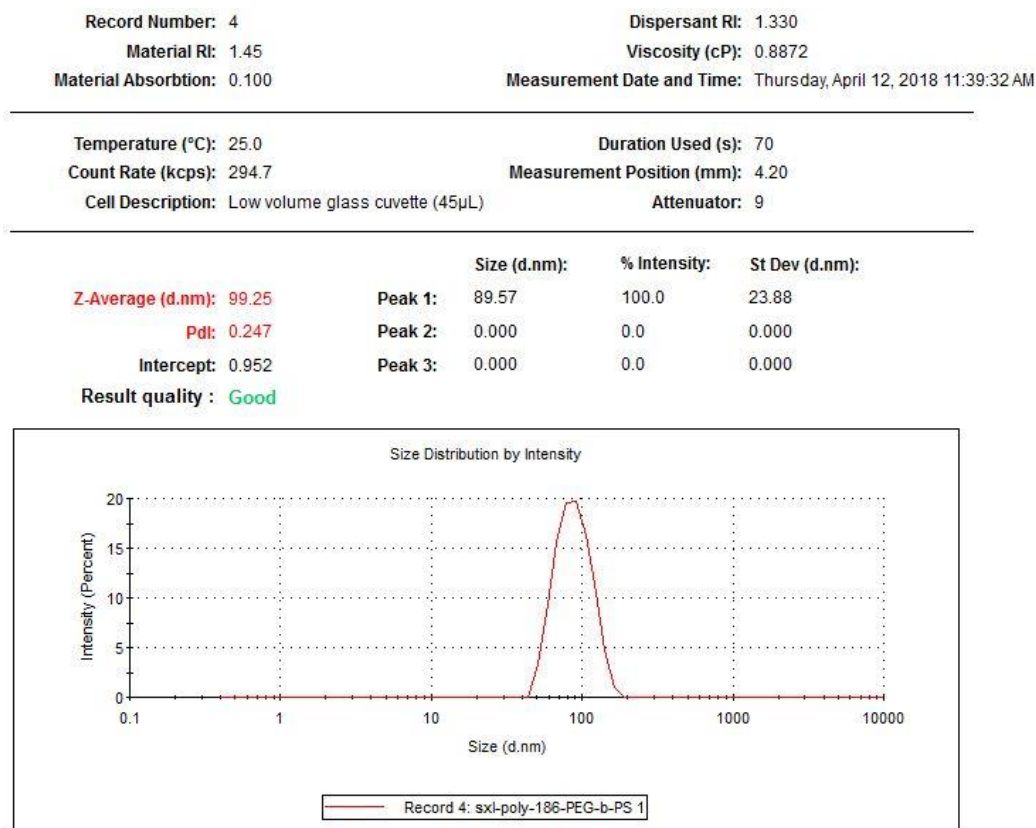


Figure 2.12 Size distribution by intensity of amphiphilic polymer **16** in water.

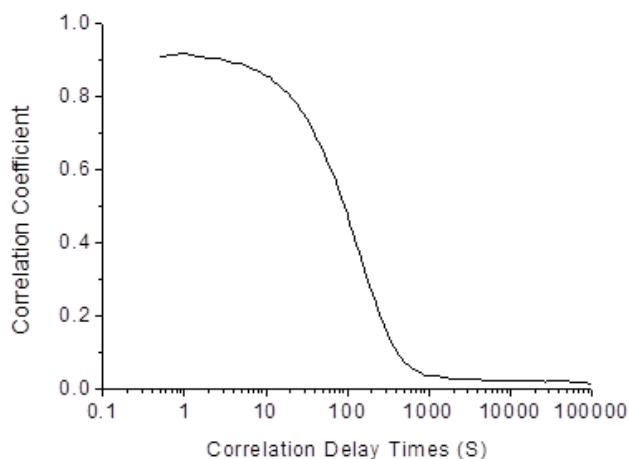


Figure 2.13 Relationship between correlation coefficient and correlation delay time for the amphiphilic polymer **16** in water.

2.2.4 Hydrophobic polymer transformations to lightly cross-linked and amphiphilic co-polymers

The linear hydrophobic polymer **13** was obtained through step-growth CuAAC polymerization between **3** and 1,4-di(azidomethyl)benzene **25**, which afforded a yellow solid ($M_n = 5,300 \text{ g mol}^{-1}$, $D = 1.35$) after precipitation and purification. (**Scheme 2.5** and **Figure 2.14**). Simple addition of 1,3,5-triaminomethylbenzene **9** to **13** resulted in a distinctive change in the polymer backbone as well as cross-linking. UV-Vis time-kinetics displayed a blue-shift due to amine scrambling (*i.e.* analogous of **1** to **2**), giving a clean isosbestic point at $\lambda = 325 \text{ nm}$ (**Figure 2.9B**). $^1\text{H NMR}$ spectroscopy titrations of **13** with **9** demonstrated amine-induced scrambling and complete thiol release (**Figure 2.15**). This topological change releases dangling thiols in the polymer, and we took advantage of this to further cross-link the material. Thus, oxidation of the dangling thiols to disulfides was performed by addition of H_2O_2 , generating lightly cross-linked polymer **17** ($M_n = 21.0 \text{ kg mol}^{-1}$, $D = 1.18$, **Figure 2.9H**, **Table 2.2** and **Figure 2.16**). In **Figure 9H**, the prominent shoulders are likely due to smaller molecular weight polymers/oligomers

with different extents of cross-linking. The approximate molecular weight of these shoulders is 200 g/mol and below. To further determine the role of H₂O₂, we checked if sulfoxides were formed by oxidation of the thioethers of the Meldrum's acid derivatives. LC-MS was used to monitor the reaction between **1** and H₂O₂. This was conducted using the same conditions used in creating polymer **17**, and there was no chemical reaction (**Figure 2.17**). Also, an additional experiment was carried out with an excess of H₂O₂, and again no reaction was found. All the above data shows that polymer **17** was constructed by two covalent attachments, one through the thiol/amine conjugate such as **2**, and the other through disulfide bonds. Thus, we triggered both backbone and cross-linking interchanges from a hydrophobic polymer to a lightly cross-linked network.

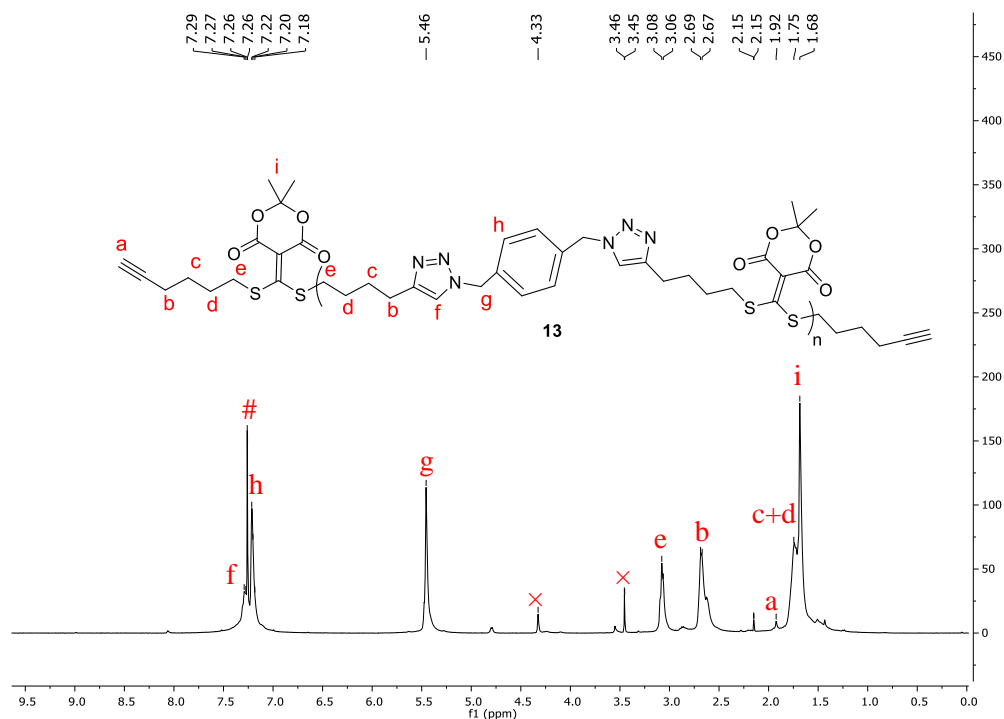


Figure 2.14 ¹H NMR for linear polymer **13** in CDCl₃.

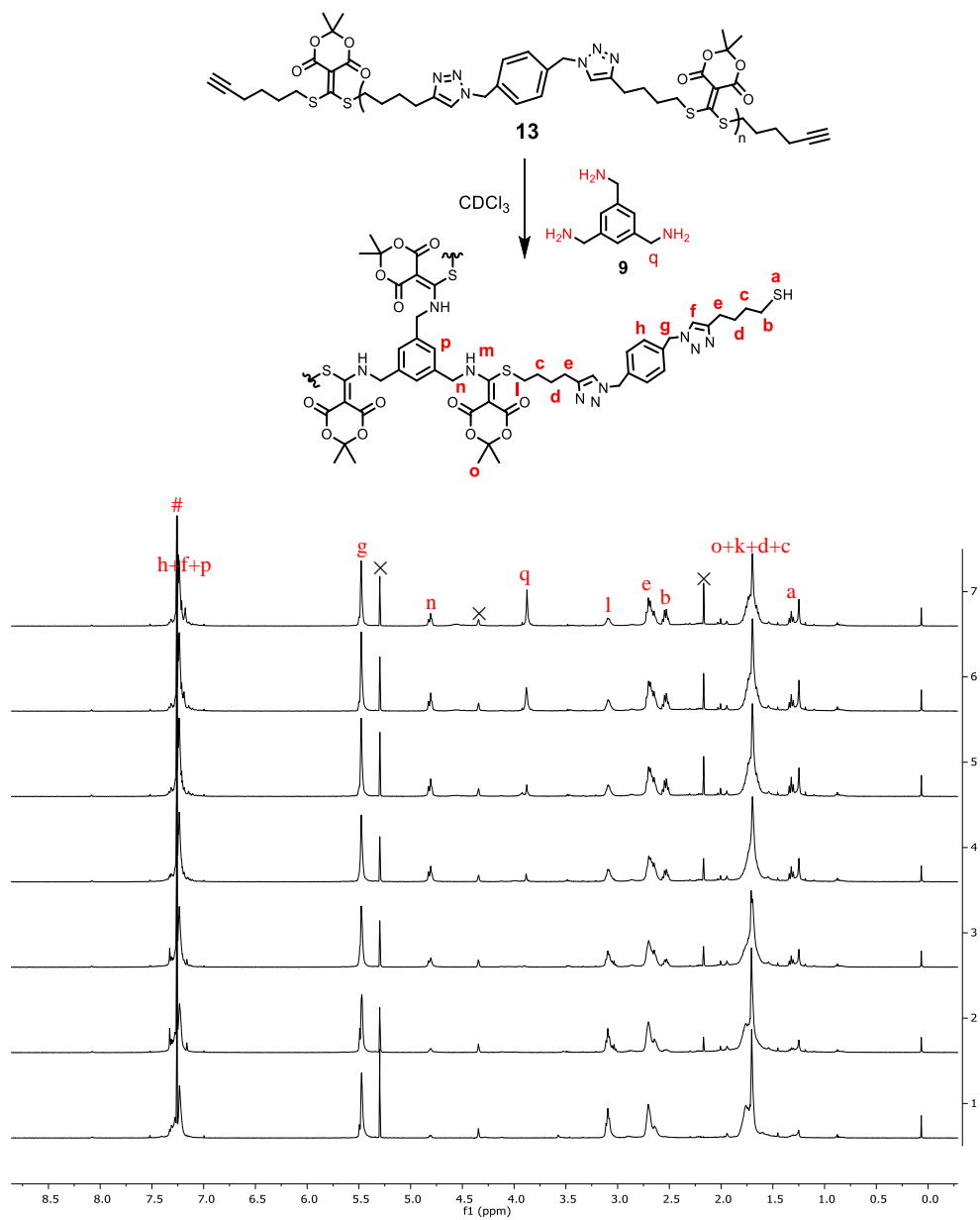


Figure 2.15 ^1H NMR spectrum titration for **13** (14 mg/mL) with **9** in CDCl_3 .

Polymer	M_n (Daltons)	M_w (Daltons)	\bar{D} (PDI)
12	2300	3300	1.43 (chloroform)
13	5300	7200	1.36 (chloroform)
	2800	5100	1.82 (DMF)
14	14900	17200	1.15 (chloroform)
16	5800	7500	1.29 (chloroform)
17	21000	24900	1.19(DMF)
18	38900	54400	1.40 (chloroform)

Table 2.2 GPC data for the topological polymers.

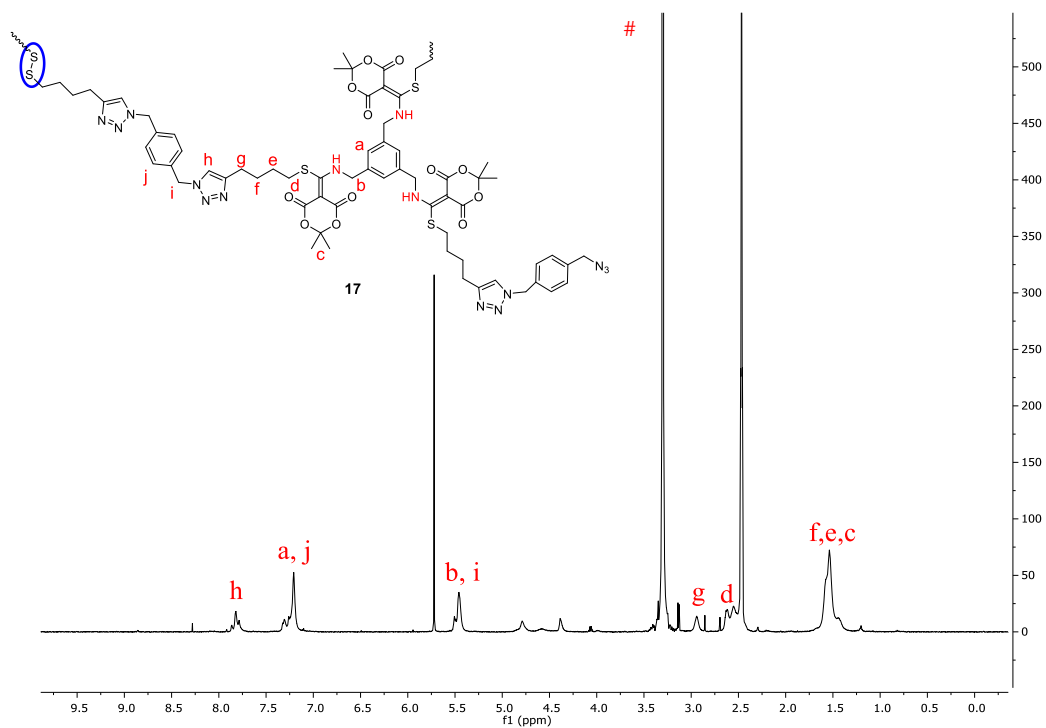
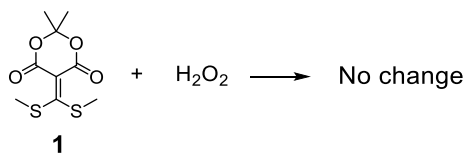
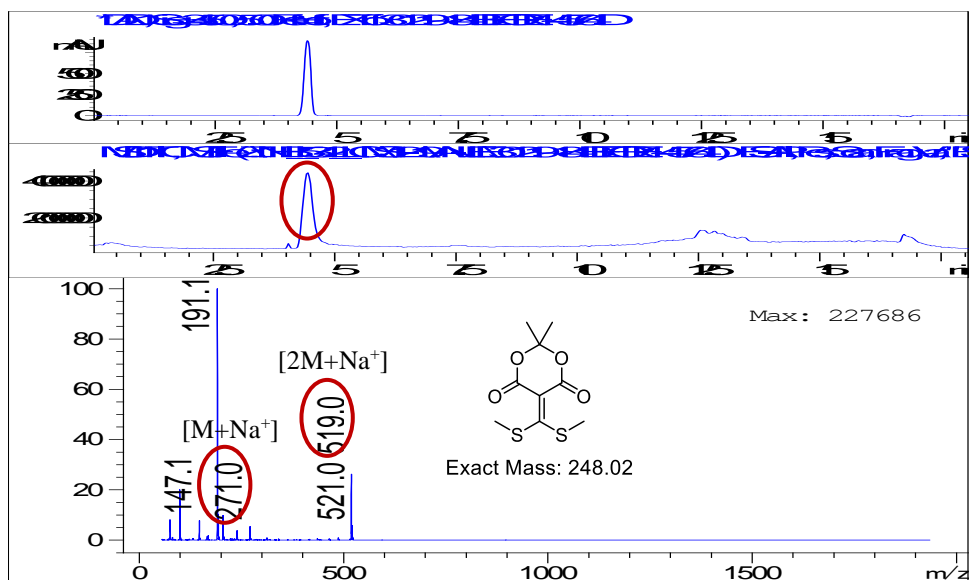


Figure 2.16 ^1H NMR spectrum for **17** in DMSO.



1) Before adding H₂O₂ to **1**



2) After adding H₂O₂ to **1**

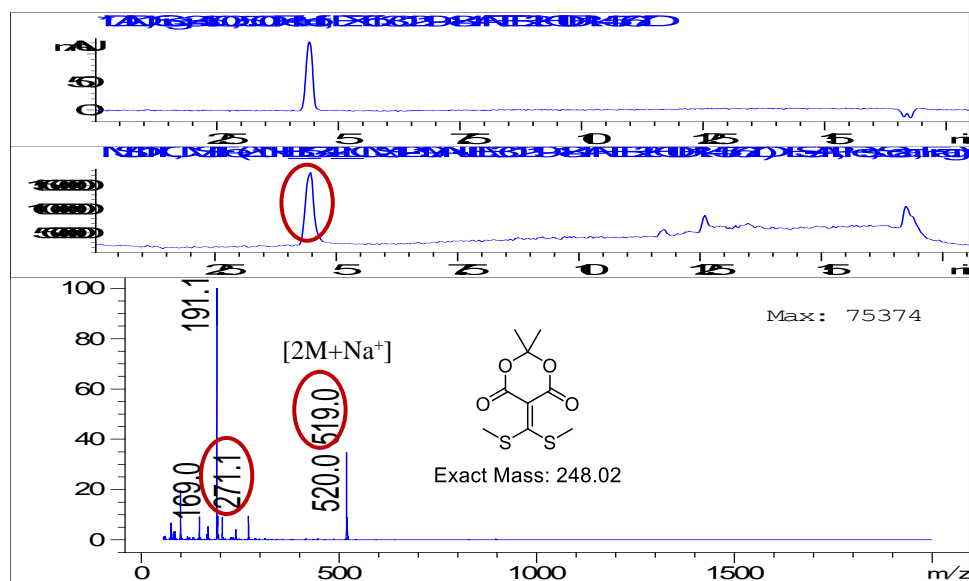


Figure 2.17 LC-MS data for **1** before and after adding H₂O₂. To a solution of **1** (10mg, 0.04 mmol) in THF/DMF (50/50 = v/v), hydrogen peroxide (10 μ L, 30% aqueous solution) was added. After 2 hours, it was monitored.

In the next transformation, poly(ethylene glycol) diamine **26** ($M_n = 6,000 \text{ g mol}^{-1}$) was used to functionalize **13**, again via thiol displacement. Following the reaction between **13** and **26** in 1:1 ratio, product **18** was precipitated from cold methanol. UV-Vis spectroscopy again demonstrated a decrease in the absorbance of 350 nm and increase at 310 nm (**Figure 9C**) while GPC displayed a lower retention time and higher molecular weight ($M_n = 38.9 \text{ kg mol}^{-1}$, $D = 1.39$, **Table 2.2**) for **18**, indicating the formation of longer random copolymers (**Figure 9G**). Additionally, analysis of the ^1H NMR spectrum (**Figure 2.18**) revealed the presence of peaks corresponding to PEG backbone protons. These data demonstrate successful chemically-triggered remodeling of the linear polymers through amine/thiol scrambling.

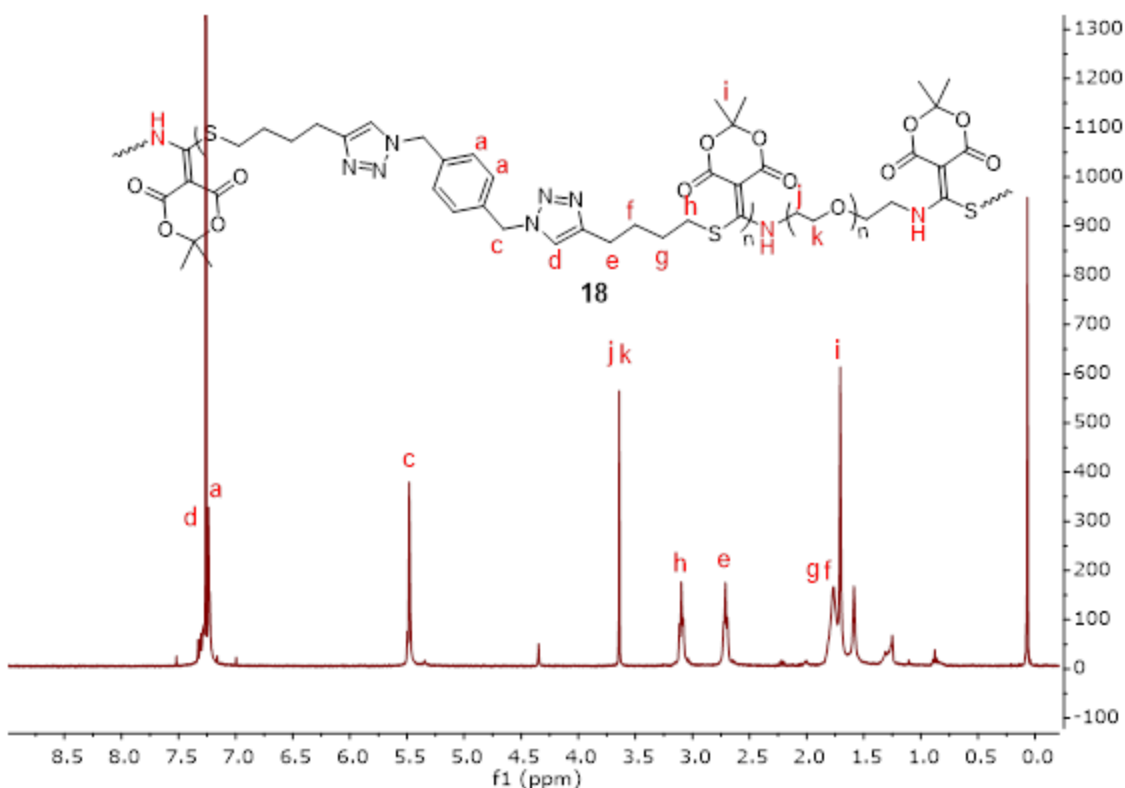


Figure 2.18 Proton NMR spectrum for **18** in CDCl_3 .

2.2.5 Lightly cross-linked polymer transformations to cross-linked polymer

Lightly cross-linked polymer **14** was synthesized through the copper-catalyzed click reaction between **3** and 1,3,5-tris(azidomethyl)benzene **27** (**Scheme 2.5** and **Figure 2.19**). GPC with multiangle light scattering detection gave the molecular weight for **14** ($M_n = 14.9 \text{ kg mol}^{-1}$, $D = 1.16$, **Figure 2.9I**, **Table 2.2**). Using ^1H NMR analysis ala the method of Moore,³⁷ an approximate degree of branching of 65% was obtained. Similar to the reaction of **12** or **13**, UV-Vis kinetics of the reaction of **14** with the triamine **9** demonstrated a blue shift, and new ^1H NMR spectroscopy resonances appeared in a time-dependent manner (**Figure 2.9D** and **2.20**). The analyses confirmed the remolding of the architecture and the release of thiol moieties.³⁸ The product was directly oxidized with H_2O_2 resulting in a highly cross-linked polymer **19** in a DMF/THF mixture which exists as a gel (**Figure 2.21**). Rheometric tests found the storage modulus (G') to be an average of 5.5 kPa and the loss modulus (G'') to be 1.5 kPa on average, slightly increasing with the change of angular frequency in the range of 0.1 – 100 rad/s (**Figure 9J**). In summary, lightly cross-linked polymeric backbones were morphed, resulting in gels in situ by simple addition of a cross-linking unit.

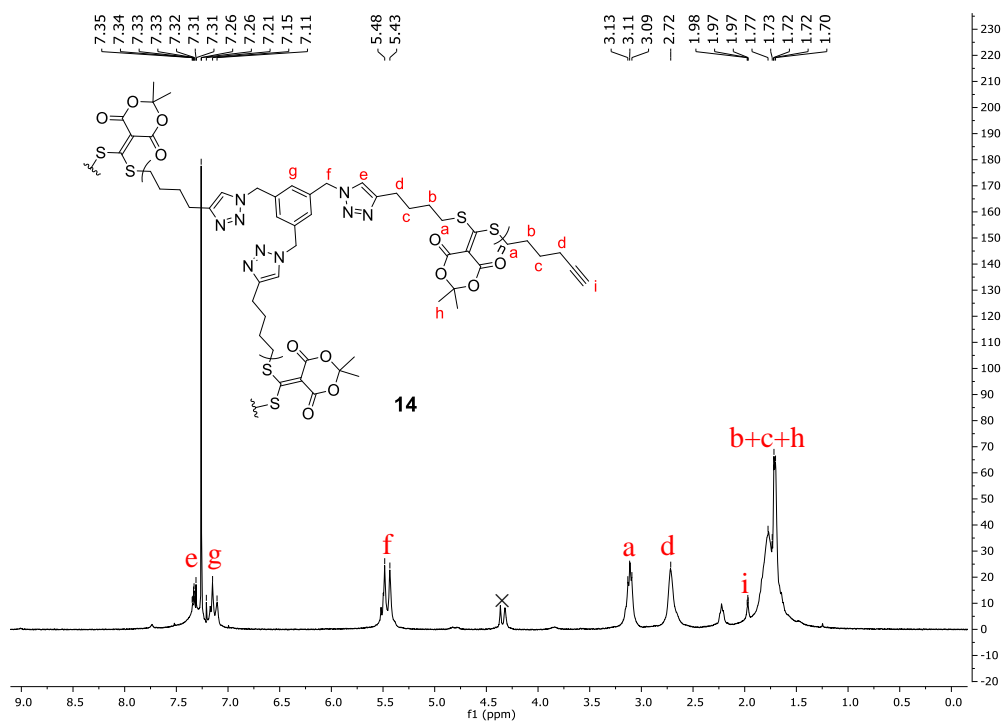


Figure 2.19 ^1H NMR for hyperbranched polymer **14** in CDCl_3 .

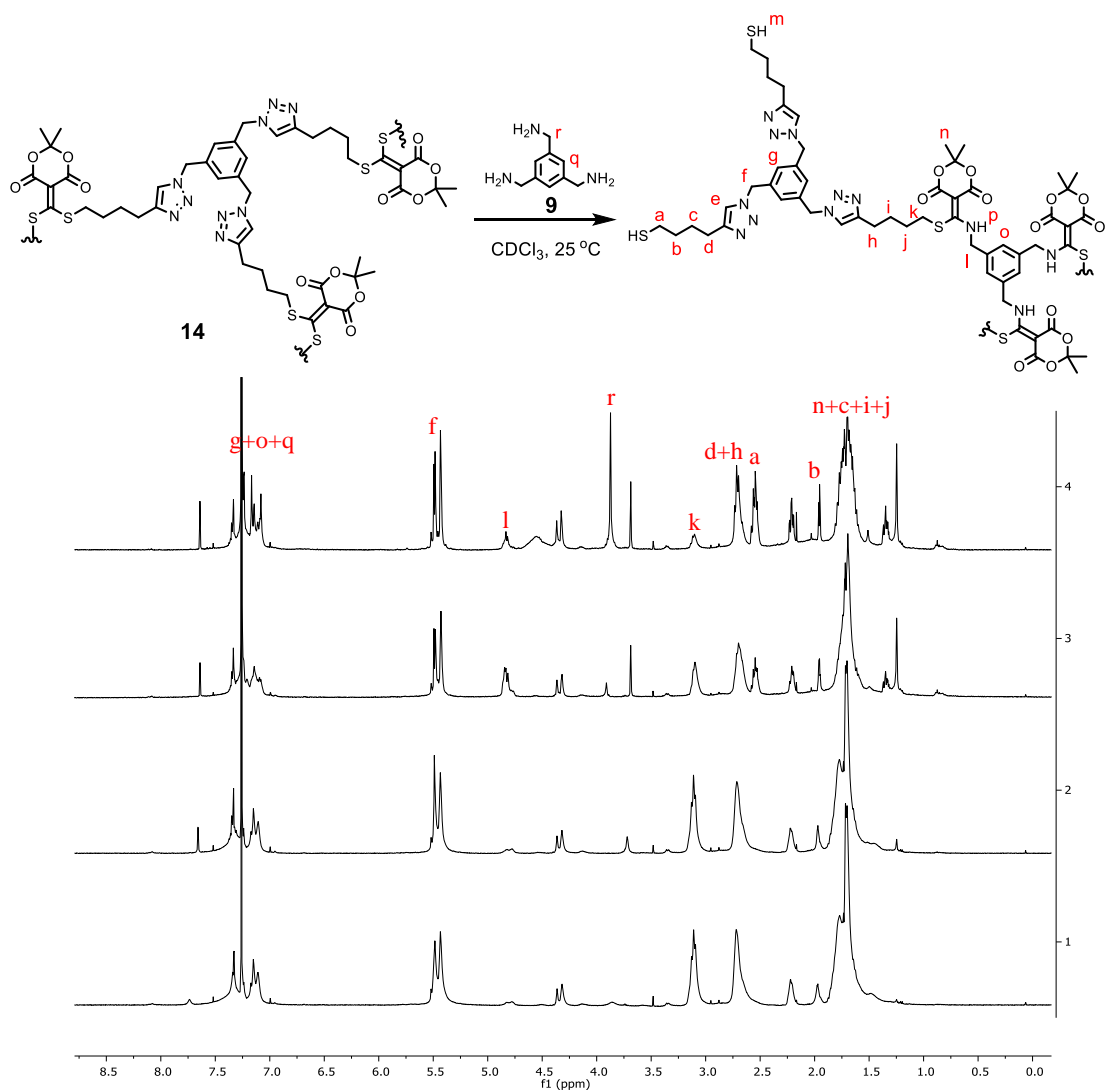


Figure 2.20 ^1H NMR spectrum titration for **14** with **9** in CDCl_3 .

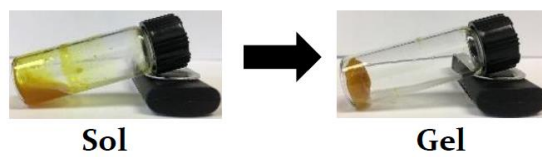


Figure 2.21 Macroscopic transformation of **14** to crosslinked gel network **19**.

2.2.6 Hydrogel transformations to mono- and double networking hydrogels

In addition to polymers, the strategies discussed here were applied to matrix hydrogels. Initially, hydrogel **15** was synthesized via click reaction between **3** and four-arm poly(ethylene glycol) azide **28** ($M_n \sim 10.0 \text{ kg mol}^{-1}$) in a water/*tert*-butanol mixture (**Scheme 2.5**). The volume of the hydrogel was expanded after swelling in water due to the hydrophilic network, resulting in a frequency-independent storage modulus of 2.2 kPa (**Figure 2.9K**).

Next, DTT was used to degrade the hydrogel by cleaving the linkage at conjugate acceptor core **3**, leading to the quantitative generation of four-arm PEG thiol **29** (**Figure 2.22E**) in pH 7.3 HEPES (4-(2-hydroxyethyl)-1-piperazine-ethanesulfonic acid) buffer. After removal of **4** and residual DTT by dialysis, the resulting system containing numerous free thiols was cross-linked through disulfide bonds by addition of H_2O_2 , generating a new networking matrix: hydrogel **20** (**Table 2.1** and **Figure 2.23**). Gel **20** demonstrated a softened elastic modulus of only 260 Pa corresponding to lower overall cross-link density (**Figure 2.9K**). Continuing with the theme, we employed four-arm poly(ethylene glycol) amine **30** (M_n ca. 2.0 kg mol^{-1}) to construct hydrogel **21**, using multiple amines separated by long PEG chains that expanded the matrix of the hydrogel through scrambling thiols on the conjugate acceptor. Visibly, hydrogel **15** became a viscous liquid after mixing with **30** for six hours (1:1 ratio to the conjugate acceptor), liberating the thiols along with a noticeable odor. Subsequent addition of H_2O_2 linked the free thiols as disulfides in a second crosslinking, leading to hydrogel **21** (**Figure 2.24**). Rheometric testing gave an even softer storage modulus (75 Pa) for the swelled hydrogel, which supported our proposed role of **30** to expand the hydrogel matrix. Next, four-arm PEG thiol **31** (M_n ca. 5.0 kg mol^{-1} , 1:1 ratio to the conjugate acceptor) was utilized to morph the matrix of hydrogel **15**, of which the thiols would exchange between a bis-

vinyllogous thiol esters in **15** and thiol-terminated derivative **31**. Subsequently, released free thiols enabled the second cross-linking through formation of disulfides, generating hydrogel **22** (**Figure 2.25**). With this different cross-linking, the storage modulus became to 230 Pa. Thus, numerous hydrogels of differing physical properties resulting from backbone alternations were readily created via simple mixing of reagents.

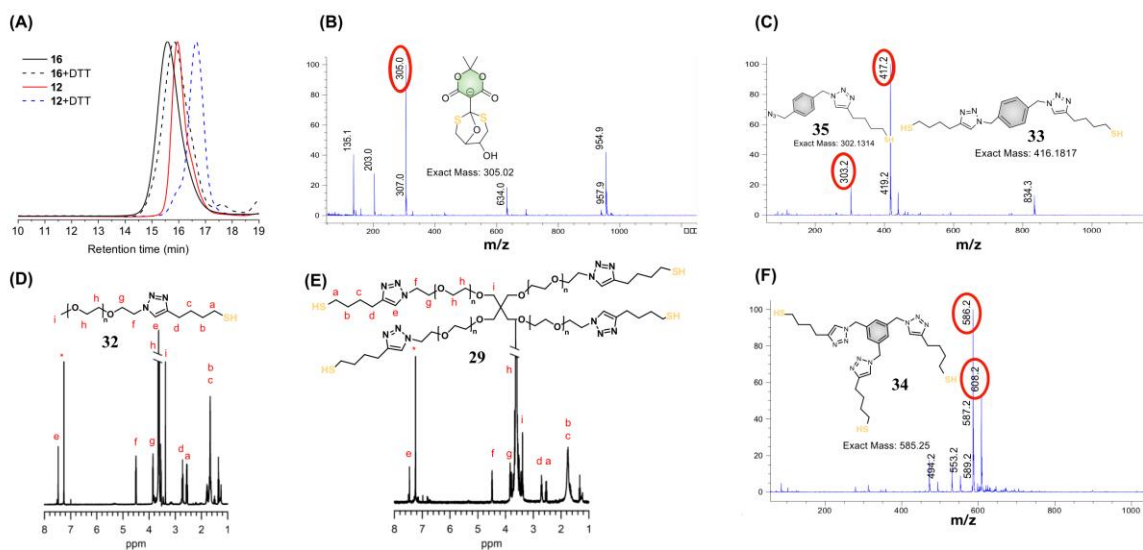


Figure 2.22 GPC, ^1H NMR spectroscopy, and LC-MS for the polymer degradation. (A) GPC of **12** and **16** before and after degradation; (B) Mass spectra for tricyclic product **4** observed in LC-MS; (C) Masses for **33** and **35** observed in LC-MS, resulted from decomposition of **13**, **17** and **18**; (D) ^1H NMR for the thiol-terminated PEG product **32** released from **12**; (E) ^1H NMR for the four-arm PEG thiol **29** degraded from hydrogel **15**; (F) Mass spectra for **34** released from **14** and **19** in LC-MS.

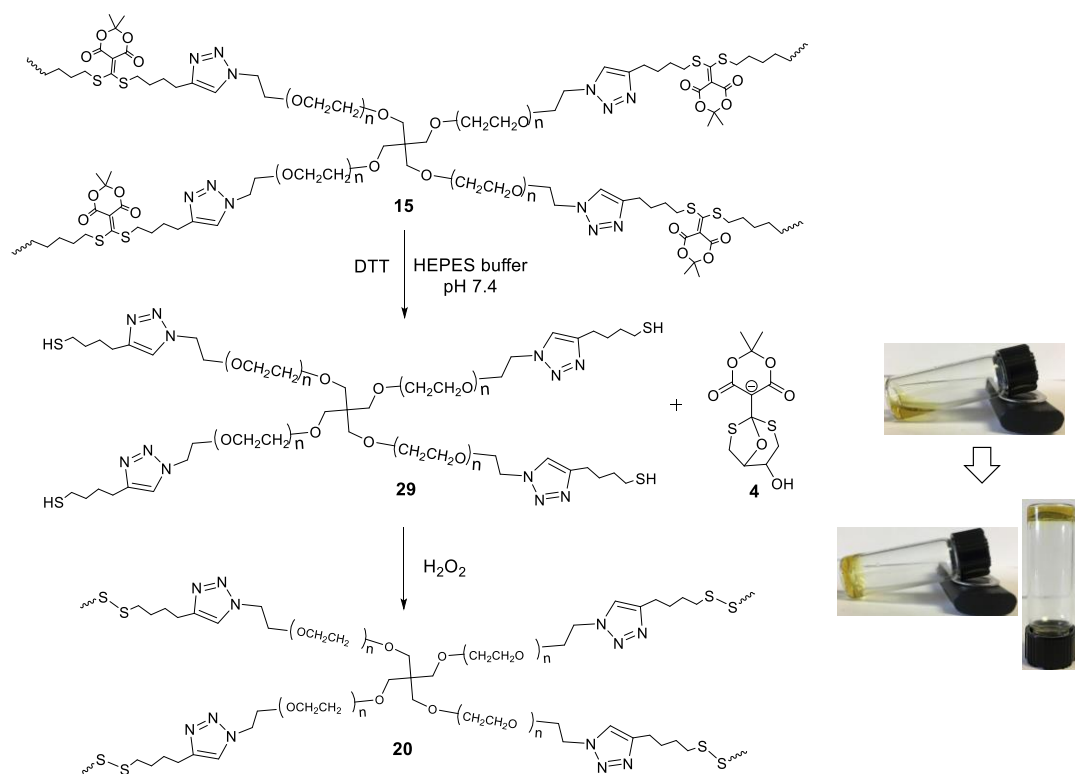


Figure 2.23 After swollen in HEPES buffer (pH 7.3), **15** was treated with excess DTT (> 10 eq. of conjugate acceptor) for three hours in HEPES buffer and the hydrogel became sol liquid with release of quantitative four-arm PEG thiol **29**. The resulting suspension was placed on dialysis tubing (1.0 kDa molecular weight cut-off) and suspended in deionized water for 24 hours to remove the small molecules. After dry under lyophilizer, solid four-arm PEG thiol was obtained. Next, after addition of hydrogen peroxide (20 mM) to the aqueous solution of four-arm PEG thiol (180 mg/mL), free thiols cross-linked together via disulfide bonds to offer hydrogel **20**.

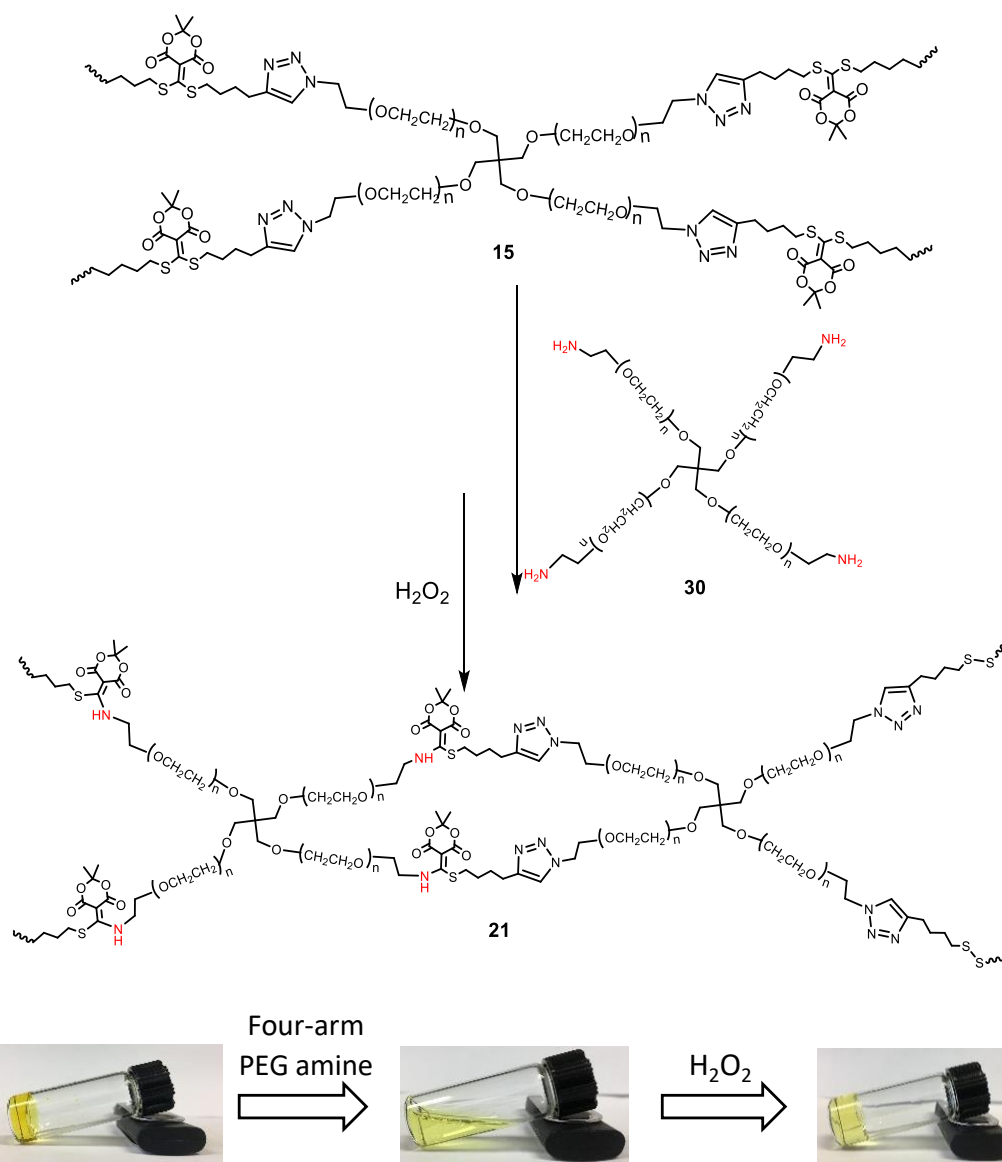


Figure 2.24 After swollen in HEPES buffer (pH 7.3), **15** was mixed with four-arm poly(ethylene glycol) amines **30** ($M_n = 2,000$, 1 : 1 ratio of amine : conjugate acceptor **1**) for six hours and the hydrogel became sol with release of quantitative terminal thiols. Next, addition of hydrogen peroxide (20 mM) cross-linked free thiols together via disulfide bonds to offer hydrogel **21**.

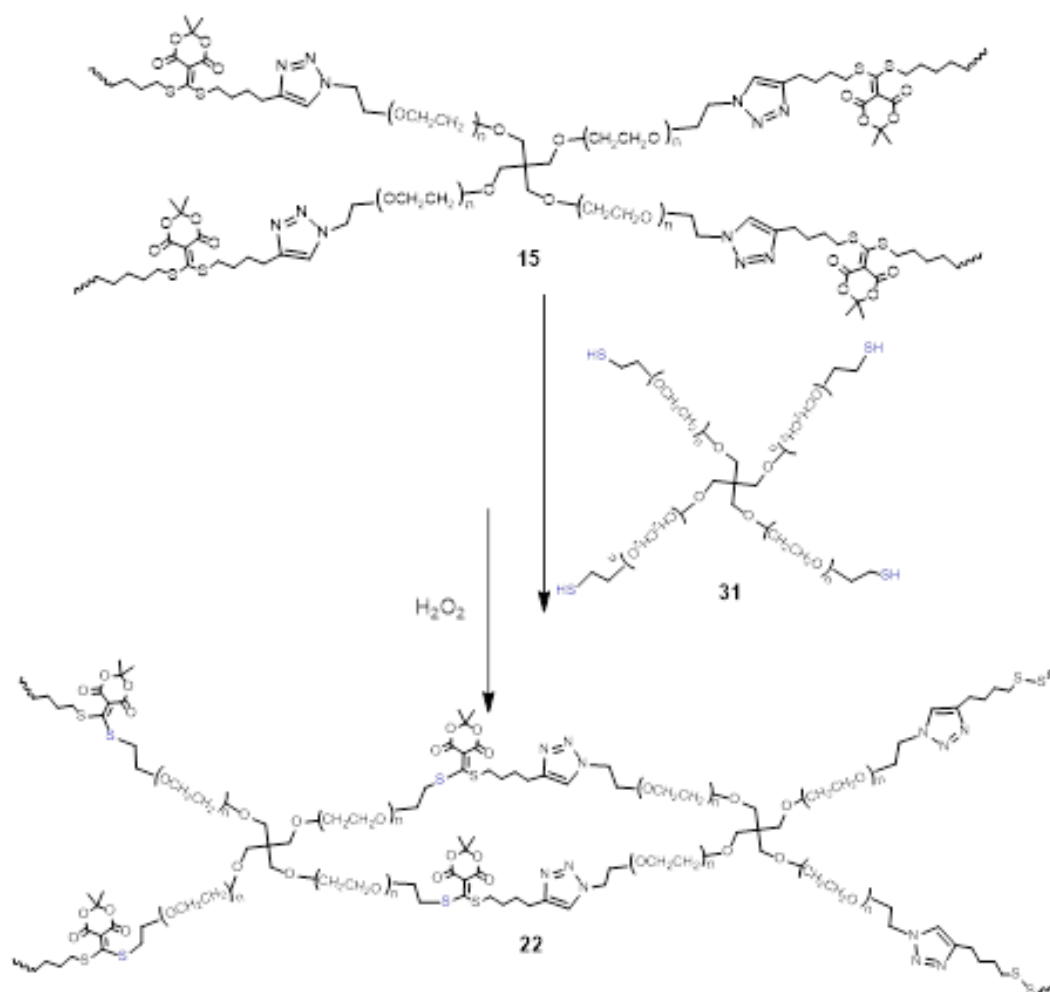


Figure 2.25 After swollen in HEPES buffer (pH 7.3), **15** was mixed with four-arm poly(ethylene glycol) thiol **31** ($M_n = 5,000$, 1 : 1 ratio of free thiol : conjugate acceptor) for six hours and the hydrogel firstly became sol state with release of quantitative terminal thiols. Next, addition of hydrogen peroxide cross-linked free thiols together via disulfide bonds to offer hydrogel **22**.

Significantly, all of the topological remodeling of the polymer and hydrogel backbones and cross-linkers were performed in neutral aqueous condition at ambient temperature by simply adding new monomers, cross-linkers, polymers or an oxidant. The

resulting spatiotemporal regulation of material properties is promising in the applications of drug delivery system, cells encapsulation, and cell migration.

2.2.7 Macromolecular degradation into small molecules

Remodeling and transforming polymeric architectures via chemically-triggered synthesis has been described above. Another critical property of a polymer is its ability to degrade, which facilitates controlled removal of plastic pollutants once the material has served its purpose. Further, such triggerable material degradation should hold wide applicability in biomedicine and drug-delivery. As we have stressed throughout, all of the bis-vinylous thiol esters analogous to **1**, bis-vinylous thiol amine structures containing linkages as in **2**, and disulfide bonds, could be decoupled by various chemical reagents. Further, with the co-existence of two or more crosslinking chemical bonds, we could control and tune the degradation through different declicking reactions.

First, **12** was treated with DTT in HEPES buffer (pH 7.3) for three hours and the solution was then placed in dialysis tubing (1.0 kDa molecular weight cut-off) and suspended in deionized water for 40 hours (changing the solvent every ten hours) to remove small molecules (**Figure 2.26**). The thiol-terminated product **32** was confirmed by ¹H NMR spectroscopy (**Figure 2.22D**) and GPC, where a longer retention time (**Figure 2.22A**) indicated success of the decoupling reactions. Next, **16** was declicked using DTT for 36 hours in HEPES buffer (50% acetonitrile as co-solvent, **Figure 2.27**). After dialysis, GPC data showed that the result had a lower molecular weight (**Figure 2.22A**). Next, polymers **13**, **14**, **17**, **18** and **19** were all processed in HEPES buffer in the presence of DTT (overnight for **13** and **14**; two days for **17** and **18**; five days for **19**). As expected, the polymers containing amine/thiol conjugate acceptors such as structure **2**, were more difficult to decompose than the polymers containing thiol ester conjugate

acceptors such as with **1**, due to the amine being less labile as a leaving group. Yet, all species did entirely degrade with DTT. A macroscopic surface-accessible degradation occurred, which can be seen by the naked-eye and analyzed by LC-MS. LC-MS data showed the tricyclic product **4** (**Figure 2.22B**) with a mass/charge ratio (m/z) = 305.0 for all polymers declicked by DTT, and bis-thiol terminated derivative **33** released from **13**, **17** and **18** (m/z = 417.2, **Figure 2.22C** and **Figure 2.28-2.30**); three-arm thiol derivative **34** released from **14** and **19** (m/z = 586.2, 608.2; Fig. 2F, Fig. S30–S31), respectively. We also observed the azide-containing side products **35** and **36**, **37** (**Figure 2.22C** and **Figure 2.28-32**) from declick reaction mentioned above, due to incomplete CuAAC click reaction.

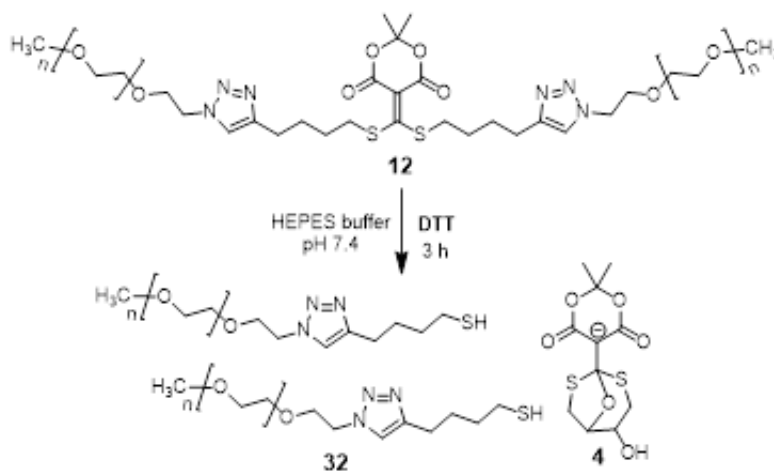


Figure 2.26 20 mg **12** and 6.0 mg DTT were added into HEPES buffer ($\text{pH} = 7.3$) and the mixture was stirred under room temperature for three hours. The resulting suspension was placed on dialysis tubing (1.0 kDa molecular weight cut-off) and suspended in deionized water for 40 hours (change the solvent every ten hours) to remove the small molecules. After dry under lyophilizer, solid PEG-SH **32** was obtained.

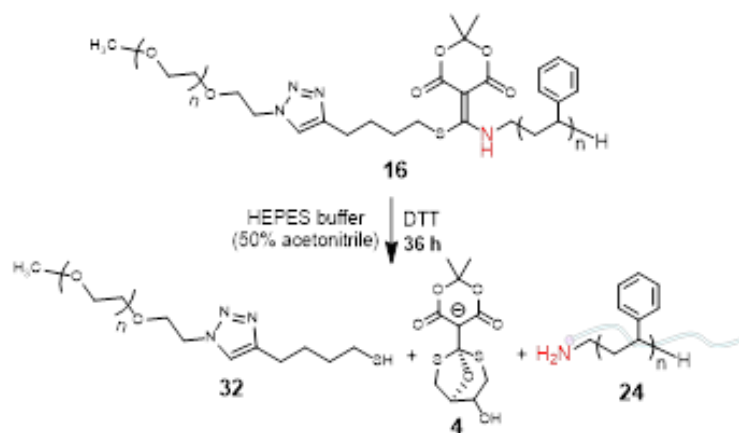
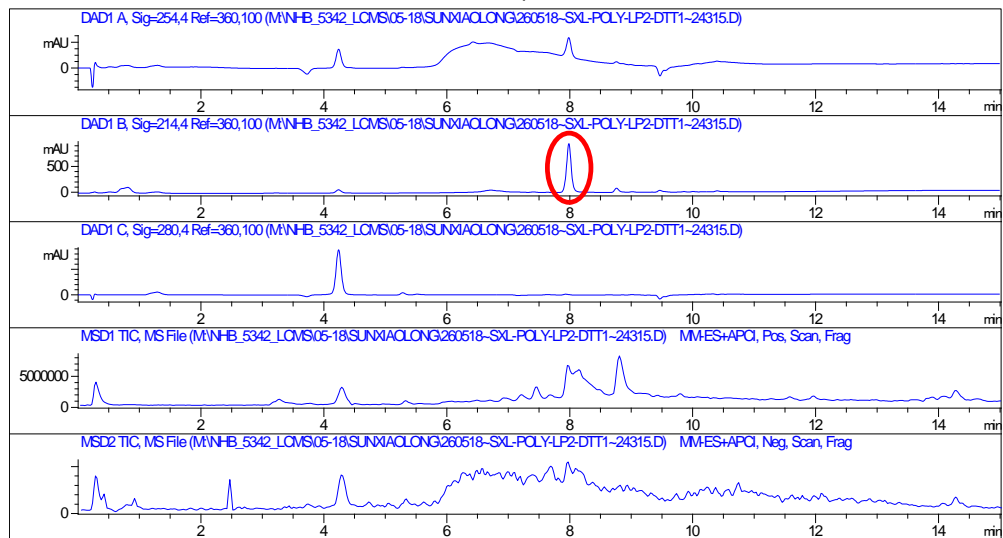
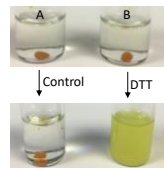
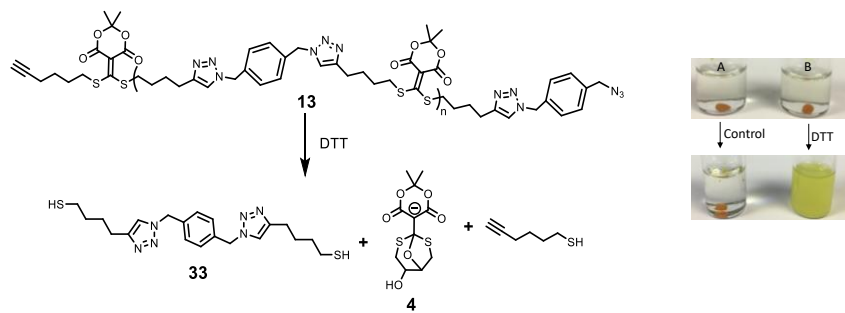


Figure 2.27 20 mg **16** and 20 mg DTT were added into HEPES buffer (pH = 7.3, 50% acetonitrile as co-solvent) and the mixture was stirred under room temperature for 36 hours. The resulting suspension was placed on dialysis tubing (1.0 kDa molecular weight cut-off) and suspended in deionized water for 40 hours (change the solvent every ten hours) to remove the small molecules.



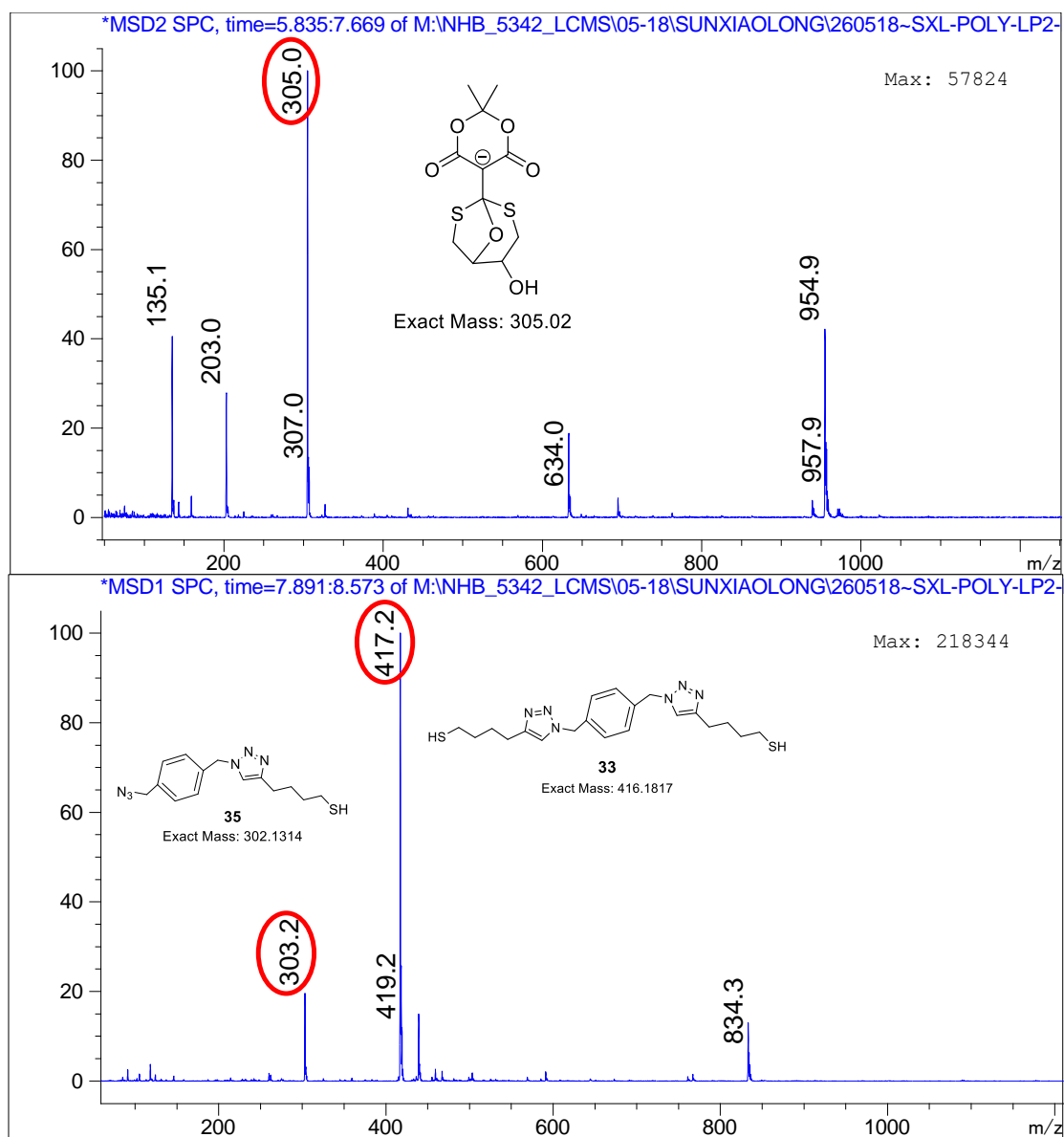
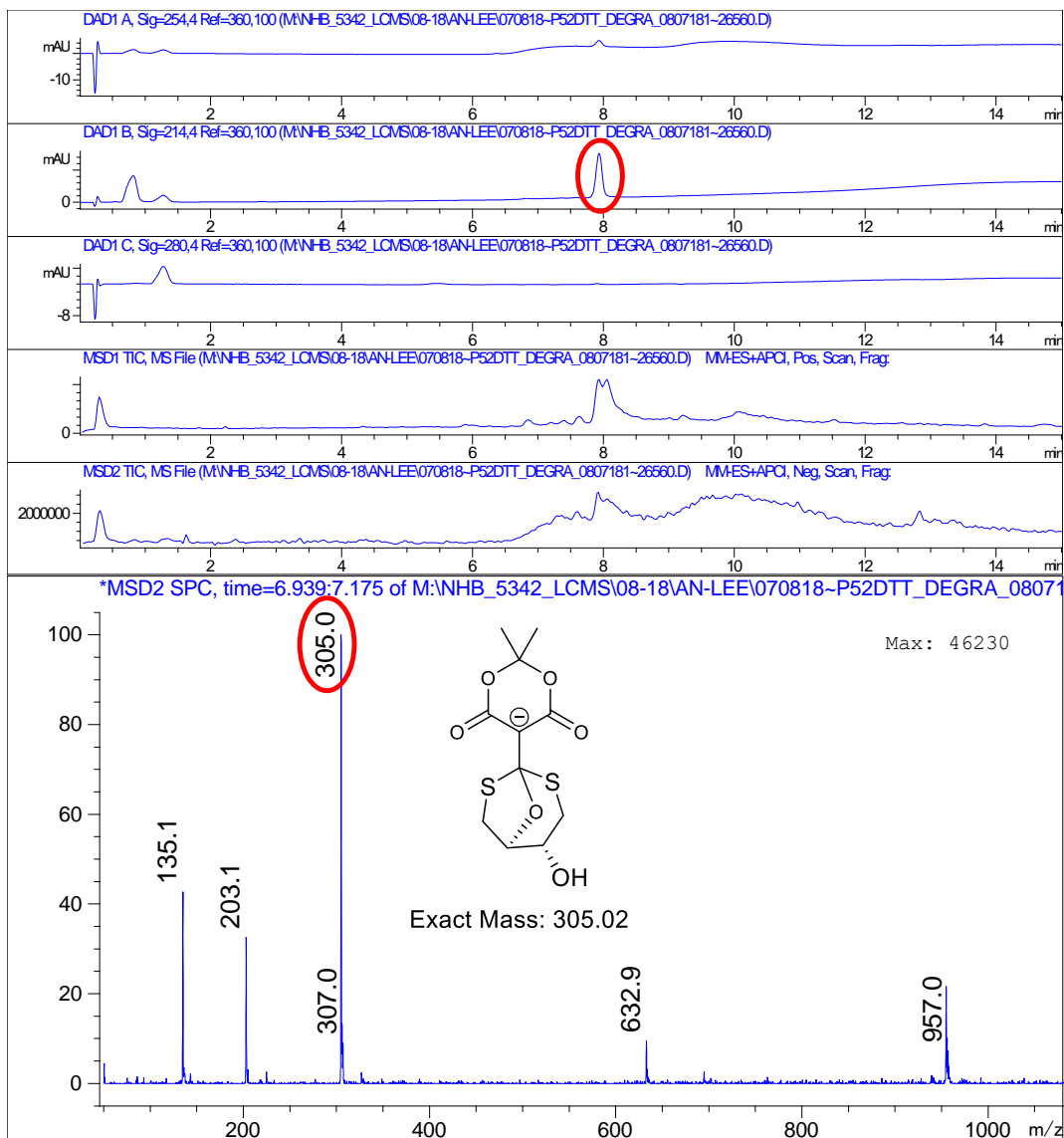
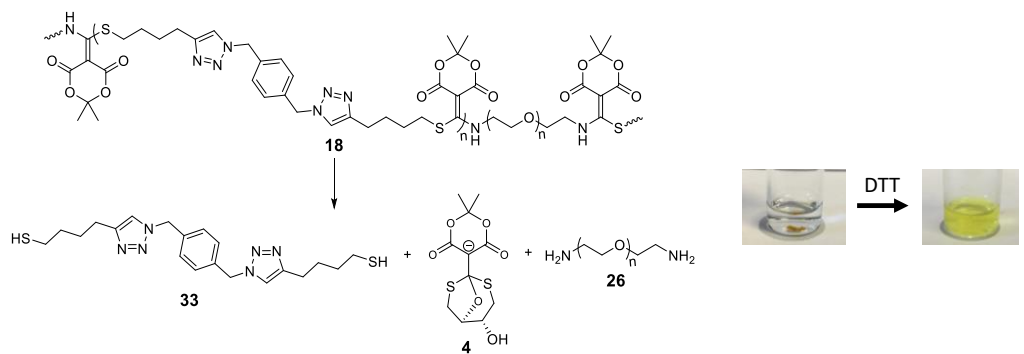


Figure 2.28 Degradation of **13** (5 mg) in the presence of DTT (20 mM) in HEPES buffer (pH = 7.3, 50% acetonitrile as co-solvent). Vial A is control sample without DTT; vial B is sample with DTT. After overnight shaking, solid in vial B was dissolved to form the yellow suspension. LC-MS tracked the main products: **4** and **33** in different retention times. Also the azide molecule **35** was observed due to insufficient CuAAC click reaction.



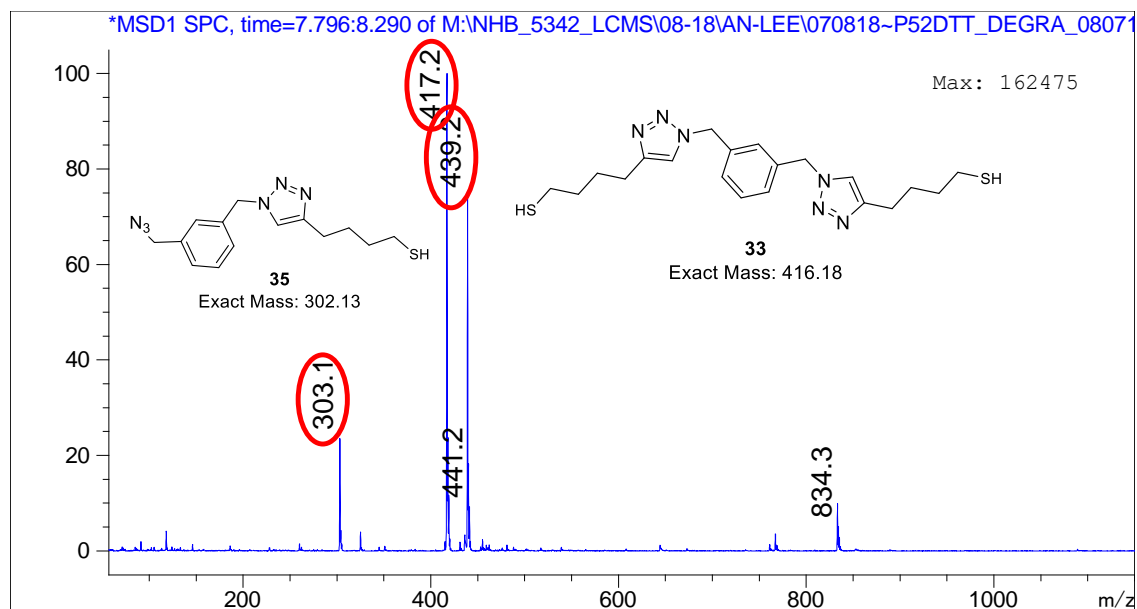
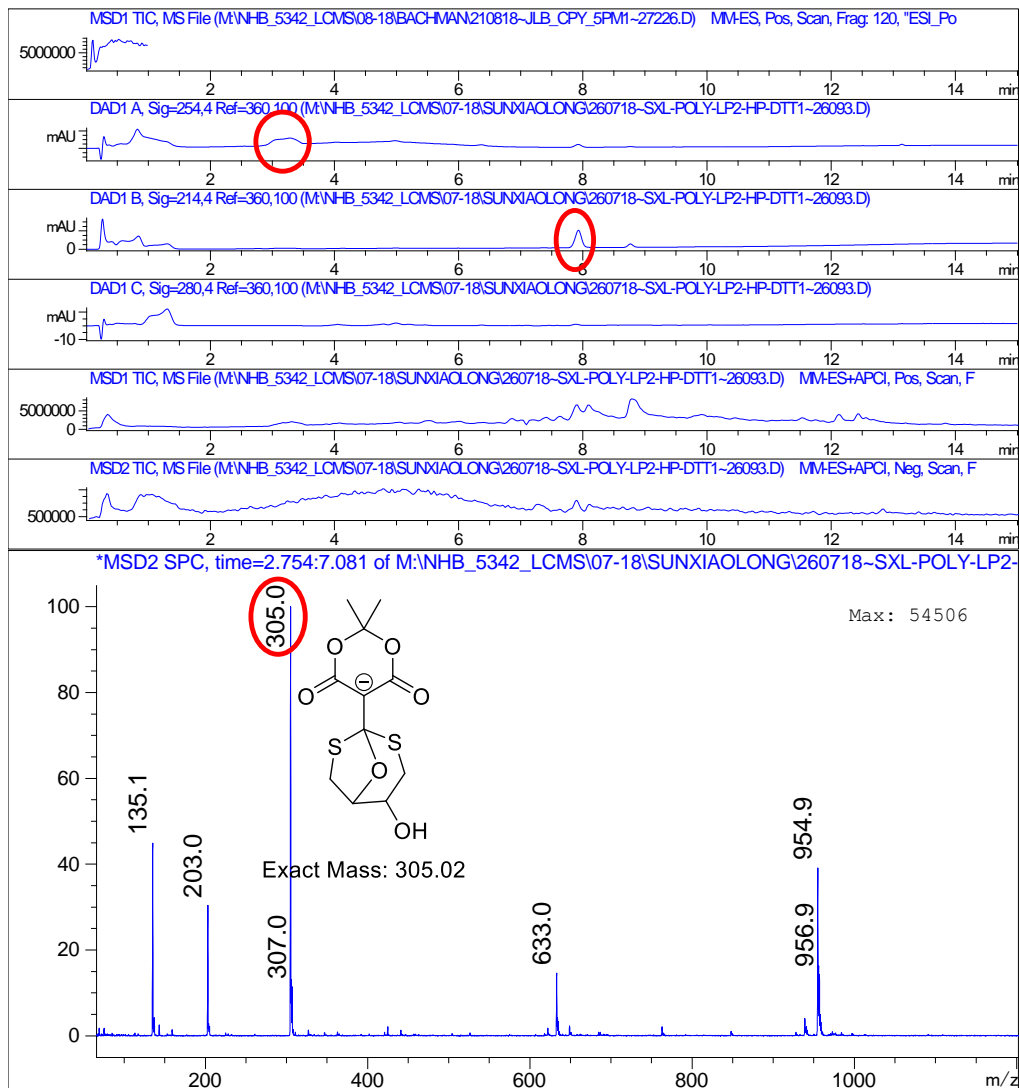
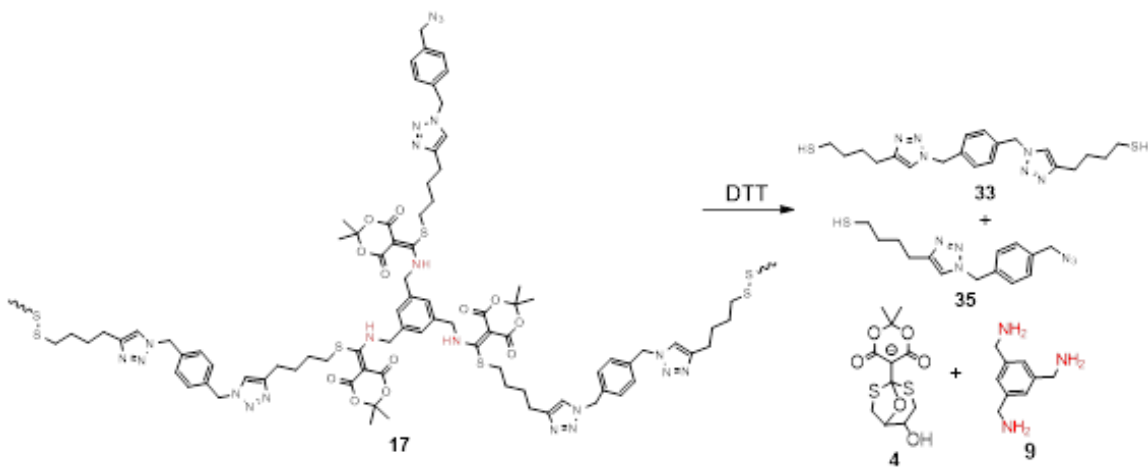


Figure 2.29 Degradation of **18** in the presence of DTT in HEPES buffer (pH = 7.3, 50% acetonitrile as co-solvent). After 48 hours shaking, solid in vial was dissolved to form the yellow suspension. LC-MS tracked the main products: **4** and **33**, **35** in different retention times. Azide molecule was observed due to insufficient reaction.



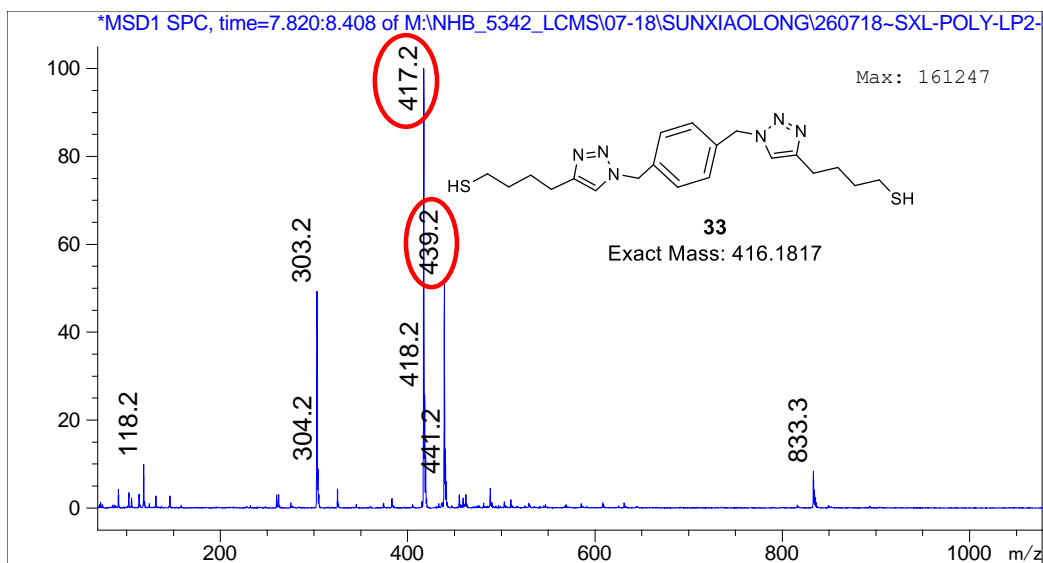
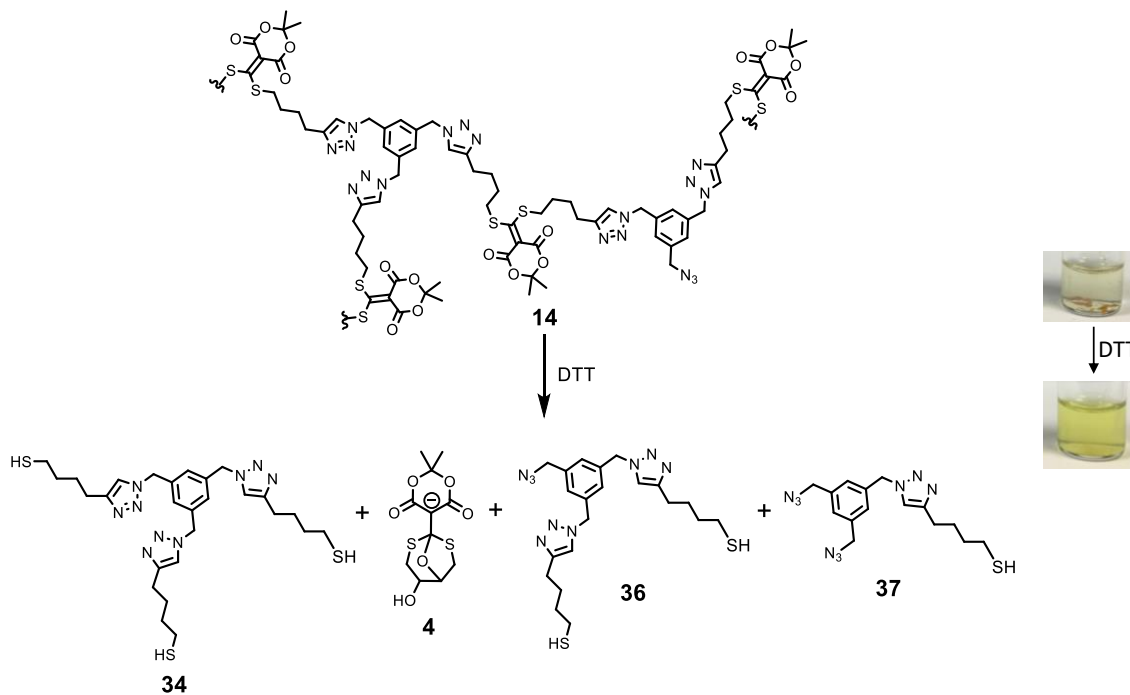
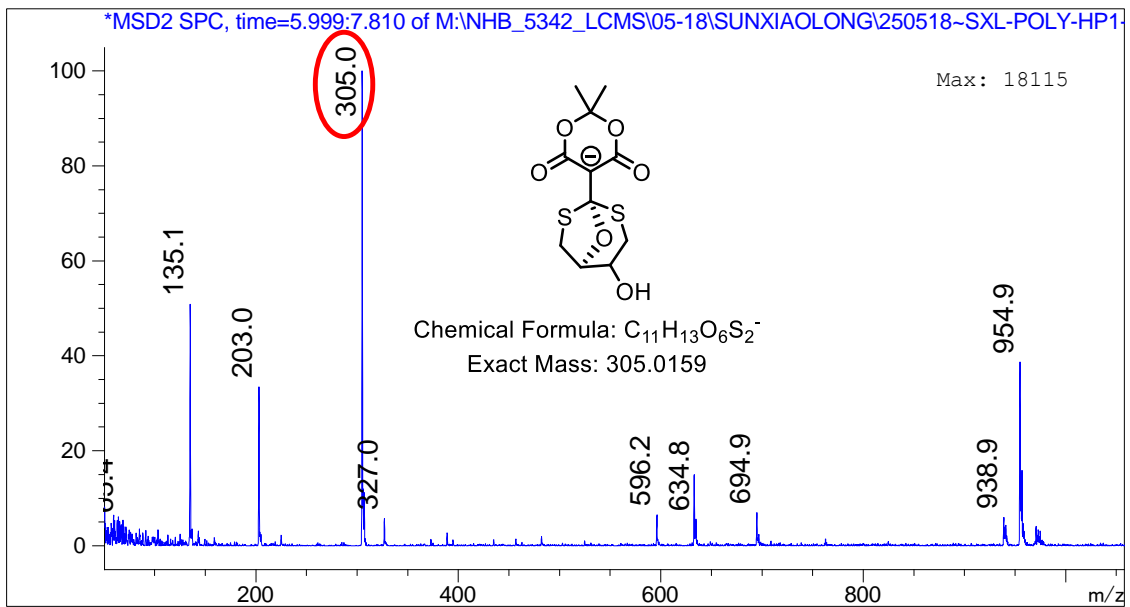
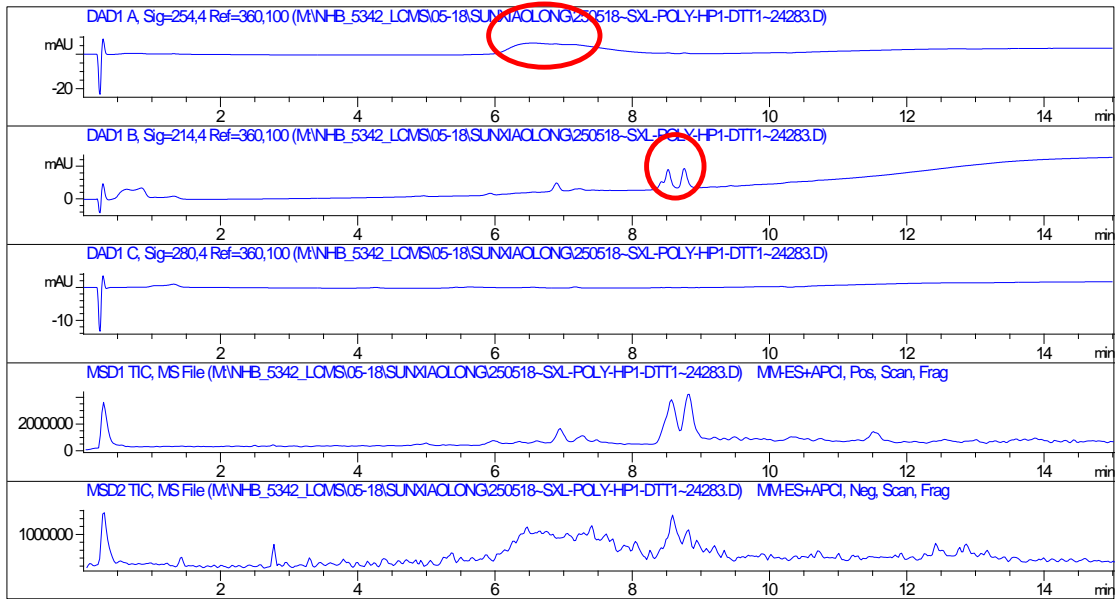


Figure 2.30 Degradation of **17** in the presence of DTT in HEPES buffer (pH = 7.3, 50% acetonitrile as co-solvent). After 48 hours shaking, solid was dissolved to form the yellow suspension. LC-MS tracked the main products: **4** and **33**, **35** in different retention times.





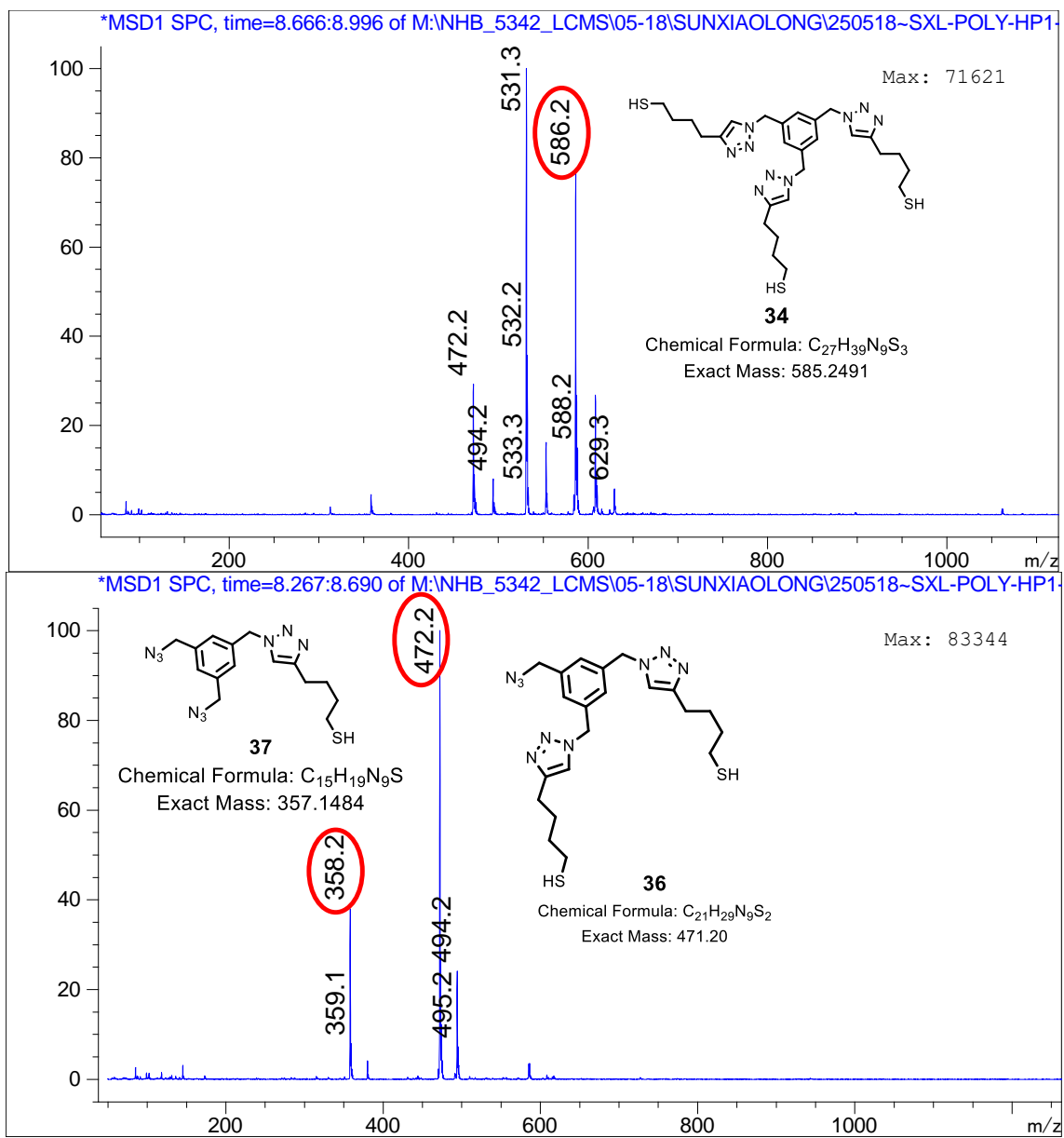
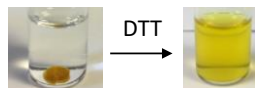
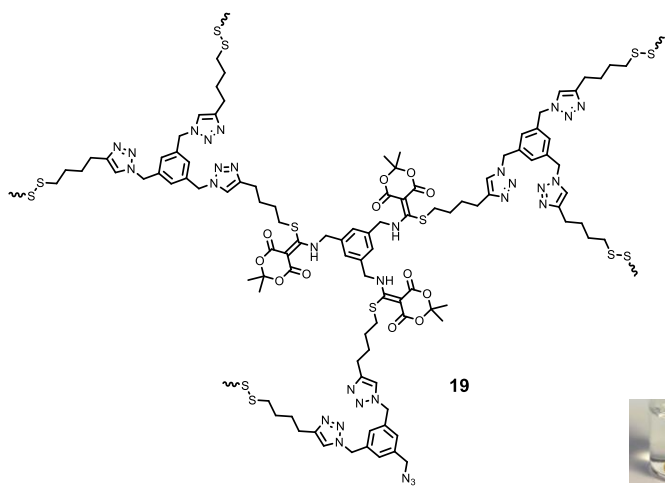
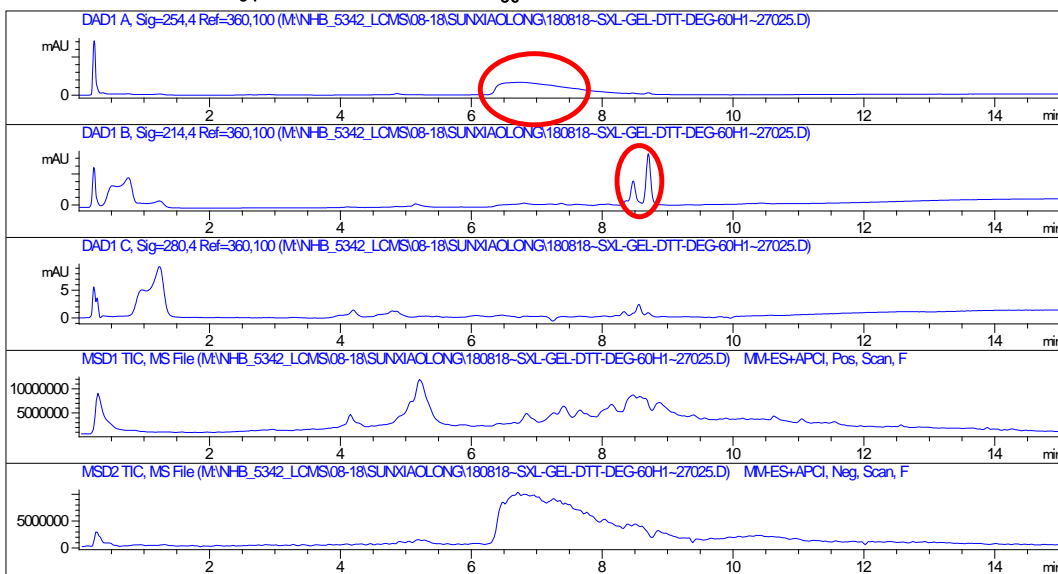
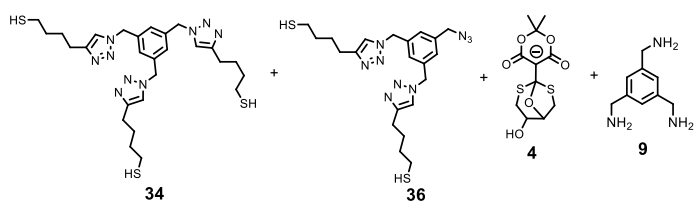


Figure 2.31 Degradation of **14** in the presence of DTT under HEPES buffer (pH 7.3, 50 % acetonitrile as cosolvent). After overnight shaking, solid in vial was dissolved to form the yellow suspension. LC-MS tracked the main products: **4** and **34** in different retention times. Also the azide molecules **36**, **37** were observed due to insufficient click reaction.



5 days DTT



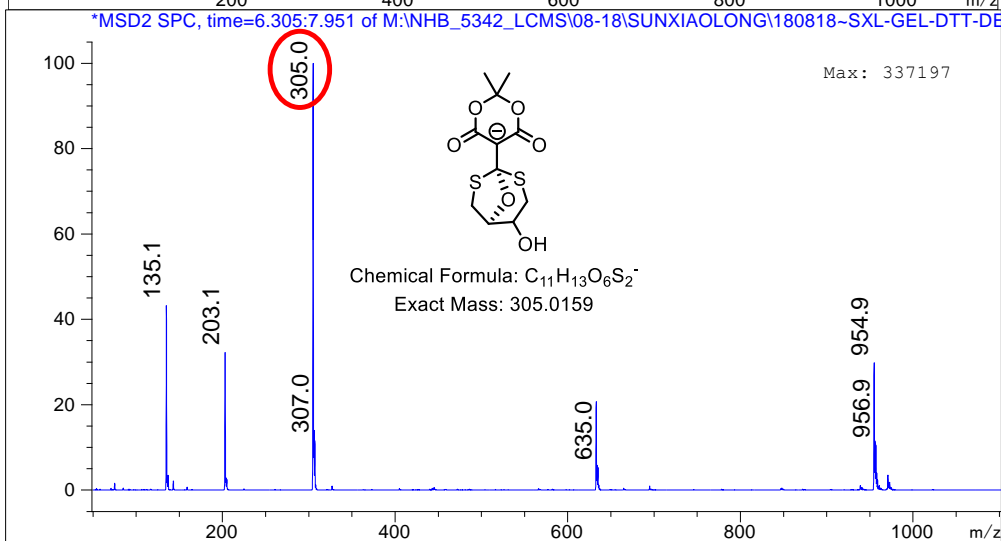
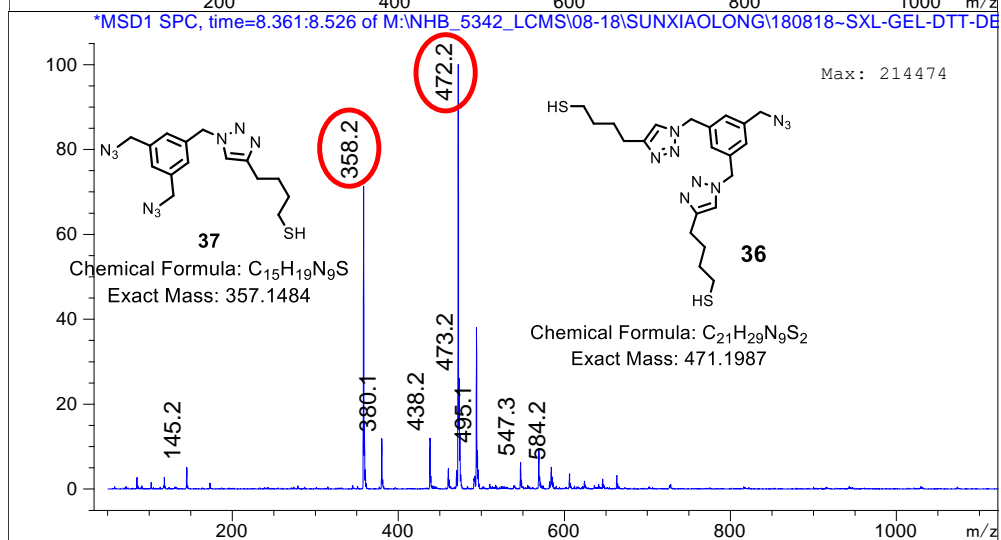
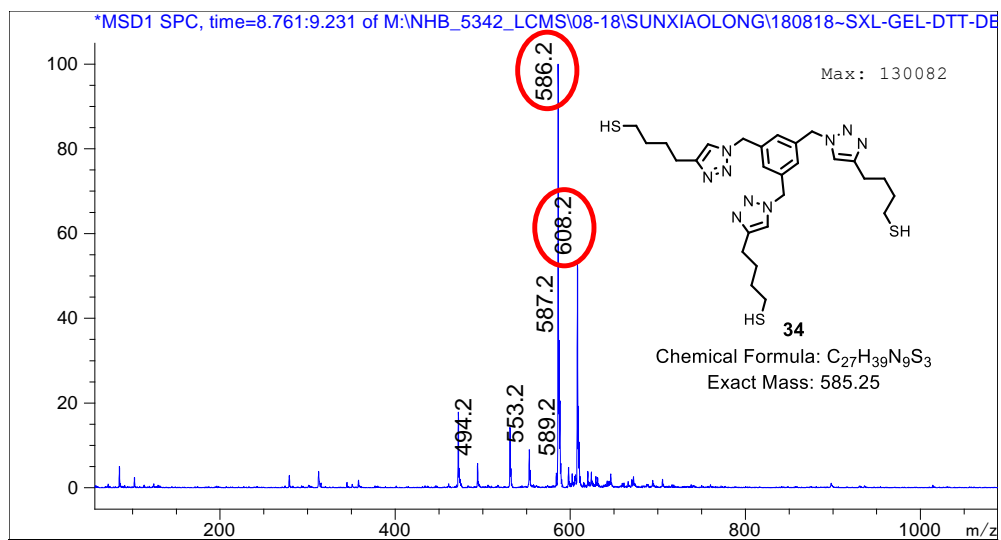
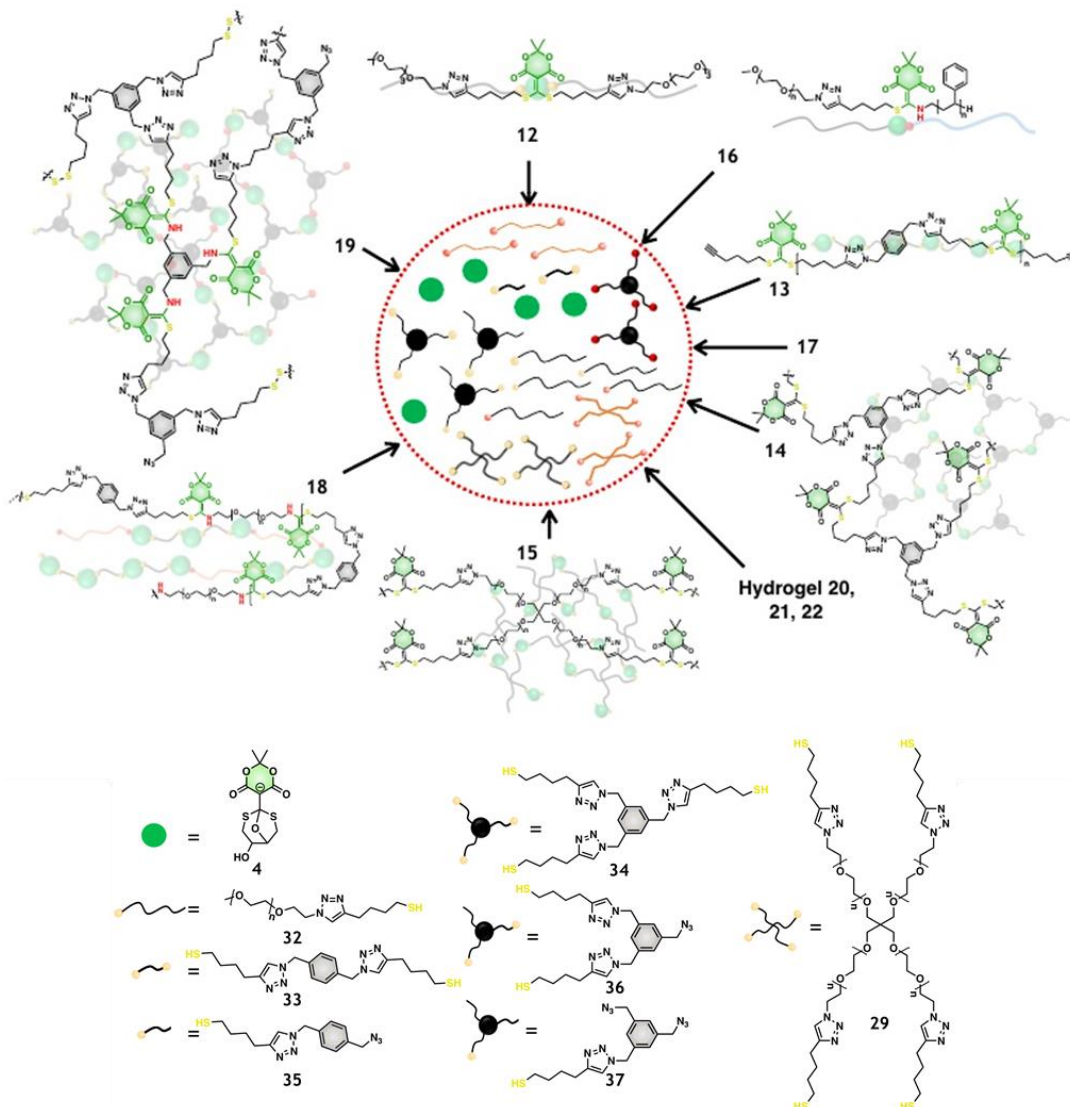
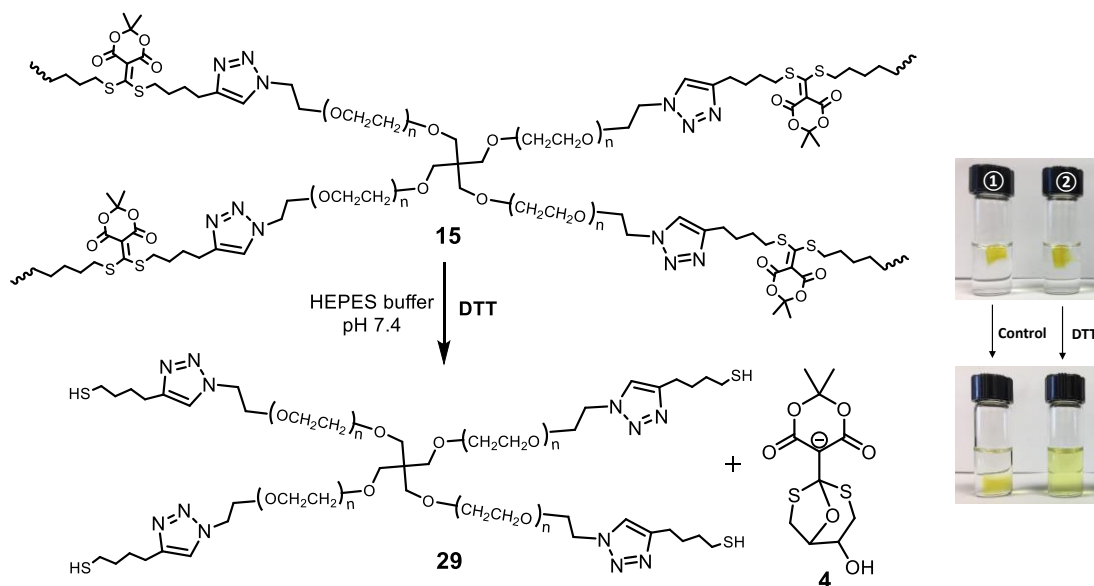


Figure 2.32 Degradation of **19** in the presence of DTT in HEPES buffer (pH = 7.3, 25% acetonitrile/25% methanol as co-solvent). Inset photos were Gel samples before and after DTT decoupling. LC-MS tracked the main product **4** and **34**. Also the azide molecule **36** and **37** was observed due to insufficient reaction.



Scheme 2.6 Schematic depiction of polymer degradation induced in the presence of DTT or tris(2-carboxyethyl)phosphine (TCEP)/ethanolamine in neutral HEPES buffer. The degradation process was triggered either by the cyclization between a bis-vinyllogous derivatives of **3** with DTT, or disulfide cleavage by reduction with TCEP, or ethanolamine-induced decoupling of structures such as **1**, respectively.

DTT was also successfully used to declick the hydrogels into small molecules. The 3D network **15** was processed in HEPES buffer in the presence of DTT, and after 20 minutes the yellow gel disassembled, with no disassembly of the control sample without DTT (inset picture in **Figure 2.33**). LC-MS verified the generation of **4** (**Figure 2.33**), and following dialysis, ^1H NMR spectroscopy confirmed formation of **29** (**Figure 2.22E**). Furthermore, kinetic studies from the rheometer displayed a decreasing of the storage modulus (G') due to degradation of hydrogel **15** following addition of DTT, indicating gradual breakage of the matrix (**Figure 2.34** and **Figure 2.35**). Next, the viscoelasticity of a soft hydrogel **20** (storage modulus $G' = 28$ Pa) was transformed rapidly into a solution state ($G' < G''$) due to the cleavage of disulfide bonds by tris(2-carboxyethyl)phosphine (TCEP) (**Figure 2.34B**). Following dialysis, the solution state was reversed into a gel under hydrogen peroxide due to the reformation of disulfide bonds (**Figure 2.36**).



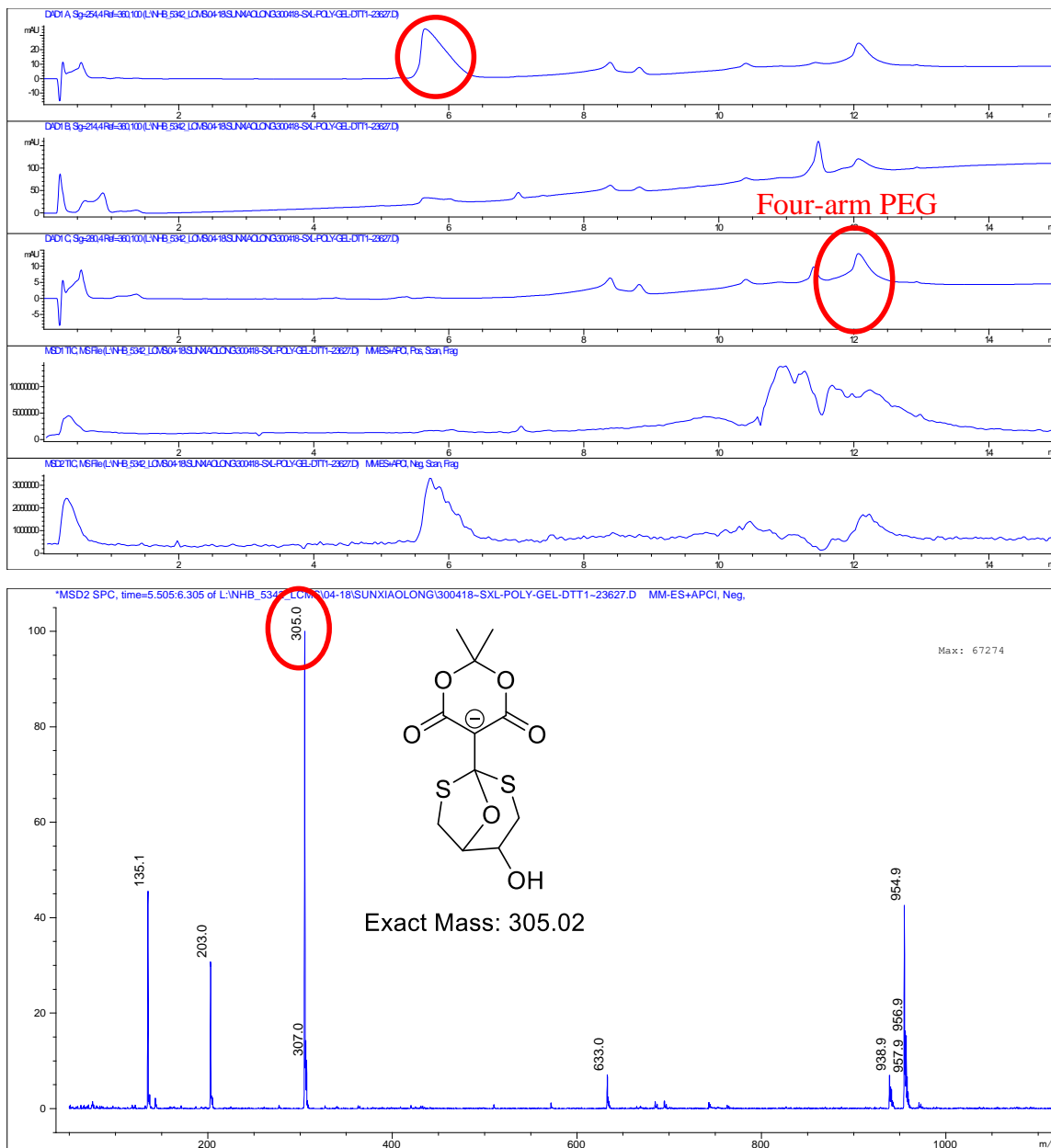


Figure 2.33 Degradation of hydrogel **15** in the presence of DTT under HEPES buffer (pH 7.3). Vial 1 is control sample without DTT; vial 2 is sample with DTT. After 20 mins shaking, hydrogel in vial 2 was dissolved to form the yellow suspension.

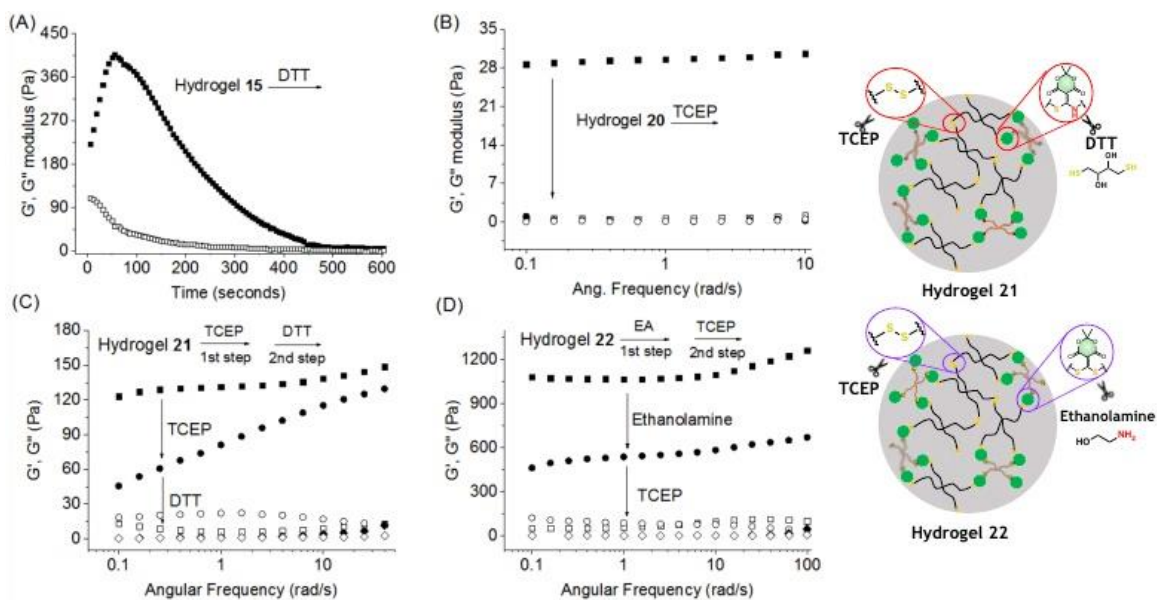


Figure 2.34 Monitoring hydrogel degradation by rheometer. (A) Time-based kinetics for degradation of hydrogel **15** in the presence of DTT; (B) TCEP-induced disulfide reduction for hydrogel **20** degradation; (C) Two cross-linked networks: disulfide bond and amine/thiol conjugate acceptor linked in hydrogel **21** were degraded by TCEP and DTT, respectively; (D) Two cross-linked networks: a bis-vinyllogous thiol-ester such as **1** and disulfide bond linking hydrogel **22** were degraded by ethanolamine and TCEP, respectively. Storage modulus and loss modulus for hydrogels **20**, **21** and **22** were scanned before and after degradation.

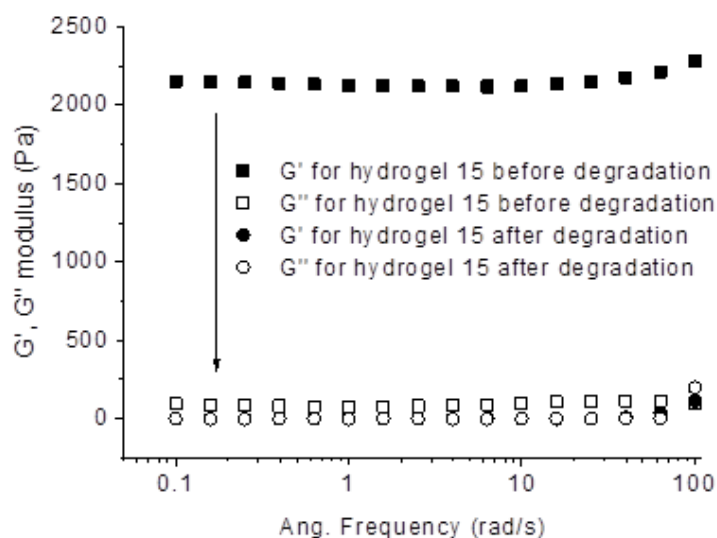


Figure 2.35 Changes of storage modulus and loss modulus of hydrogel **15** before and after degradation. Hydrogel **15** was processed in the presence of DTT for 10 mins.

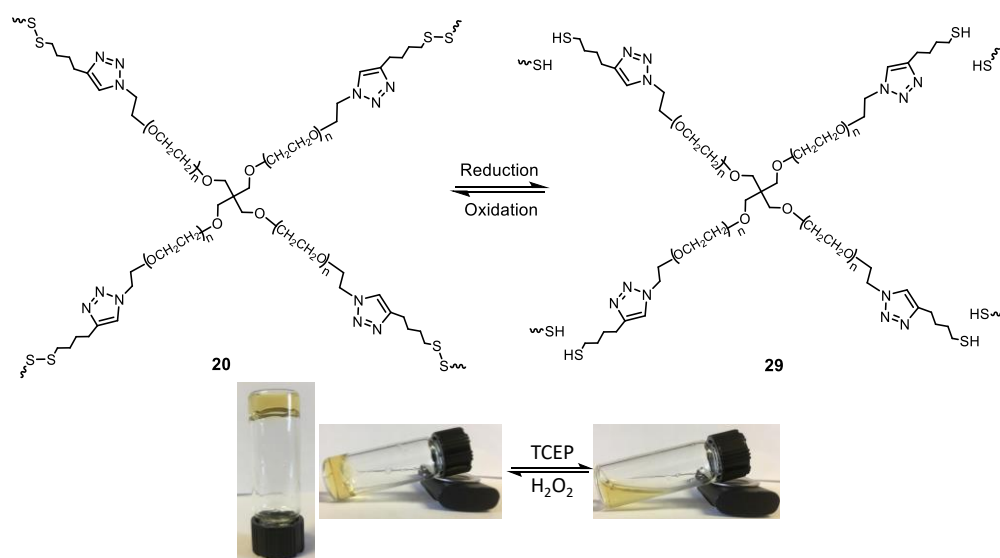


Figure 2.36 Reversibility of hydrogel **20** degradation and reformation in the presence of TCEP and H_2O_2 . After adding TCEP, hydrogel **20** decomposed into four-arm PEG thiol **29** and then dialysis tubing to remove TCEP/oxidized TCEP. Next, hydrogen peroxide reversed the sol into hydrogel through thiol oxidation.

The crosslinked matrixes **21** and **22** could also be tuned and controlled by different decoupling reagents. The matrix of hydrogel **21** ($G' \sim 130$ Pa), containing both the amine/thiol conjugate and disulfide bonds, were tuned separately by TCEP for the reduction of disulfides ($G' \sim 70$ Pa), and subsequently by DTT for the cleavage of the thiol-amine conjugate analogous to **2** ($G' \sim 5$ Pa, **Figure 2.34C** and **2.37**). While for hydrogel **22** ($G' \sim 1000$ Pa), ethanolamine was employed to cut off the bis-vinylogous thiol ester core analogous to **1** ($G' \sim 500$ Pa), and then TCEP was used to reduce the disulfide bonds ($G' \sim 5$ Pa), decomposing the cross-linked hydrogel entirely into small molecules (**Figure 2.34D** and **2.38**). The tunable and degradable properties of the hydrogels, particularly the ability to tune the two dynamically cross-linked samples under physiological conditions, are potentially applicable in drug delivery systems and tissue bioengineering.

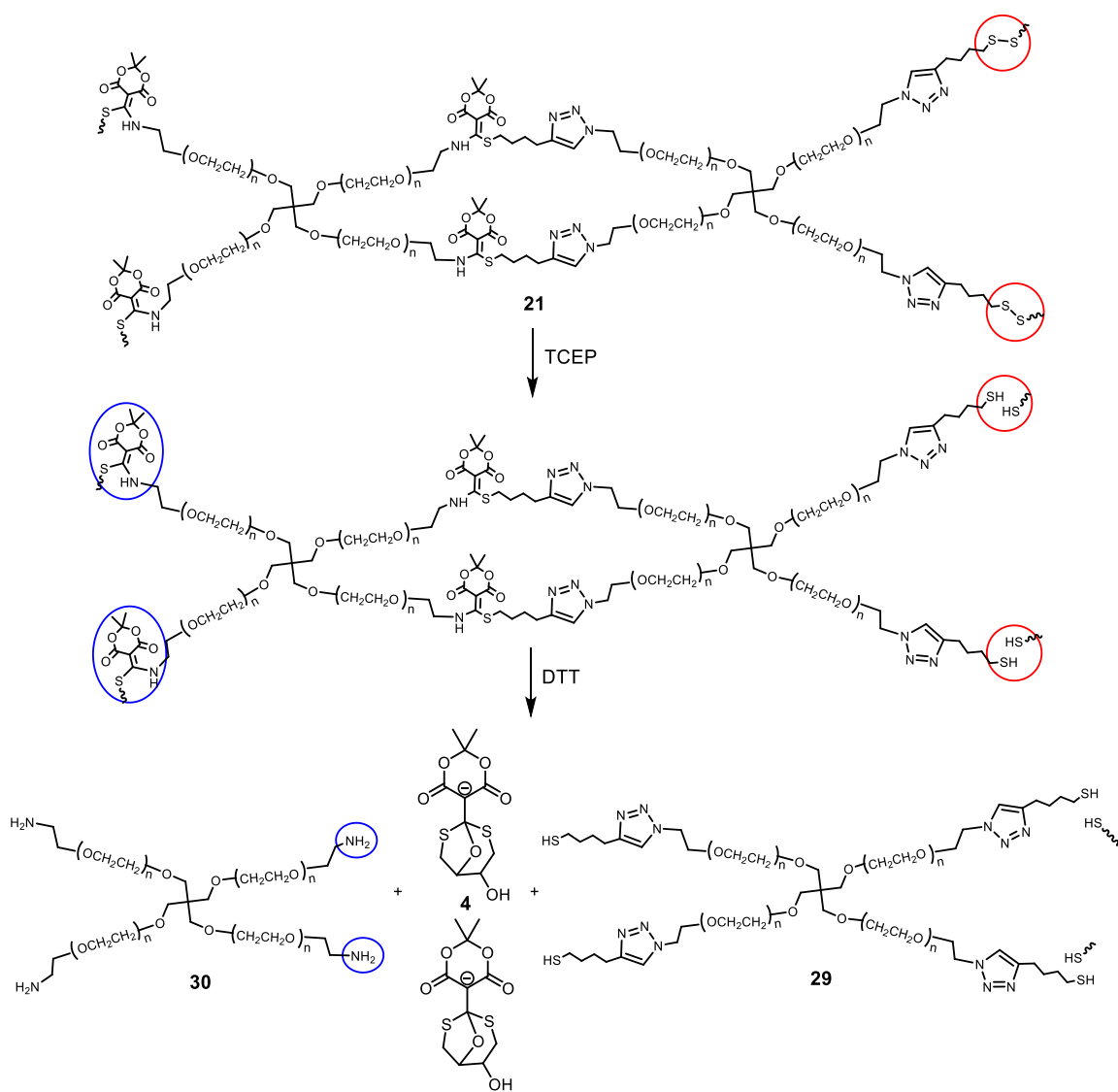


Figure 2.37 Degradation of conjugate acceptor and disulfide-linked hydrogel **21** in the presence of TCEP and DTT. TCEP firstly reduced the disulfide bonds while DTT subsequently cleaved the conjugate acceptors to release the tricyclic product, **29** and **30**.

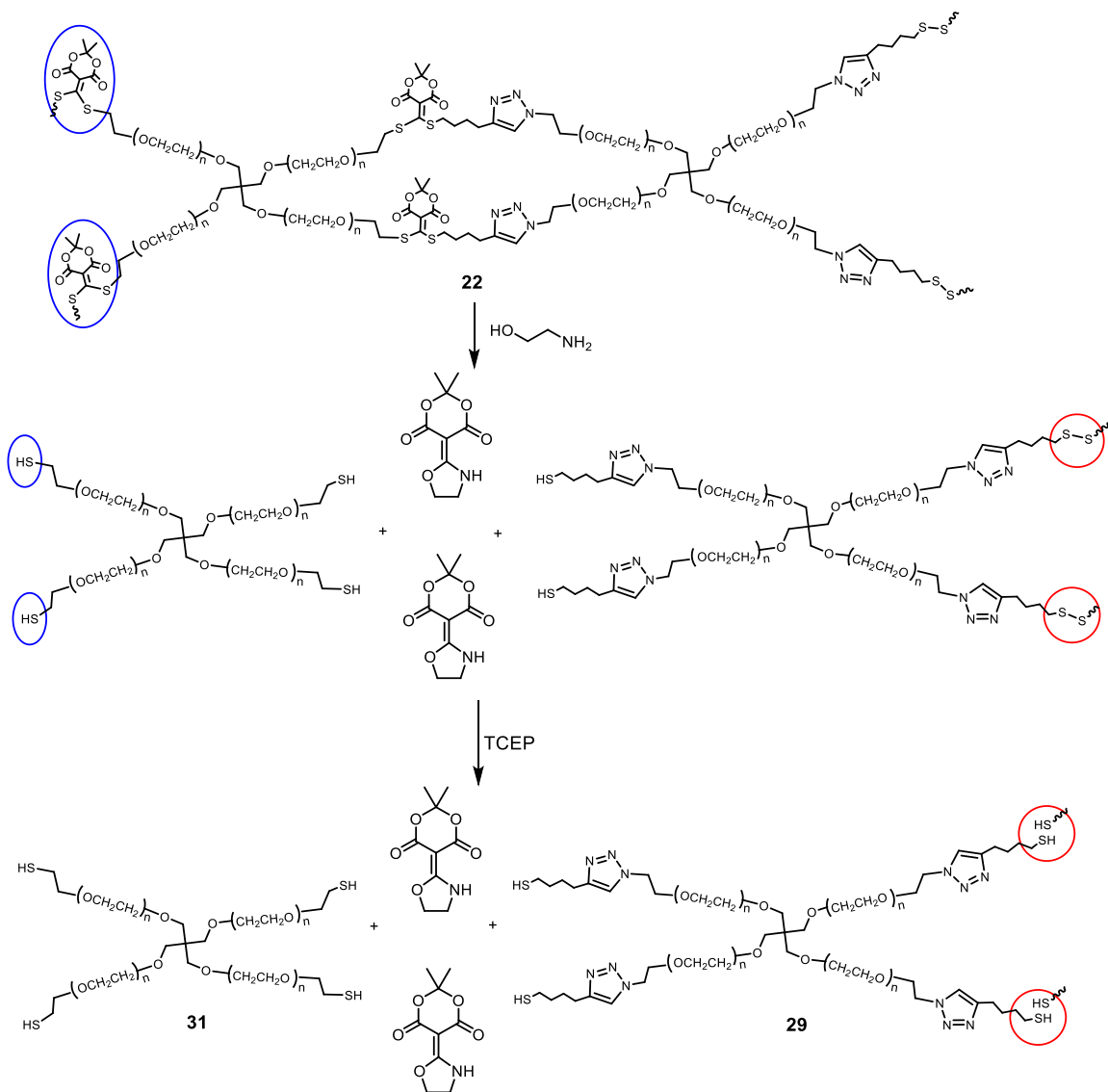


Figure 2.38 Degradation of bis-vinyllogous thiol ester and disulfide-linked hydrogel **22** in the presence of ethanolamine and TCEP. Ethanolamine decoupled the conjugate linker and then TCEP reduce the disulfide bond rapidly.

2.3 CONCLUSION

We have demonstrated in macromolecular constructs the versatility of being able to click thiols, and amines and thiols, via structures analogous to **1** to make morphable soft materials. By simply controlling the sequence of addition of monomers, cross-linkers or polymers, we could chemically trigger interconversion of backbone architectures and crosslinks, control polymer morphologies, and alter macroscopic properties, all at ambient temperature in aqueous media. In specific, the reversible conjugate additions inherent in the organic chemistry of **1** and its analogs introduced herein, coupled with thiol-disulfide scrambling, led to very simple approaches that interconvert linear hydrophobic, hydrophilic, and amphiphilic polymers, as well as lightly cross-linked polymers and hydrogels; further even allowing interconversion of random co-polymers with other lightly cross-linked polymers. In addition, in a facile fashion 4 different hydrogels could be created via manipulating the components allowed to react with structures containing the reactivity of **1**. The choice of amines and thiols used herein are specific to this study, but clearly the possibilities are vast given the numbers of amine and thiol units that can be imagined. Lastly, and potentially just as important, all the soft materials are degradable with various chemical triggers, albeit specifically DTT was used in this study. Owing to the mild reaction conditions and ease of use in a wide variety of applications, this method is expected to have numerous material applications.

2.4 EXPERIMENTAL SECTION

2.4.1 Methods and Instruments

Nuclear Magnetic Resonance (NMR)

^1H and ^{13}C NMR spectra were recorded on Varian DirectDrive or Varian INOVA 400 MHz NMR spectrometers. The NMR spectra were referenced to solvent and the spectroscopic solvents (CDCl_3 , CD_3CN , D_2O , $\text{DMSO-}d_6$, etc.) were purchased from Cambridge Isotope Laboratories and stored over 3 Å molecular sieves.

Liquid Chromatography–Mass Spectrometry (LC-MS)

Finnigan MAT-VSQ 700 and DSQ spectrometers were used to obtain mass spectra. HR electrospray ionization (ESI) mass spectra were recorded using either Agilent 6530 Accurate-Mass Q-TOF LC/MS or MALDI-TOF (Vogayer, PerSeptive Biosystem).

Gel Permeation Chromatography (GPC)

Size exclusion chromatography (SEC) was carried out on an Agilent system with a 1260 Infinity isocratic pump, degasser, and thermostated column chamber held at 30 °C containing Agilent 5 μm MIXED-C columns with a combined operating range of 200–2000 000 g mol^{-1} relative to polystyrene standards. Chloroform with 50 ppm amylene and DMF with 10 mM LiCl were used as the mobile phases. SEC system was equipped with an Agilent 1260 Infinity refractometer, bi dual angle dynamic and static light scattering.

Dynamic Light Scattering (DLS)

DLS size analysis of aggregates formed by amphiphilic block copolymer PS-b(EVA)-PEG was carried out using Malvern Zetasizer Nano ZS model equipped with He-Ne laser source (633 nm; Max 4mW). The measurements were run in triplicate with 20 scans per measurement.

High-Resolution Mass Spectrometry (HRMS)

High-resolution mass spec (HRMS) analysis was conducted by the University of Texas Mass Spectrometry Facility using Agilent Technologies 6530 Accurate Mass Q-TOF LC/MS system. MALDI-TOF MS analysis was performed using an AB-Sciex Voyager-DE PRO MALDI-TOF equipped with a 337 nm nitrogen laser in linear mode using CHCA as a matrix.

UV-Vis Spectroscopy

The UV-Vis absorbance spectra and kinetics were obtained in Cary 100 UV-Vis spectrophotometer from Agilent Technology. The spectra were run in Cary WinUV software: Scan, Kinetics and Scanning Kinetics, respectively.

Rheometry

Rheological measurements for gel and hydrogel were conducted at 25 °C on Discovery HR-2 Hybrid Rheometer (TA Instrument) using a 40 mm flat plate.

2.4.2 Materials

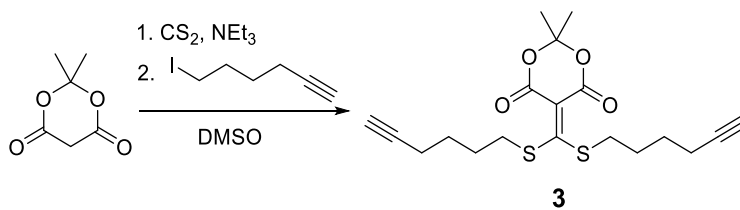
The copper (I) iodide (Sigma-Aldrich, 99%), CuSO₄·5H₂O (Fisher Scientific, 101.7%) and sodium L-ascorbate (Sigma Aldrich, 99%) were used for click reactions as received. Tris(benzyltriazolylmethyl)amine (TBTA) ligand was synthesized according to literature protocol.³⁹ Meldrum's acid were purchased from Oakwood Chemical and made in China. 6-Iodo-1-hexyne (97%); Polystyrene, amine terminated average $M_n = 5,000$ Da, PDI ≤ 1.2 ; Poly(ethylene glycol) methyl ether azide PEG average $M_n = 1,000$ Da were all from Sigma-Aldrich. Four-arm poly(ethylene glycol) azide (> 95%, $M_n = 10,000$ Da), four-arm poly(ethylene glycol) amine ($M_n = 2,000$ Da, PDI ≤ 1.05) and four-arm poly(ethylene glycol) thiol (> 90%, $M_n = 5,000$ Da) was purchased from JenKem

Technology. Other chemical reagents were purchased from Tokyo Chemical Industry, Sigma Aldrich, Acros Organics, et al. and used without further purification.

In the experiments described in this paper, the unpleasantness of the thiol smell released from the reactions was equivalent to or slightly worse than the odor of natural gas. However, as a precaution against even these levels of exposure, the reactions were carried out in a fume hood.

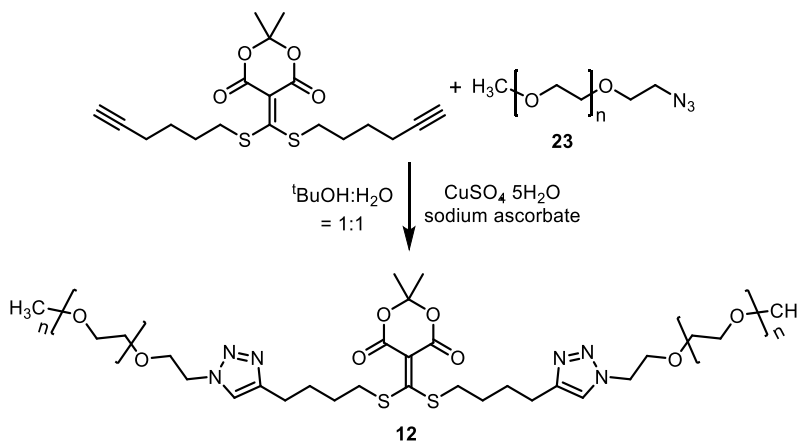
All cuvettes made by fused quartz were purchased from Starna Cells with standard screw and septum top.

2.4.3 Synthesis

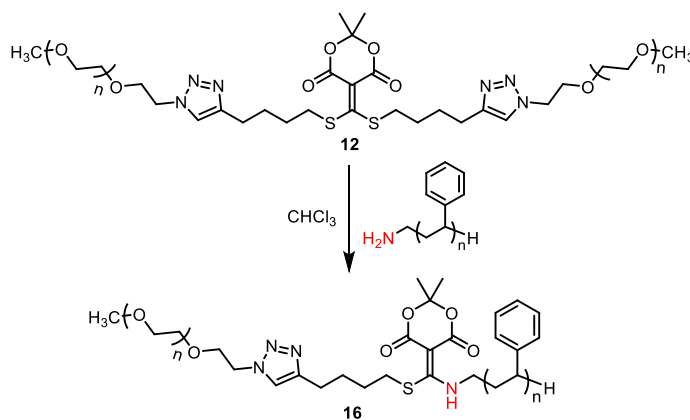


5-(bis(hex-5-yn-1-ylthio)methylene)-2,2-dimethyl-1,3-dioxane-4,6-dione:²⁷ In a flame dried, 25 mL round bottom flask, Meldrum's acid (0.5 g, 3.47 mmol) was dissolved in DMSO followed by the addition of triethylamine (0.7 g, 6.94 mmol) and carbon disulfide (0.26 g, 3.47 mmol). Resulting red solution was stirred at room temperature for 1 hour. After 1 hour, 6-iodo-1-hexyne (1.44 g, 6.94 mmol) was added to the solution dropwise. The resulting solution was brown in color and the whole round bottom flask was wrapped in aluminium foil and allowed to stir over night (~ 18 h). The solution was added over ice and extracted with chloromethane (50 mL × 3). Organic phase was collected and dried with sodium sulfate. After evaporation under vacuum, the crude liquid product was purified by column chromatography with hexane/ethyl acetate = 10/1 (vol/vol) as eluent to offer yellow oily product **3** (0.4 g, 31%). ¹H NMR (400 MHz, CDCl₃) δ 3.18 – 3.04 (m, 4H), 2.21 (td, *J* = 6.8, 2.6 Hz, 4H), 1.95 (t, *J* = 2.7 Hz, 2H),

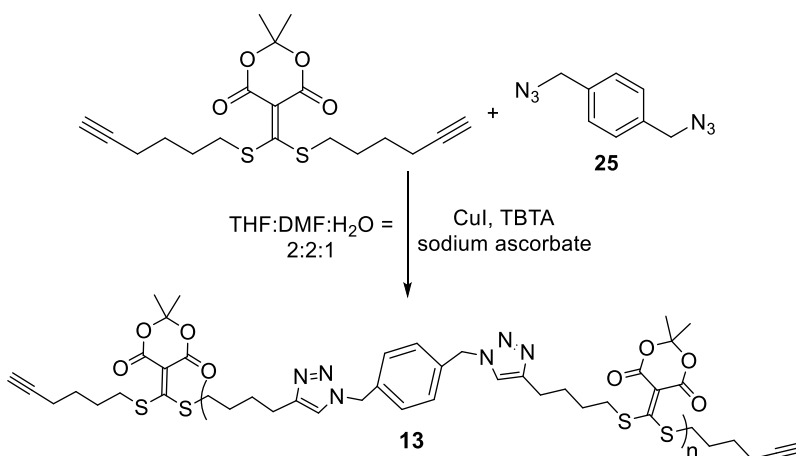
1.88 – 1.79 (m, 4H), 1.71 (s, 6H), 1.68 – 1.58 (m, 4H). ¹³C NMR (101 MHz, CDCl₃) δ 190.07, 160.04, 103.81, 103.14, 83.25, 69.25, 38.03, 27.52, 27.30, 26.92, 17.92; HRMS (ES⁺) m/z calc. for [M + Na]⁺, 403.1008; found, 403.0996.



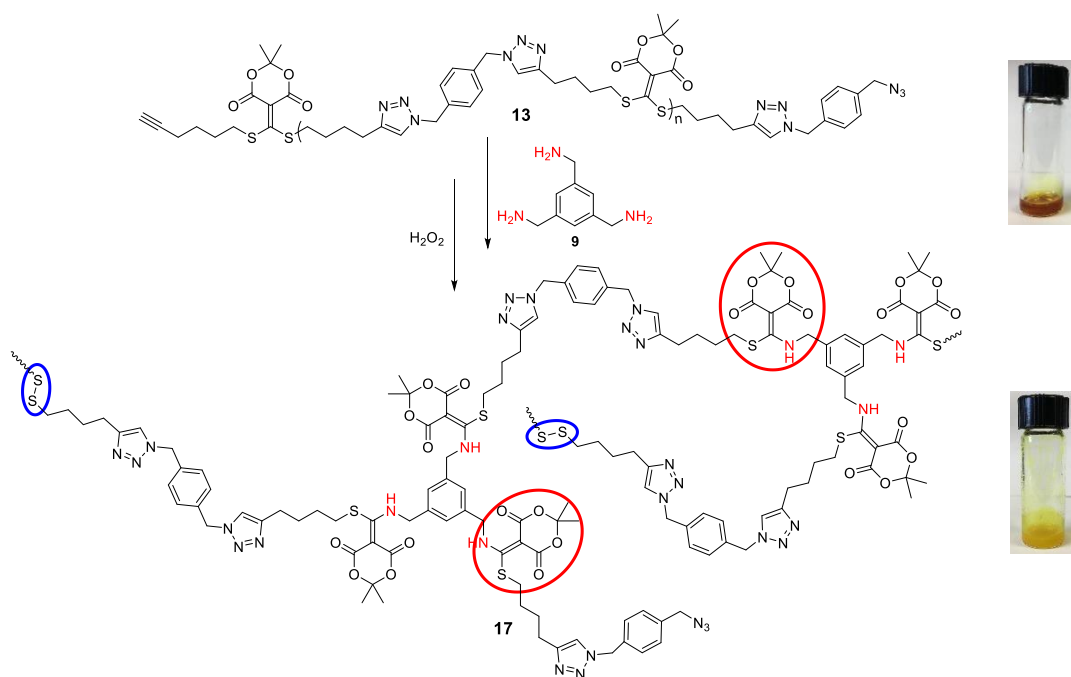
12: In a 5 mL vial, conjugate acceptor **3** (20 mg, 0.23 mmol) and poly(ethylene glycol) methyl ether azide **23** (107 mg, PEG average $M_n = 1,000$ Da) were dissolved in *tert*-butyl alcohol (60 μ L) and water (60 μ L). CuSO₄·5H₂O (0.6 mg, 0.002 mmol) and sodium ascorbate (1.25 mg, 0.006 mmol) was dissolved in water (30 μ L). The two ingredients were mixed together and stirred in a shaker at 40 °C for 24 hours. The suspension was diluted with chloroform and precipitated from cold ether (Redisolve and precipitate, repeat the process for three times). Then dry the product under vacuum.



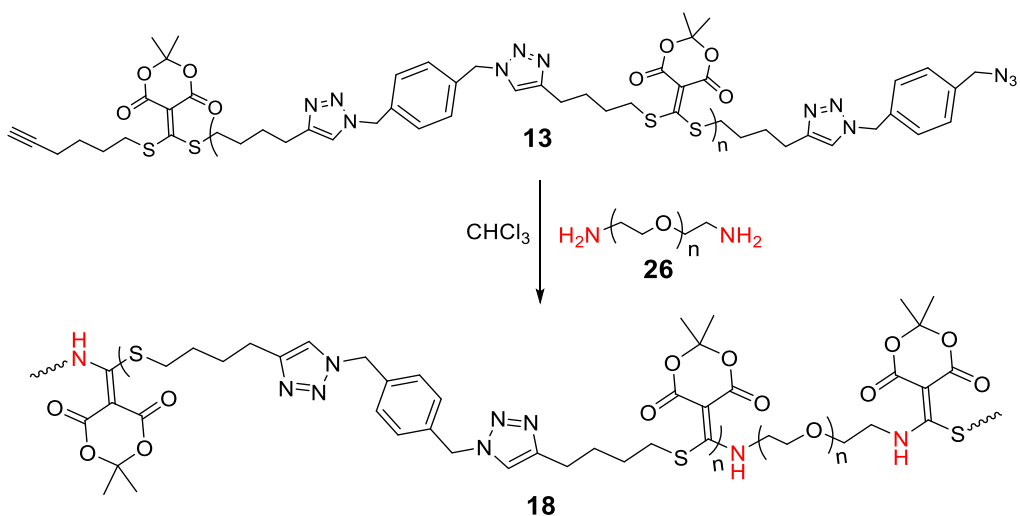
16: Polymer **12** (47.6 mg) and polystyrene amine terminated **24** (average $M_n = 5,000$, PDI ≤ 1.2) (100 mg) were dissolved in 100 μL chloroform. The suspension was stirred at room temperature for 40 hours. The brown oily mixture was diluted with 1 mL chloroform and then precipitate from cold methanol. After centrifuge, the solid was re-dissolved with minimum chloroform and precipitate from cold methanol. Repeat the procedure for three times and then dry under vacuum to offer light yellow powder **16**.



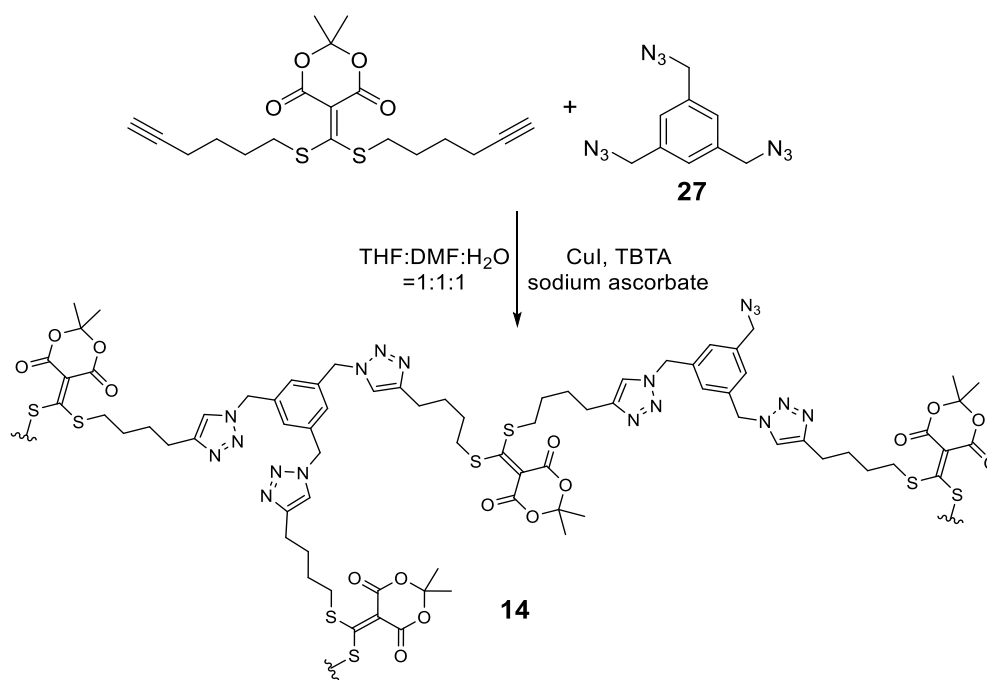
13: In a 5 mL vial, conjugate acceptor **3** (100 mg, 0.26 mmol) and 1,4-di(azidomethyl)benzene **25** (49 mg, 0.26 mmol) were dissolved in THF (40 μL). CuI (5.0 mg, 0.026 mmol) and TBTA (27.9 mg, 0.052 mmol) were dissolved in DMF (40 μL). Sodium ascorbate (15.6 mg, 0.079 mmol) was dissolved in mili-Q water (20 μL). The three ingredients were mixed together and stirred in a shaker at room temperature for two days. The suspension was diluted and dissolved with chloroform and precipitated from cold methanol (repeat the process for three times). The product was placed on dialysis tube (1.0 kDa molecular weight cut-off) for further purification and then dried under vacuum to offer yellow solid **13**.



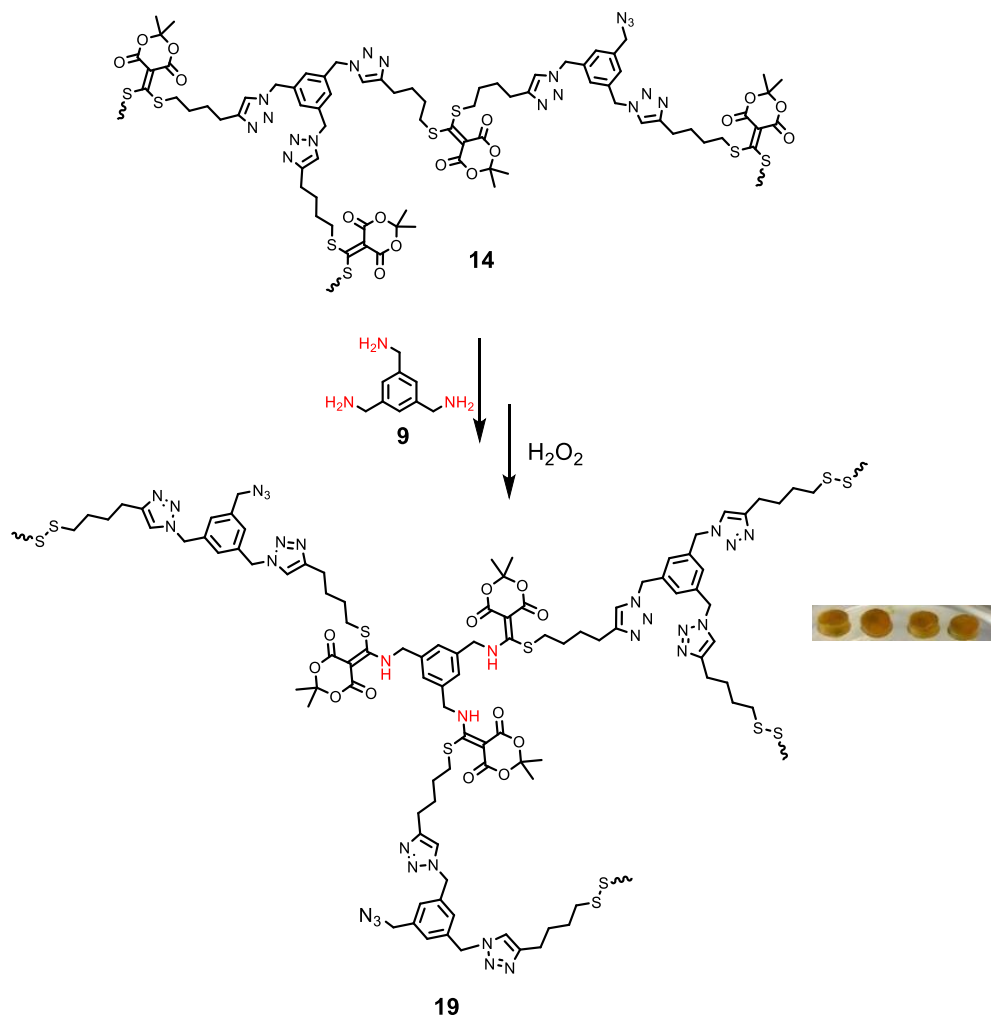
17: **13** (20 mg, $M_n = 5400 \text{ g mol}^{-1}$) was dissolved in THF/DMF mixture and **9** (10 mg, 0.061 mmol) was added into the suspension. The suspension was shaking for three hours and strong odor smell generated which indicated the scrambling process of amine-thiol in the conjugate acceptors. Subsequently, hydrogen peroxide (7 μL , 30% aqueous solution) was utilized to oxidize the thiols into disulfide and a very viscose solution was produced. Next, the suspension was diluted and dissolved with chloroform and precipitated from cold methanol (repeat the purification process for three times). The product was dried under vacuum to offer product **17**.



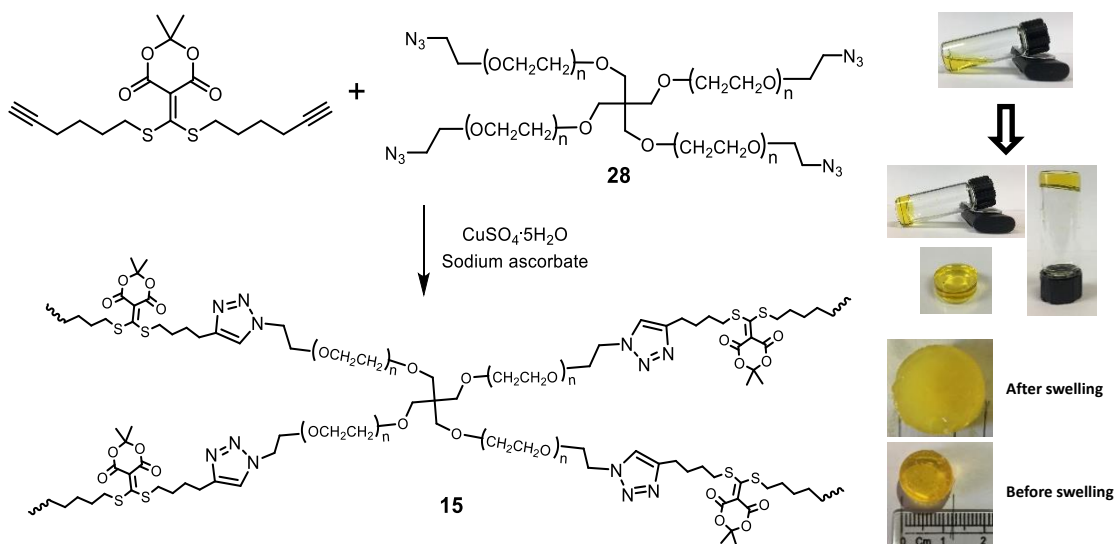
18: **13** (20 mg, $M_n = 5.4$ kg/mol) was dissolved in chloroform and PEG diamines **26** (20 mg, $M_n = 6.0$ kg/mol) was added into the yellow solution. The mixture was stirred for 24 hours and was diluted with chloroform and precipitated from cold methanol. The crude sample was placed on dialysis tube (4.0 kDa molecular weight cut-off) and then precipitated from cold methanol (repeat the purification process for three time). The product was dried under vacuum to offer a light-yellow product **18**.



14: In a 5 mL vial, conjugate acceptor **3** (200 mg, 0.52 mmol) and 1,3,5-tris(azidomethyl)benzene **27** (77 mg, 0.31 mmol) were dissolved in tetrahydrofuran (80 μ L). CuI (7 mg, 0.03 mmol) and TBTA (28 mg, 0.05 mmol) were dissolved in DMF (80 μ L). Sodium ascorbate (21 mg, 0.10 mmol) was dissolved in mili-Q water (80 μ L). The three ingredients were mixed together and shaken overnight. The viscous mixture was diluted with chloroform and then the solid was precipitated from cold methanol. The crude sample was placed on dialysis tube (4.0 kDa molecular weight cut-off) for overnight and dried under vacuum to offer a light-yellow product **14**.



19: **14** (70 mg, $M_n = 14.9$ kg/mol) was dissolved in THF/DMF mixture and **9** (10 mg, 0.061 mmol) was added into the suspension. The suspension was shaking for three hours. Subsequently, hydrogen peroxide (10 μL , 30% aqueous solution) was utilized to oxidize the thiols into disulfide and a cross-linked networking gel **19** was formed.



15: To a small vial was added **3** (7.5 mg, 20.0 μmol), four-arm PEG azides **28** ($M_n = 10.0$ kg/mol, 100 mg, 10.0 μmol), sodium ascorbate (2.0 mg, 10.0 μmol), copper sulfate (2.0 mg, 8.0 μmol) and then *tert*-butanol/Milli-Q water=1/1. The suspension was stirred to give a clear yellow solution.⁴⁰ Then the reaction mixture was stirred under a shaker for 30 mins and upon separation of the vial to offer a yellowish uniform hydrogel **15**. The hydrogel was washed in a neutral EDTA aqueous solution (10%) to extract the trapped copper, remove sodium ascorbate and noncross-linked molecules. Finally, the hydrogel was allowed to reach maximum water absorbance in HEPES buffer (pH 7.3) solution.

2.5 REFERENCES

1. Stuart, M. A. C.; Huck, W. T.; Genzer, J.; Müller, M.; Ober, C.; Stamm, M.; Sukhorukov, G. B.; Szleifer, I.; Tsukruk, V. V.; Urban, M., Emerging Applications of Stimuli-Responsive Polymer Materials. *Nat. Mater.* **2010**, *9* (2), 101-113.
2. Blum, A. P.; Kammeyer, J. K.; Rush, A. M.; Callmann, C. E.; Hahn, M. E.; Gianneschi, N. C., Stimuli-Responsive Nanomaterials for Biomedical Applications. *J. Am. Chem. Soc.* **2015**, *137* (6), 2140-2154.
3. Montero de Espinosa, L.; Meesorn, W.; Moatsou, D.; Weder, C., Bioinspired Polymer Systems with Stimuli-Responsive Mechanical Properties. *Chem. Rev.* **2017**, *117* (20), 12851-12892.
4. Shafrank, R. T.; Millik, S. C.; Smith, P. T.; Lee, C.-U.; Boydston, A. J.; Nelson, A., Stimuli-Responsive Materials in Additive Manufacturing. *Prog. Polym. Sci.* **2019**, *93*, 36-67.
5. Delplace, V.; Nicolas, J., Degradable Vinyl Polymers for Biomedical Applications. *Nat. Chem.* **2015**, *7* (10), 771-784.
6. Lamb, J. B.; Willis, B. L.; Fiorenza, E. A.; Couch, C. S.; Howard, R.; Rader, D. N.; True, J. D.; Kelly, L. A.; Ahmad, A.; Jompa, J., Plastic Waste Associated with Disease on Coral Reefs. *Science* **2018**, *359* (6374), 460-462.
7. Christensen, P. R.; Scheuermann, A. M.; Loeffler, K. E.; Helms, B. A., Closed-Loop Recycling of Plastics Enabled by Dynamic Covalent Diketoenamine Bonds. *Nat. Chem.* **2019**, *11* (5), 442-448.
8. Su, W.-F., Chemical and Physical Properties of Polymers. In *Principles of Polymer Design and Synthesis*, Springer Berlin Heidelberg: Berlin, Heidelberg, 2013; pp 61-88.
9. Scheutz, G. M.; Lessard, J. J.; Sims, M. B.; Sumerlin, B. S., Adaptable Crosslinks in Polymeric Materials: Resolving the Intersection of Thermoplastics and Thermosets. *J. Am. Chem. Soc.* **2019**, *141* (41), 16181-16196.
10. Reuther, J. F.; Dahlhauser, S. D.; Anslyn, E. V., Tunable Orthogonal Reversible Covalent (TORC) Bonds: Dynamic Chemical Control over Molecular Assembly. *Angew. Chem. Int. Ed.* **2019**, *58* (1), 74-85.

11. Cudjoe, E.; Herbert, K. M.; Rowan, S. J., Strong, Rebondable, Dynamic Cross-Linked Cellulose Nanocrystal Polymer Nanocomposite Adhesives. *ACS Appl. Mater. Interfaces* **2018**, *10* (36), 30723-30731.
12. Rowan, S. J.; Cantrill, S. J.; Cousins, G. R.; Sanders, J. K.; Stoddart, J. F., Dynamic covalent chemistry. *Angew. Chem. Int. Ed.* **2002**, *41* (6), 898-952.
13. Sun, H.; Kabb, C. P.; Sims, M. B.; Sumerlin, B. S., Architecture-Transformable Polymers: Reshaping the Future of Stimuli-Responsive Polymers. *Prog. Polym. Sci.* **2019**, *89*, 61-75.
14. Sun, H.; Kabb, C. P.; Dai, Y.; Hill, M. R.; Ghiviriga, I.; Bapat, A. P.; Sumerlin, B. S., Macromolecular Metamorphosis via Stimulus-Induced Transformations of Polymer Architecture. *Nat. Chem.* **2017**, *9*, 817-823.
15. Kolb, H. C.; Finn, M.; Sharpless, K. B., Click Chemistry: Diverse Chemical Function from a Few Good Reactions. *Angew. Chem. Int. Ed.* **2001**, *40* (11), 2004-2021.
16. Kolb, H. C.; Sharpless, K. B., The Growing Impact of Click Chemistry on Drug Discovery. *Drug. Discov. Today* **2003**, *8* (24), 1128-1137.
17. Qin, A.; Lam, J. W. Y.; Tang, B. Z., Click Polymerization. *Chem. Soc. Rev.* **2010**, *39* (7), 2522-2544.
18. Arslan, M.; Tasdelen, M. A., Click Chemistry in Macromolecular Design: Complex Architectures from Functional Polymers. *Chemistry Africa* **2018**, *2* (2), 195-214.
19. Binder, W. H.; Sachsenhofer, R., 'Click' Chemistry in Polymer and Materials Science. *Macromol. Rapid Commun.* **2007**, *28* (1), 15-54.
20. Binder, W. H.; Sachsenhofer, R., 'Click' Chemistry in Polymer and Material Science: an update. *Macromol. Rapid Commun.* **2008**, *29* (12-13), 952-981.
21. Diehl, K. L.; Kolesnichenko, I. V.; Robotham, S. A.; Bachman, J. L.; Zhong, Y.; Brodbelt, J. S.; Anslyn, E. V., Click and Chemically Triggered Declick Reactions through Reversible Amine and Thiol Coupling via a Conjugate Acceptor. *Nat. Chem.* **2016**, *8* (10), 968-973.
22. Johnson, A. M.; Anslyn, E. V., Reversible Macrocyclization of Peptides with a Conjugate Acceptor. *Org. Lett.* **2017**, *19* (7), 1654-1657.

23. Sun, X.; Anslyn, E. V., An Auto-Inductive Cascade for the Optical Sensing of Thiols in Aqueous Media: Application in the Detection of a VX Nerve Agent Mimic. *Angew. Chem. Int. Ed.* **2017**, *129* (32), 9650-9654.
24. Sun, X.; Shabat, D.; Phillips, S. T.; Anslyn, E. V., Self-Propagating Amplification Reactions for Molecular Detection and Signal Amplification: Advantages, Pitfalls, and Challenges. *J. Phys. Org. Chem.* **2018**, DOI: 10.1002/poc.3827.
25. Sun, X.; Boulgakov, A. A.; Smith, L. N.; Metola, P.; Marcotte, E. M.; Anslyn, E. V., Photography Coupled with Self-Propagating Chemical Cascades: Differentiation and Quantitation of G- and V-Nerve Agent Mimics via Chromaticity. *ACS Cent. Sci.* **2018**, *4* (7), 854-861.
26. Ishibashi, J. S. A.; Kalow, J. A., Vitrimeric Silicone Elastomers Enabled by Dynamic Meldrum's Acid-Derived Cross-Links. *ACS Macro Lett.* **2018**, *7* (4), 482-486.
27. Ben Cheikh, A.; Chuche, J.; Manisse, N.; Pommelet, J. C.; Netsch, K. P.; Lorencak, P.; Wentrup, C., Synthesis of Alpha.-Cyano Carbonyl Compounds by Flash Vacuum Thermolysis of (Alkylamino) Methylene Derivatives of Meldrum's Acid. Evidence for Facile 1, 3-Shifts of Alkylamino and Alkylthio Groups in Imidoylketene Intermediates. *J. Org. Chem.* **1991**, *56* (3), 970-975.
28. Meadows, M. K.; Sun, X.; Kolesnichenko, I. V.; Hinson, C. M.; Johnson, K. A.; Anslyn, E. V., Mechanistic Studies of a "Declick" Reaction. *Chem. Sci.* **2019**, *10* (38), 8817-8824.
29. Bräse, S.; Banert, K., *Organic Azides: Syntheses and Applications*; Wiley: Chichester, U.K., 2010.
30. Chawla, K. K.; Meyers, M., *Mechanical Behavior of Materials*. Prentice Hall: 1999.
31. Zheng, Y.; Li, S.; Weng, Z.; Gao, C., Hyperbranched Polymers: Advances from Synthesis to Applications. *Chem. Soc. Rev.* **2015**, *44* (12), 4091-4130.
32. Oliva, N.; Conde, J.; Wang, K.; Artzi, N., Designing Hydrogels for On-Demand Therapy. *Acc. Chem. Res.* **2017**, *50* (4), 669-679.
33. Zhu, Z.; Yang, C. J., Hydrogel Droplet Microfluidics for High-Throughput Single Molecule/Cell Analysis. *Acc. Chem. Res.* **2017**, *50* (1), 22-31.
34. Förster, S.; Antonietti, M., Amphiphilic Block Copolymers in Structure-Controlled Nanomaterial Hybrids. *Adv. Mater.* **1998**, *10* (3), 195-217.

35. Rösler, A.; Vandermeulen, G. W.; Klok, H.-A., Advanced Drug Delivery Devices via Self-Assembly of Amphiphilic Block Copolymers. *Adv. Drug Deliv. Rev.* **2001**, *53* (1), 95-108.
36. Alexandridis, P.; Lindman, B., *Amphiphilic Block Copolymers: Self-Assembly and Applications*. Elsevier: 2000.
37. Markoski, L.; Thompson, J.; Moore, J., Indirect Method for Determining Degree of Branching in Hyperbranched Polymers. *Macromolecules* **2002**, *35* (5), 1599-1603.
38. Mohapatra, H.; Phillips, S. T., Using Smell To Triage Samples in Point-of-Care Assays. *Angew. Chem. Int. Ed.* **2012**, *51* (44), 11145-11148.
39. Von Delius, M.; Geertsema, E. M.; Leigh, D. A., A Synthetic Small Molecule that can Walk Down a Track. *Nat. Chem.* **2010**, *2*, 96-101.
40. Malkoch, M.; Vestberg, R.; Gupta, N.; Mespouille, L.; Dubois, P.; Mason, A. F.; Hedrick, J. L.; Liao, Q.; Frank, C. W.; Kingsbury, K.; Hawker, C. J., Synthesis of Well-Defined Hydrogel Networks using Click Chemistry. *Chem. Commun.* **2006**, *26*, 2774-2776.

Chapter 3: A Self-Degradable Hydrogel Sensor for a Nerve Agent Tabun Mimic through a Self-Propagating Cascade²

Nerve agents which irreversibly deactivate the enzyme acetylcholinesterase are extremely toxic weapons of mass destruction used in acts of terror and criminal warfare. Thus, developing methods to detect these lethal chemicals are of the utmost importance. To create an optical sensor for a surrogate of the nerve agent tabun, as well as a physical barrier that dissolves in response to this analyte, we devised a network hydrogel that decomposes via a self-propagating cascade. A Meldrum's acid-derived linker was incorporated into a hydrogel which undergoes a declick reaction in response to thiols, thereby breaking network connections, which release more thiols; propagating the response throughout the gel. In essence, the gel is self-degrading upon being triggered. A combination of chemical reactions triggered by the addition of the tabun mimic initiates the cascade. The dissolving barrier was used to release dyes, as well as nanoparticles that undergo a spontaneous aggregation. Thus, this sensing system for tabun generates a physical response and the delivery of chemical agents, in response to an initial trigger.

²This chapter was adapted from the article: Lee, D.-H.; Valenzuela, S. A.; Dominguez, M. N.; Otsuka, M.; Milliron, D. J.; Anslyn, E. V. A Self-Degradable Hydrogel Sensor for a Nerve Agent Tabun Mimic through a Self-Propagating Cascade. *Cell Reports Physical Science* **2021**, in press.

3.1 INTRODUCTION

A hydrogel is a network in which a hydrophilic polymer forms a three-dimensional architecture that gels water. Hydrogels do not dissolve in an aqueous environment, instead they can swell and contain large amounts of water.^{1,2} Due to these characteristics, hydrogels are flexible enough to act like natural tissues. In addition, it is feasible to control the mechanical integrity, porosity, and degradation properties of hydrogels by adjusting parameters such as synthesis conditions, types of polymers used in the gel, molecular weight, and crosslinking density. As a result, hydrogels are widely used in biomedical applications such as contact lenses, hygiene products, wound dressings, scaffolds for protein recombination, and drug delivery systems.^{3,4}

Hydrogels applied to delivery systems are employed to load and release drugs by exploiting their porous structure and/or degradation.^{3,5} Their porosity can be changed by controlling the crosslinking density as well as the polymer's affinity for water in the matrix. One can load a drug by mixing it with a precursor of the hydrogel or by swelling the hydrogel in a solution of the drug. The release proceeds through various mechanisms such as diffusion control, swelling control, chemical control, and environment-reactive release.⁶ Therefore, the loading and degradation ability of hydrogels is a critical factor in delivery systems. We envisioned that environment-reactive release could be used both in the detection of, and for triggering a response to, chemical warfare agents.

Chemical warfare agents (CWAs) are highly hazardous compounds that have been used in terrorism as well as in wars. Among CWAs, nerve agents that contain an organophosphorus functional group have been the most exploited weaponized agent. They trigger activation of the parasympathetic nervous system, causing fatal injuries to humans. Since first developed during World War II, nerve agents have been employed in the Iraq-Iran conflict during the 1980-1988,⁷ the Syrian civil war in 2013, an

assassination in 2017 of a North Korean political affiliate, and the death of a former Russian military officer family in the UK in 2018. Even though CWAs were banned by OPCW and 193 member states joined the convention,⁸ they are still employed because of their low price and ease of synthesis. To avoid these threats, it is important to detect and eliminate them.

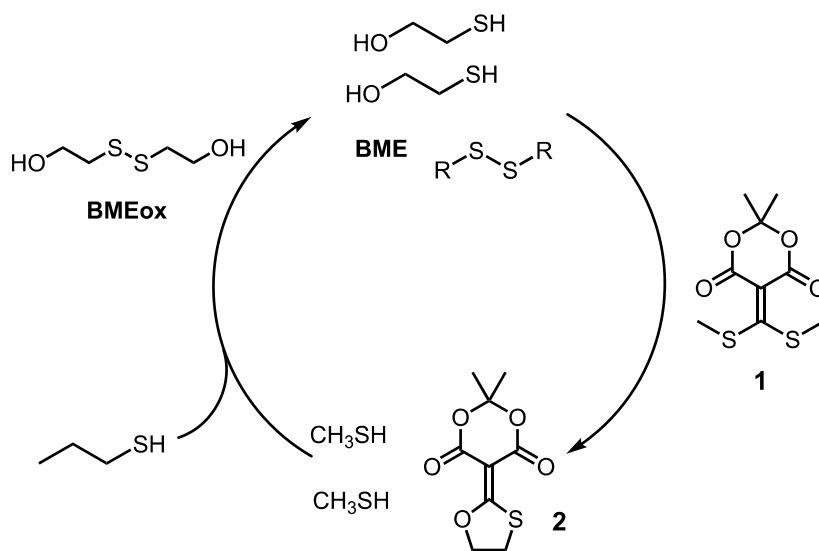
Hydrogels have been used previously in nerve agent detection, including studies on the release of entities attached to the gels,^{9,10} fluorescence sensors using fluorophore-integrated smart hydrogels,¹¹ and photonic crystal hydrogel sensors.^{12,13} However, these studies induced small changes in the signaling units included in the hydrogel or the particle spacing.

Herein, we report a hydrogel that self-degrades via a self-propagating cascade in response to a surrogate of the nerve agent tabun. The hydrogel undergoes a large physical change, *i.e.*, complete degradation when triggered to do so via a chemical agent generated from the nerve agent mimic, thereby transforming the hydrogel from a gel to a sol easily seen with the naked eye. Further, because this reaction is carried out via a self-propagating cascade, less than an equivalent of the trigger is needed to induce dissolution. The self-propagating cascade amplifies the detection through a cascade cycle, so only ppb levels of analyte are needed.¹⁴ Further, this sensor was designed to detect the tabun surrogate selectively among a variety of nerve agents. Because only tabun has a cyanide as a leaving group, a series of reactions initiated by cyanide that generate a thiol trigger was developed, thereby imparting selectivity to the sensing event.

3.2 DESIGN CRITERIA

We previously reported that derivatives of Meldrum's acid, **1**, shown in **Scheme 1**, can click together different thiols, or amines with thiols, following by a declicking with

β -mercaptoethanol (**BME**) or dithiothreitol (**DTT**), respectively.¹⁵ In the context of an auto-inductive cascade, such a monomer can be used to amplify the number of thiols present in a solution via addition of ppb levels of a thiol trigger.¹⁴ As **Scheme 3.1** portrays, addition of the trigger to a solution of disulfide-linked **BME** (**BMEox**) leads to disulfide exchange, releasing **BME** that declicks **1** to release two equivalents of methanethiol and product **2**, thus doubling the number of thiol-triggers each time the cycle turns over until all of **1** is consumed. This cascade was previously used to create an exquisitely sensitive sensor for V-nerve agent surrogates because thiols are the biproducts of their hydrolysis.¹⁴



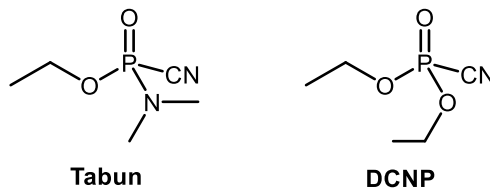
Scheme 3.1 A thiol auto-inductive cascade in the previous work.

Tabun, however, is not a V-nerve agent, and thus does not release thiols, but instead releases cyanide upon hydrolysis.¹⁶ Thus, in order to trigger the auto-inductive cascade of **Scheme 3.1** we required a series of reactions that could occur with a tabun

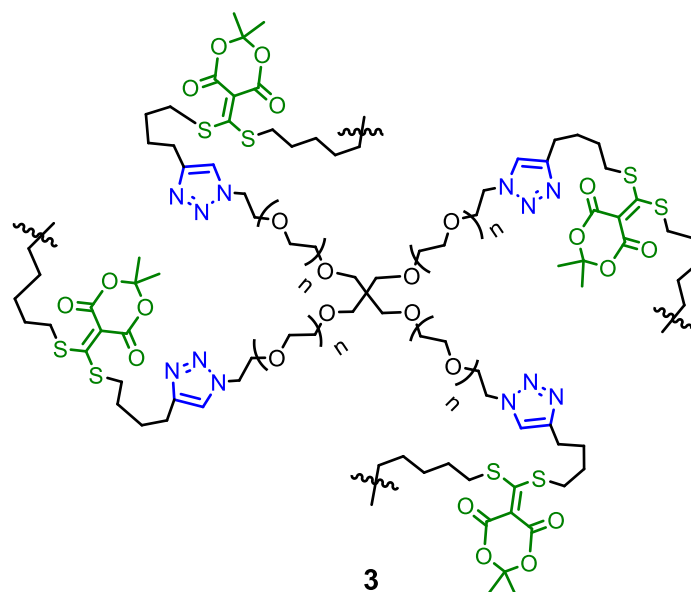
mimic to ultimately generate an equivalent of thiol for each equivalent of the mimic. Due to the risks associated with working with nerve agents, experiments are generally performed using surrogate molecules that are safer to handle than real CWAs, but with similar chemical behavior and structure.¹⁷⁻²⁰ We choose diethyl cyanophosphate (**DCNP**) as the tabun mimic, and as described below two reactions initiated by cyanide to release a thiol were devised (**Scheme 3.2a**). Admittedly, for the real agent the experimental conditions may need to be adjusted to accommodate small differences in reactivity.

We have also previously reported that Meldrum's acid derivatives analogous to **1** can be used as linkers to generate hydrogels using thiol containing monomers, and that the gels can be degraded to small molecules with equal equivalents of **BME** or **DTT** to the Meldrum's acid linker.²¹ In this work, hydrogel **3**, shown in **Scheme 2B**, was prepared via copper-catalyzed azide-alkyne cycloaddition (CuAAC) reactions to introduce branched monomers (PEG-azide ($MW = 10,000$)) and create triazole linkers (blue), while the Meldrum's acid linkers (green) were used to degrade in response to the addition of **BME** or **DTT**. Similarly, the Kalow group has recently reported a series of polymers using analogous linking units. They developed vitrimeric silicone elastomers with a Meldrum's acid derivative and thiol-functionalized polydimethylsiloxane through a conjugate addition of thiols. Adding 1-mercapto-2-propanol to the expanded network permanently disrupted the network cross-linking, resulting in complete dissolution.²²

(a)

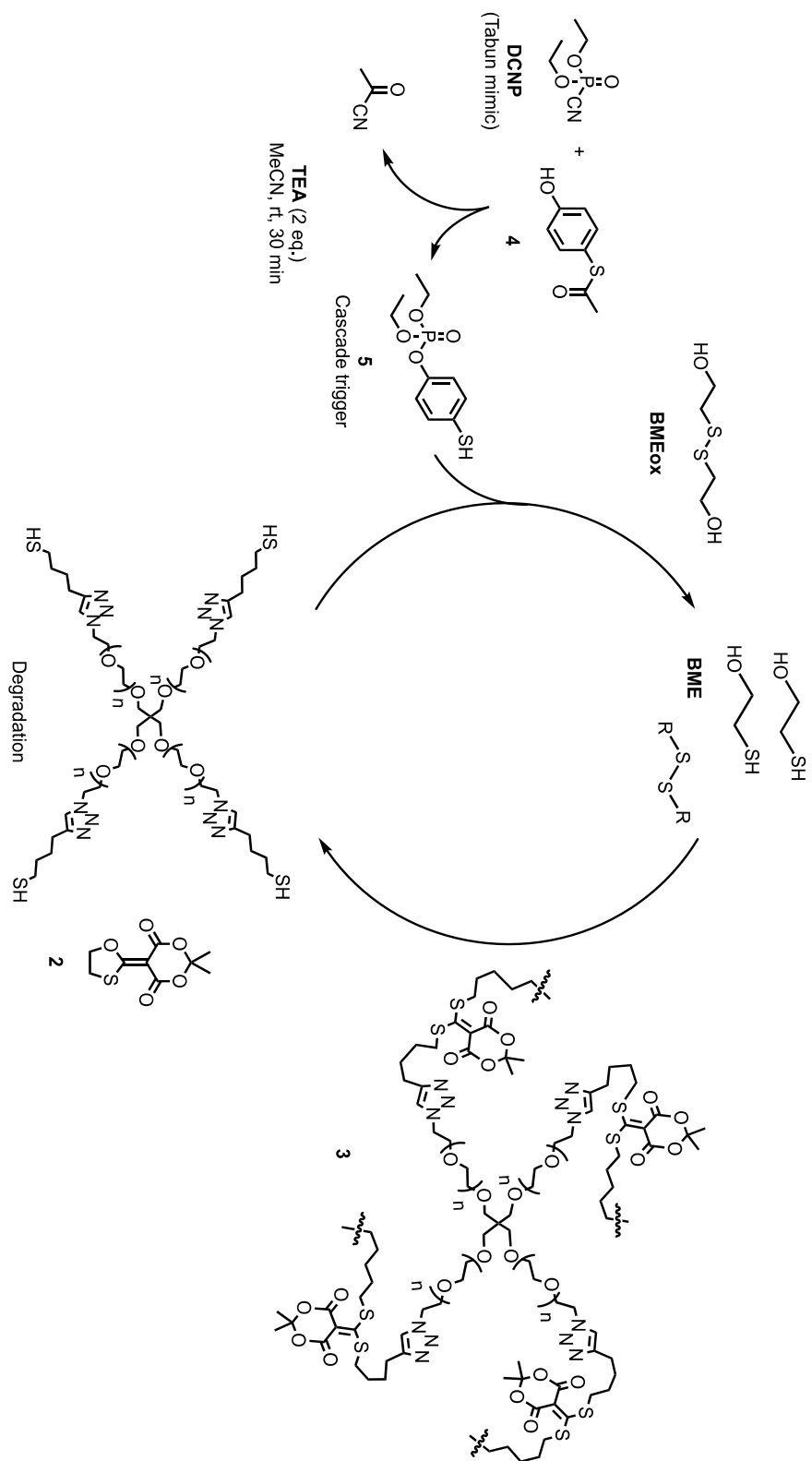


(b)



Scheme 3.2 Selected tabun mimic and synthesized hydrogel.

The goal of the study presented here was to combine the auto-inductive cascade of **Scheme 1** with the degradable hydrogel shown in **Scheme 2B**. The hypothesis was that upon **BME** declick of any of the Meldrum's acid-derived linkages in **3** would result in two equivalents of thiol being generated, analogous to the two equivalents of methanethiol generated in the cascade shown in **Scheme 1**. Thus, the gel generates the thiols that propagate the cycle as the degradation proceeds, each time creating the five-membered ring product **2** (**Scheme 3**). In essence, the gel self-degrades upon being triggered with a thiol. Finally, we envisioned that triggering the auto-inductive degradation of a physical barrier created by the self-degrading hydrogel could be used to release chemical agents, and we demonstrate this with both colorimetric indicators and nanocrystals.

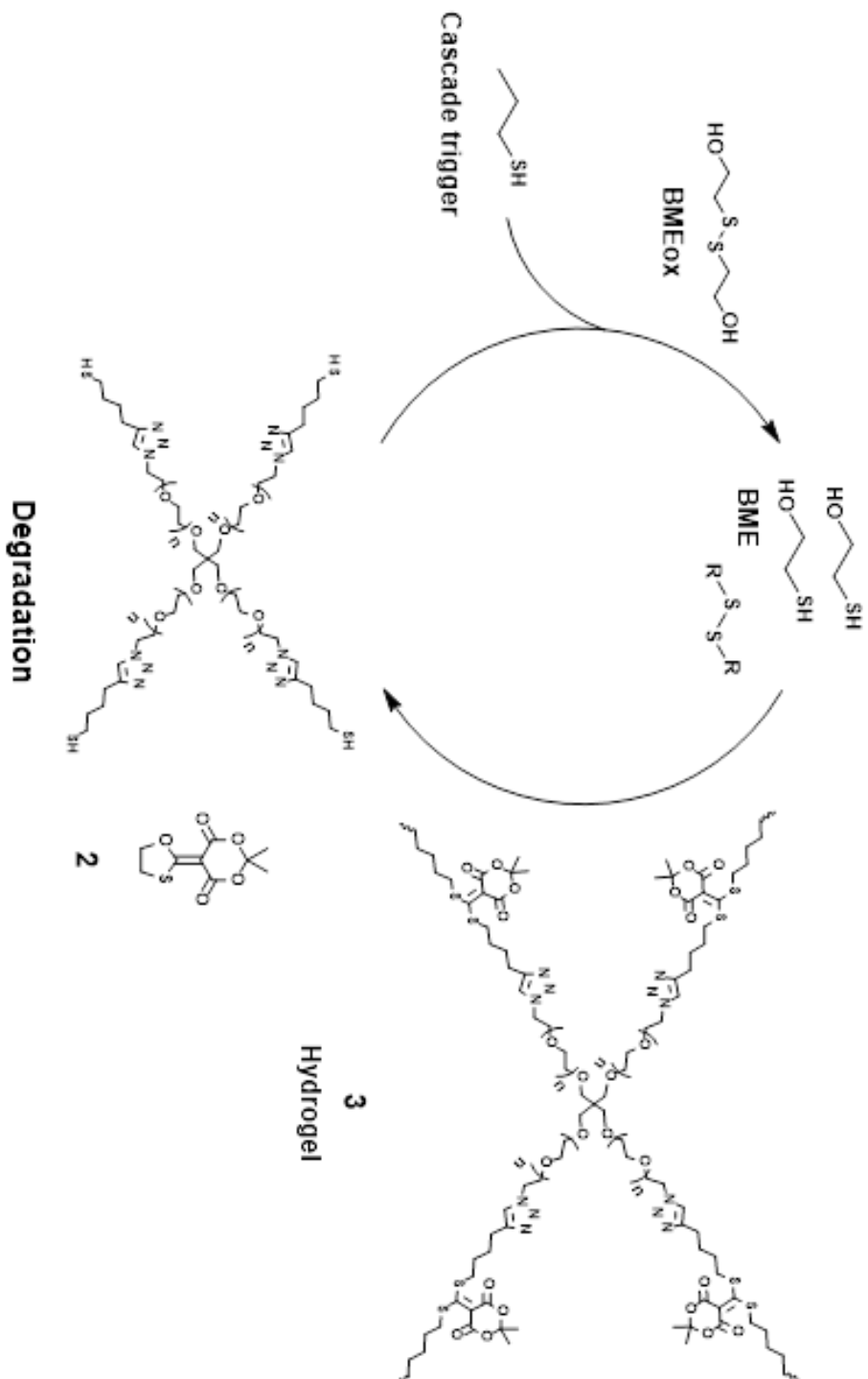


Scheme 3.3 Detection of a tabun mimic via a self-propagating cascade with perturbation of gel formation.

3.3 RESULTS AND DISCUSSION

3.3.1 Preliminary Test

In our previous work, compound **1** was successfully used in the auto-inductive cascade shown in **Scheme 1** using butanethiol as the trigger in a pH 10 buffered solution (borax/sodium hydroxide buffer).¹⁴ Before carrying out the detection of a tabun mimic, a preliminary test was conducted to determine if placement of Meldrum's acid linkers analogous to **1** within gel **3** would lead to a similar cascade (**Scheme 3.4, Figure 3.1**). Rhodamine 6-G (**R6G**) was added during the synthesis of hydrogel **3** to confirm the changes with a quantitative analysis. Kinetics experiments were conducted with the **R6G**-containing gel, 2-hydroxyethyl disulfide (**BMEox**) and butanethiol at different concentrations. The equivalents were determined relative to the number of the Meldrum's acid linking units in **3**. Each compound was added to centrifuge tubes with 5 ml of pH 10 buffer. After shaking the tubes for time periods of 5, 10, 20, 30, 40, 50 and 60 minutes, 100 μ l of solution was collected by a pipette for optical analysis. According to these time points, gel **3** was entirely degraded after 40 minutes in both 0.1 and 0.3 equivalents of butanethiol, whereas the changes in the two other samples at pH 10, without the thiol trigger, showed only 15% to 20% as much **R6G** release (**Figure 3.1-3**), presumably due to some extent of gel degradation or diffusion of **R6G** out of the hydrogel. Another key difference with the study reported here is the use of pH 7.3, which nearly eliminates all degradation and **R6G** release without addition of a thiol (**Figure 3.4**). Thus, this study confirmed that if a substance capable of reducing **BMEox** was introduced to the gel,²³ the auto-inductive cascade would be triggered to commence, and the gel thereby entirely self-degraded.



Scheme 3.4 A hydrogel self-propagating cascade into a solution via degradation in preliminary test.

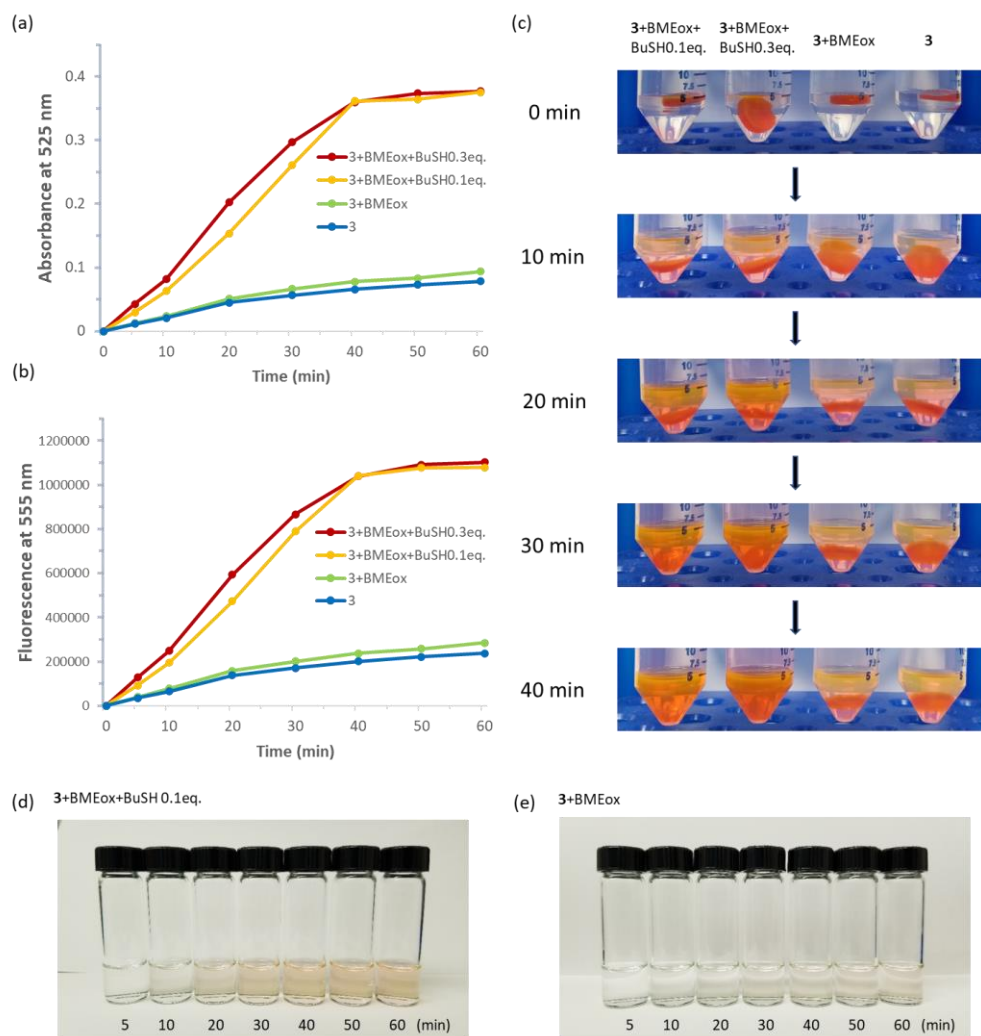


Figure 3.1 Kinetics experiments for the preliminary test results of **Scheme 3.3**. Butanethiol was exploited as the thiol trigger and it was conducted in pH 10 (borax/sodium hydroxide buffer). **3** was synthesized with Meldrum's acid derivative 5 μmol and four-arm PEG azides 2.5 μmol . Rhodamine 6-G was added during the synthesis of **3**. There were four samples **3** + 2-hydroxyethyl disulfide (BMEox) 5 μmol + butane thiol 0.5 μmol (0.1 equivalent), **3** + BMEox 5 μmol + butane thiol 1.5 μmol (0.3 equivalent), **3** + BMEox 5 μmol and only **3**. (a) Absorbance spectra at 525 nm. (b) Fluorescence intensity at 555 nm. It was obtained by excitation at 470 nm. (c) Photograph showing changes of **3** from a hydrogel to a solution. (d) Optical changes of the first sample (**3** + BMEox 5 μmol + butane thiol 0.5 μmol (0.1 equivalent)) with extracted solution. (e) Optical changes of the third sample (**3** + BMEox 5 μmol) with extracted solution.

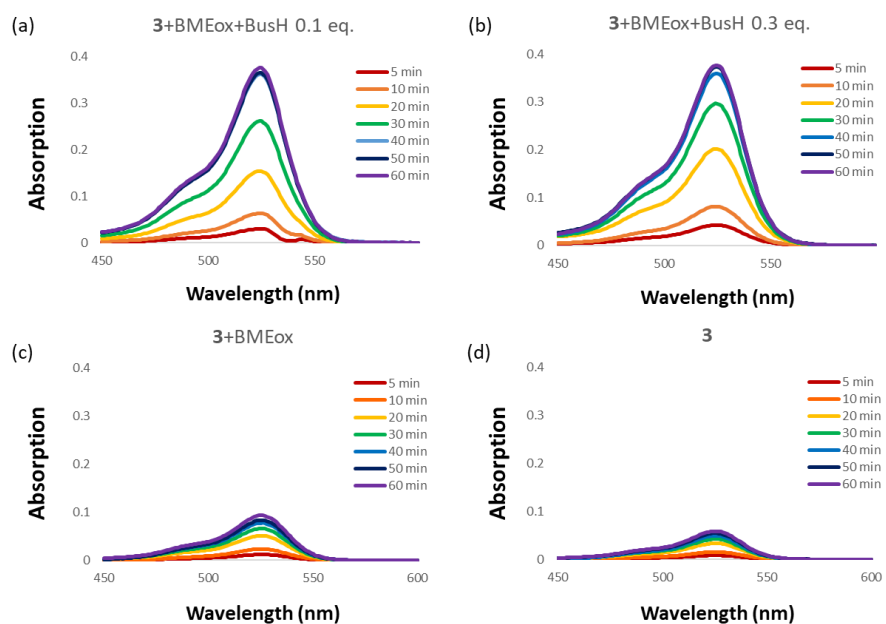


Figure 3.2 Absorption data of the preliminary test. (**Figure 3.1a**) (a) **3** + BMEox + butane thiol 0.1 equivalent, (b) **3** + BMEox + butane thiol 0.3 equivalent, (c) **3** + BMEox, (d) **3** were added in 5 ml of pH 10 buffer.

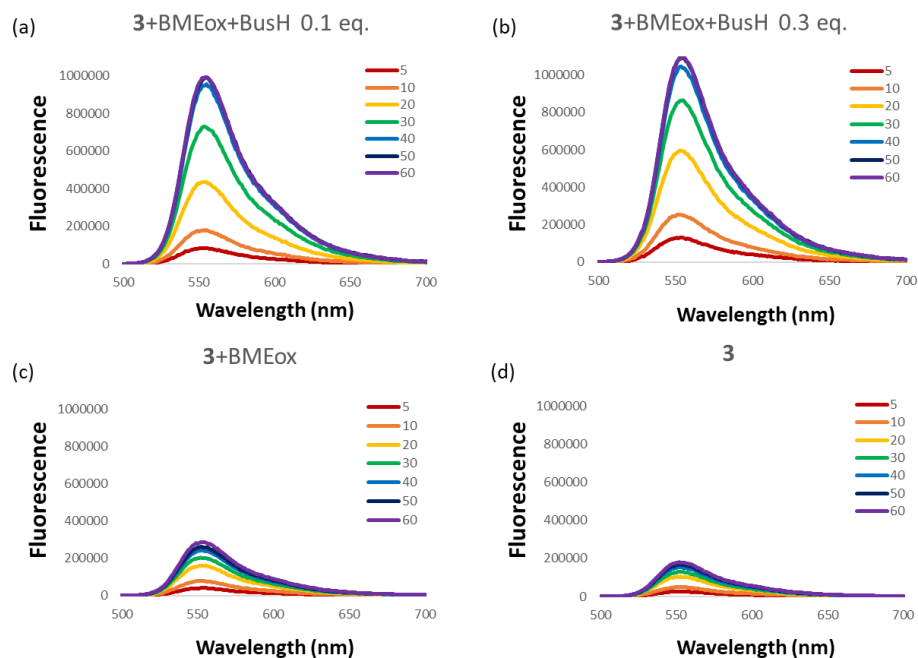


Figure 3.3 Fluorescence data of the preliminary test ($\lambda_{ex} = 470$ nm). (**Figure 3.1b**) (a) **3** + BMEox + butane thiol 0.1 equivalent, (b) **3** + BMEox + butane thiol 0.3 equivalent, (c) **3** + BMEox, (d) **3** were added in 5 ml of pH 10 buffer.

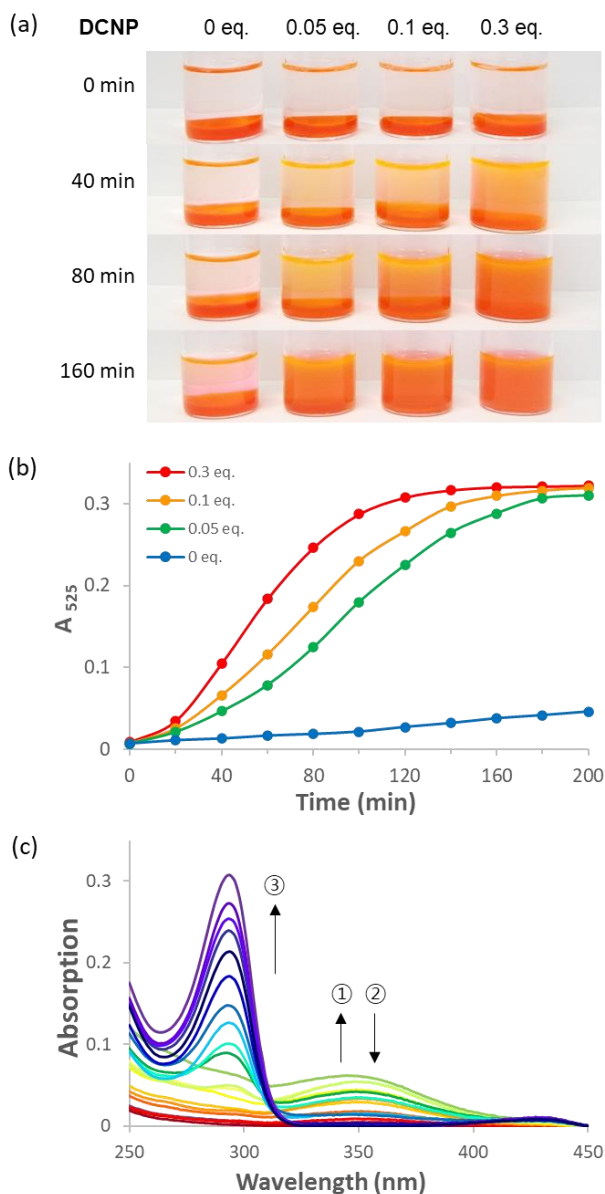
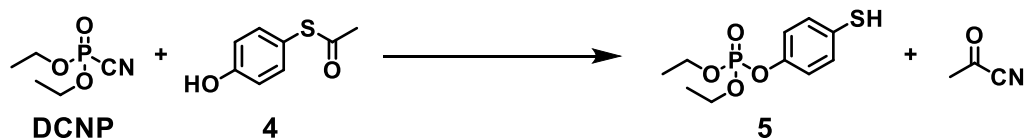


Figure 3.4 A titration study at physiological pH (phosphate-buffered saline (PBS)). After reacting **4** (1.5 μmol), **DCNP** (0, 0.25, 0.5, and 1.5 μmol), and triethylamine (3 μmol) in acetonitrile for 30 minutes, the resulting mixture was added to 5 ml PBS buffer in the presence of **BME-ox** (5 μmol) and **3** with **R6G**. The reactions were then shaken. (a) Photos of the four samples with different amount of **DCNP**. (b) Absorption data for the time dependent release of **R6G** from the degradation of **3** at 525 nm. (c) Absorption spectra of kinetic data with 0.25 μmol of **DCNP**. The spectra were changed according to the numbers and arrows.

3.3.2 Optimized Conditions and Rate Constant for the Thiol Trigger

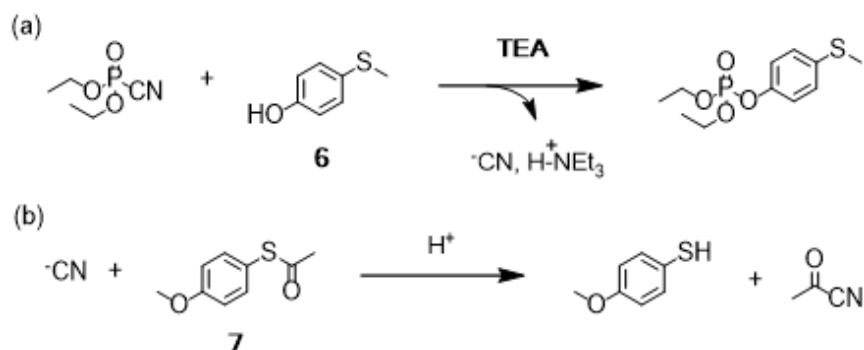
To generate a thiol trigger for detection of tabun surrogate **DCNP**, initiator **4** was designed (**Scheme 3.3**). We anticipated that the phenol group of **4** would add to the phosphoryl center of **DCNP** and the thioester would be electrophilic enough to capture the cyanide leaving group, thereby generating aromatic thiol **5** that could be used to trigger the dissolution of gel **3**. Compound **4** is both nucleophilic (the phenol) and electrophilic (the thioester), yet it is a stable white powder and does not react with itself in solution at pH 7. However, as previously stated, to generate product **5** the phenol must react with **DCNP**^{24,25} while the thioester must react with cyanide.²⁶ Thus, we sought to explore the relative rates of these two reactions that involve **4**. We first varied four conditions to maximize the yield of **5**: solvent, temperature, time, and basicity. Acetonitrile, acetone, DMF, DMSO, and water were tested as solvents. Among them, acetonitrile had the highest yield of **5**. Similarly, we varied temperature, time, and basicity. As a result, an optimized condition for the highest yield of **5** was obtained: 25 °C, 30 minutes, and 2 equivalents of triethyl amine (TEA) in acetonitrile (**Table 3.1**).



m/z (-ESI)	167	261	385	521
Retention time in LC/MS	5.0 min	7.2 min	9.3 min	10.1 min
Solvent (TEA 2 eq., 25°C, 1h) (%)				
MeCN	5	73	0	22
DMF	20	61	3	16
THF	11	69	1	18
acetone	5	73	1	20
water	25	59	2	15
DMSO	18	61	2	19
Amount of TEA (MeCN, 25°C, 1h) (%)				
0.1 eq.	100	0	0	0
0.5 eq.	58	22	2	18
1 eq.	36	43	2	19
2 eq.	5	73	0	22
10 eq.	15	47	7	31
70 eq.	9	13	24	54
Temperature (TEA 2 eq., MeCN, 1h) (%)				
25 °C	5	73	0	22
50 °C	30	47	3	20
75 °C	22	52	6	20
Time (TEA 2 eq., MeCN, 25°C) (%)				
10 min	16	50	2	32
0.5 h	6	73	1	20
1 h	5	73	0	22

Table 3.1 Experiment results to find optimized conditions to obtain **5** from LC/MS data. The numbers in the table are the ratio (%) among the four products above. Between 0.5 and 1 hour, the yield of **5** did not significantly change. Due to the negligible yield difference between 0.5 and 1 hour, the 0.5-hour reaction time was adopted due to the relative speed to obtaining results.

Using these conditions, we set out to explore model reactions to analyze the relative rates of the reactions that would initiate the cascade of **Scheme 3.5**. There were two model reactions. The first was a model of the phenol attacking the phosphorus center of **DCNP** (**Scheme 3.5a**), and the second was a model for the released cyanide reacting with a thioester (**Scheme 3.5b**). In **6** the thioester of initiator **4** was replaced with a thioether and in **7** the phenol of **4** was protected with a methyl group. The kinetic studies were carried out via UV-Vis spectroscopy. While keeping the concentration of **6** and **7** constant, the change of the reaction was followed for 2 hours with different **DCNP** and cyanide concentrations (1, 2, 3, and 4 equivalents), respectively (**Figure 3.5** and **3.7**). For the reaction of cyanide anion with **7**, we employed 18-crown-6 (50 μM) to dissolve potassium cyanide (50 μM). The concentrations of **6** and **7** were monitored, and using these results, rate constants were calculated.²⁷ The 2nd order rate constant of the reaction between **6** and **DCNP** was $0.66 \text{ M}^{-1} \text{ min}^{-1}$ (**Figure 3.5d**) and for the reaction between **7** and cyanide anion the rate constant was $2.67 \text{ M}^{-1} \text{ min}^{-1}$ (**Figure 3.7d**). Thus, the reaction of the phenol with **DCNP** is approximately 4 times slower than the reaction of cyanide with the thioester. Hence, it is the reaction between the trigger and the tabun surrogate that limits the rate of the initiator **4** to trigger the cascade.



Scheme 3.5 Model studies for rate constant. (a) Model reaction to release cyanide. (b) Model reaction for cyanide capture and thiol release.

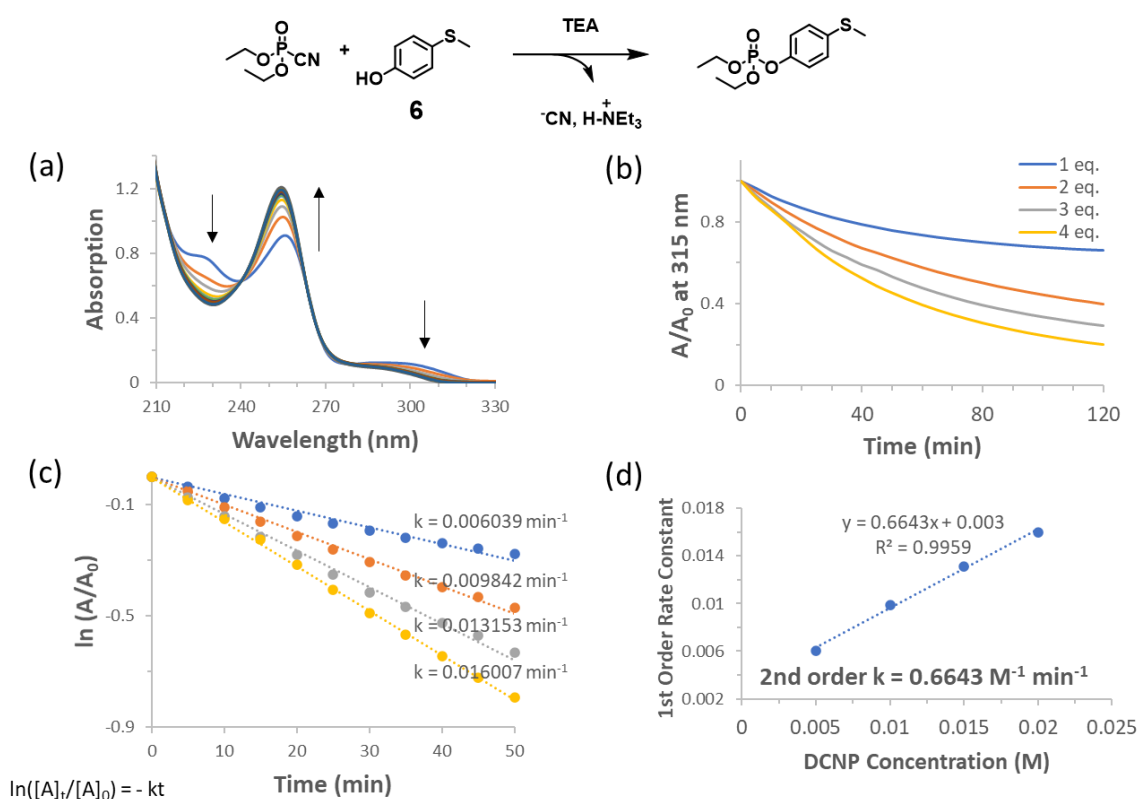


Figure 3.5 (a) Time kinetic studies with absorption changes of DCNP and **6** in acetonitrile in the presence of 2 equivalent of triethyl amine. (b) Time kinetic results for a concentration of **6** based on the absorption data spectra. 1, 2, 3, and 4 equivalents DCNP were added separately into acetonitrile in the presence of **6** (5 mM), and triethyl amine (10 mM). (c) First order rate constant was calculated from (b). Y-axis is $-kt$, so the slope is regarded as $-k$. (d) Second order rate constant was calculated with concentration of DCNP and the first order rate constant (c).

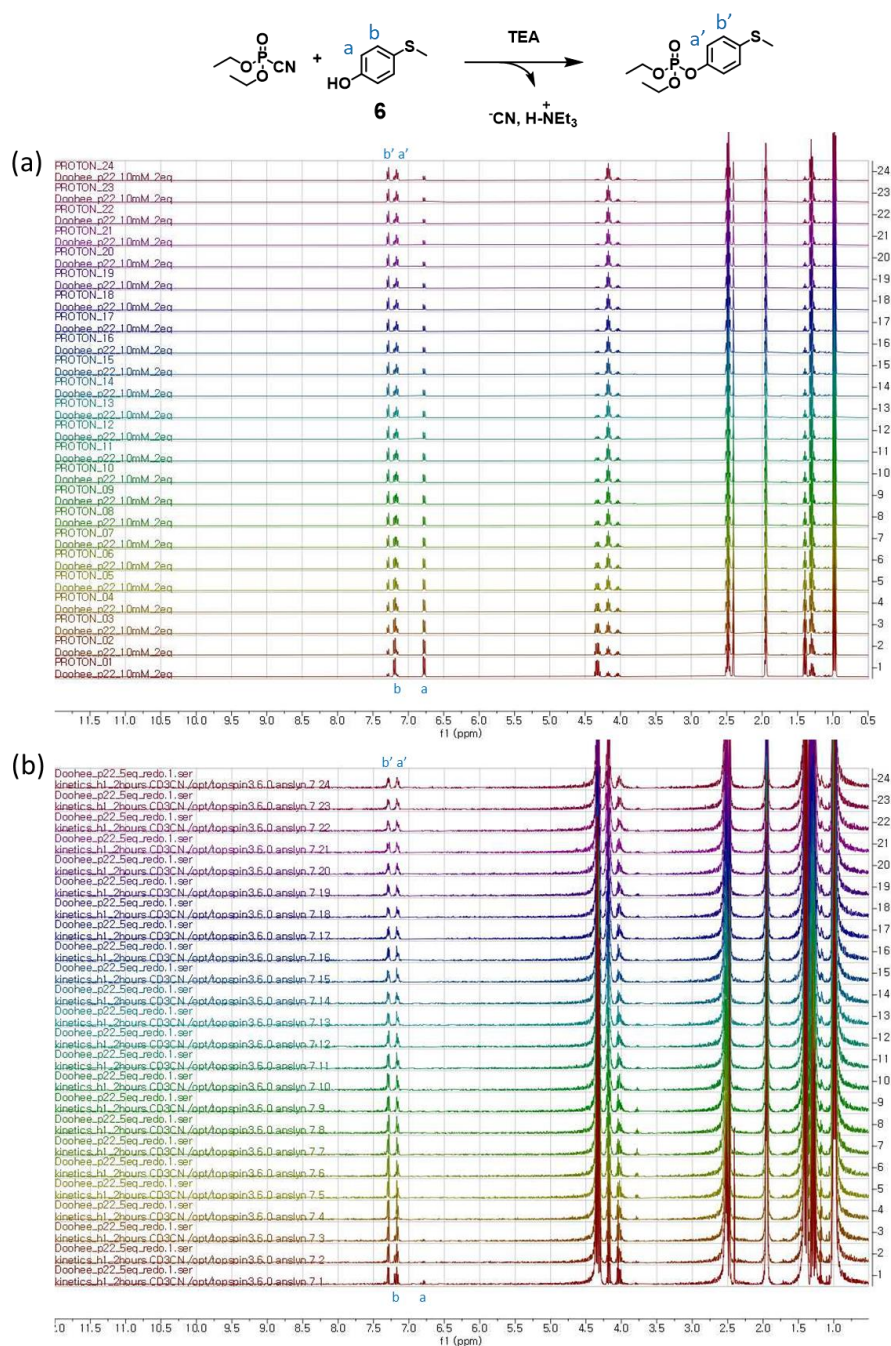


Figure 3.6 ¹H NMR kinetic studies between DCNP and **6**. There are 24 NMR results each and they were taken every 5 minutes for 2 hours. (a) 2 equivalents DCNP (20 mM) was added into acetonitrile-d in the presence of **6** (10 mM), and triethyl amine (20 mM). The disappearance of **a** was monitored over time. (b) 5 equivalents DCNP (50 mM) was added into acetonitrile-d in the presence of **6** (10 mM), and triethyl amine (20 mM).

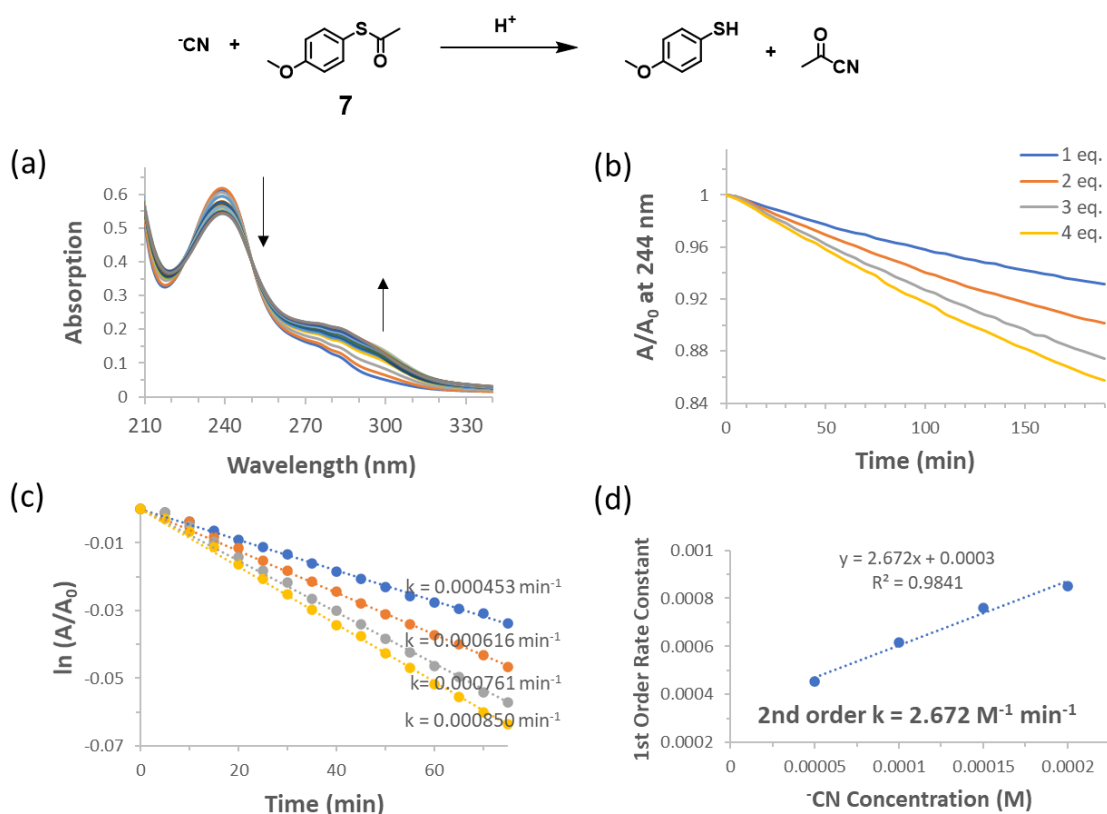


Figure 3.7 (a) Time kinetic studies with absorption changes of cyanide and **7** in acetonitrile. Cyanide was prepared from the mixture of potassium cyanide and 18-crown-6. (b) Time kinetic results for a concentration of **7** based on the absorption data spectra. 1, 2, 3, and 4 equivalents cyanide were added separately into acetonitrile in the presence of **7** (50 μM). (c) First order rate constant was calculated from (b). Y-axis is $-kt$, so the slope is regarded as $-k$. (d) Second order rate constant was calculated with concentration of cyanide and the first order rate constant (c).

3.3.3 Titration Studies at pH 10 and 7.3

Once the conditions for the reactions that would initiate the auto-inductive cascade and their model kinetics were obtained, we turned to triggering the dissolution of hydrogel **3**. After the initiation step was conducted in acetonitrile to generate the thiol trigger, aliquots were transferred to aqueous solutions containing the gels and the cascade studies were performed in pH 10 buffer (as were the preliminary tests using butanethiol described above). There were four samples of equal weight of gel **3** (128 mg) and equal concentrations of probe **4** (300 μM), while the amount of **DCNP** was varied between 0, 0.05, 0.1 and 0.3 equivalents relative to the Meldrum's acid linkers in hydrogel **3**. As anticipated, the three samples containing **DCNP** led to hydrogel degradation (**Figure 3.8**) while zero equivalents gave far less degradation. This result is meaningful because it confirmed that probe **4** released a thiophenol that in turn triggered the dissolution of the hydrogel.

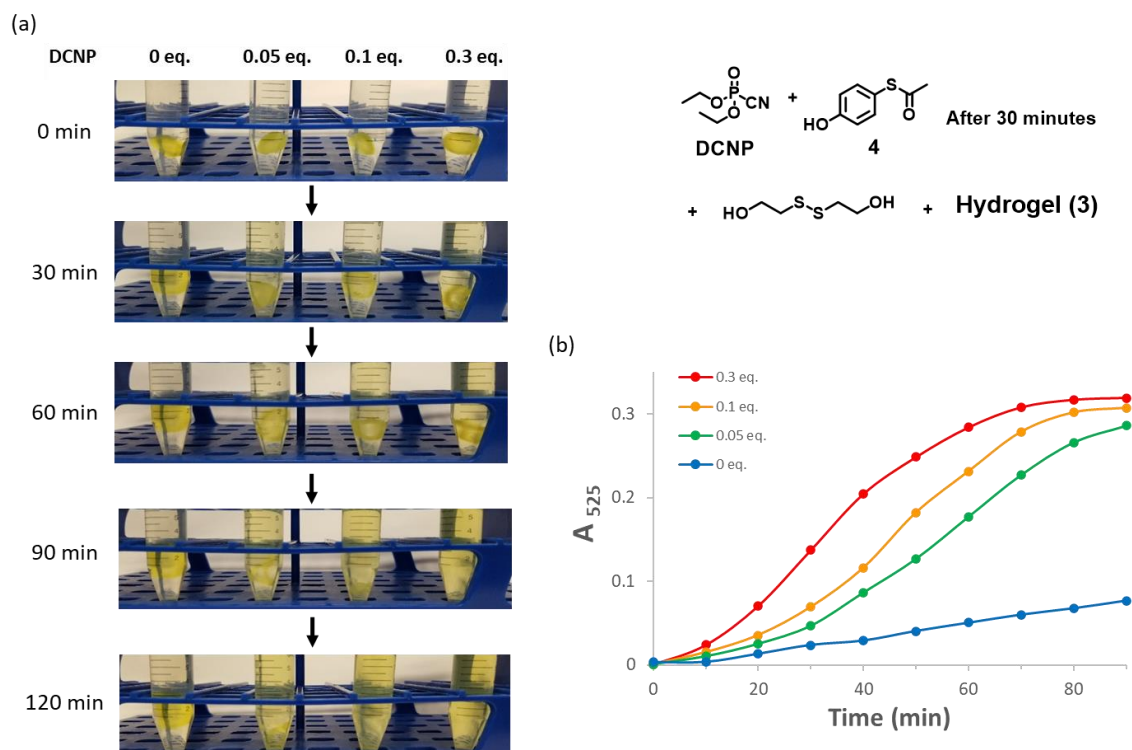


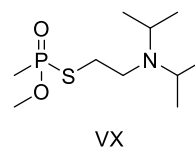
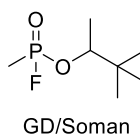
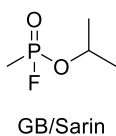
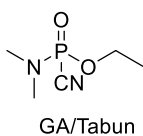
Figure 3.8 Kinetics titration study at pH 10 buffer (borax/sodium hydroxide buffer). After reacting **4** (5 μmol), DCNP (0, 0.25, 0.5, and 1.5 μmol), and triethylamine (10 μmol) in acetonitrile for 30 minutes, the resulting mixture was added to the pH 10 buffer 5 mL in the presence of 2-hydroxyethyl disulfide (5 μmol) and **3**. (a) Photos of the four samples with varying amounts of DCNP without Rhodamine 6G. The equivalent (eq.) is the ratio between the conjugate acceptor in **3** and DCNP: 0, 0.05, 0.1, and 0.3 (left to right). (b) Absorption data of time dependent titration for degradation of **3** with Rhodamine 6G. Absorption (525 nm) was measured by extracting 100 μL of each solution at intervals of 10 minutes for a total of 90 minutes.

We next explored physiological pH 7.3 instead of pH 10, all other conditions remaining the same. At pH 7.3, thiophenols (such as **5**) are substantially ionized while alkylthiols (such as butanethiol, recall **Figures 3.1-3.3**) are not,²⁸ and hence we expected the cascade to still function well at this lower pH. Indeed, the results were similar except that the hydrogel took longer to degrade (time dependent data, **Figure 3.4b**). The shape of the time-dependent data plots shows an initiation period as the cascade starts degrading, an exponential rise due to auto-induction, followed by a plateau as all the Meldrum's acid linkers in **3** are consumed. Importantly very little degradation occurs without **DCNP**. Further, at either pH 10 or 7.3, the Meldrum's acid linkers in gel **3** could be observed to generate **2** via UV-Vis absorption spectroscopy due to a hypsochromic shift of the I_{\max} of 350 nm \rightarrow 290 nm (**Figure 3.4c**), as we have observed in previous systems.¹⁴ Hence, **Figure 3.4** shows three different ways to follow the optical response to the tabun mimic **DCNP**. While these three responses could be used to quantitate the concentration of **DCNP** as we have done in other contexts,¹⁴ the goal for this study was to trigger gel degradation and use it as a delivery agent. Interestingly, however, there is another informative aspect to the UV-Vis traces given in **Figure 3.4c** that gives insight into the time-evolution of gel degradation. As the peak at 350 nm increased and decreased according to the time sequence, the peak at 290 nm indicative of **2** continually increased. Initially, because hydrogel **3** was in a solid state the solution did not show its absorbance. However, as **3** gradually degraded, some of gel with the Meldrum's acid linker (a chromophore itself) dissolved and was observed at 350 nm. As the cascade continued the Meldrum's acid linker entirely broke down to product **2**, thereby continuing to increase the peak at 290 nm.

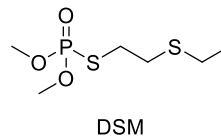
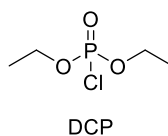
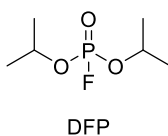
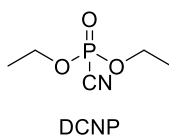
3.3.4 Selectivity Test

After confirming that this hydrogel sensor was working properly for **DCNP**, a selectivity experiment was performed. A unique characteristic of tabun is the cyanide moiety, which acts as a leaving group and a nucleophile. The Kumar group has reported the analysis of cyanide due to its nucleophilic ability after being released from an analogous mimic.²⁹⁻³¹ In our study, the two reactions that use initiator **4** were anticipated to impart selectivity to the sensing event. To test this, we conducted experiments on three nerve agent surrogates (**Figure 3.9 and 3.10**). First, the reaction between the initiator **4** with the nerve mimics **DCNP** (a GA-agent mimic), diisopropylfluorophosphate (**DFP**, a GB/GD-agent mimic), and demeton-S-methyl (**DSM**, a V-agent mimic) were followed by LC-MS. The thiophenol compound **5** was only observed in the reaction with **DCNP**. In the reaction of **4** with **DFP** phosphoryl transfer to the phenol did occur, but the thioacetate remained intact. With **DSM** there was no reaction with initiator **4**. We also attempted to initiate the auto-inductive cascade to degrade gel **3** using the three nerve agent mimics. As expected, the hydrogel was degraded only when **DCNP** was added, and the absorption increased compared to **DFP** and **DSM**. Similarly, in a study by the Martínez-Máñez group, it was reported that when comparing **DFP** and **DCNP**, only **DCNP** reacted with both the aldehyde and phenol moiety within their probe.³²

- Nerve Agents



- Nerve Agent Mimics



Scheme 3.6 Nerve agents and their mimics. DCNP (diethylcyanophosphonate) is a simulant of a tabun, and both DFP (diisopropylfluorophosphate) and DCP (diethylchlorophosphate) are surrogates of a sarin and a soman. DSM (demeton-S-methyl) is employed as a mimic of VX.

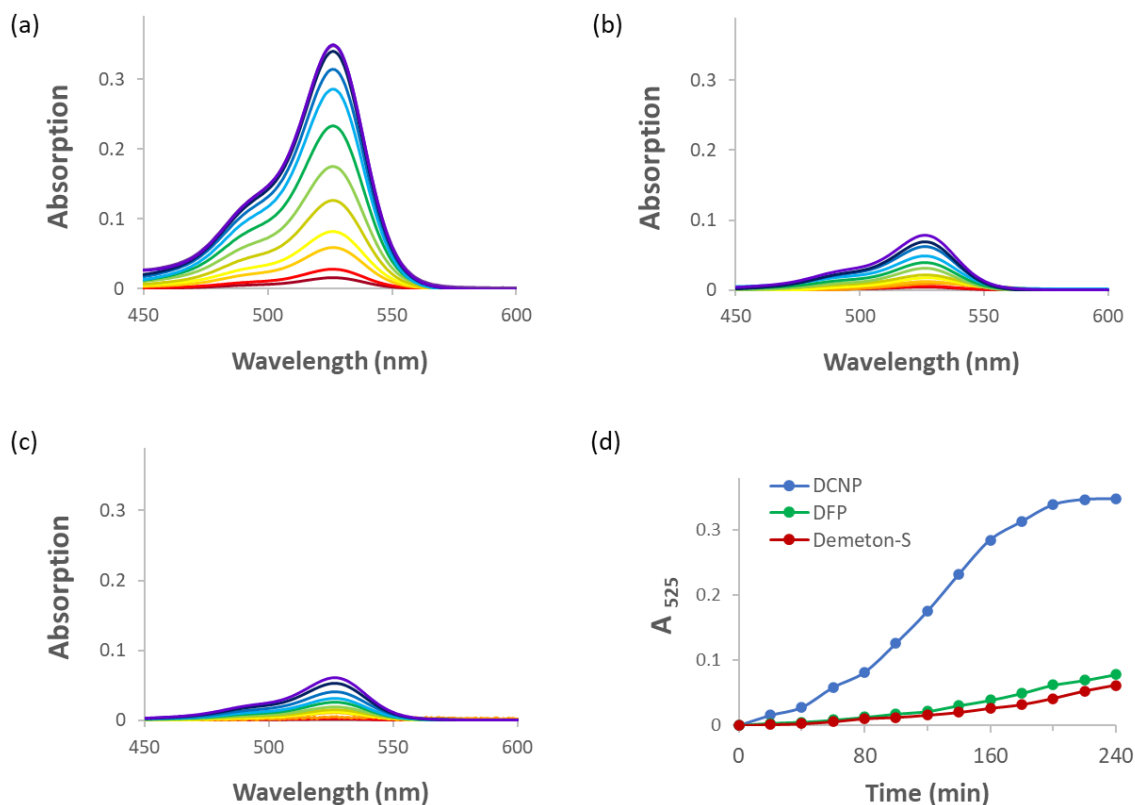


Figure 3.9 Selectivity test. Absorption data of time dependent titration for **3** degradation with DCNP (a tabun mimic), DFP (a sarin and soman mimic), and Demeton-S-methyl (a VX mimic) in physiological pH (Phosphate-buffered saline). After reacting **4** (5 μmol), triethylamine (10 μmol), and (a) DCNP 0.5 μmol (0.1 equivalent); (b) DFP 5 μmol (1 equivalent); (c) DSM 5 μmol (1 equivalent) in acetonitrile for 30 minutes, the result mixture was added to the PBS 5 mL in the presence of 2-hydroxyethyl disulfide (5 μmol) and **3** with Rhodamine 6G (5 μmol). Absorption was measured by extracting 100 μL of the solution at intervals of 20 minutes for 240 minutes. (d) shows absorbance spectra of (a), (b), and (c) at 525 nm.

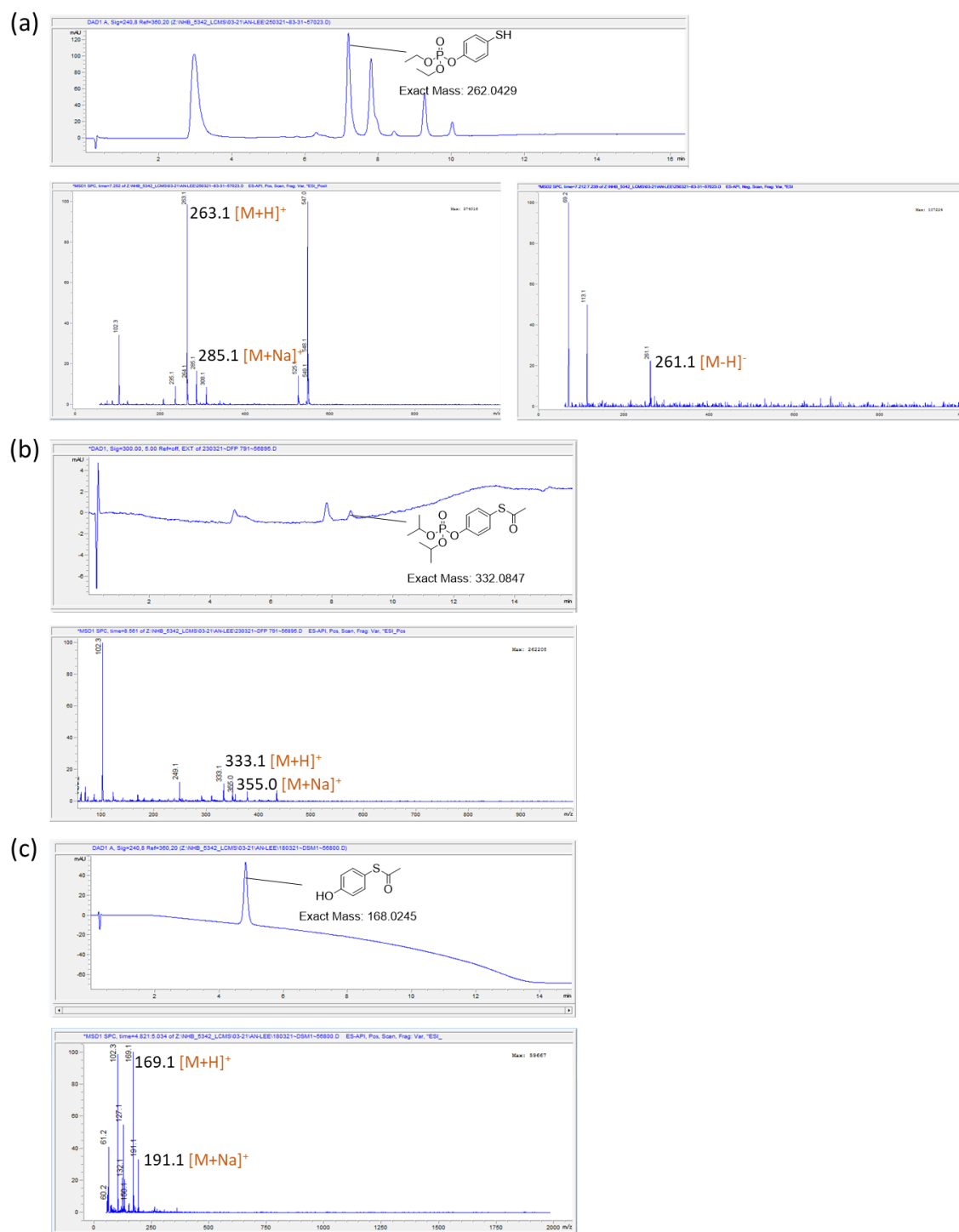


Figure 3.10 LC-MS data of the reaction **4** (10 mM) and triethylamine (20 mM) with (a) DCNP (10 mM); (b) DFP (10 mM); (c) DSM (10 mM) in acetonitrile for 90 minutes.

3.3.5 Membrane Degradation

We next turned to using hydrogel **3** as a physical barrier to time the release of reagents in response to **DCNP** using an “hourglass” like study. While in a real-life application the reagents could be tabun antidotes or capture agents, we mimicked such entities using dyes and nanocrystals, respectively. We anticipated that solutions resulting from the reaction of **4** and **DCNP** could be used to trigger degradation of a membrane created from **3** in a time dependent manner depending upon the thickness of the membrane. Hydrogels of four different thicknesses were prepared and affixed to vial adaptors. To do so, the masses of reactants and quantities of solvent (*t*-butanol and water) were controlled to make different thickness of membranes (**Figure 3.11**). Indeed, we visually confirmed that the membrane decomposition time varies contingent on the thickness of the hydrogel because the thicker the membranes, the longer it took for the gels to dissolve and release the red solution containing **R6G** into the bottom vial. Several factors must influence this phenomenon, each of which could be tuned for a specific application: 1) the degradation rate of the hydrogel induced by **DCNP** is dependent upon pH, 2) the weight of the top solution, and 3), the surface tension of the solvent (water in our case) that impedes the solution from passing through the membrane.

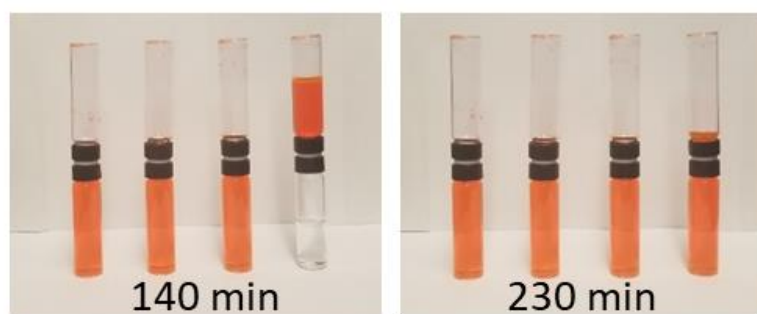
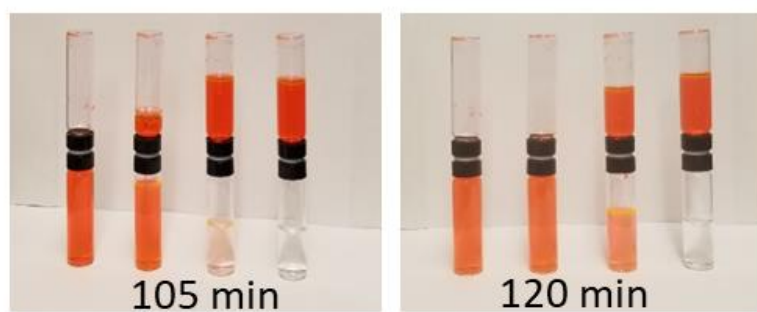
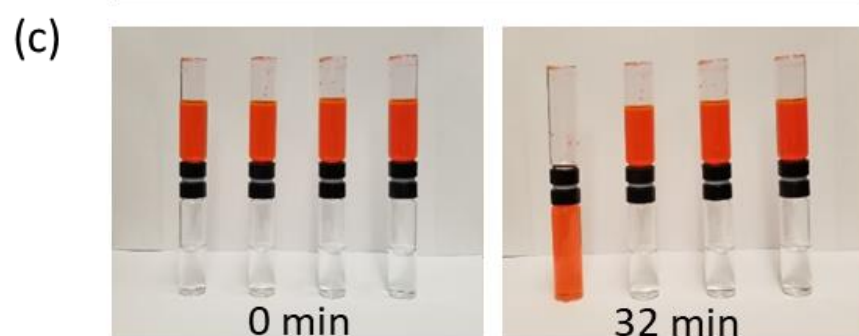
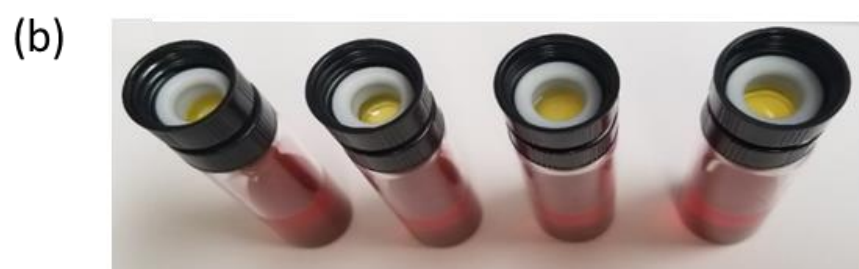


Figure 3.11 Membrane degradation test of **3**. There were four different weights and thicknesses of gels created with **3** which were synthesized with 5 μmol , 7 μmol , 9 μmol , and 11 μmol of the Meldrum's acid linker in the gel. (a) Thickness of **3**: 1.7 mm, 2.2 mm, 2.6 mm, and 3.2 mm. (b) A photo for the four samples before connecting the top vial. (c) Visualization for the kinetic samples designated 1, 2, 3, and 4 (left to right). Four different sets were made of **3** containing 5 μmol , 7 μmol , 9 μmol , and 11 μmol of the conjugate acceptor for samples 1, 2, 3, and 4, respectively. Each sample was made in a 1 dram vial, however, the reactants and solvent varied to make alter the thickness of the membrane. The conditions for each sample shown above was: 1. Meldrum's acid linker (1.90 mg, 5 μmol , 1 equiv.), four-arm PEG azides (25 mg, 2.5 μmol , 0.5 equiv.), tert-butanol (50 μL), Milli-Q water (50 μL), sodium ascorbate (0.5 mg, 2.5 μmol , 0.5 equiv.), and copper sulfate (0.5 mg, 2 μmol , 0.40 equiv.), 2. Meldrum's acid linker (2.66 mg, 7 μmol , 1 equiv.), four-arm PEG azides (35 mg, 3.5 μmol , 0.5 equiv.), tert-butanol (70 μL), Milli-Q water (70 μL), sodium ascorbate (0.7 mg, 3.5 μmol , 0.5 equiv.), and copper sulfate (0.7 mg, 2.8 μmol , 0.4 equiv.), 3. Meldrum's acid linker (3.42 mg, 9 μmol , 1 equiv.), four-arm PEG azides (45 mg, 4.5 μmol , 0.5 equiv.), tert-butanol (90 μL), Milli-Q water (90 μL), sodium ascorbate (0.9 mg, 4.5 μmol , 0.5 equiv.), and copper sulfate (0.9 mg, 3.6 μmol , 0.4 equiv.), and 4. Meldrum's acid linker (4.18 mg, 11 μmol , 1 equiv.), four-arm PEG azides (55 mg, 5.5 μmol , 0.5 equiv.), tert-butanol (110 μL), Milli-Q water (110 μL), sodium ascorbate (1.1 mg, 5.5 μmol , 0.5 equiv.), and copper sulfate (1.1 mg, 4.4 μmol , 0.4 equiv.).

Further, we anticipated that the membrane could be used to release particles, such as potentially capture agents. To study this, we followed the change in morphology of nanocrystal (NC) particles upon mixing solutions because they give an optical response. We found that Sn:In₂O₃ nanocrystals (ITO NCs) functionalized with mixed aldehyde and benzyl-terminal oligo(ethylene oxide) ligands can be dispersed in polar solvents.³³ Specifically, we found that these functionalized ITO NCs form stable dispersions in aqueous solutions above pH 8, but aggregate at low pH. Thus, to explore the ability to release particles, we followed the pH-controlled aggregation using the self-

degradable hydrogel. The top vial was filled with a dispersion of 12 nm diameter NCs (pH 10), which was triggered to fall into the bottom vial (pH ~3) using the same procedure as described in the previous paragraph. Once the membrane dissolved and the NC solution mixed with the acidic water, they flocculated out of solution. We believe this occurs from a destabilized ligand shell from ligand exchange/removal and etching conditions created by the use of the strong acid (**Figure 3.12a**).^{34,35} The blue color of the NCs in the top vial is due to the high energy tail of the localized surface plasmon resonance (LSPR) absorbing red light, while the aggregated NCs (where strong coupling of LSPR in neighboring NCs is expected) appear light green in color (**Figures 3.12b,c, and d**). Thus, physical changes of NCs can also be used to monitor/sense the gel dissolution response to the tabun surrogate.

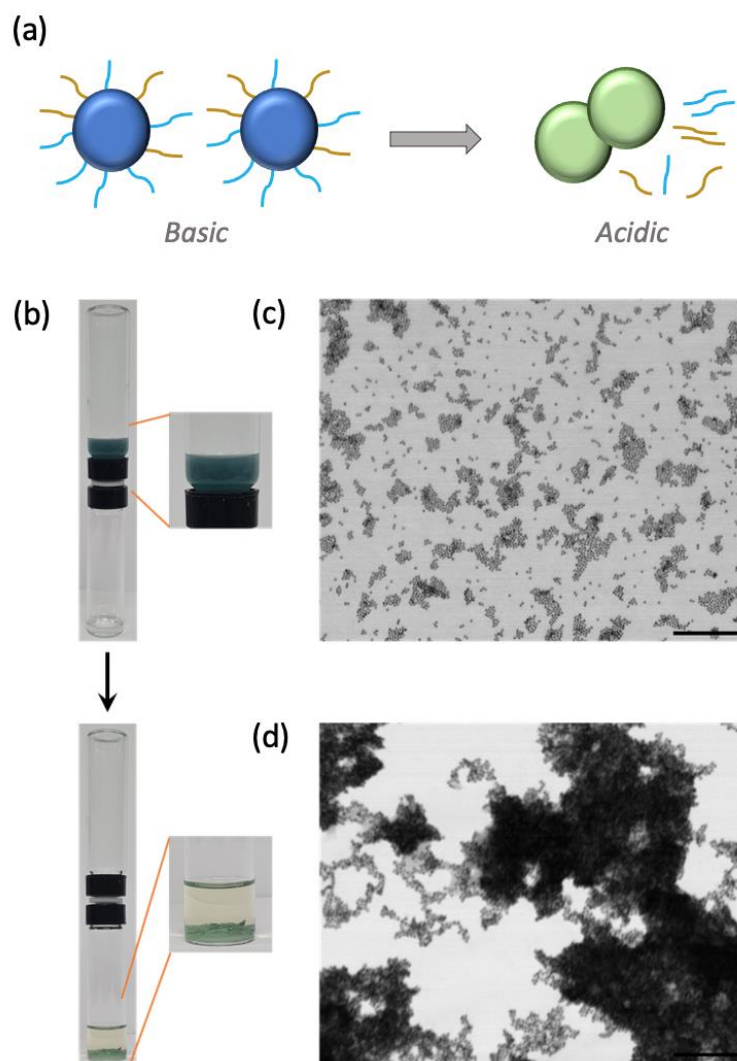


Figure 3.12 Experiment showing the alteration in degree of dispersion of nanocrystals due to a change in pH induced by membrane decomposition. (a) Representation of the **ITO NCs** with the ligands functionalized on the **NC** surface. Acidic conditions cause the ligands to be stripped from the **NCs** causing **NC** degradation and aggregation. (b) Top is a picture before the membrane degradation, and the bottom is a picture after degradation. The top vial contained a pH 10 aqueous solution (4 mL) containing dispersed colloidal **NCs**, and the bottom was pH 3 water (1 mL). (c) and (d) are STEM images before and after, respectively, the membrane degradation. Both scalebars are 250 nm.

3.4 CONCLUSION

A degradable hydrogel was used as both an optical and physical-change sensor for a surrogate of the nerve agent tabun. Using a self-propagating cascade that degrades the gel due to the release of thiols that then further propagates its own degradation, we could monitor absorbance changes, dye release, and physical changes of the gel. The initiation of the cascade was performed via two sequential reactions using an initiator that reacts with the tabun surrogate, releases cyanide, and subsequently releases a thiophenol to trigger gel degradation. Confirmation of the anticipated two reaction sequence was done by monitoring the kinetics of model reactions. In addition, the hydrogel was used as a membrane to study the decomposition rate depending on the membrane thickness, thus generating an hourglass like change in the mixing of solutions of colored dyes and nanocrystals that undergo dispersion changes, albeit one can imagine the delivery of other chemical agents upon triggering with tabun or surrogates. For a practical application with a real agent, the kinetics of this proof-of-principle system will need to be sped up because an hour or more response time is too slow to be practical. Thus, on another front we are working on more rapid self-propagating cascades that can be incorporated into gels. However, based on our results, we expect that the concept of triggerable self-degradable hydrogels can also be applied in other fields, such as bio- and nanomaterials.

3.5 EXPERIMENTAL SECTION

3.5.1 Methods and Instruments

Nuclear Magnetic Resonance (NMR)

NMR spectra were recorded from The University of Texas at Austin NMR facility. Varian DirectDrive or Varian INOVA 400 MHz NMR spectrometers were employed on Synthesized compounds characterization. Time kinetics studies with NMR were recorded on Bruker AVIII HD 500 MHz cryoprobe. The NMR spectra were referenced to solvent and the spectroscopic solvents (CDCl_3 , CD_3CN) were purchased from Cambridge Isotope Laboratories. All NMR spectral data was processed with the Mestrenova software package.

Liquid Chromatography–Mass Spectrometry (LC-MS)

Finnigan MAT-VSQ 700 and DSQ spectrometers were used to obtain mass spectra. HR electrospray ionization (ESI) mass spectra were recorded using either Agilent 6530 Accurate-Mass Q-TOF LC/MS or MALDI-TOF (Vogayer, PerSeptive Biosystem).

High-Resolution Mass Spectrometry (HRMS)

High-resolution mass spec (HRMS) analysis was conducted by the University of Texas Mass Spectrometry Facility using Agilent Technologies 6530 Accurate Mass Q-TOF LC/MS system.

UV-Vis Spectroscopy

The UV-Vis absorbance spectra and kinetics were obtained in Cary 100 UV-Vis spectrophotometer from Agilent Technology. The spectra were run in Cary WinUV software: Scan, Kinetics and Scanning Kinetics, respectively.

Fluorescence Spectroscopy

Fluorescence spectra were recorded on a Photon Technology International Fluorescence Master fluorimeter. The source was a 75 W Xenon short arc lamp.

Solid Phase Peptide Synthesis, Purification, and Identification Equipment

The solid phase peptide synthesis was conducted via CEM Liberty Blue Microwave Peptide Synthesizer and all syntheses were done at the 0.25 mmol scale. Upon completion, HPLC was used to purify the desired product. The HPLC used was a Shimadzu Prominence system furnished with a Zorbax SB-C18 preparatory column (21.2 x 250 mm) with 7.0 μm packing material. The University of Texas at Austin Mass Spectrometry Facility used an Agilent Technologies 6530 Accurate Mass Q-TOF LC/MS for any high-resolution mass spectrometry (HRMS) data. A liquid chromatography mass spectrometry (LC-MS) instrument: Agilent Technologies 6125B Single Quadrupole LC-MS, was used to collect all UV-traces and MSD-TIC(+) data.

Scanning Transmission Electron Microscopy (STEM).

Samples were prepared by drop-casting dilute (0.1mg/mL) NC dispersions onto carbon-coated 400 mesh copper grids, with imaging performed on a Hitachi S5500 scanning transmission electron microscope (STEM) operating in the TEM mode with an accelerating voltage of 30 kV. Sizing NCs using the bright-field TEM images with the use of image j found NC sizes to be $9.8\text{nm} \pm 3.5\text{nm}$.³⁶

3.5.2 Materials

Cascade Materials

All materials were used as received unless otherwise stated. Meldrum's acid was purchased from Oakwood Chemical. 6-Iodo-1-hexyne (97%), diethyl cyanophosphonate (DCNP), diisopropylfluorophosphate (DFP), *O,O*-Dimethyl *S*-2-(ethylsulfanyl)ethyl phosphorothioate (demeton-S-methyl), Dulbecco's phosphate buffered saline, 2-

hydroxyethyl disulfide, 4-mercaptophenol, tetrabutylammonium cyanide, Indium(III) acetate ($\text{In}(\text{ac})_3$, 99.99%), tin (IV) acetate ($\text{Sn}(\text{ac})_4$, >99.9%), oleic acid (OA, 90%, technical grade), oleyl alcohol (OleOH, 98%), KOH (>85%), sodium L-ascorbate (99%), potassium cyanide, 18-crown-6, and triethylamine (>99.9%) were all from MilliporeSigma. 4-(Methylthio)phenol was from Tokyo Chemical Industry. Four-arm poly(ethylene glycol) azide (> 95%, $M_n = 10,000$ Da) was purchased from JenKem Technology. $\text{CuSO}_4 \cdot 5\text{H}_2\text{O}$ was bought from Fisher Scientific. Borax / sodium hydroxide buffer solution pH 10 was purchased from Fluka. Other chemical reagents were purchased from MilliporeSigma, Acros Organics, Fisher Scientific and so on.

All cuvettes made by fused quartz were purchased from Starna Cells with standard screw and septum top.

Solid Phase Peptide Synthesis Materials

All solid phase peptide syntheses were completed using an automated microwave peptide synthesizer, CEM Liberty, at a 0.25 mmol scale. Unless otherwise stated, all of the following reagents listed were used as received. The solvent, ACS grade dimethylformamide (DMF) was purchased from Fischer Scientific. Piperidine (99%) was purchased from Alfa Aesar. Ethyl(hydroxyamino)cyanoacetate (99.7%) was purchased from CHEM-IMPEX INT'L Inc. N, N'-Diisopropylcarbodiimide (99.5%) was purchased from CHEM-IMPEX INT'L Inc. The ACS grade acetic anhydride (99.7%) was purchased from Fisher Chemical. Fmoc-azidolysine (98%) was purchased from Novabiochem. The Fmoc-NH-PEG2-CH₂CH₂COOH (97%) was purchased from PUREPEG. Both the Fmoc-Asp(OtBu)-OH (98%) and Fmoc-Asp(OtBu)-Wang Resin (mesh:100-200, Subst.: 0.51 mmol/g) were purchased from P3BioSystems.

Solid Phase Click Reactions Materials

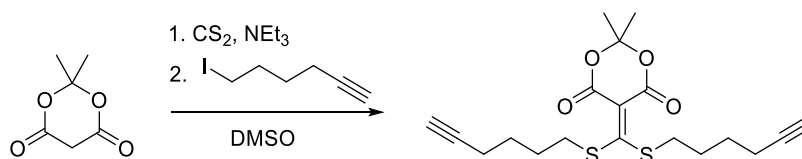
All the follow reagents and solvents were used as received unless otherwise stated. The solvent, DMF, used for were purchased from Fisher Scientific. The 4-ethynylbenzaldehyde (98%) was purchased from Ark Pharm, Inc. The 4-phenyl-1-butyne (97%) was purchased from Sigma Aldrich. Additionally, the copper (I) iodide (99%), and sodium L-ascorbate were both purchased from Sigma Aldrich. The synthesis of tris((1-benzyl-4-triazolyl)methyl)amine (TBTA) was accomplished following literature protocol.³⁷

Solid Phase Peptide Synthesis Cleavage, Precipitation, and Purification

Materials

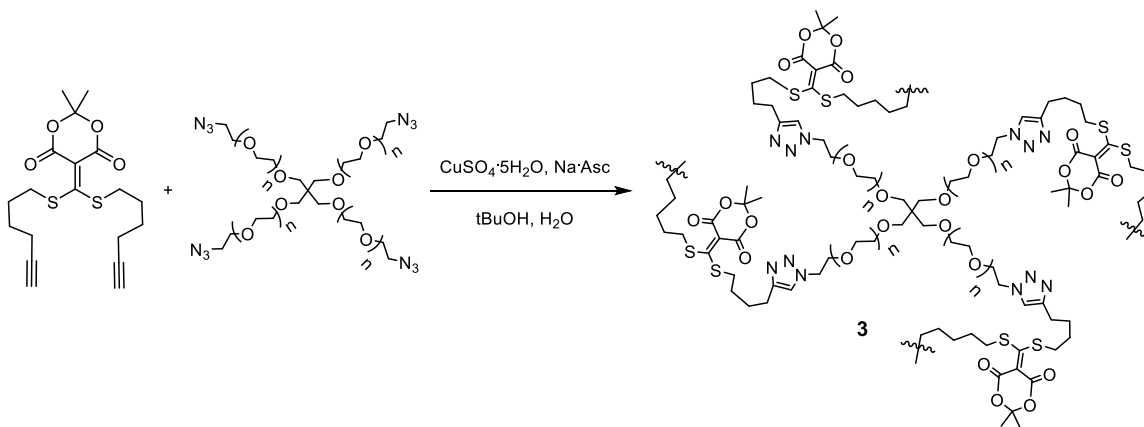
Cleavage: Trifluoroacetic acid (99.9%) was purchased from CHEM-IMPEX INT'L Inc. and the triisopropylsilane (98%) was purchased from Aldrich Chemistry. Precipitation: The solvent, ACS grade ether, was purchased from Fisher Chemical. Purification: For the high-performance liquid chromatography (HPLC) both solvents methanol and nanopore water were altered by adding 0.1% formic acid. The formic acid (99%) was purchased by Acros Organics. Nanopure water is provided by The University of Texas at Austin. The Optima Methanol was purchased from Fisher Chemical.

2.4.3 Synthesis



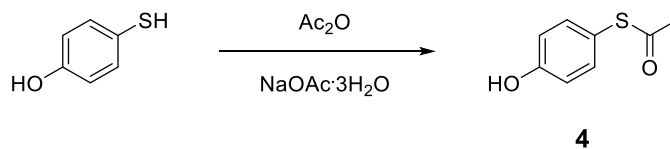
5-(bis(hex-5-yn-1-ylthio)methylene)-2,2-dimethyl-1,3-dioxane-4,6-dione: To a flask in the presence of Meldrum's acid (2 g, 13.9 mmol, 1 equiv.) in DMSO (10 mL) under argon gas, triethylamine (7.82 ml, 55.6 mmol, 4 equiv.) and carbon disulfide (0.84 mL, 13.9 mmol, 1 equiv.) were added in order. After stirring the mixture for 1 hour, 6-

iodo-1-hexyne (4.59 mL, 34.75 mmol, 2.5 equiv.) was added to the mixture carefully. The resulting mixture was a clear dark red color and left to stir overnight. The solution was added over ice and extracted with dichloromethane. The organic phase was dried with magnesium sulfate and evaporated via rotary evaporation. The crude product was purified by a column chromatography with ethyl acetate/hexane (1/5, v/v) and yellow viscous oil was obtained (2.94 g, 56%). ¹H NMR (400 MHz, CDCl₃) δ 3.18 – 3.04 (m, 4H), 2.21 (td, *J* = 6.8 Hz, 2.6 Hz, 4H), 1.95 (t, *J* = 2.7 Hz, 2H), 1.88 – 1.79 (m, 4H), 1.71 (s, 6H), 1.68 – 1.58 (m, 4H). ¹³C NMR (101 MHz, CDCl₃) δ 190.07, 160.04, 103.81, 103.14, 83.25, 69.25, 38.03, 27.52, 27.30, 26.92, 17.92; HRMS (ES⁺) *m/z* calc. for [M + Na]⁺, 403.1008; found, 403.0996.



Hydrogel (3): To a 1 dr vial, 5-(bis(hex-5-yn-1-ylthio)methylene)-2,2-dimethyl-1,3-dioxane-4,6-dione (1.9 mg, 5 μmol, 1 equiv.), four-arm PEG azides (M_n = 10,000 g/mol, 25 mg, 2.5 μmol, 0.5 equiv.) and tert-butanol (50 μL) was added. Milli-Q water (35 μL) containing sodium ascorbate (0.5 mg, 2.5 μmol, 0.5 equiv.) was added to the mixture and stirred to give a homogeneous yellow solution using a vortexer and a sonicator. After dissolving the mixture completely, copper sulfate (0.5 mg, 2 μmol, 0.4 equiv.) in water (15 μL) was added and stirred for 1 minute with a vortexer. The mixture

was stirred under a shaker for 1 hour. After removing the vial, a clear yellow hydrogel (**3**) was obtained. The hydrogel was purified in a neutral EDTA aqueous solution (10%) to extract the copper, remove sodium ascorbate and unreacted molecules. At last, **3** was ready to swell in water as a hydrogel.



S-(4-hydroxyphenyl) ethanethioate (4): 4-Mercaptophenol (1.252 g, 10 mmol), acetic anhydride (1.021 g, 10 mmol), and sodium acetate trihydrate (136.1 mg, 1 mmol) were stirred at room temperature (23-24 °C) overnight (12-18 hrs). The mixture was extracted with dichloromethane in the presence of sodium bicarbonate. The organic phase was dried with magnesium sulfate and evaporated via rotary evaporation. The crude product was purified by a column chromatography with ethyl acetate/hexane (1/5, v/v) and the white powder was obtained (1.18 g, 71%). ¹H NMR (400 MHz, CDCl₃) δ 7.20 (m, 2H), 6.73 (m, 2H), 6.08 (s, 1H), 2.42 (s, 3H). ¹³C NMR (101 MHz, CDCl₃) δ 197.90, 157.46, 136.23, 117.65, 116.72, 30.00; HRMS (-ESI) m/z calc. for [M - H]⁻, 167.0172; found, 167.0171.

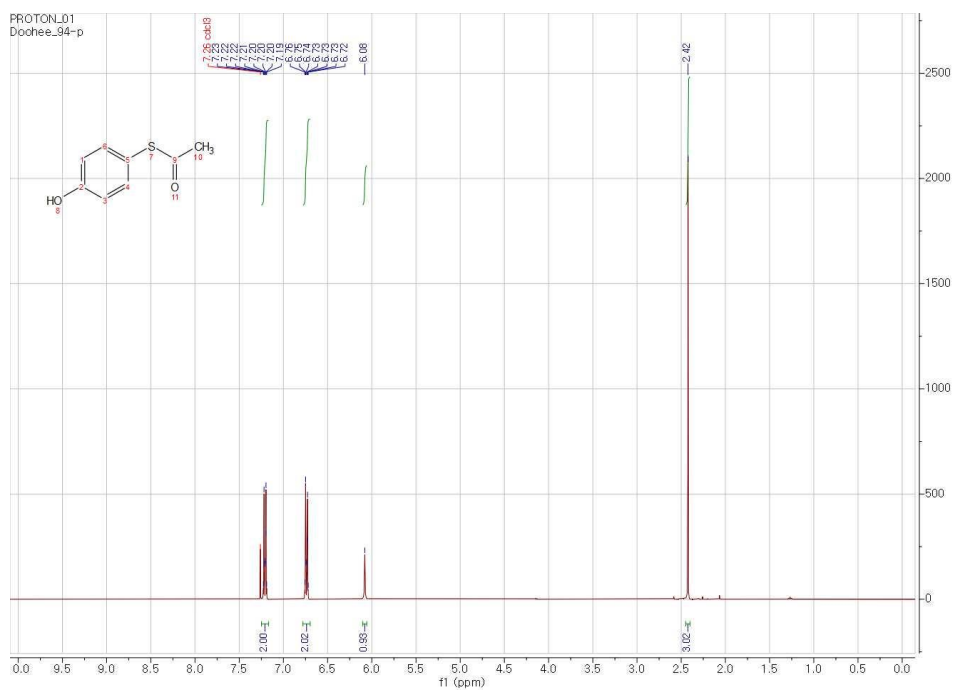


Figure 3.13 ^1H NMR spectrum of **4** (CDCl_3).

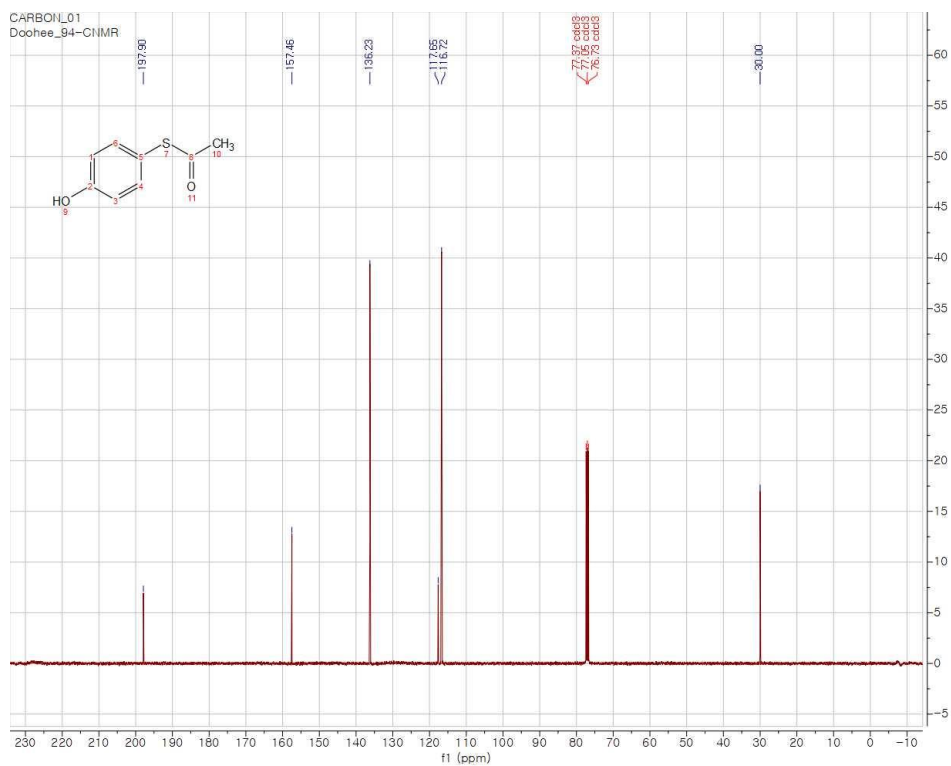


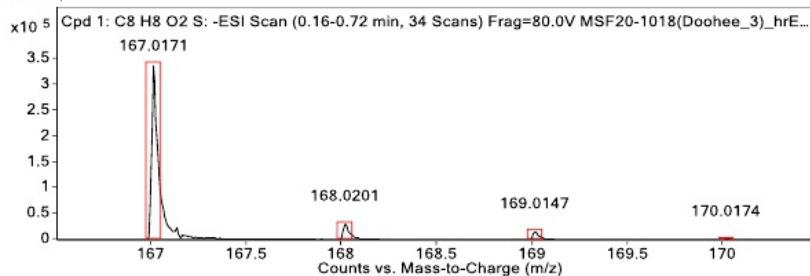
Figure 3.14 ^{13}C NMR spectrum of **4** (CDCl_3).

Target Compound Screening Report

Results Acquired by The University of Texas at Austin Mass Spectrometry Facility

Data File	MSF20-1018(Doohee_3)_hrESIneg1.d	Sample Name	1018(Doohee_3)	Comment	1018(Doohee_3)
Position	P1-E7	Instrument Name	Instrument 1	User Name	
Acq Method	FIA_neg.m	Acquired Time	10/2/2020 2:39:29 PM	DA Method	KS.m

MS Zoomed Spectrum



MS Spectrum Peak List

Obs. m/z	Calc. m/z	Charge	Abundance	Formula	Ion Species	Tgt Mass Error (ppm)
167.0171	167.0172	1	343543	CBH8O2S	(M-H) ⁻	1.02
168.0201	168.0203	1	31243	CBH8O2S	(M-H) ⁻	1.19
169.0147	169.0145	1	16194	CBH8O2S	(M-H) ⁻	-1.19
170.0174	170.0174	1	1476	CBH8O2S	(M-H) ⁻	-0.28
171.0294	171.0175	1	230	CBH8O2S	(M-H) ⁻	-70.02

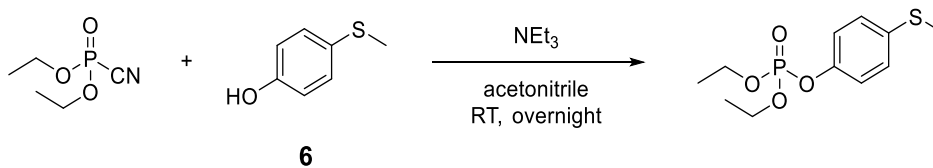
--- End Of Report ---

Agilent Technologies

Page 1 of 1

Printed at: 2:40 PM on:10/2/2020

Figure 3.15 High resolution mass data of **4**.



Diethyl (4-(methylthio)phenyl) phosphate: Diethyl phosphorocyanidate (196 mg, 1.2 mmol) was added to a solution acetonitrile (8 mL) containing 4-(methylthio)phenol (126 mg, 1 mmol) and triethyl amine (202 mg, 2 mmol) at room temperature (23-24 °C). After stirring overnight (12-18 hrs), the mixture was extracted with dichloromethane (DCM) and water with sodium bicarbonate. The organic phase was dried with magnesium sulfate and evaporated via rotary evaporation. The crude product was purified by a column chromatography with DCM/hexane (1/1, v/v) to DCM and the colorless clear liquid was obtained (236 mg, 85%). ¹H NMR (400 MHz, CD₃CN) δ 7.29 (d, J = 8.7 Hz, 2H), 7.16 (d, J = 8.9 Hz, 2H), 4.23 – 4.11 (m, 4H), 2.47 (s, 3H), 1.31 (t, J

= 7.0 Hz, 6H). ^{13}C NMR (101 MHz, CD_3CN) δ 148.49, 135.01, 127.91, 120.72, 64.60, 15.43, 15.34; HRMS (+ESI) m/z calc. for $[\text{M} + \text{Na}]^+$, 299.0477; found, 299.0475.

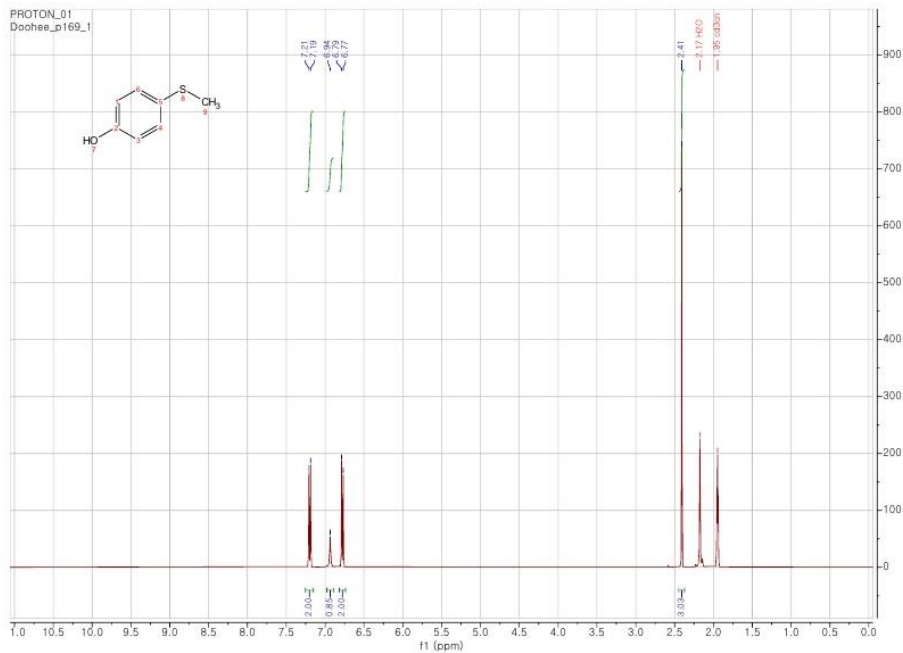


Figure 3.16 ^1H NMR spectrum of **6** (CD_3CN).

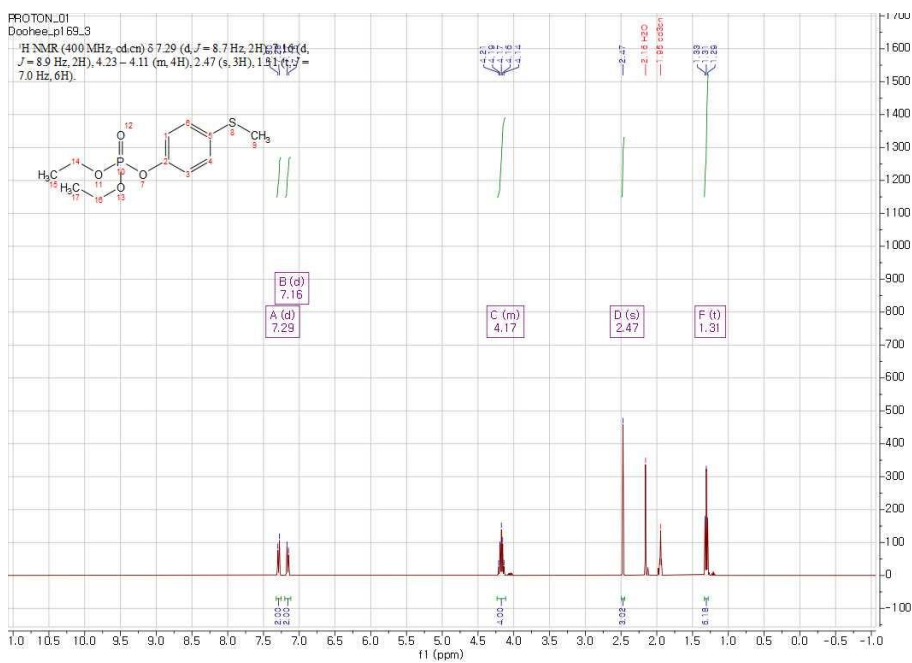


Figure 3.17 ^1H NMR spectrum of diethyl (4-(methylthio)phenyl) phosphate (CD_3CN).

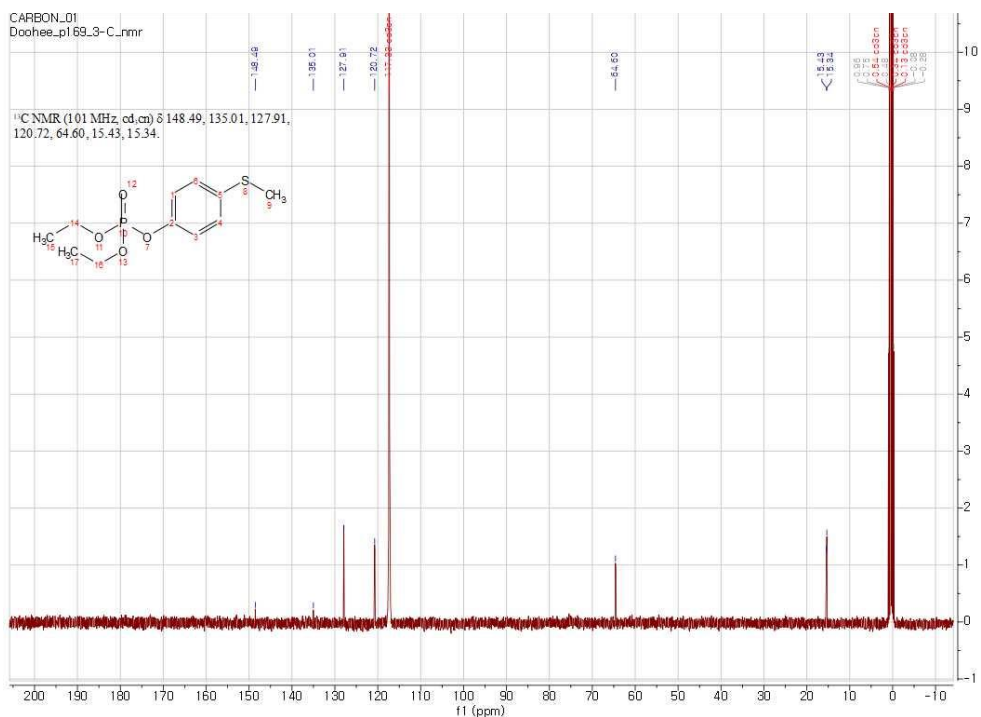


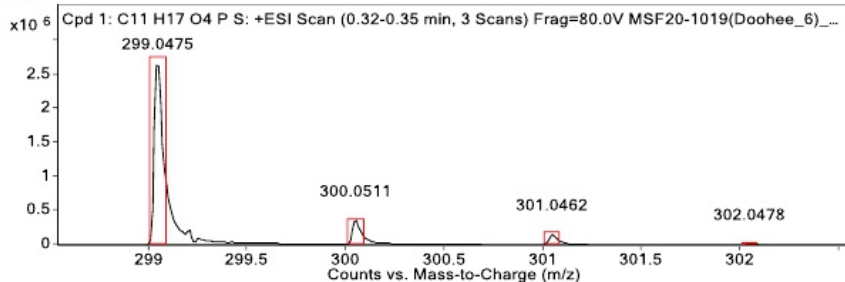
Figure 3.18 ¹³C NMR spectrum of diethyl (4-(methylthio)phenyl) phosphate (CD₃CN).

Target Compound Screening Report

Results Acquired by The University of Texas at Austin Mass Spectrometry Facility

Data File	MSF20-1019(Doohee_6)_hrESIPos1.d	Sample Name	1019(Doohee_6)	Comment	1019(Doohee_6)
Position	P1-E8	Instrument Name	Instrument 1	User Name	
Acq Method	FIA_pos.m	Acquired Time	10/2/2020 2:23:08 PM	DA Method	KS.m

MS Zoomed Spectrum

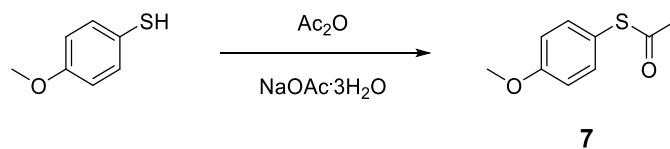


MS Spectrum Peak List

Obs. m/z	Calc. m/z	Charge	Abundance	Formula	Ion Species	Tgt Mass Error (ppm)
299.0475	299.0477	1	2754743	C ₁₁ H ₁₇ O ₄ PS	(M+Na) ⁺	0.81
300.0511	300.0509	1	363998	C ₁₁ H ₁₇ O ₄ PS	(M+Na) ⁺	-0.52
301.0462	301.0460	1	159334	C ₁₁ H ₁₇ O ₄ PS	(M+Na) ⁺	-0.63
302.0478	302.0487	1	17534	C ₁₁ H ₁₇ O ₄ PS	(M+Na) ⁺	3.01
303.0479	303.0492	1	2218	C ₁₁ H ₁₇ O ₄ PS	(M+Na) ⁺	4.4

--- End Of Report ---

Figure 3.19 High resolution mass data of diethyl (4-(methylthio)phenyl) phosphate.



S-(4-methoxyphenyl) ethanethioate (7): 4-Methoxythiophenol (701 mg, 5 mmol), acetic anhydride (510 mg, 5 mmol), and sodium acetate trihydrate trihydrate (680.4 mg, 5 mmol) were stirred at room temperature (23-24 °C) overnight (12-18 hrs). The mixture was extracted with dichloromethane in the presence of sodium bicarbonate. The organic phase was dried with magnesium sulfate and concentrated using rotary evaporation. The crude product was purified by a column chromatography with ethyl acetate/hexane (1/20, v/v) and the colorless clear liquid was obtained (756 mg, 83%). ¹H NMR (400 MHz, CDCl₃) δ 7.32 (d, J = 8.9 Hz, 2H), 6.94 (d, J = 9.0 Hz, 2H), 3.81 (s, 3H), 2.39 (s, 3H). ¹³C NMR (101 MHz, CDCl₃) δ 195.15, 160.68, 136.09, 118.70, 114.88, 55.33, 29.94; HRMS (+ESI) m/z calc. for [M + Na]⁺, 205.0294; found, 205.0296.

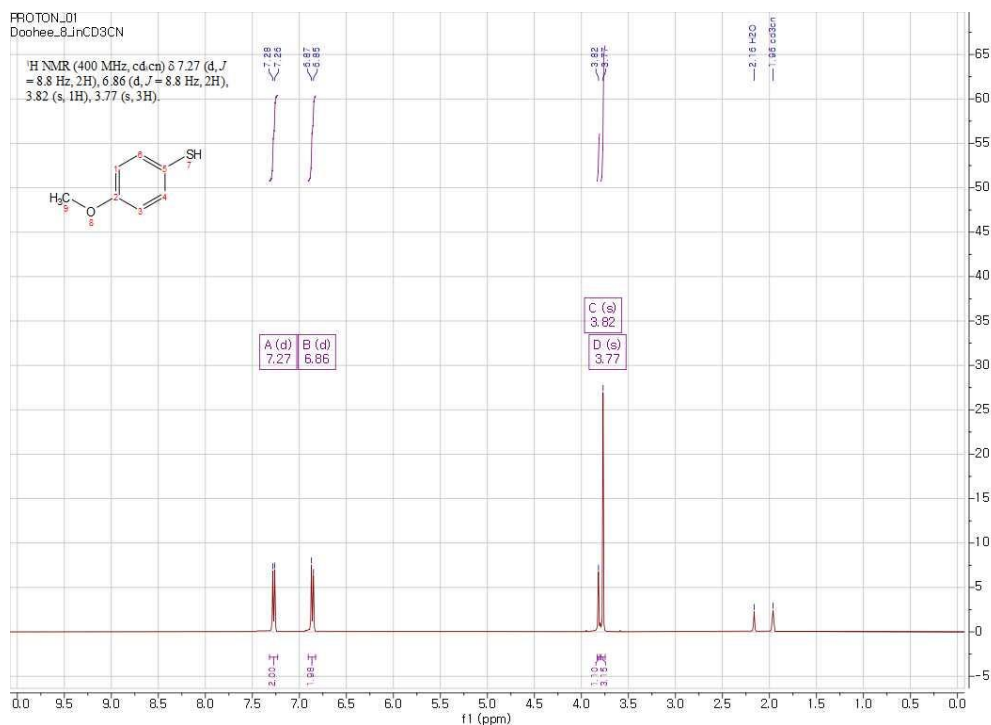


Figure 3.20 ¹H NMR spectrum of 4-methoxybenzenethiol (CD₃CN).

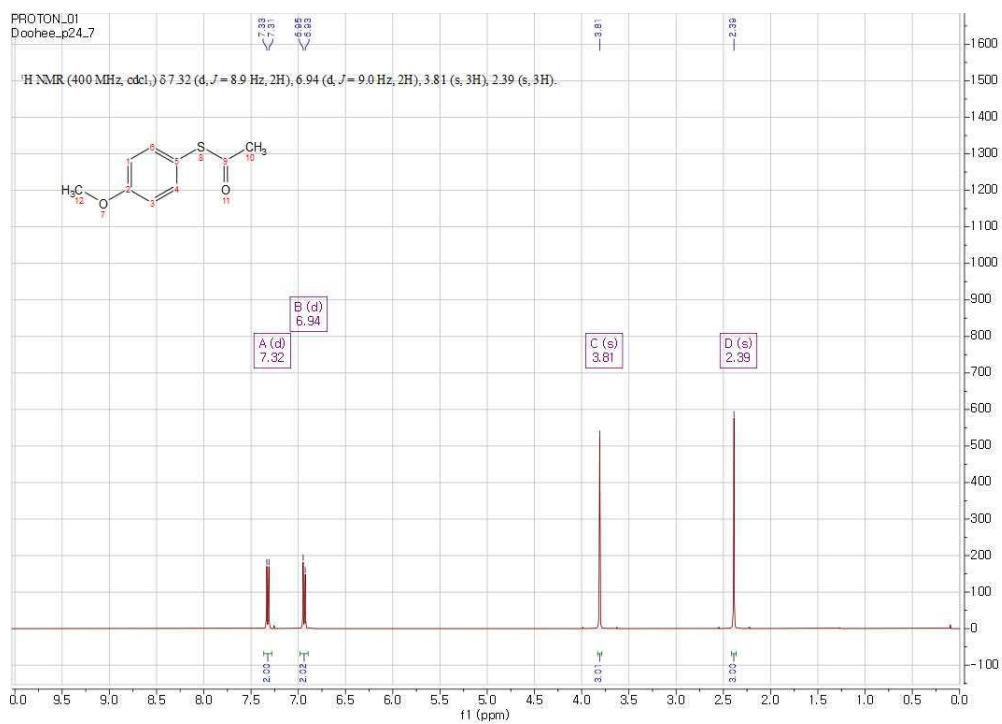


Figure 3.21 ^1H NMR spectrum of **7** (CDCl_3).

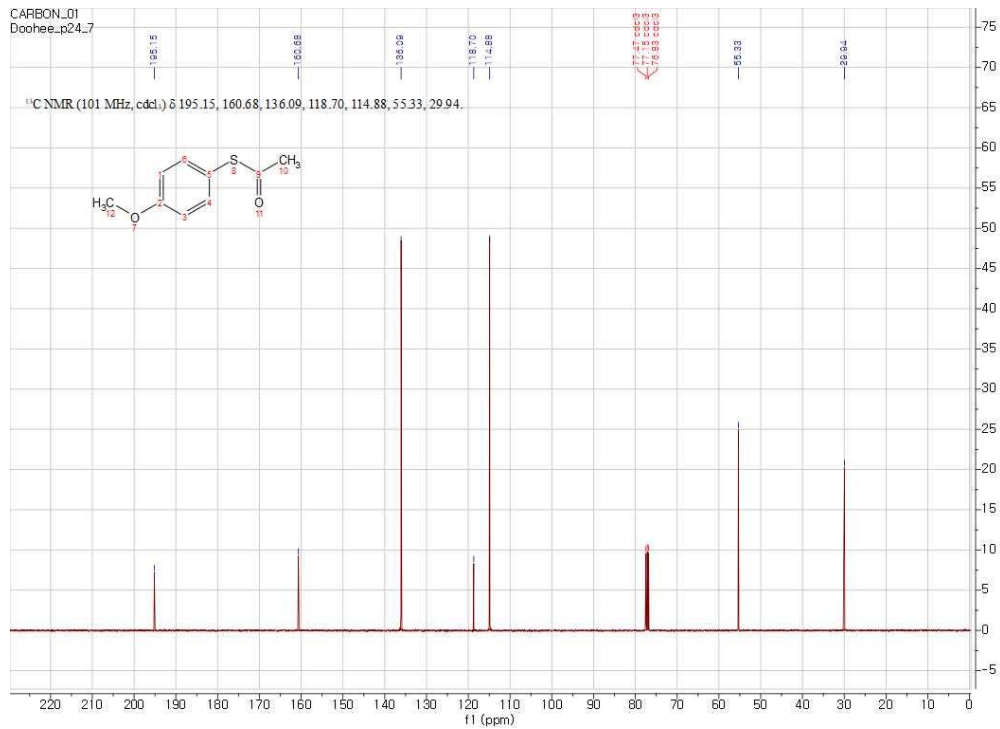


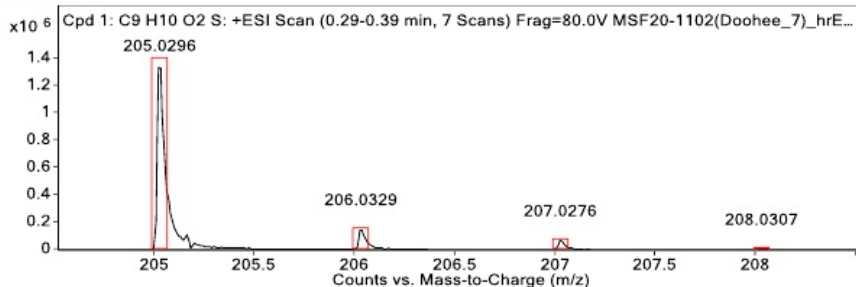
Figure 3.22 ^{13}C NMR spectrum of **7** (CDCl_3).

Target Compound Screening Report

Results Acquired by The University of Texas at Austin Mass Spectrometry Facility

Data File	MSF20-1102(Doohee_7)_hrESIpos2.d	Sample Name	1102(Doohee_7)	Comment	1102(Doohee_7)
Position	P1-F4	Instrument Name	Instrument 1	User Name	
Acq Method	FIA_pos.m	Acquired Time	10/12/2020 3:29:06 PM	DA Method	KS.m

MS Zoomed Spectrum



MS Spectrum Peak List

Obs. m/z	Calc. m/z	Charge	Abundance	Formula	Ion Species	Tgt Mass Error (ppm)
205.0296	205.0294	1	1400105	C9H10O2S	(M+Na)+	-1.02
206.0329	206.0325	1	150787	C9H10O2S	(M+Na)+	-2.2
207.0276	207.0268	1	69270	C9H10O2S	(M+Na)+	-3.68
208.0307	208.0296	1	6256	C9H10O2S	(M+Na)+	-5.27

--- End Of Report ---

Figure 3.23 High resolution mass data of **7**.

Microwave Assisted Peptide Synthesis

Using the peptide synthesizer, the ligands were made using standard Fmoc-deprotection using piperidine and the desired natural or unnatural amino acid, and PEG were coupled using diisopropylcarbodiimide (DIC)/Ethyl(hydroxyamino)cynoacetate (Oxyma) amide coupling conditions. The ligands were synthesized using Wang resin. The microwave assisted peptide synthesizer coupled the amino acids with DIC/Oxyma in two steps: 1) 75 °C, 170 W for 15 seconds, and 2) 90 °C, 30 W for 110 seconds. All Fmoc-deprotections were completed using a piperidine/DMF (20:100) solution in two phases: 1) 75 °C, 155 W for 15 seconds, and 2) 90 °C, 30 W for 50 seconds. Following the same standard synthesis procedures, the N-terminus of the ligand was deprotected and

capped with acetic anhydride. All resins were sequentially washed with DMF (25 mL), DCM (25 mL), and MeOH (25 mL). The resin was dried under vacuum for at least three hours prior to the solid phase copper (I)-catalyzed alkyne-azide cycloaddition reaction.

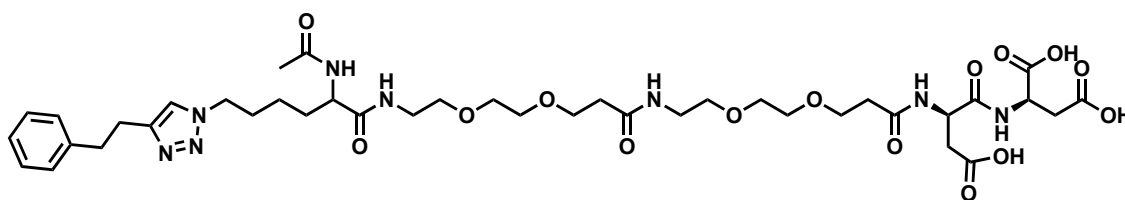
Solid Phase Copper(I)-Catalyzed Alkyne-Azide Cycloaddition

Solid Phase Copper(I)-Catalyzed Alkyne-Azide Cycloaddition (SP-CuAAC), was performed using the following described procedure to install the desired alkyne (4-phenyl-1-butyne or 4-ethynylbenzaldehyde) onto the azide of the ligand. The resin was transferred to a 20 mL dram vial and suspended in 4 mL of DMF. With 1.1 equivalencies (azide/alkyne, 1:1.1), the desired alkyne was added to the vial. The vial was then sealed and degassed with N₂ gas. The catalyst solution was made in a separate vial under inert conditions. The catalyst was prepared by combining tris(1-benzyl-4-triazolylmethyl) amine (TBTA)/sodium ascorbate/copper iodide (0.4: 0.4:0.2 eq.) and dissolving the solids in a total of 3.4 mL of DMF and 1.6 mL of H₂O. The catalyst solution was added to the dram vial containing the resin and alkyne and the solution was equipped with a N₂ balloon. The resulting mixture was left on a shaker for 12-24 hours at room temperature. Once completed the resin was washed with DMF (40 mL), DCM (40 mL), and MeOH (40 mL). The resin was left to dry under vacuum for at least four hours prior to cleaving the ligand off the resin.

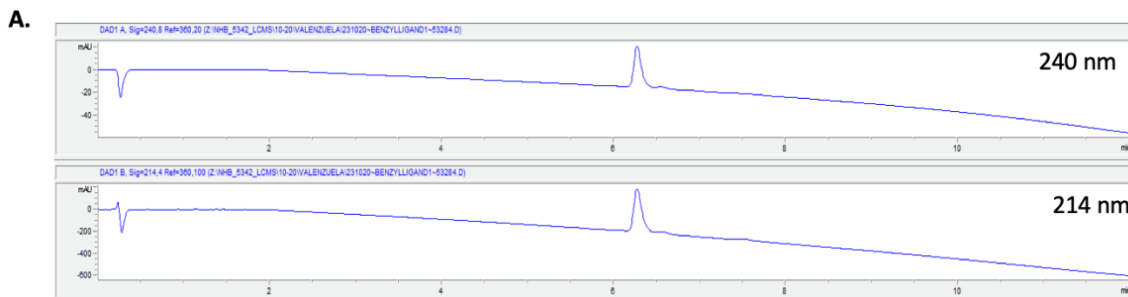
Once the resin was dried the ligand was cleaved off the resin. For the resin that was subjected to the SP-CuAAC with 4-ethynylbenzaldehyde, the cleavage solution consisted of TFA/H₂O (90:10). For the resin that was subjected to the SP-CuAAC with 4-phenyl-1-butyne, the cleavage solution consisted of TFA/TIS/H₂O (95:2.5:2.5). In both cases the resin was agitated for 2.5-3 hours with their respective cleavage solution. The cleavage solution was removed, and the ligand was precipitated with ether. Upon removal of the ether, the precipitant was analyzed using an LCMS (5% to 95% MeOH gradient

over 12 minutes, MeOH/H₂O binary system) to display the desired products. The peaks in the LCMS were identified using MS. Further purification using a HPLC (gradient: isocratic binary system, MeOH/H₂O 10% to 95% over 90 minutes, both the MeOH and H₂O were altered with 0.1% formic acid) removed residual biproducts. The desired ligand was collected and the MeOH was removed using a rotatory evaporation. The residual water was lyophilized to yield a white powder for all ligands made.

Benzyl-Ligand



Yield: 87.93 mg (98.5 μmol), 11.3%, white solid. HRMS(+ESI)/ Da: M = C₄₀H₆₀N₈O₁₅, (M+Na)⁺_{theoretical} = 915.4076, (M+Na)⁺_{observed} = 915.4070, Target Mass Error = -0.72 ppm.



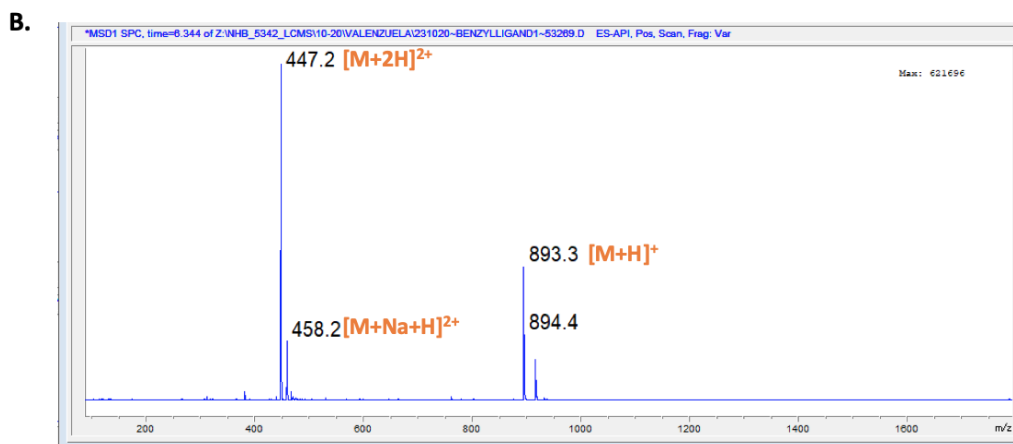


Figure 3.24 The benzyl-ligand purity conformation via LC-MS. (a) The UV-trace at both 240 and 214 nm over a 12 minutes (LCMS Trace: 5% to 95% MeOH gradient) displays only one peak. (b) The MSD-TIC (+) of the single peak shown in (a) displaying the mass of the desired ligand.

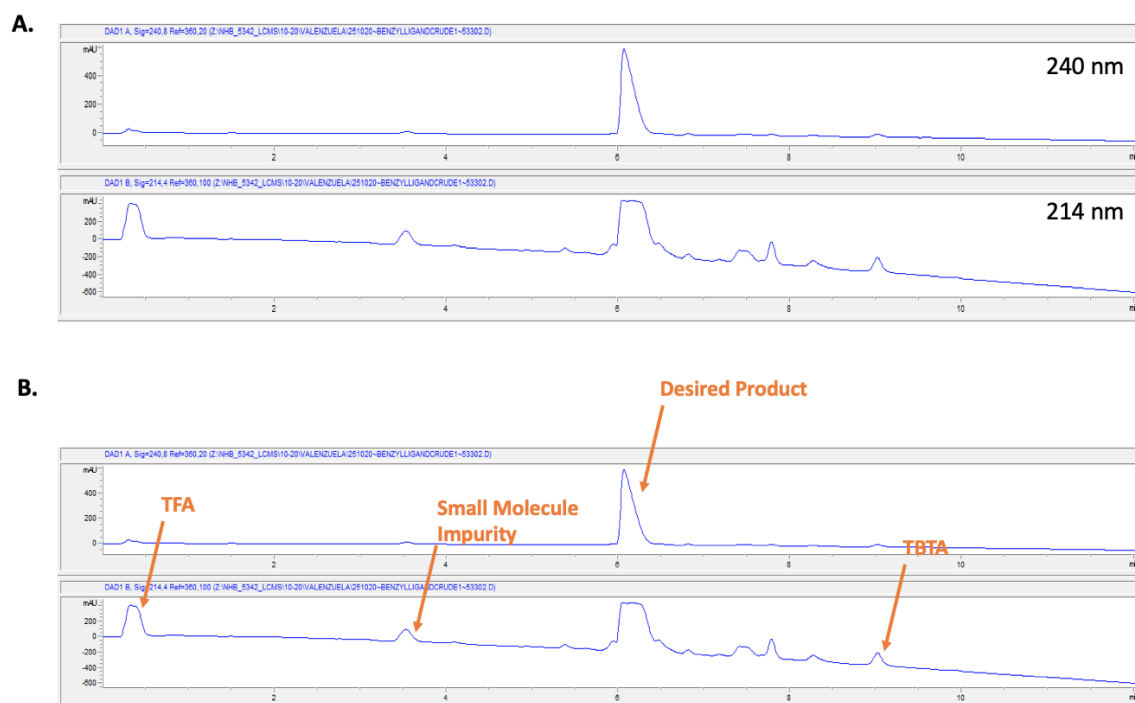
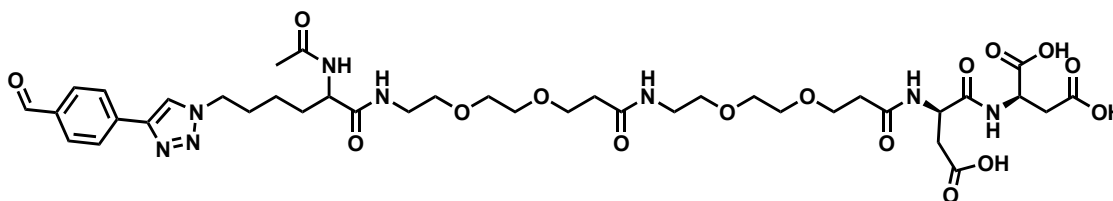


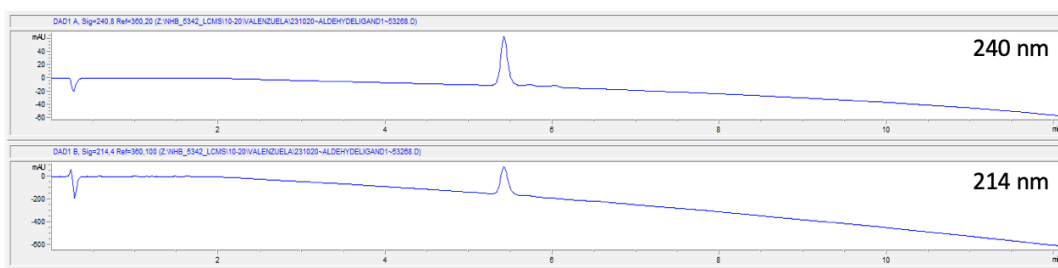
Figure 3.25 The LCMS-trace of the benzyl-ligand prior to HPLC purification. (a) The crude UV-trace of the benzyl-ligand at 240 and 214 nm. (b) The identities of known impurities.

Aldehyde-Ligand



Yield: 105.45 mg (118.1 μmol), 12.0%, white solid. HRMS(+ESI)/ Da: $M = \text{C}_{39}\text{H}_{56}\text{N}_8\text{O}_{16}$, $(M+\text{Na})^+_{\text{theoretical}} = 915.3712$, $(M+\text{Na})^+_{\text{observed}} = 915.3706$, Target Mass Error = -2.49 ppm.

A.



B.

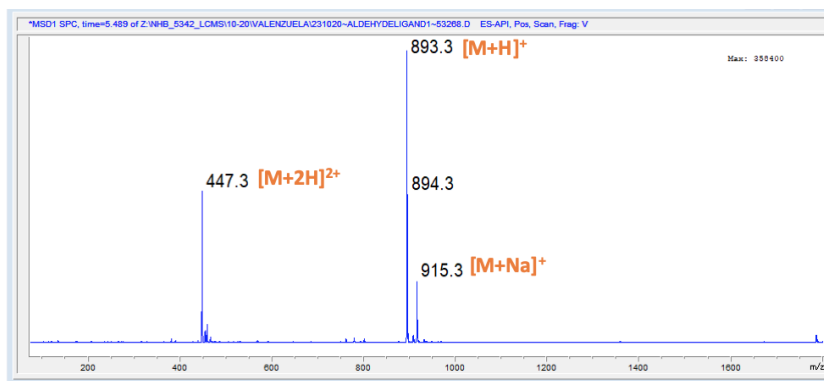


Figure 3.26 The Aldehyde-ligand purity conformation via LC-MS. (a) The UV-trace at both 240 and 214 nm over a 12 minutes (LCMS Trace: 5% to 95% MeOH gradient) displays only one peak. (b) The MSD-TIC (+) of the single peak shown in (a) displaying the mass of the desired ligand.

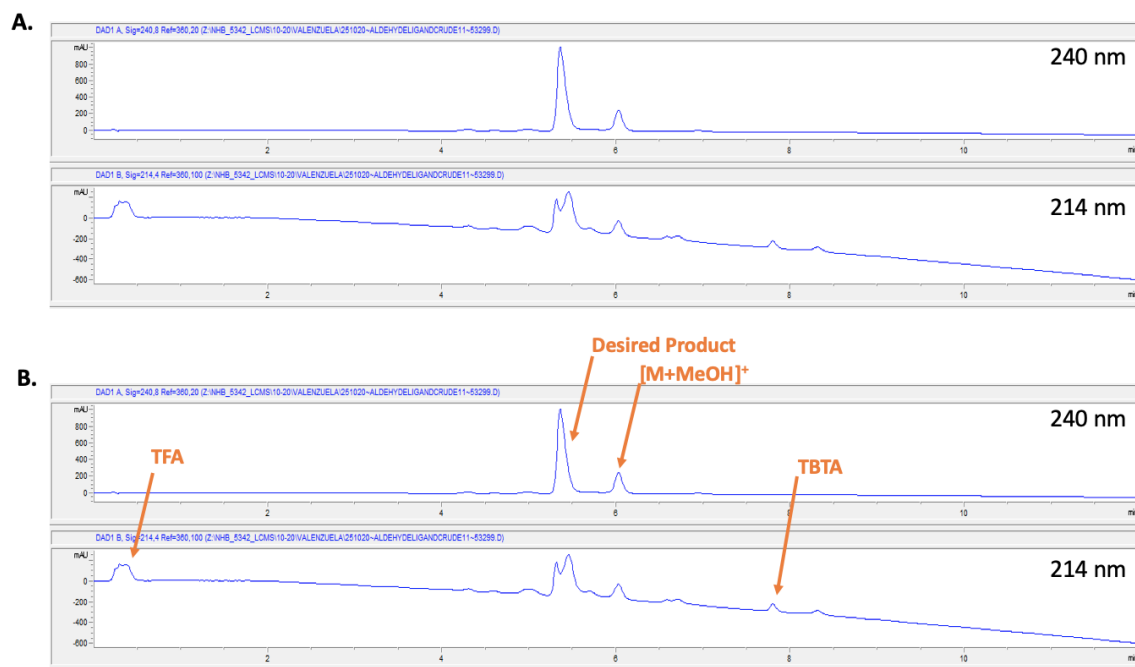


Figure 3.27 The LCMS-trace of the Aldehyde-ligand prior to HPLC purification. (a) The crude UV-trace of the Aldehyde-ligand at 240 and 214 nm. (b) The identities of known impurities.

Synthesis of Colloidal nanocrystals (NCs)

Colloidal nanocrystals (NCs) were synthesized by the modification of a slow injection method to synthesize monodispersed spheres.³⁸ A metal precursor solution (4.75 mmol In(III)acetate, 0.25 mmol Sn(IV)acetate, 10 mL oleic acid) was slow injected into 13 mL of oleyl alcohol held at 290 °C under inert atmosphere. After the reaction, NCs were washed five times with ethanol and redispersed in hexane. NCs were functionalized using a direct ligand exchange method. Oleate-capped NCs in hexane were again flocculated with ethanol and introduced to polar ligand solution (0.01 M ligand in DMF) and sonicated (15 mins). NCs were then flocculated using an ethanol:hexane (1:1) mixture and introduced to a basic solution of water (0.1M KOH pH 14) sonicated (15 mins). The NC precipitate was then centrifuged and dispersed with a second basic

solution (TEA pH 12) and sonicated for (15 mins). The NCs were centrifuged using a filtered centrifuged tube for spin dialysis and redispersed in pure water maintain some basicity (5mL pH 10). Particles were characterized using ^1H NMR, UV/Vis, and STEM (Figure 3.28-3.30).

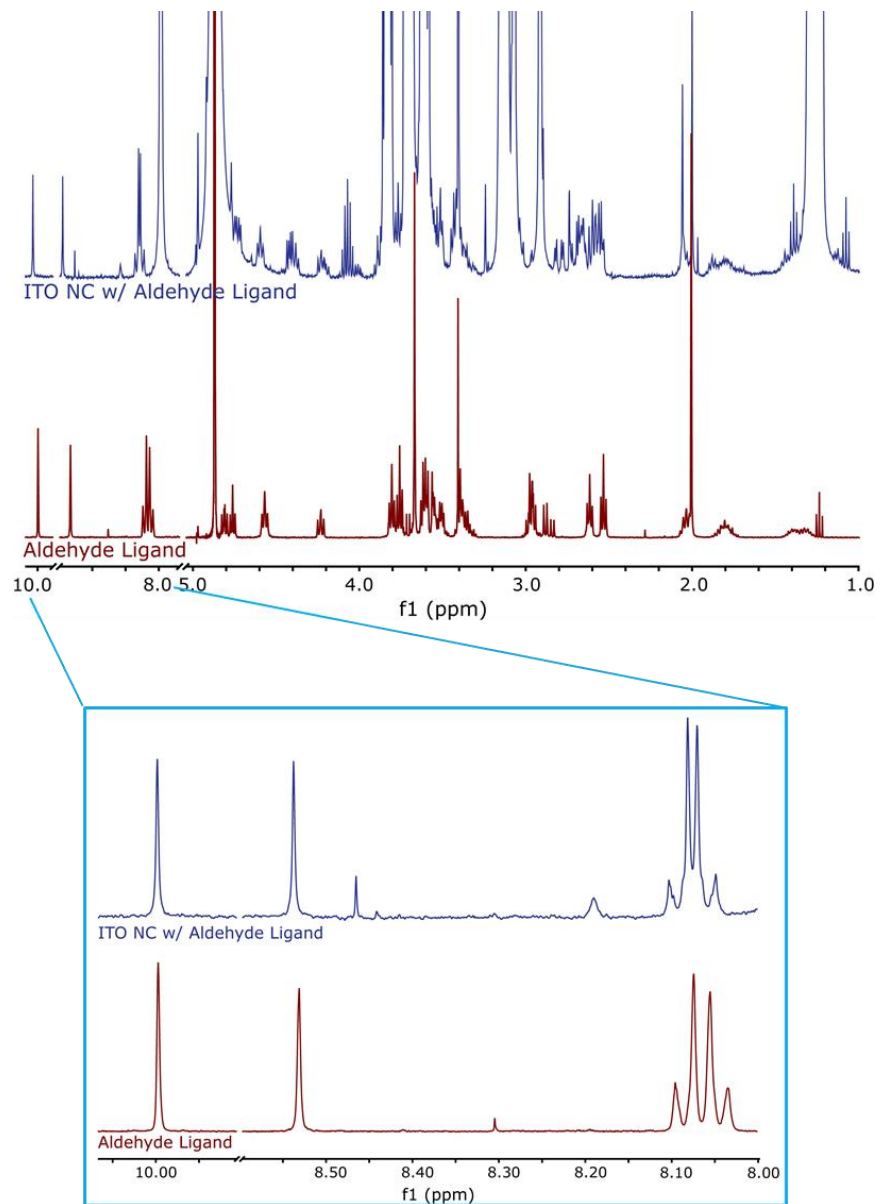


Figure 3.28 ^1H NMR spectrum of NCs.

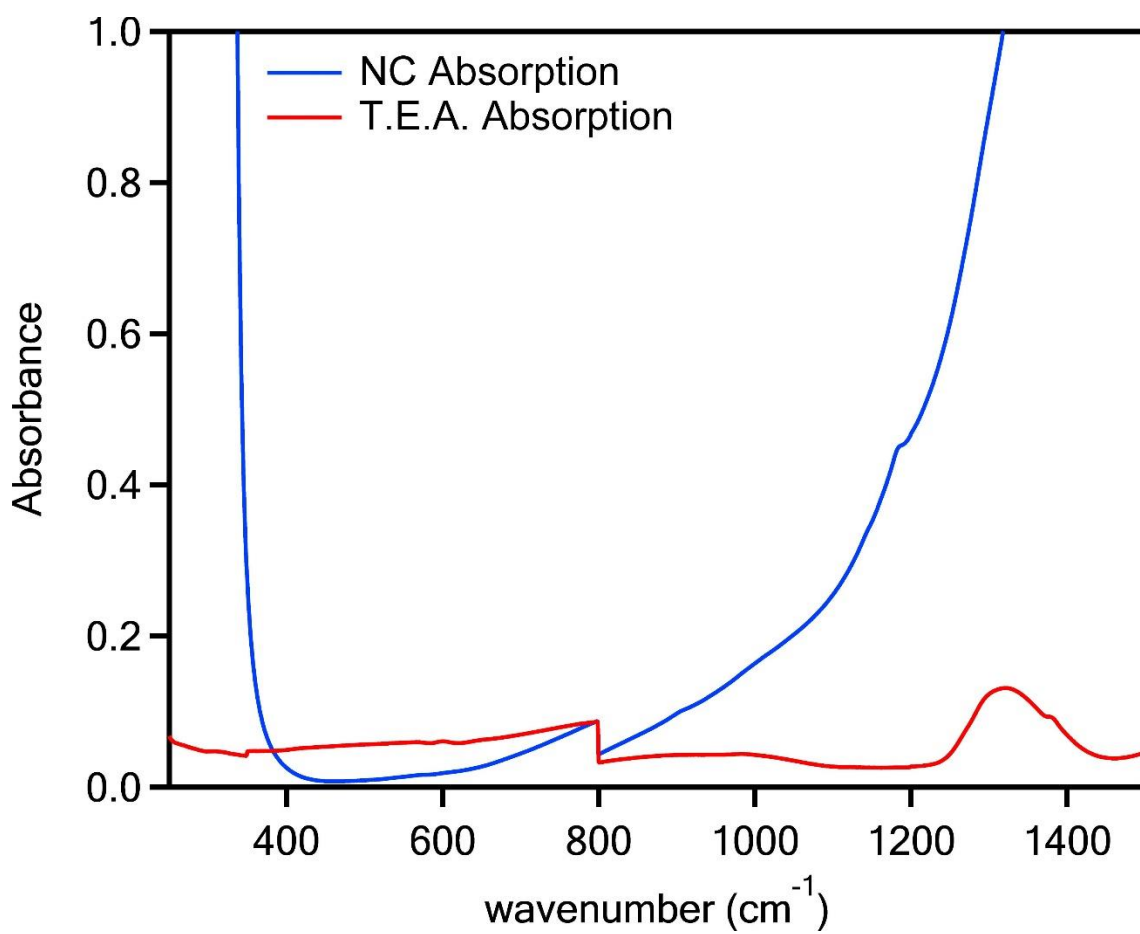


Figure 3.29 Absorbance data of NCs and triethylamine (TEA).

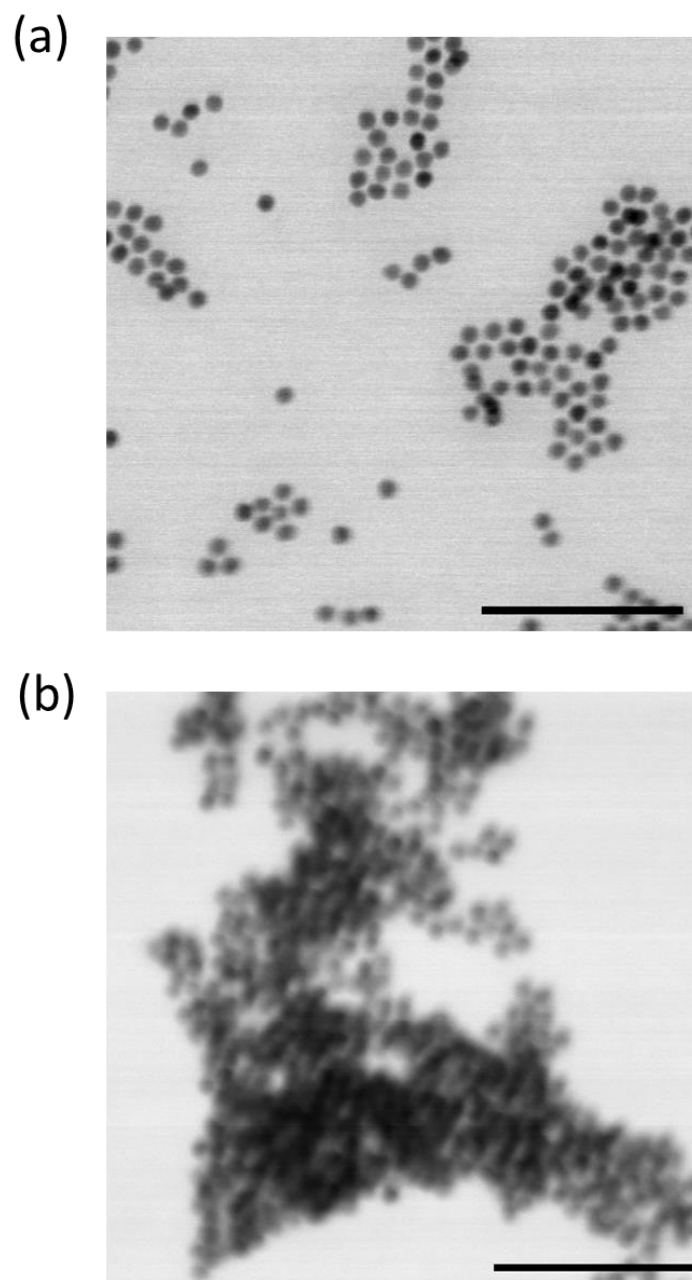


Figure 3.30 (a) and (b) are STEM images before (a) and after (b) the membrane degradation. Both scalebars are 100 nm.

3.6 REFERENCES

1. Thakur, S.; Thakur, V. K.; Arotiba, O. A. *History, Classification, Properties and Application of Hydrogels: An Overview. Hydrogels. Gels Horizons: From Science to Smart Materials*; Springer, Singapore, 2018; pp 29-50.
2. Bahram, M.; Mohseni, N.; Moghtader M. *An Introduction to Hydrogels and Some Recent Applications, Emerging Concepts in Analysis and Applications of Hydrogels*; IntechOpen, 2016; pp 9-38.
3. Caló, E.; Khutoryanskiy, V. V. Biomedical Applications of Hydrogels: A Review of Patents and Commercial Products. *European Polymer Journal* **2015**, *65*, 252-267.
4. Ozcelik, B. *Degradable Hydrogel Systems for Biomedical Applications. Biosynthetic Polymers for Medical Applications*; Elsevier, Australia, 2016; pp 173-188.
5. Ashley, G. W.; Henise, J.; Reid, R.; Santi, D. V. Hydrogel Drug Delivery System with Predictable and Tunable Drug Re-lease and Degradation Rates. *PNAS* **2013**, *110*, 2318-2323.
6. Kim, S. W.; Bae, Y. H.; Okano, T. Hydrogels: Swelling, Drug Loading, and Release. *Pharmaceutical Research* **1992**, *9*, 283-290.
7. Stuart, J. A.; Ursano, R. J.; Fullerton, C. S.; Norwood, A. E.; Murray, K. Belief in Exposure to Terrorist Agents: Reported Exposure to Nerve or Mustard Gas by Gulf War Veterans. *J. Nerv. Ment. Dis.* **2003**, *191*, 431-436.
8. Organisation for the Prohibition of Chemical Weapons (OPCW) Home Page. <https://www.opcw.org> (accessed Feb 03, 2021).
9. Belger, C.; Weis, J. G.; Egap, E.; Swager, T. M. Colorimetric Stimuli-Responsive Hydrogel Polymers for the Detection of Nerve Agent Surrogates. *Macromolecules* **2015**, *48*, 7990-7994.
10. Ali, M. A.; Tsai, T.-H.; Braun, P. V. Amplified Detection of Chemical Warfare Agents Using Two-Dimensional Chemical Potential Gradients. *ACS Omega* **2018**, *3*, 14665-14670.
11. Whitaker, C. M.; Derouin, E. E.; O'connor, M. B.; Whitaker, C. K.; Whitaker, J. A.; Snyder, J. J.; Kaufmann, N. R.; Gilliard, A. N.; Reitmayer, A. K. Smart Hydrogel Sensor for Detection of Organophosphorus Chemical Warfare Nerve Agents. *Journal of Macromolecular Science, Part A* **2017**, *54*, 40-46.

12. Jeremy, P. W.; Sanford A. A. Acetylcholinesterase-Based Organophosphate Nerve Agent Sensing Photonic Crystal. *Anal. Chem.* **2005**, *77*, 1596-1600.
13. Fenglian Q.; Chunxiao Y.; Zihui M.; Shuguang L.; Jiayu X.; Xiaochun H.; Min X. Acetylcholinesterase-Functionalized Two-Dimensional Photonic Crystal for the Sensing of G-Series Nerve Agents. *Analytical and Bioanalytical Chemistry* **2019**, *411*, 2577-2585.
14. Sun, X.; Anslyn, E. V. An Auto-Inductive Cascade for the Optical Sensing of Thiols in Aqueous Media: Application in the Detection of a VX Nerve Agent Mimic. *Angew. Chem.* **2017**, *129*, 9650-9654.
15. Diehl, K. L.; Kolesnichenko, I. V.; Robotham, S. A.; Bachman, J. L.; Zhong, Y.; Brodbelt, J. S.; Anslyn, E. V. Click and Chemically Triggered Declick Reactions through Reversible Amine and Thiol Coupling via a Conjugate Acceptor. *Nature Chemistry* **2016**, *8*, 968-973.
16. Kim, K.; Tsay, O. G.; Atwood, D. A.; Churchill, D. G. Destruction and Detection of Chemical Warfare Agents. *Chem. Rev.* **2011**, *111*, 5345-5403.
17. Balasubramanian, S.; Kulandaisamy, A. J.; Babu, K. J.; Das, A.; Rayappan, J. B. B. Metal Organic Framework Functionalized Textiles as Protective Clothing for the Detection and Detoxification of Chemical Warfare Agents: A Review. *Ind. Eng. Chem. Res.* **2021**, *60*, 4218-4239.
18. Climent, E.; Biyikal, M.; Gawlitza, K.; Dropa, T.; Urban, M.; Costero, A. M.; Martinez-Manez, R.; Rurack, K. Determination of the Chemical Warfare Agents Sarin, Soman and Tabun in Natural Waters Employing Fluorescent Hybrid Silica Materials. *Sens. Actuators B Chem.* **2017**, *246*, 1056-1065.
19. Cavalcante, S. F. D.; Simas, A. B. C.; Kuca, K. Nerve Agents' Surrogates: Invaluable Tools for Development of Acetylcholinesterase Reactivators. *Curr. Org. Chem.* **2019**, *23*, 1539-1559.
20. Bobbitt, N. S.; Mendonca, M. L.; Howarth, A. J.; Islamoglu, T.; Hupp, J. T.; Farha, O. K.; Snurr, R. Q. Metal-Organic Frameworks for the Removal of Toxic Industrial Chemicals and Chemical Warfare Agents. *Chem. Soc. Rev.* **2017**, *46*, 3357-3385.
21. Sun, X.; Chwatko, M.; Lee, D.-H.; Bachman, J. L.; Reu-ther, J. F.; Lynd, N. A.; Anslyn, E. V. Chemically Triggered Synthesis, Remodeling, and Degradation of Soft Materials. *J. Am. Chem. Soc.* **2020**, *142*, 3913-3922.

22. Ishibashi, J. S. A.; Kalow, J. A. Vitrimeric Silicone Elastomers Enabled by Dynamic Meldrum's Acid-Derived Cross-Links. *ACS Macro Lett.* **2018**, *7*, 482-486.
23. DeCollo, T. V.; Lees, W. J. Effects of Aromatic Thiols on Thiol-Disulfide Interchange Reactions that Occur during Protein Folding. *J. Org. Chem.* **2001**, *66*, 4244-4249.
24. Ganesan, K.; Raza, S. K.; Vijayaraghavan, R. Chemical Warfare Agents. *J. Pharm. Bioallied Sci.* **2010**, *2*, 166-178.
25. Kucernak, A. R. J.; Fahy, K. F.; Sundaram, V. N. N. Facile Synthesis of Palladium Phosphide Electrocatalysts and Their Activity for the Hydrogen Oxidation, Hydrogen Evolutions, Oxygen Reduction and Formic Acid Oxidation Reactions. *Catalysis Today* **2016**, *262*, 48-56.
26. Gregory, M. J.; Bruce, T. C. Nucleophilic Displacement Reactions at the Thiol Ester Bond. V. Reactions of 2,2,2-Trifluoroethyl Thioloacetate. *J. Am. Chem. Soc.* **1967**, *89*, 2121-2127.
27. Anslyn, E. V.; Dougherty, D. A. *Modern Physical Organic Chemistry*; University Science Books, 2006; pp 355-419.
28. Jiang, W.; Cao, Y.; Liu, Y.; Wang, W. Rational Design of a Highly Selective and Sensitive Fluorescent PET Probe for Discrimination of Thiophenols and Aliphatic Thiols. *Chem. Commun.* **2010**, *46*, 1944-1946.
29. Kumar, V.; Rana, H. Chromogenic and Fluorogenic Detection and Discrimination of Nerve Agents Tabun and VX. *Chem. Commun.* **2015**, *51*, 16490-16493.
30. Kumar, V.; Raviraju, G.; Rana, H.; Rao, V. K.; Gupta, A. K. Highly Selective and Sensitive Chromogenic Detection of Nerve Agents (sarin, tabun and VX): A Multianalyte Detection Approach. *Chem. Commun.* **2017**, *53*, 12954-12957.
31. Kumar, V.; Rana, H.; Raviraju, G.; Garg, P.; Baghel, A.; Gupta, A. K. Chromogenic and Fluorogenic Multianalyte Detection with a Tuned Receptor: Refining Selectivity for Toxic Anions and Nerve Agents. *RSC Adv.* **2016**, *6*, 59648-59656.
32. Barba-Bon, A.; Costero, A. M.; Gil, S.; Martínez-Mañez, R.; Sancenón, F. Selective Chromo-Fluorogenic Detection of DFP (a Sarin and Soman Mimic) and DCNP (a Tabun Mimic) with a Unique Probe Based on a Boron Dipyrromethene (BODIPY) Dye. *Org. Biomol. Chem.* **2014**, *12*, 8745-8751.

33. Dominguez, M. N.; Howard, M. P.; Maier, J. M.; Valenzuela, S. A.; Sherman, Z. M.; Reuther, J. F.; Reimnitz, L. C.; Kang, J.; Cho, S. H.; Gibbs, S. L.; Menta, A. K.; Zhuang, D. L.; Van der Stok, A.; Kline, S. J.; Anslyn, E. V.; Truskett, T. M.; Milliron, D. J. Assembly of Linked Nanocrystal Colloids by Reversible Covalent Bonds. *Chem. Mater.* **2020**, *32*, 10235-10245.
34. Boles, M.; Ling, D.; Hyeon, T.; Talapin, D. V. The Surface Science of Nanocrystals. *Nature Mater.* **2016**, *15*, 141-153.
35. Dong, A.; Ye, X.; Chen, J.; Kang, Y.; Gordon, T.; Kikkawa, J. M.; Murray, C. B. A Generalized Ligand-Exchange Strategy Enabling Sequential Surface Functionalization of Colloidal Nanocrystals. *J. Am. Chem. Soc.* **2011**, *133*, 998-1006.
36. Jansons, A. W.; Hutchison, J. E. Continuous Growth of Metal Oxide Nanocrystals: Enhanced Control of Nanocrystal Size and Radial Dopant Distribution. *ACS Nano* **2016**, *10*, 6942-6951.
37. von Delius, M.; Geertsema, E. M.; Leigh, D. A. A Synthetic Small Molecule that can Walk Down a Track. *Nat. Chem.* **2010**, *2*, 96-101.
38. Schneider, C. A.; Rasband, W. S.; Eliceiri, K. W. NIH Image to ImageJ: 25 Years of Image Analysis. *Nat. Methods* **2012**, *9*, 671-675.

Chapter 4: A Bis-Pyridinium Calix[4]pyrrole Derivative for Remediation and Detection of Nerve Agents

A bis-pyridinium calix[4]pyrrole appended with anthracene subunits was employed to remediate and detect nerve agents through hydrogen bonding interactions and anion binding, respectively. The system provides a recognition-based approach to facilitating hydrolysis with subsequent detection of the nerve agent's leaving groups.

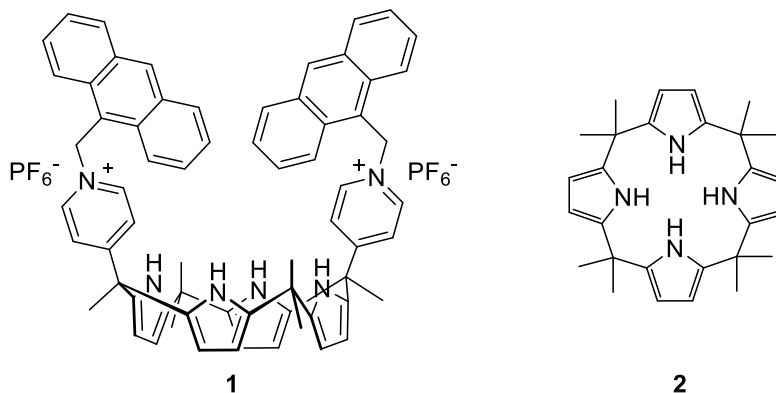
4.1 INTRODUCTION

Chemical warfare agents (CWAs) are one of the most hazardous weapons due to their rapid toxic reactions and sometimes severe chronic sequelae. Although the use of CWAs has been forbidden by the Chemical Weapons Convention, their low cost, potency, and easy mass production makes them attractive for use in warfare and terrorism.^{1,2}

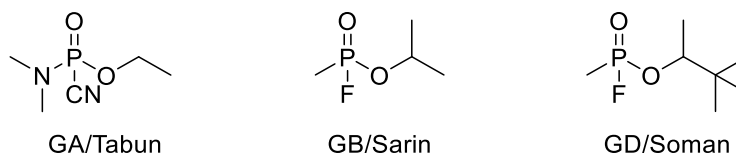
Nerve agents, the most commonly used CWAs, are organo-phosphorus compounds. These agents inhibit the degradation of acetylcholine by inactivation of the enzyme acetylcholinesterase. To prevent, or reverse, their binding with this enzyme, nerve agents can be hydrolyzed.³⁻⁷ Their hydrolysis rate at neutral pH and room temperature is relatively slow. As examples, several hydrolysis half-lives of nerve agents (Figure 1) are as follows: GA (8.5 hours at pH 7), GB (39 hours at pH 7), GD (45 hours at pH 6.6), and VX (1,000 hours at pH 7).^{7,8} Therefore, catalytic acceleration of the hydrolysis of nerve agents would be advantageous for their destruction.

Recently, progress toward achieving this goal has been made using supramolecular and receptor-based approaches.⁹ Gale and co-workers reported neutral 1,3-diindolylureas as organocatalysts for the accelerated hydrolysis of the nerve agent mimics (Figure 1) diethyl cyanophosphonate (DCNP) and diisopropyl fluorophosphate (DFP).¹⁰ These catalysts enhanced the hydrolysis rate of these nerve agent surrogates through hydrogen bonding and hydrophobic effects, and a separate indicator was employed to measure the hydrolysis rate based on a pH change. Moreover, the same group reported tripodal amide/histidine-containing receptors capable of increasing the rate of GD hydrolysis *via* hydrogen bonding interactions.¹¹

- Receptors



- G-Nerve Agents



- Nerve Agent Simulants

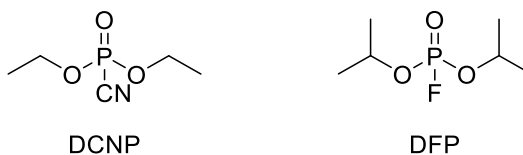
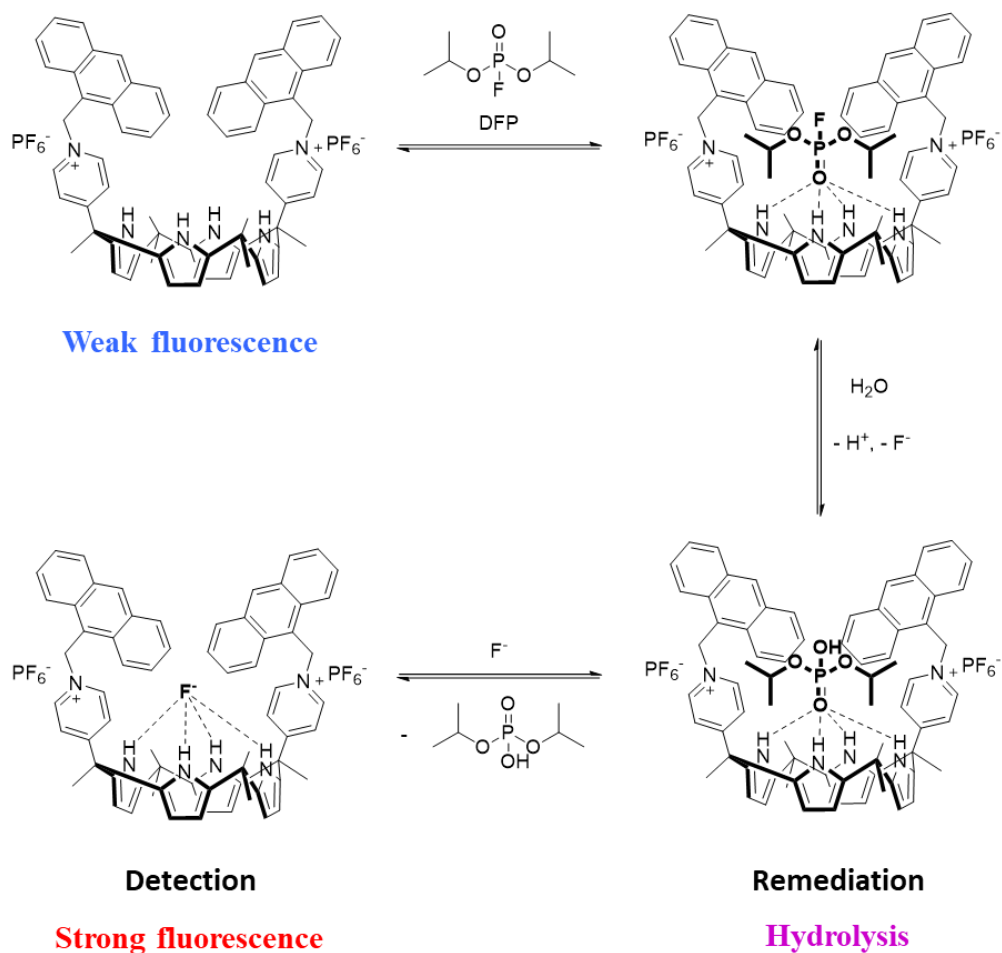


Figure 4.1 Receptors **1** and **2** used for nerve agent remediation and detection, G-series nerve agents and their simulants.

Calix[4]pyrroles are non-aromatic tetrapyrrolic macrocycles that have been extensively studied as anion receptors, ion-pair receptors, transmembrane transporters, and molecular containers.¹²⁻¹⁶ We postulated that a dicationic calix[4]pyrrole functionalized with fluorophores would not only enhance the hydrolysis of the nerve agents, but also result in a fluorescence turn-on by binding with the departed anionic leaving groups. This led to the design of calix[4]pyrrole **1** (**Figure 4.1**). This bis-pyridinium calix[4]pyrrole bearing fluorogenic anthracene subunits was expected to

polarize the P=O bond of the nerve agent upon binding through four hydrogen bonds, and to do so more than the neutral calix[4]pyrrole **2** due to its cationic charges. The polarization via hydrogen bonding and field effects were postulated to increase in the hydrolysis rate by facilitating nucleophilic attack by water. Furthermore, the anion released from the nerve agent during hydrolysis was anticipated to bind the receptor stronger than the phosphate anionic product, and thus would replace the hydrolyzed nerve agent from receptor **1** (Scheme 4.1).

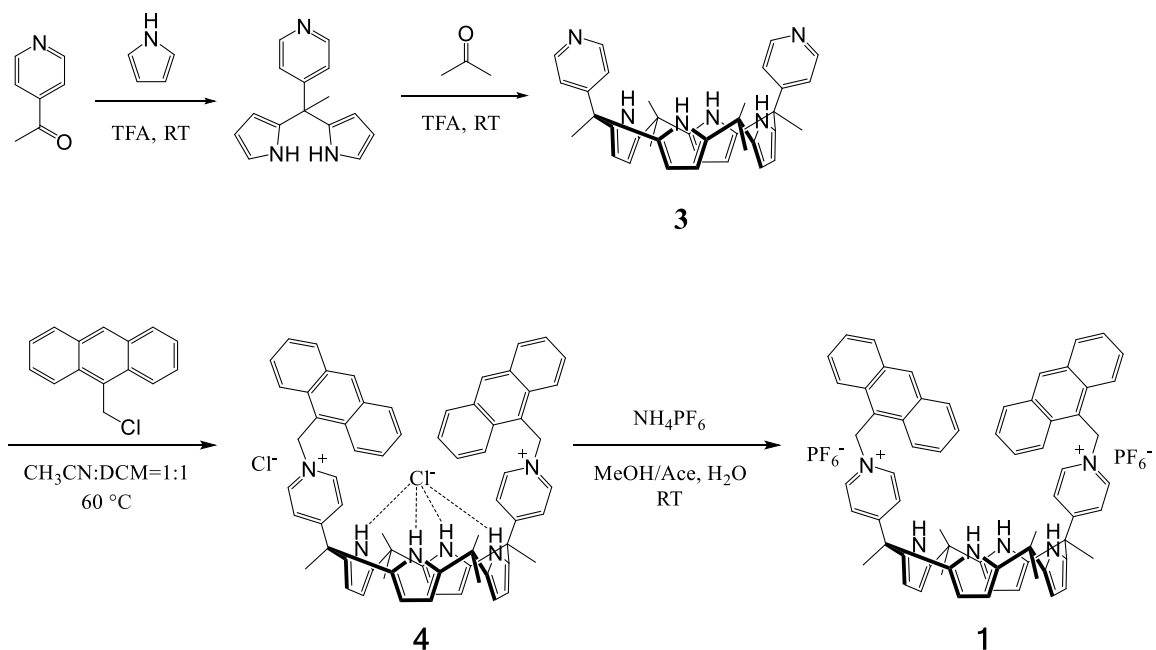


Scheme 4.1 The proposed scheme for remediation and detection of a nerve agent simulant, incorporating **1** and DFP.

4.2 RESULTS AND DISCUSSION

4.2.1 Synthesis of the Receptor 1

The synthesis of receptor **1** is shown in Scheme S1. Coupling of *cis*-bispyridine-functionalized calix[4]pyrrole derivative with 9-(chloromethyl)anthracene gave the tetrachloride salt of the compound **1**, which afforded receptor **1** as the tetrahexafluorophosphate salt in a good yield followed by the anion exchange reaction. All compounds were characterized by standard spectroscopic methods (see the section 4.4.3 for details).



Scheme 4.2 Scheme of synthesis of **1**.

4.2.2 ^1H NMR Studies of Receptors with Nerve Agent Simulants

To explore the catalysis of hydrolysis and the binding of the leaving groups, ^1H NMR spectroscopy was conducted using receptors **1** and **2** and the nerve agent surrogates DCNP and DFP in CD_3CN (**Figure 4.2a-d**). These mimics have been reported to show similar reactivity to the actual toxic agents.^{17,18} In the presence of either DCNP or DFP, the N-H signals of the calix[4]pyrrole core were observed to shift downfield as a result of forming hydrogen bonds between the pyrrole NH protons and nerve agent surrogates. The pyrrole N-H resonances of **1** were shifted with DCNP (**Figure 4.2a**) and DFP (**Figure 4.2b**) more than those of **2** with DCNP (**Figure 4.2c**) and DFP (**Figure 4.2d**). Job plot analysis provided evidence for the formation of a 1:1 complex stoichiometry between receptor **1** and both nerve agent surrogates (**Figure 4.3**). By fitting the ^1H NMR titration curves to a standard 1:1 binding profile, association constants (K_a) corresponding to the interactions between **1** and the nerve agent mimics were determined (**Figure 4.4, 4.5**). Receptor **1** was found to exhibit a higher affinity towards DCNP than towards DFP ($K_a=4.8\pm 0.8 \times 10 \text{ M}^{-1}$ and $1.1\pm 0.1 \times 10 \text{ M}^{-1}$ for DCNP and DFP, respectively). In contrast, negligible binding of **2** with both surrogates was observed ($K_a < 1 \text{ M}^{-1}$). Thus, the ^1H NMR spectroscopic analyses led to the conclusion that dicationic receptor **1** has a higher affinity for nerve agent surrogates than **2**. This finding was ascribed to a combined participation of hydrogen bonding with the pyrrole NHs and electrostatic field effects.

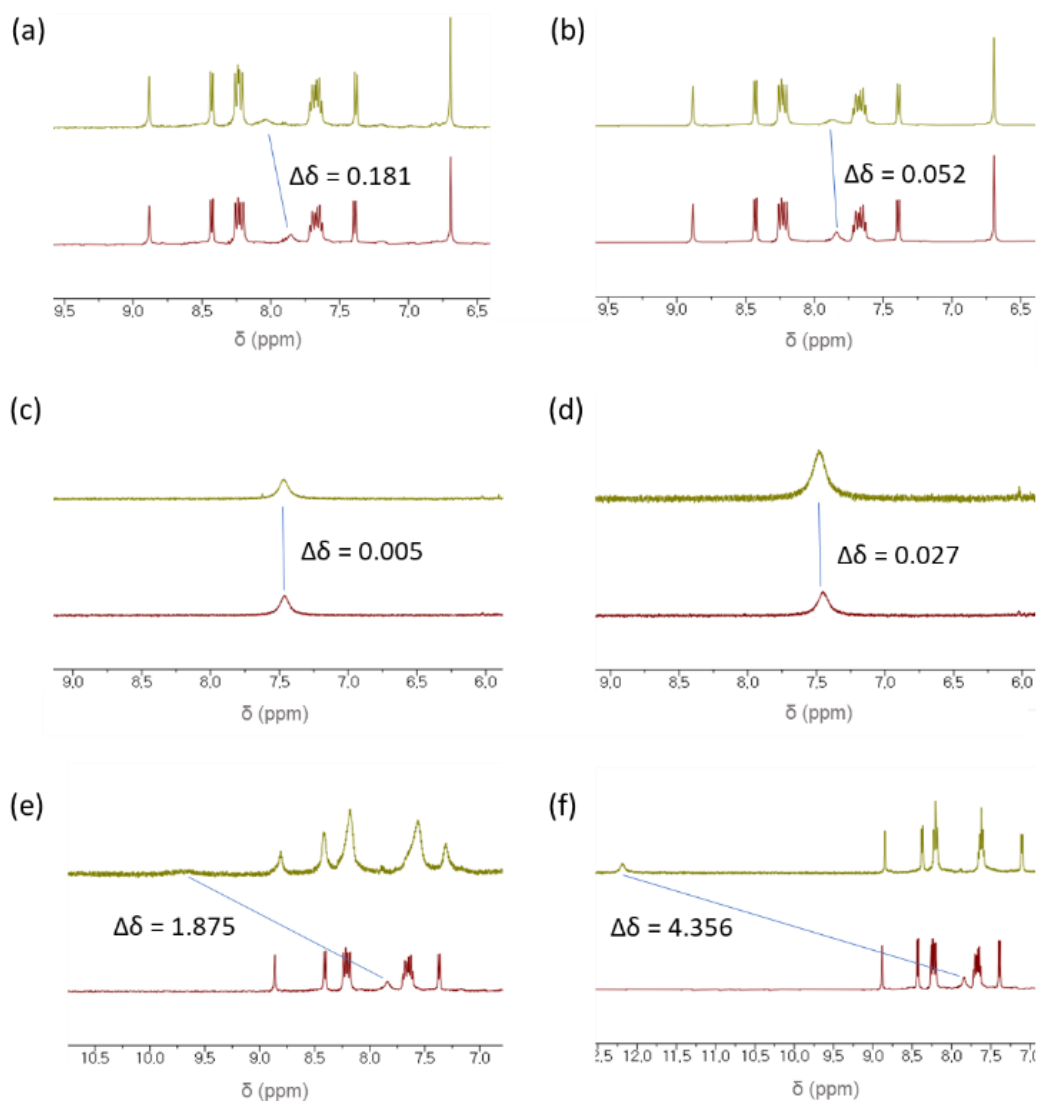


Figure 4.2 ^1H NMR spectra of receptors for pyrrole protons in acetonitrile- $[\text{d}_3]$. (a) Initial free compound **1** (bottom) and **1** with the addition of 1 equivalent of DCNP (top). (b) Initial free compound **1** (bottom) and **1** with the addition of 1 equivalent of DFP (top). (c) Initial free compound **2** (bottom) and **2** with the addition of 1 equivalent of DCNP (top). (d) Initial free compound **2** (bottom) and **2** with the addition of 1 equivalent of DFP (top). (e) Initial free compound **1** (bottom) and **1** with the addition of 1 equivalent of TBACN (top). (f) Initial free compound **1** (bottom) and **1** with the addition of 1 equivalent of TBAF.

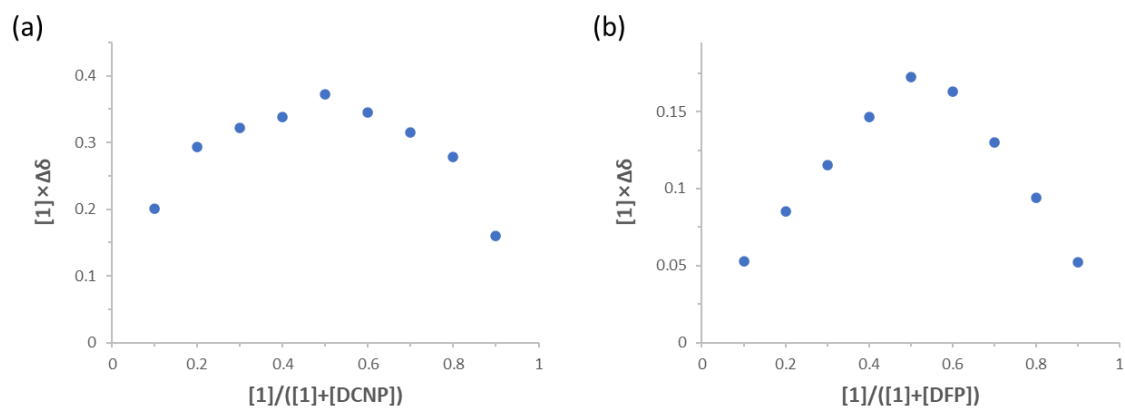


Figure 4.3 Job plot obtained from ^1H NMR titration of **1** with (a) DCNP and (b) DFP in CD_3CN for which $[1]+[\text{DCNP}] = 5 \text{ mM}$ and $[1]+[\text{DFP}] = 5 \text{ mM}$ each.

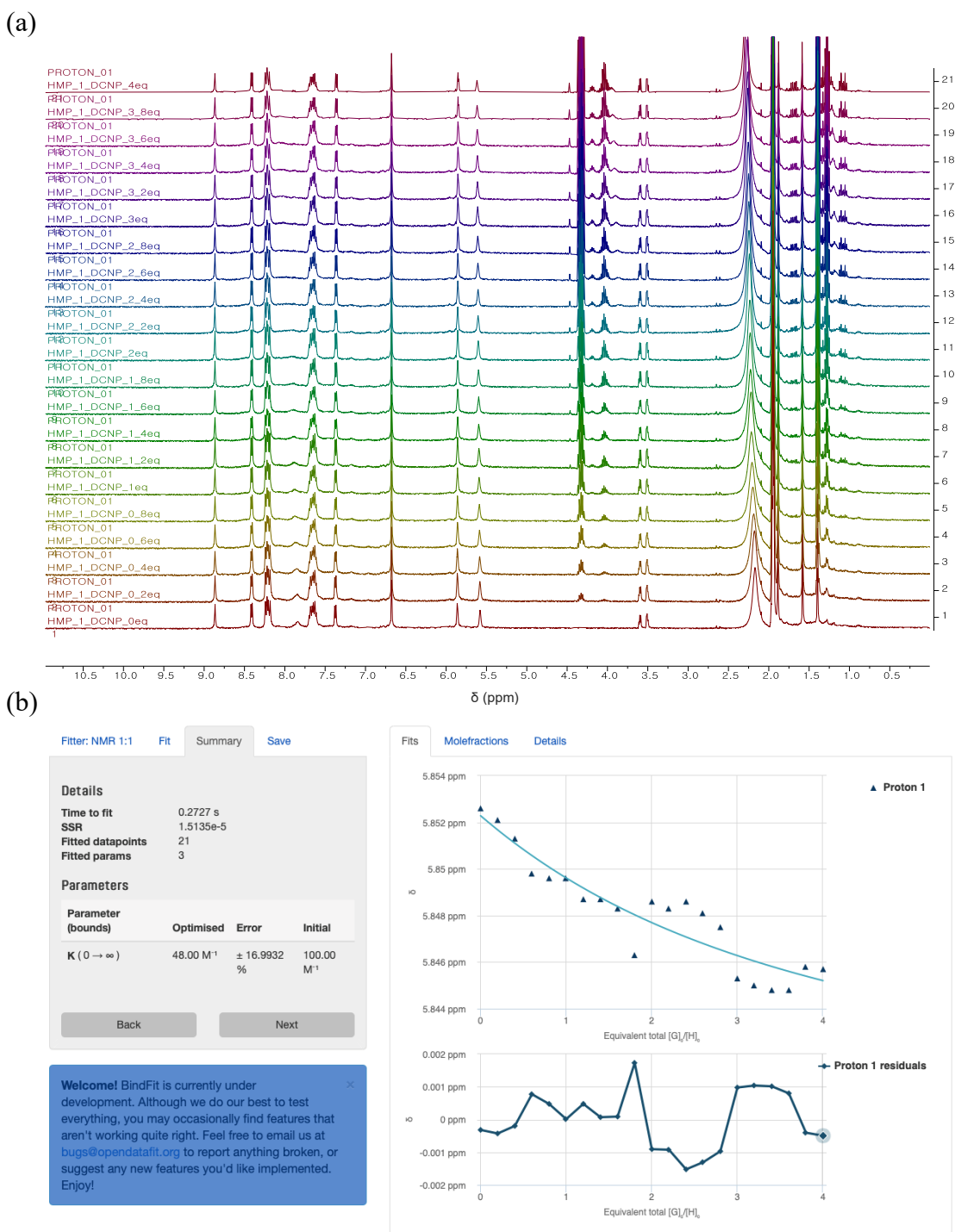


Figure 4.4 (a) ^1H NMR studies between DCNP and **1**. DCNP (0 equiv. (bottom) to 4 equiv. (top)) was gradually added to the solution of CD_3CN in the presence of **1** (6 mM). (b) Association constants of **1** with DCNP calculated with (a).

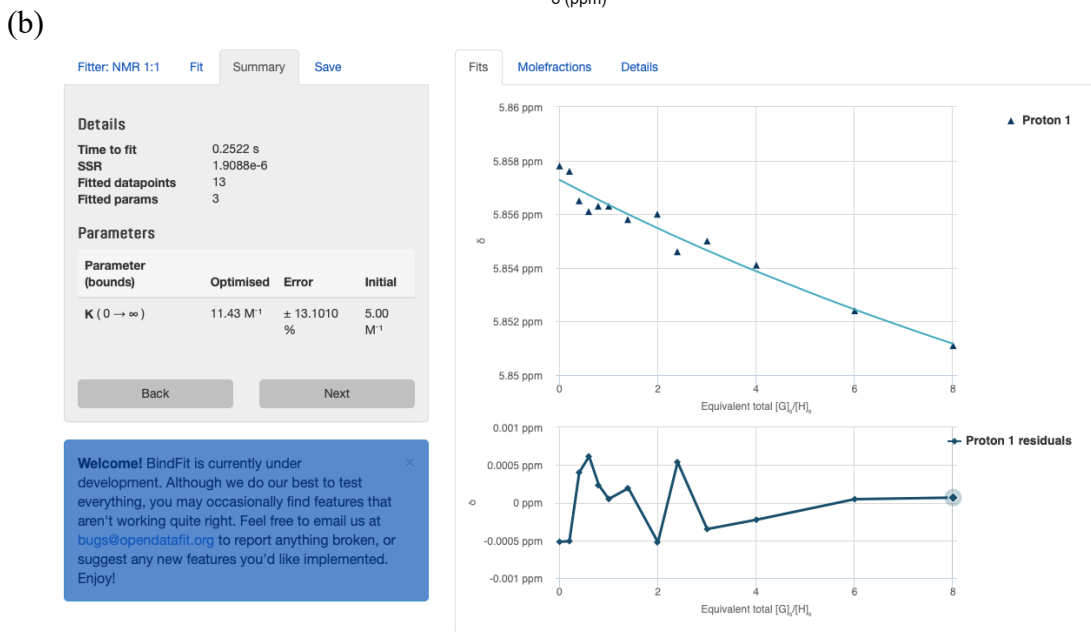
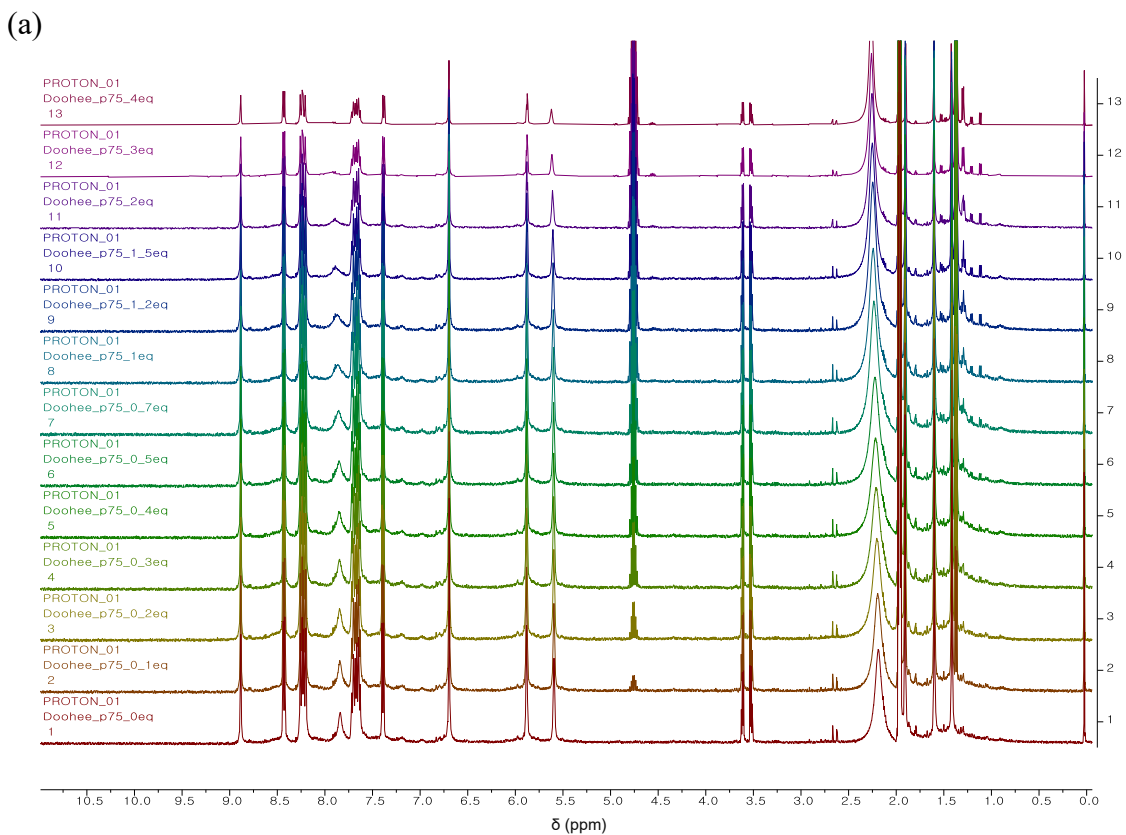


Figure 4.5 (a) ^1H NMR studies between DFP and **1**. DFP (0 equiv. (bottom) to 4 equiv. (top)) was gradually added to the solution of CD_3CN in the presence of **1** (6 mM). (b) Association constants of **1** with DFP calculated with (a).

4.2.3 Association Constants between **1** and Nerve Agents Leaving Groups

The association constants of the leaving groups from hydrolysis, CN^- and F^- anions, to receptor **1** were also measured and found to be $5.0 \pm 0.2 \times 10^3 \text{ M}^{-1}$ and $1.0 \pm 0.1 \times 10^4 \text{ M}^{-1}$, respectively (Figure 4.6 and 4.7). This finding was taken as evidence that the CN^- and F^- anions form a tighter hydrogen bonding complex with the pyrrole N–H protons, which supported our hypothesis that they will replace the pre-bound hydrolyzed nerve agent.

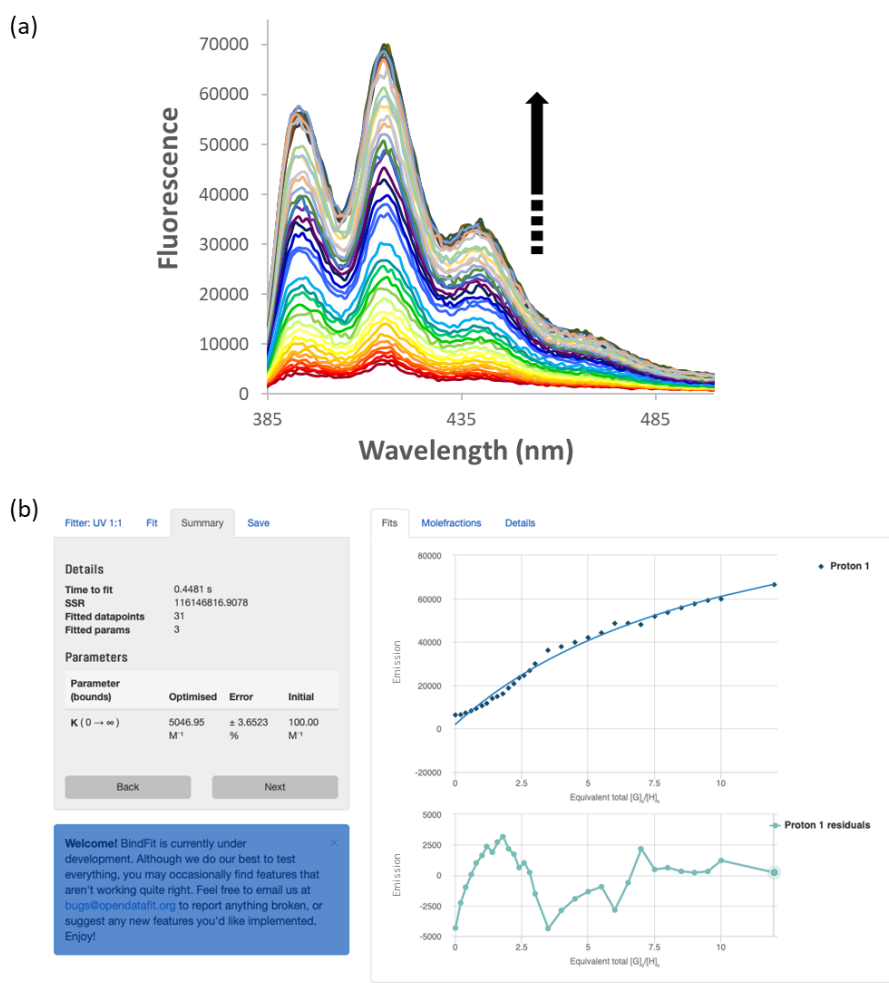


Figure 4.6 (a) Fluorescence emission spectra ($\lambda_{\text{ex}} = 372 \text{ nm}$) of **1** ($20 \mu\text{M}$) upon addition of TBACN (0-50 equivalents) along with the arrow in CH_3CN . (b) Association constant of **1** with TBACN calculated with (a) at 416 nm.

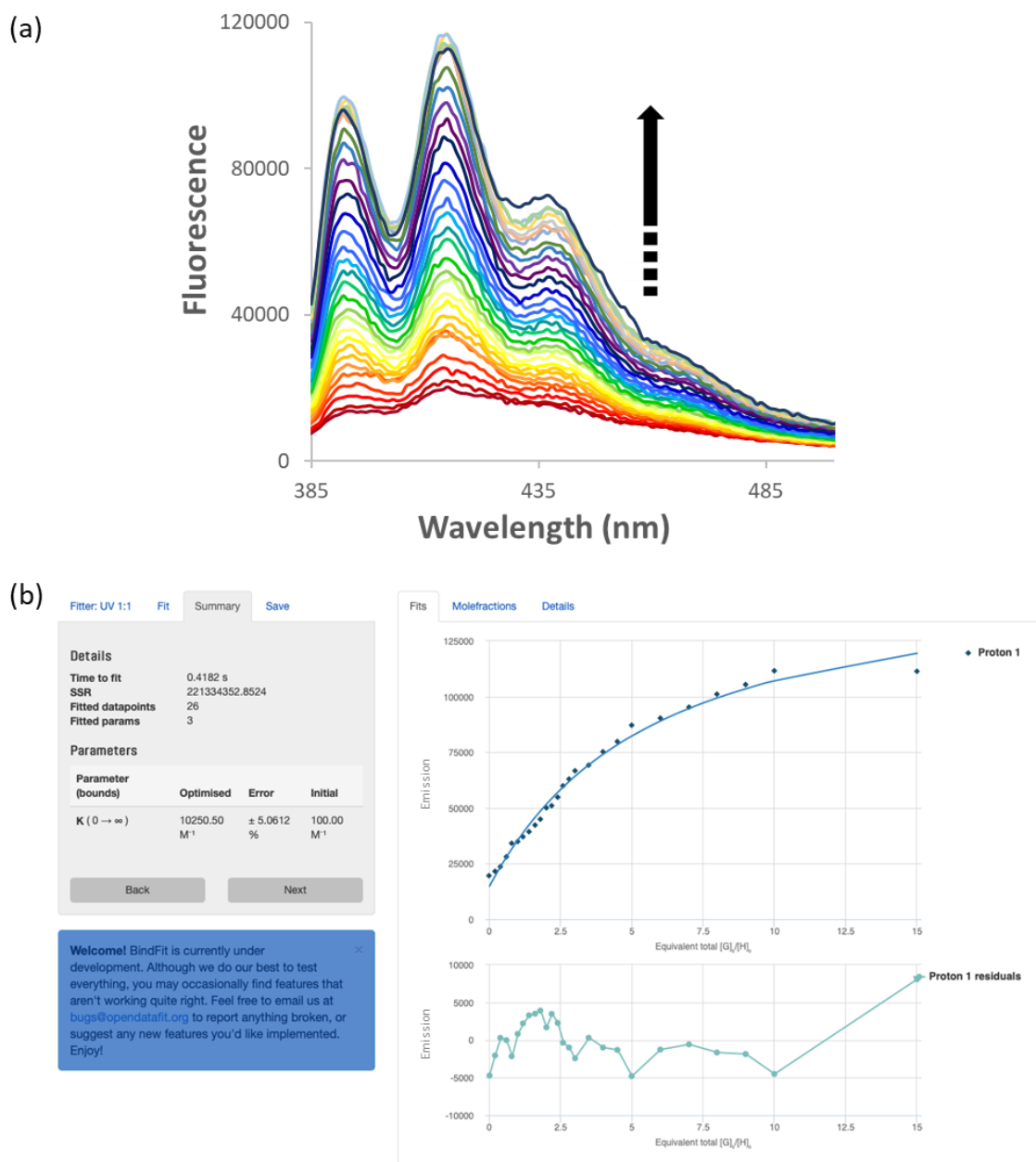


Figure 4.7 (a) Fluorescence emission spectra ($\lambda_{\text{ex}} = 372 \text{ nm}$) of **1** ($20 \mu\text{M}$) upon addition of TBAF (0-50 equivalents) along with the arrow in CH_3CN . (b) Association constants of **1** with TBAF calculated with the result of (a) at 416 nm .

To study the predicted fluorescence turn-on response of receptor **1** when binding the leaving groups of the nerve agent surrogates, these anions (as their TBA⁺ salts) were studied in CH₃CN. Receptor **1** alone showed a very weak fluorescence emission upon excitation at 372 nm. However, upon addition of either CN⁻ or F⁻ to the solution of receptor **1**, an increase in fluorescence intensity centered at 416 nm (**Figure 4.8**) was observed. This finding was rationalized in as an inhibition of photoinduced electron transfer upon CN⁻ or F⁻ binding to calix[4]pyrrole.¹⁹

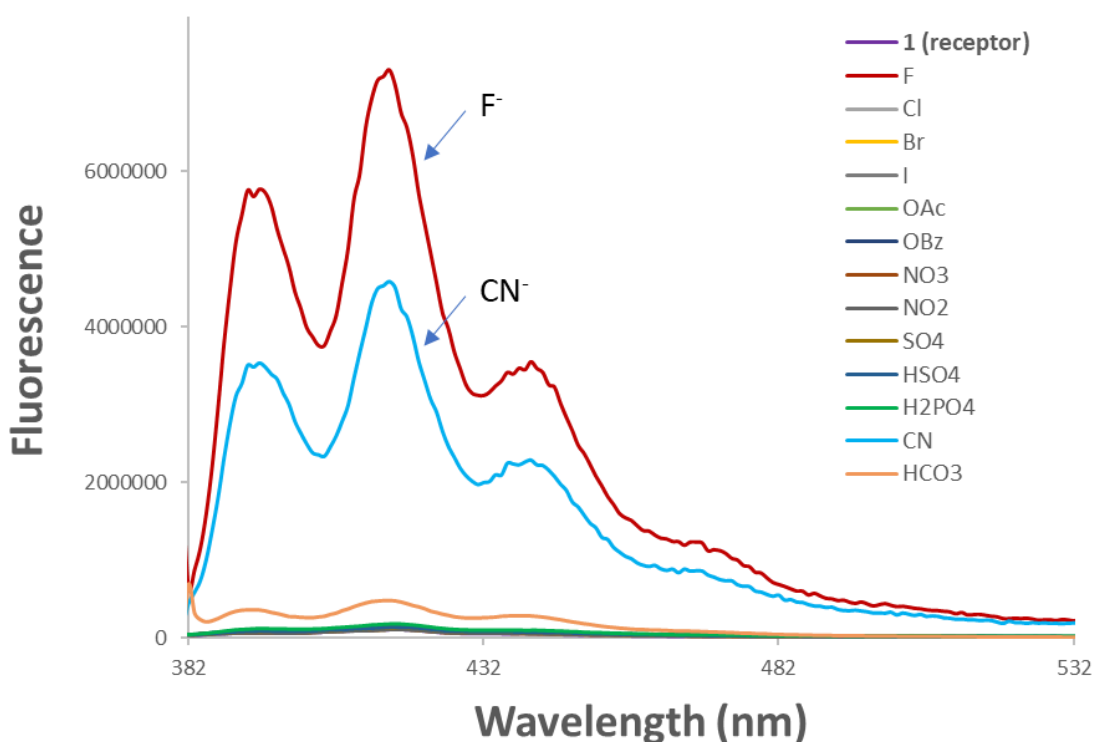


Figure 4.8 Fluorescence emission spectra ($\lambda_{\text{ex}} = 372$ nm) changes of **1** (20 μM) upon addition of various anions (100 equiv.) in CH₃CN. The anions were F⁻, Cl⁻, Br⁻, I⁻, OAc⁻, OBz⁻, NO₃⁻, NO₂⁻, SO₄²⁻, HSO₄⁻, H₂PO₄²⁻, CN⁻, HCO₃⁻ from TBA salts.

4.2.4 Hydrolysis Rates of Nerve Agent Simulants with the Receptors

We set out to measure the enhancement of hydrolysis rates using **1** and **2**. Thus, the 2nd order hydrolysis rate constants were determined in 1% H₂O in CH₃CN via following the changes in fluorescence intensity resulting from the binding of the leaving groups to receptor **1**.²⁰ The result revealed hydrolysis rate constants (k in units of mol⁻¹ · min⁻¹) of $k = 0.687$ for receptor-free, $k = 2.795$ for receptor **1**, and $k = 0.942$ for receptor **2**, respectively, in the case of DCNP (**Table 4.1**). The hydrolysis rate of DCNP is enhanced by 4.1-fold and 1.4-fold by receptor **1** and **2**, respectively. In addition, similar hydrolysis rates were seen in the case of DFP. Combined together, these results provide supports for the conclusion that the dicationic receptor **1** proved to be more effective in hydrolysis of the nerve agent surrogates than the neutral receptor **2** (see **Figure 4.9 – 4.14** for details).

Receptors	DCNP (M ⁻¹ · min ⁻¹)	DFP (M ⁻¹ · min ⁻¹)
Control*	0.687	0.525
1	2.795	2.536
2	0.942	0.771

* Only DCNP or DFP without receptors

Table 4.1 The 2nd order hydrolysis rate constants of DCNP and DFP with **1** or **2** or receptor-free in 1% H₂O in CH₃CN.

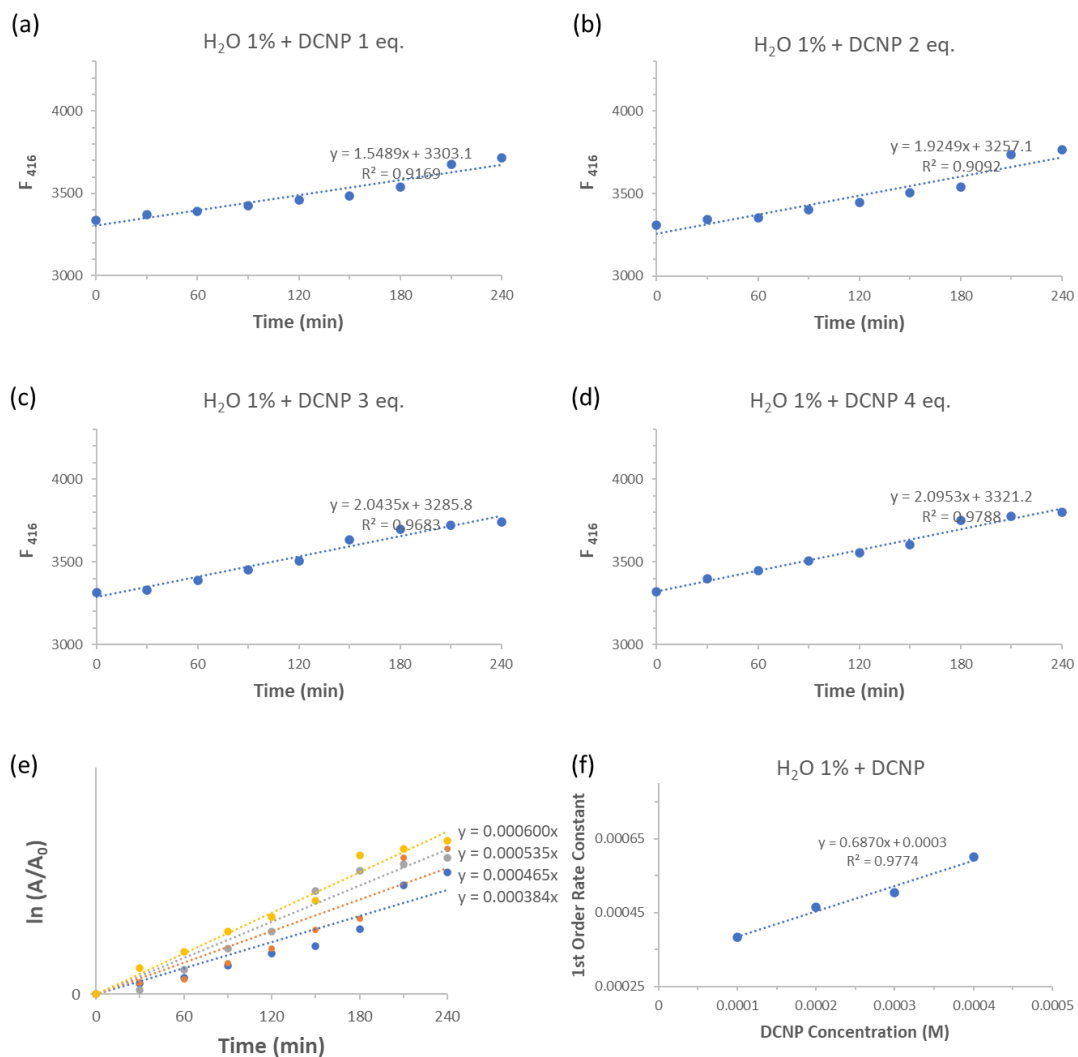


Figure 4.9 Time kinetic studies with fluorescence intensity changes of DCNP (a) 100 μM ; (b) 200 μM ; (c) 300 μM ; (d) 400 μM in acetonitrile (99%) and water (1%). Each time fluorescence was measured, the amount of released cyanide anion after hydrolysis was measured by the change in fluorescence intensity of 1 (100 μM). (e) First order rate constant was calculated from (a)-(d). Each slope represented the first order rate constant. (f) The second order rate constant was calculated from the concentration of DCNP and the first order rate constant (e). Finally, the second order rate constant was calculated to be $0.687 \text{ M}^{-1} \cdot \text{min}^{-1}$.

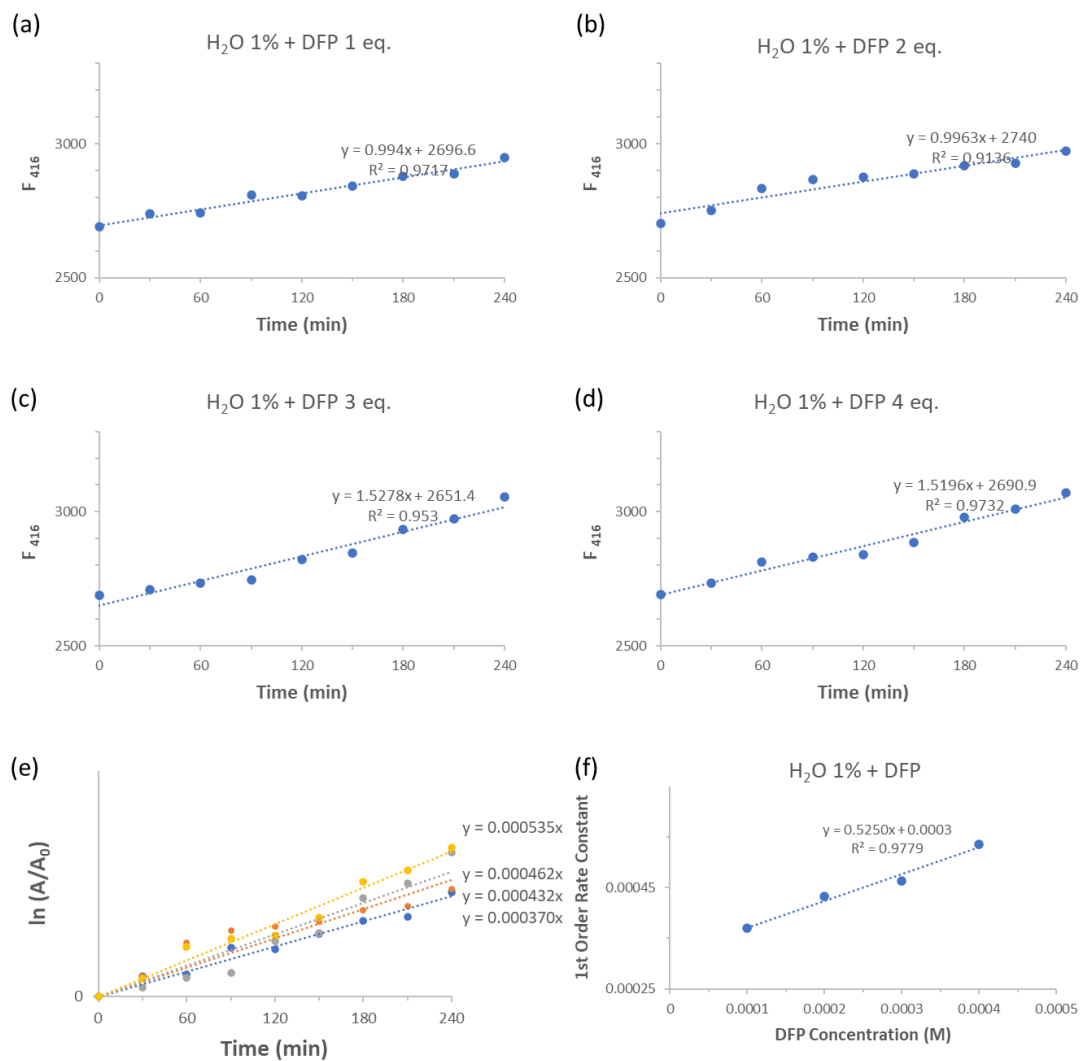


Figure 4.10 Time kinetic studies with fluorescence intensity changes of DFP (a) 100 μM ; (b) 200 μM ; (c) 300 μM ; (d) 400 μM in acetonitrile (99%) and water (1%). Each time fluorescence was measured, the amount of released fluoride anion after hydrolysis was measured by the change in fluorescence intensity of **1** (100 μM). (e) First order rate constant was calculated from (a)-(d). Each slope represented the first order rate constant. (f) The second order rate constant was calculated from the concentration of DFP and the first order rate constant (e). Finally, the second order rate constant was calculated to be $0.525 \text{ M}^{-1} \cdot \text{min}^{-1}$.

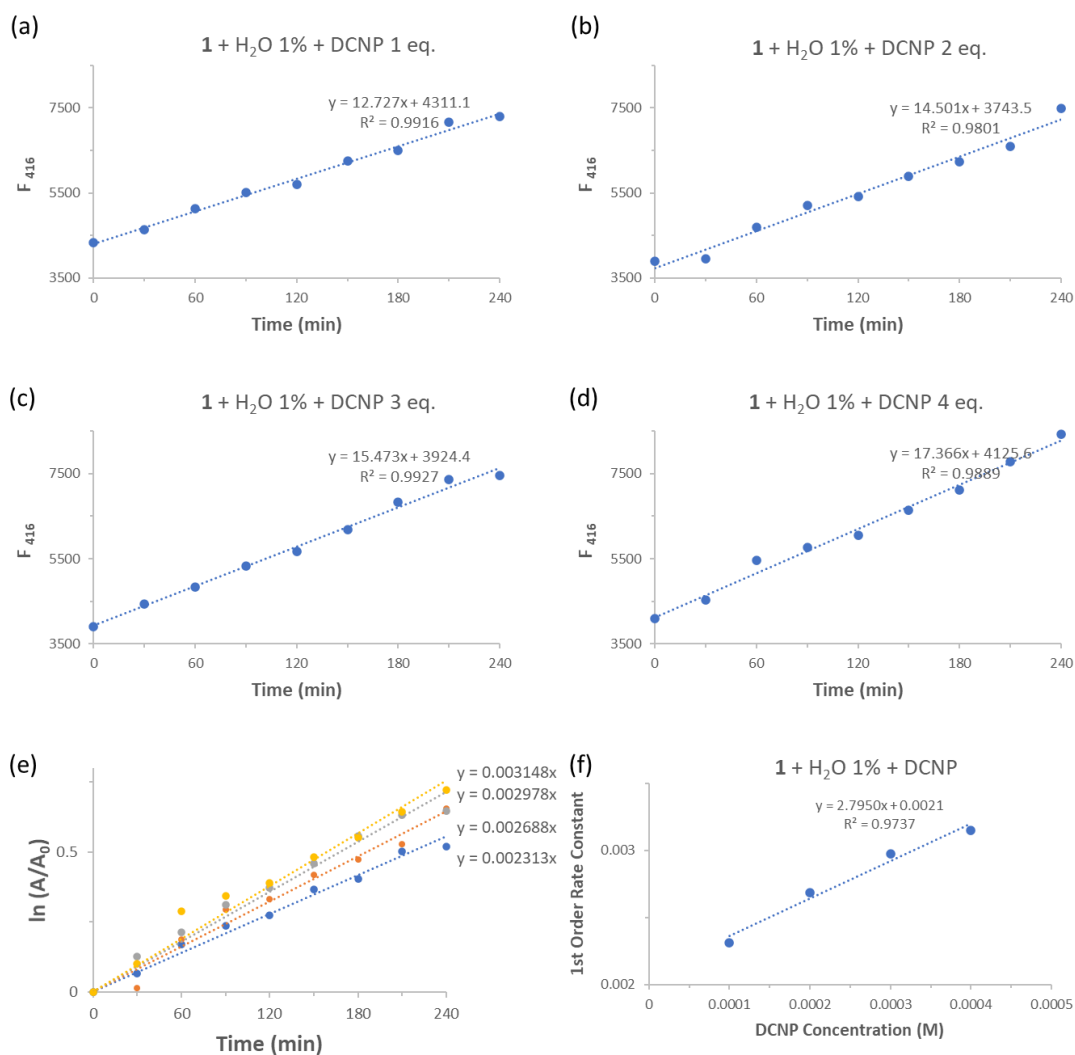


Figure 4.11 Time kinetic studies with fluorescence intensity changes of **1** (100 μM) and DCNP (a) 1; (b) 2; (c) 3; (d) 4 equivalents compared to **1** in acetonitrile (99%) and water (1%). (e) First order rate constant was calculated from (a)-(d). The slope was the first order rate constant, respectively. (f) The second order rate constant was calculated from the concentration of DCNP and the first order rate constant (e). Finally, the second order rate constant was determined to be $2.795 \text{ M}^{-1} \cdot \text{min}^{-1}$.

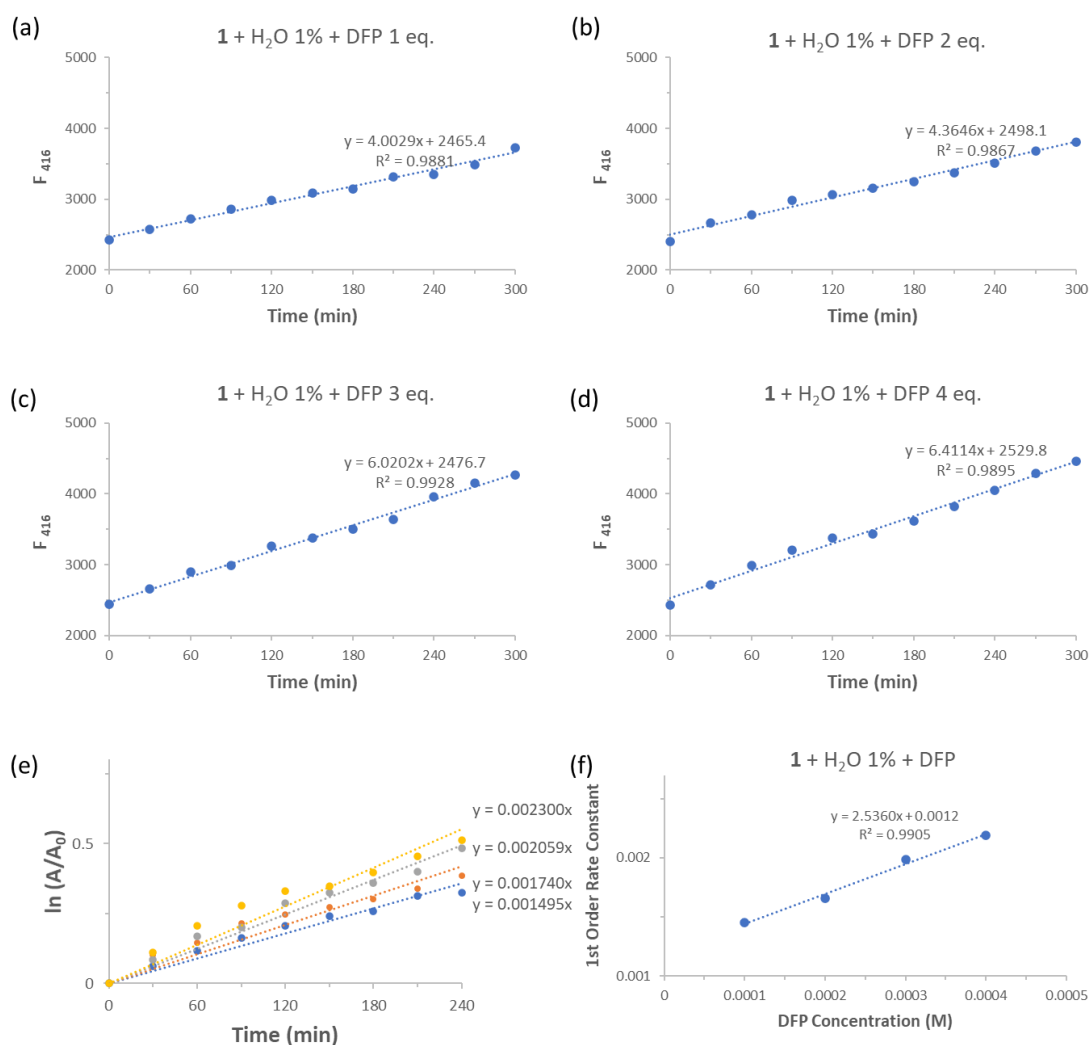


Figure 4.12 Time kinetic studies with fluorescence intensity changes of **1** (100 μM) and DFP (a) 1; (b) 2; (c) 3; (d) 4 equivalents compared to **1** in acetonitrile (99%) and water (1%). (e) First order rate constant was calculated from (a)-(d). The slope was the first order rate constant, respectively. (f) The second order rate constant was calculated from the concentration of DFP and the first order rate constant (e). Finally, the second order rate constant was determined to be $2.536 \text{ M}^{-1} \cdot \text{min}^{-1}$.

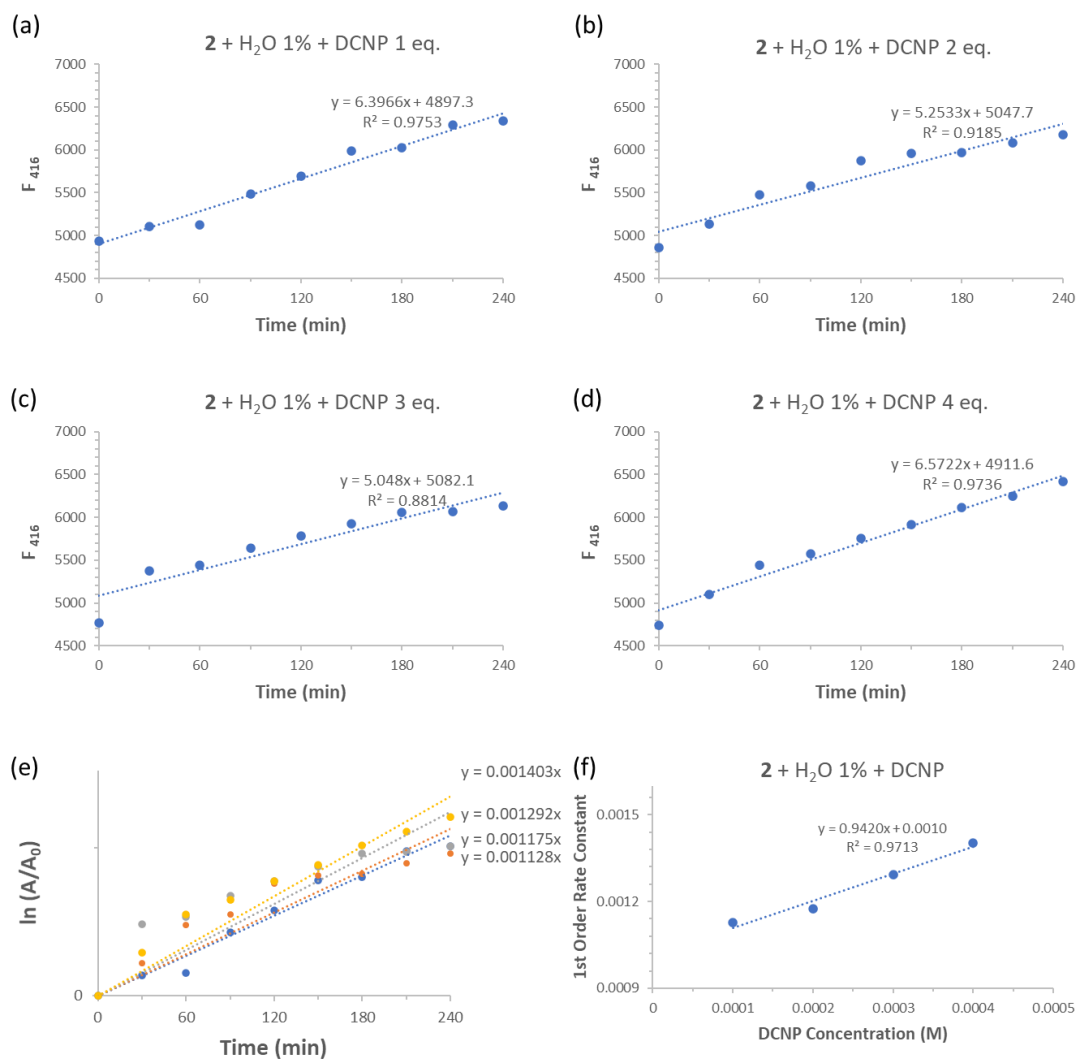


Figure 4.13 Time kinetic studies with fluorescence intensity changes of **2** (100 μM) and DCNP (a) 1; (b) 2; (c) 3; (d) 4 equivalents compared to **2** in acetonitrile (99%) and water (1%). Each time fluorescence was measured, the amount of released cyanide anion after hydrolysis was measured by the fluorescence intensity changes of **1** (100 μM). (e) First order rate constant was calculated from (a)-(d). The slope was the first order rate constant, respectively. (f) The second order rate constant was calculated from the concentration of DCNP and the first order rate constant (e). Finally, the second order rate constant was $0.942 \text{ M}^{-1} \cdot \text{min}^{-1}$.

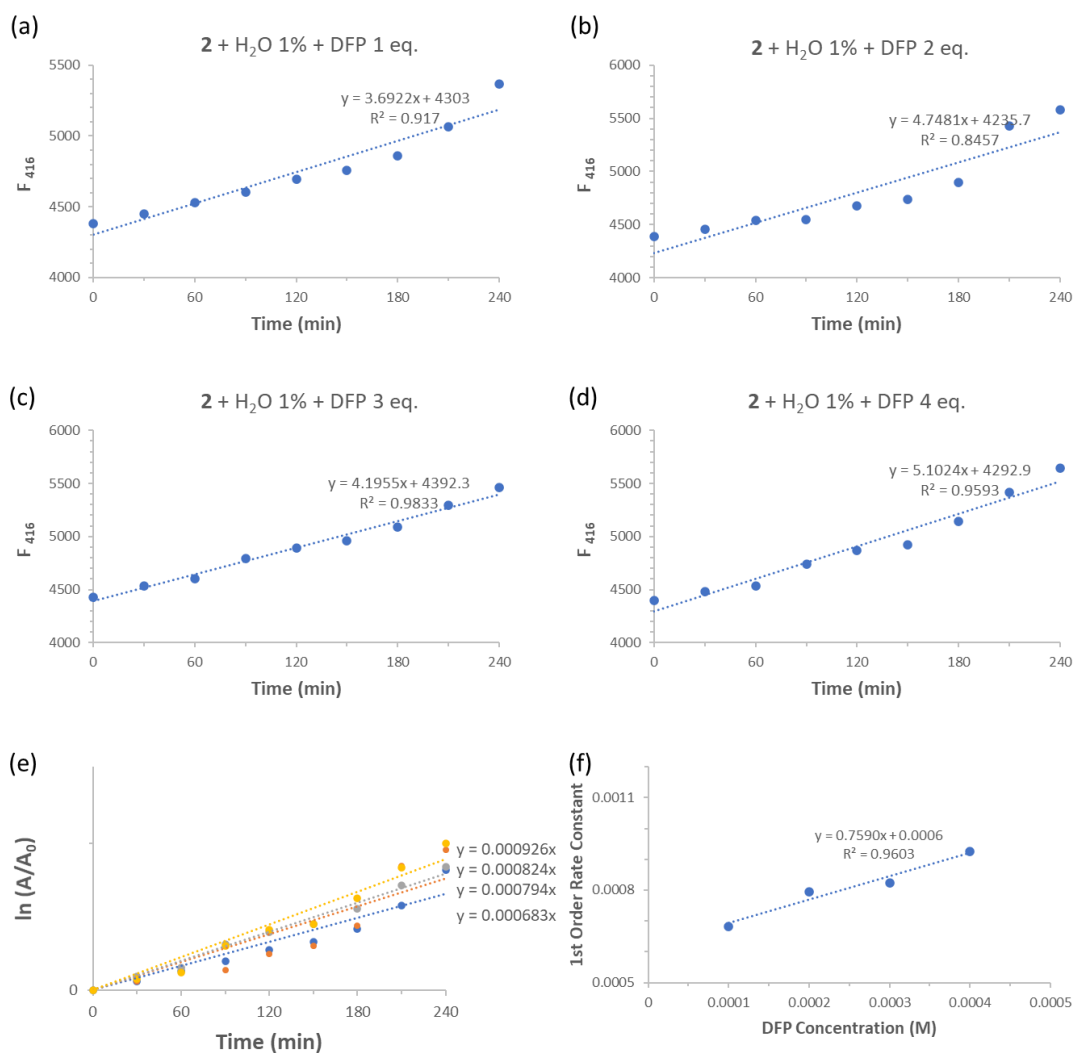


Figure 4.14 Time kinetic studies with fluorescence intensity changes of **2** (100 μM) and DFP (a) 1; (b) 2; (c) 3; (d) 4 equivalents compared to **2** in acetonitrile (99%) and water (1%). Each time fluorescence was measured, the amount of released fluoride anion after hydrolysis was measured by the fluorescence intensity changes of **1** (100 μM). (e) First order rate constant was calculated from (a)-(d). The slope was the first order rate constant, respectively. (f) The second order rate constant was calculated from the concentration of DFP and the first order rate constant (e). Finally, the second order rate constant was $0.759 \text{ M}^{-1} \cdot \text{min}^{-1}$.

4.2.5 Detection of Nerve Agent Simulants

Next, receptor **1** was applied to detect the nerve agent surrogates directly, not to remediate. When receptor **1** was exposed to either DCNP or DFP in a mixture of EtOH (1 equiv.) and DBU (1 equiv.) in CH₃CN, an immediate increase of the fluorescence intensity was seen as a result of binding of leaving groups (*i.e.*, CN⁻ or F⁻) to receptor **1** (**Figure 4.15** and **4.16**). EtOH and DBU were employed to instant nucleophilic attack to nerve agent surrogates and release leaving groups. The limit of detection (LOD) calculated by $3.3\sigma/\text{slope}$ was determined to be 1.86×10^{-6} M for DCNP and 2.25×10^{-6} M for DFP, respectively (Fig. S24 and S25). These fluorescence titration experiments demonstrated that receptor **1** could be used as a rapid sensor for the nerve agents.

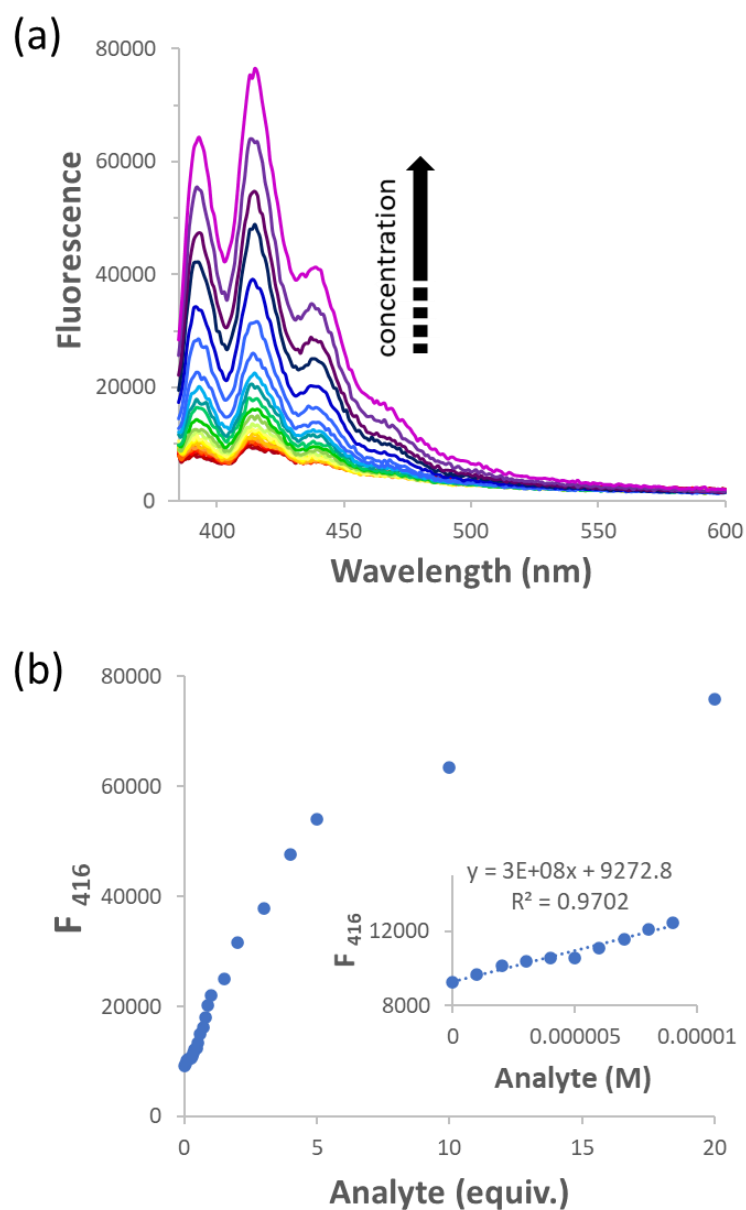


Figure 4.15 Fluorescence emission spectra of **1** (20 μ M) were obtained upon addition of 0-20 equivalents of a mixture of DCNP/EtOH/ DBU (1/1/1) in CH_3CN ($\lambda_{\text{ex}} = 372$ nm). The wavelength range was (a) 385-600 nm and (b) 416 nm, respectively. The inset of (b) is for calculating the limit of detection (LOD). The slope of the calibration curve was 336,145,733.9 and the standard deviation of the response of the curve (σ) was 189.0506. The LOD was calculated by the equation of $3.3 \times \sigma \div \text{slope}$, so the LOD was 1.86×10^{-6} .

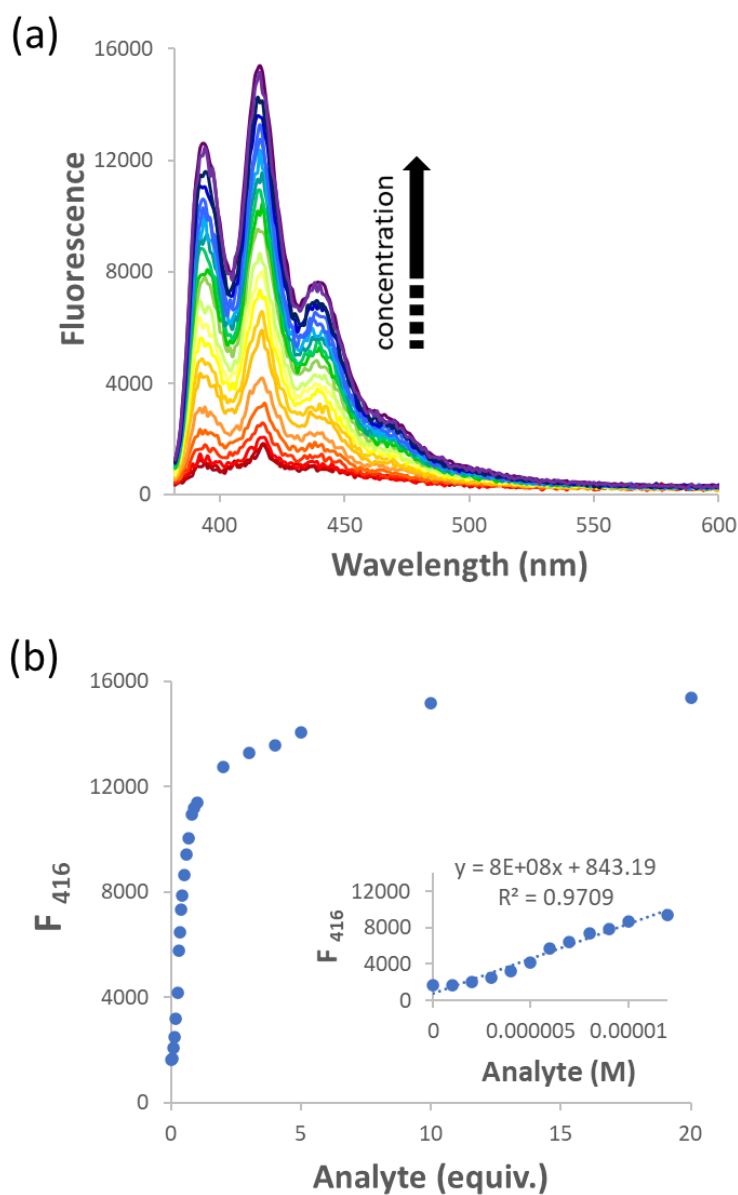


Figure 4.16 Fluorescence emission spectra of **1** (20 μ M) were obtained upon addition of 0-20 equivalents of a mixture of DFP/EtOH/ DBU (1/1/1) in CH_3CN ($\lambda_{\text{ex}} = 372$ nm). The wavelength range was (a) 382-600 nm and (b) 416 nm, respectively. The inset of (b) is for calculating the limit of detection (LOD). The slope of the calibration curve was 755,694,222.3 and the standard deviation of the response of the curve (σ) was 515.1028. The LOD was calculated by the equation of $3.3 \times \sigma \div \text{slope}$, so the LOD was 2.25×10^{-6} .

4.3 CONCLUSION

In conclusion, we have developed a bis-pyridinium calix[4]pyrrole functionalized with anthracene subunits that not only accelerates the hydrolysis rate of nerve agent surrogates, but also detects them by binding the leaving groups from hydrolysis. This was confirmed by measuring the 2nd order rate constants via fluorescence spectroscopy. Receptor **1** was found to associate with DCNP and DFP more strongly and induce faster hydrolysis than neutral receptor **2**. Moreover, DCNP and DFP were detected immediately by **1** after reacting with EtOH under basic conditions. The current work provides insights into principles that may be applied to receptor-based approaches for remediation and detection of nerve agents.

4.4 EXPERIMENTAL SECTION

4.4.1 Methods and Instruments

Nuclear Magnetic Resonance (NMR)

NMR spectra were recorded from The University of Texas at Austin NMR facility. Varian DirectDrive or Varian INOVA 400 MHz NMR spectrometers were employed on synthesized compounds characterization. The NMR spectra were referenced to solvent, and the spectroscopic solvents (CDCl_3 , CD_3CN , and $(\text{CD}_3)_2\text{SO}$) were purchased from Cambridge Isotope Laboratories. All NMR spectral data were processed with the Mestrenova software package.

High-Resolution Mass Spectrometry (HRMS)

High-resolution mass spec (HRMS) analysis was conducted by the University of Texas Mass Spectrometry Facility using Agilent Technologies 6530 Accurate Mass Q-TOF LC/MS system. MALDI-TOF MS analysis was performed using an AB-Sciex Voyager-DE PRO MALDI-TOF equipped with a 337 nm nitrogen laser in linear mode using CHCA as a matrix.

UV-Vis Spectroscopy

The UV-Vis absorbance spectra and kinetics were obtained by Cary 100 UV-Vis spectrophotometer from Agilent Technology. The spectra were run in Cary WinUV software: Scan, Kinetics and Scanning Kinetics, respectively.

Fluorescence Spectroscopy

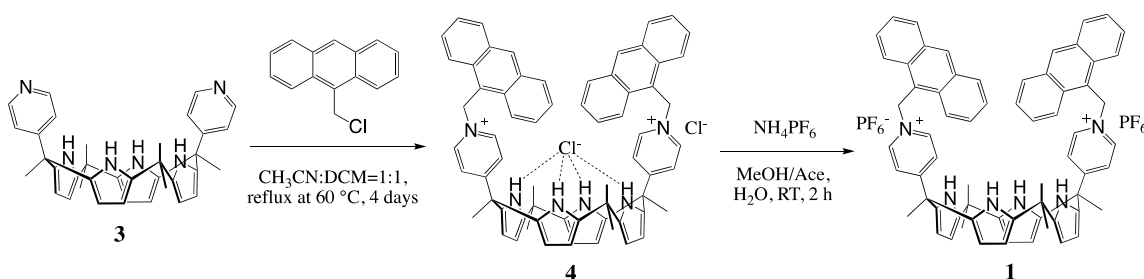
Fluorescence spectra were recorded on a Photon Technology International Fluorescence Master fluorimeter. The source was a 75 W Xenon short arc lamp.

4.4.2 Materials

All solvents and chemicals were purchased from MilliporeSigma, Acros Organics, Fisher Scientific, or and used without further purification. TLC analyses were carried out using Sorbent Technologies silica gel (200 mm) sheets. Column chromatography was performed on Sorbent silica gel 60 (40–63 mm).

4.4.3 Synthesis

Compounds **2** and **3** were prepared according to the reported procedures.^{21,22}



Scheme 4.3 Synthesis of receptor **1**.

Synthesis of **4**

To a solution of **3** (200 mg, 0.36 mmol) in dry dichloromethane/acetonitrile (1:1, 20 mL) was added 9-(chloromethyl)anthracene (204 mg, 0.9 mmol) and the mixture was stirred at 60 °C for 4 days under nitrogen atmosphere. After the volatiles were removed under reduced pressure, the residue was subjected to silica gel column eluting with acetone/methanol (20/1, v/v) to give 167 mg (46% yield) of the product as white yellow solid. ¹H NMR (400 MHz, DMSO-*d*₆) δ 10.28 (s, 4H), 8.91 (s, 2H), 8.76 (d, *J* = 6.5 Hz, 4H), 8.34 (d, *J* = 8.3 Hz, 4H), 8.23 (d, *J* = 8.2 Hz, 4H), 7.65 – 7.54 (m, 8H), 7.39 (d, *J* = 6.4 Hz, 4H), 6.90 (s, 4H), 5.75 (s, 4H), 5.69 (s, 4H), 1.82 (s, 6H), 1.55 (s, 6H), 1.40 (s, 6H). ¹³C NMR (100 MHz, DMSO-*d*₆) δ 169.27, 143.29, 140.62, 133.08, 131.34, 131.09,

131.04, 129.40, 128.27, 126.43, 125.65, 123.30, 121.53, 104.72, 101.32, 55.15, 45.02, 34.29, 30.87, 28.66, 26.62. HRMS (ESI) m/z calc. for $[M]^+$, 971.4563; found, 971.4590.

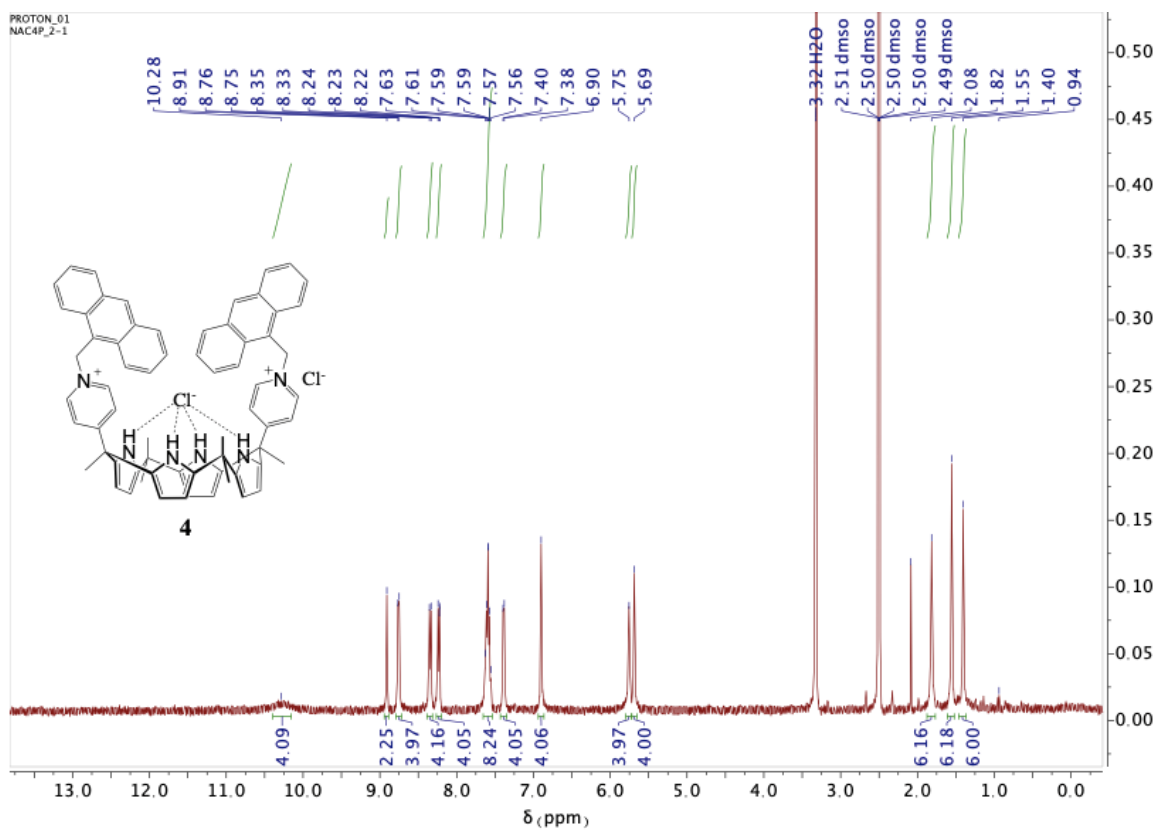


Figure 4.17 ^1H NMR spectrum of **4** recorded in $\text{DMSO-}d_6$ at 298 K.

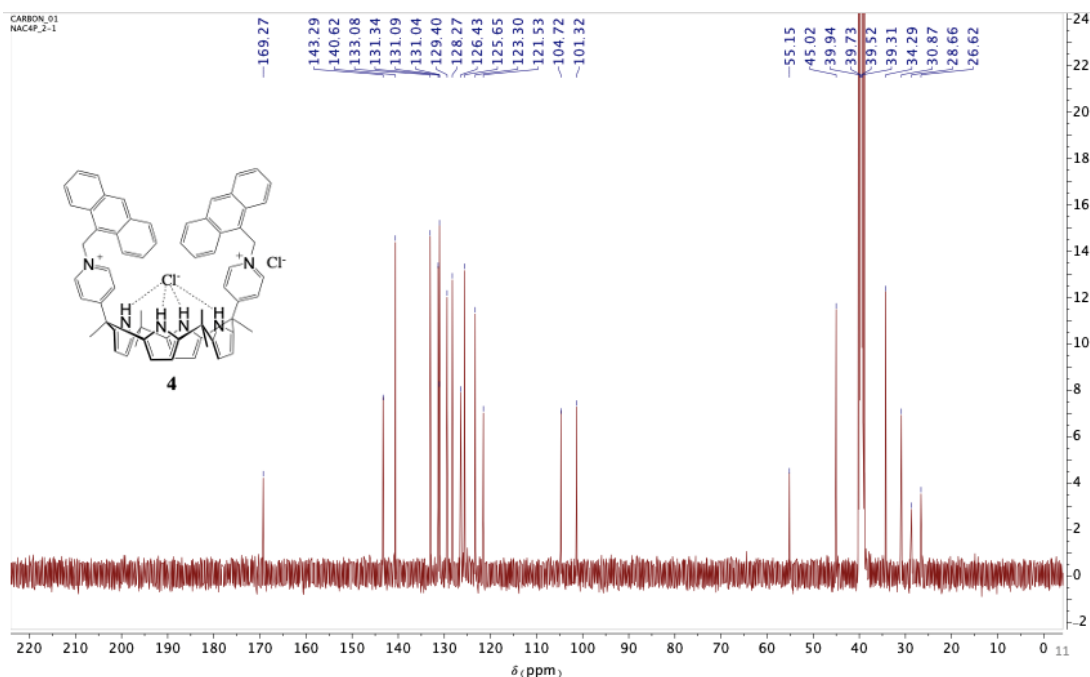


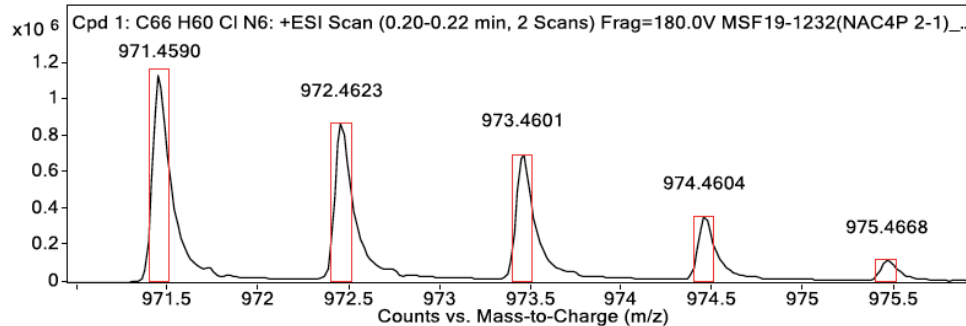
Figure 4.18 ^{13}C NMR spectrum of **4** recorded in $\text{DMSO-}d_6$ at 298 K.

Target Compound Screening Report

Results Acquired by The University of Texas at Austin Mass Spectrometry Facility

Data File	MSF19-1232(NAC4P 2-1)_hrESIpos2.d	Sample Name	1232(NAC4P 2-1)	Comment	1232(NAC4P 2-1)
Position	P1-C8	Instrument Name	Instrument 1	User Name	
Acq Method	pos.m	Acquired Time	6/28/2019 10:59:10 AM	DA Method	KS.m

MS Zoomed Spectrum



MS Spectrum Peak List

Obs. m/z	Calc. m/z	Charge	Abundance	Formula	Ion Species	Tgt Mass Error (ppm)
745.4031			5569049			
971.4590	971.4563	1	1141329	C66H60ClN6	M+	-2.85
972.4623	972.4594	1	868369	C66H60ClN6	M+	-2.95
973.4601	973.4576	1	704512	C66H60ClN6	M+	-2.6
974.4604	974.4585	1	359969	C66H60ClN6	M+	-1.9
975.4668	975.4608	1	119285	C66H60ClN6	M+	-6.2
976.4786	976.4636	1	25015	C66H60ClN6	M+	-15.36
977.4863	977.4665	1	5628	C66H60ClN6	M+	-20.27
978.4839	978.4696	1	1775	C66H60ClN6	M+	-14.67
979.4710	979.4727	1	1553	C66H60ClN6	M+	1.69

--- End of Report ---

Figure 4.19 High resolution mass data of **4**.

Synthesis of **1**

The tetrachloride salt **4** (167 mg, 0.17 mmol) was dissolved in acetone/methanol (1:1, 5 mL). Then NH_4PF_6 (277 mg, 1.7 mmol) in H_2O (10 mL) was added in one portion for the anion exchange reaction. After stirring for 2 hours at room temperature, yellow precipitate was filtered off, washed with water, and dried to afford pure **1** (146 mg, 72%). ^1H NMR (400 MHz, $\text{DMSO-}d_6$) δ 9.40 (s, 4H), 8.94 (s, 2H), 8.75 (d, $J = 6.3$ Hz, 4H), 8.39 (d, $J = 8.8$ Hz, 4H), 8.28 (d, $J = 8.4$ Hz, 4H), 7.67 (dt, $J = 19.2, 7.0$ Hz, 8H), 7.45 (d, $J = 6.4$ Hz, 4H), 6.88 (s, 4H), 5.75 (s, 4H), 5.62 (s, 4H), 1.88 (s, 6H), 1.54 (s, 6H), 1.33 (s, 6H). ^{13}C NMR (100 MHz, CD_3CN , ppm): δ 155.00, 144.00, 140.96, 133.78, 132.67, 132.65, 132.52, 130.72, 129.49, 127.71, 126.84, 123.67, 121.50, 107.42, 104.42, 73.15, 62.01, 56.88, 46.56, 35.87, 30.39, 27.15, 26.93. HRMS (ESI) m/z calc. for $[\text{M}]^{2+}$, 468.2448; found, 468.2434.

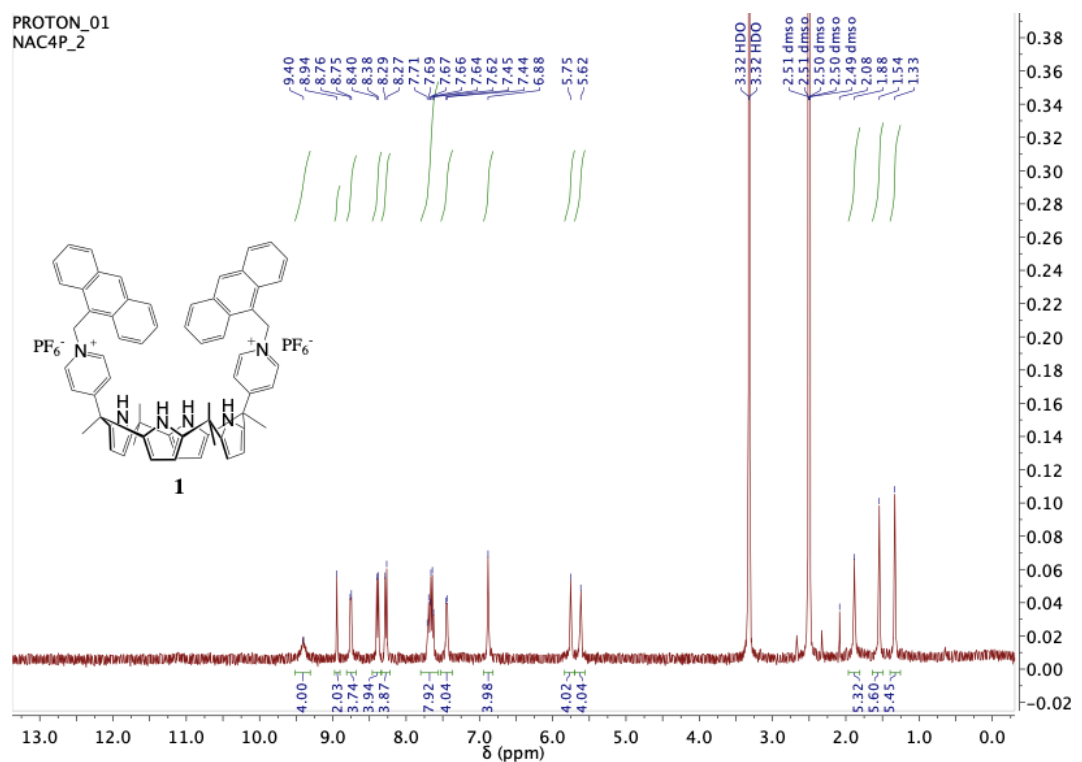


Figure 4.20 ^1H NMR spectrum of **1** recorded in $\text{DMSO-}d_6$ at 298 K.

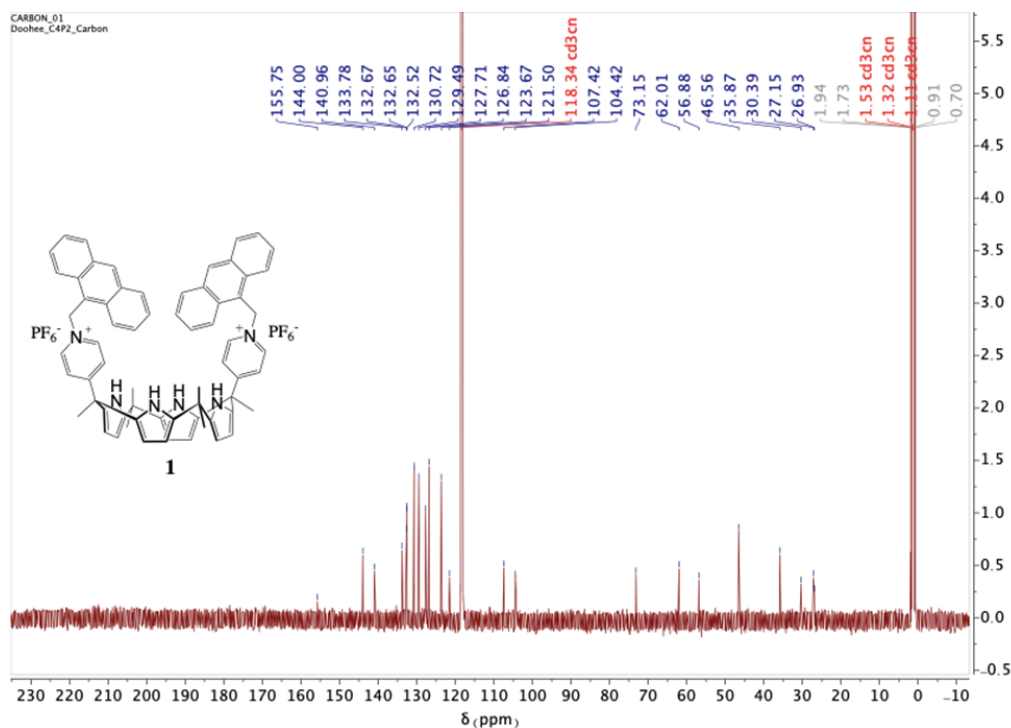


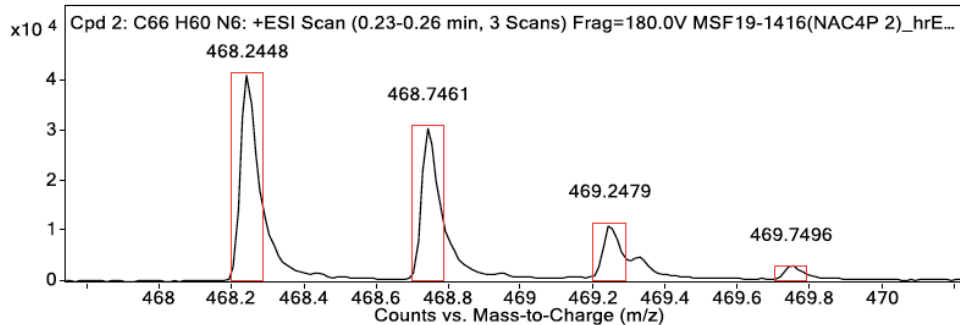
Figure 4.21 ¹³C NMR spectrum of **1** recorded in CD₃CN at 298 K.

Target Compound Screening Report

Results Acquired by The University of Texas at Austin Mass Spectrometry Facility

Data File	MSF19-1416(NAC4P 2)_hrESIpos2.d	Sample Name	1416(NAC4P 2)	Comment	1416(NAC4P 2)
Position	P1-C7	Instrument Name	Instrument 1	User Name	
Acq Method	FIA_pos.m	Acquired Time	7/19/2019 9:46:35 AM	DA Method	KS.m

MS Zoomed Spectrum



MS Spectrum Peak List

Obs. m/z	Calc. m/z	Charge	Abundance	Formula	Ion Species	Tgt Mass Error (ppm)
468.2448	468.2434	2	41133	C ₆₆ H ₆₀ N ₆	M+2	-2.96
468.7461	468.7450	2	30769	C ₆₆ H ₆₀ N ₆	M+2	-2.39
469.2479	469.2466	2	11367	C ₆₆ H ₆₀ N ₆	M+2	-2.64
469.7496	469.7482	2	2686	C ₆₆ H ₆₀ N ₆	M+2	-2.93
470.2533	470.2498	2	813	C ₆₆ H ₆₀ N ₆	M+2	-7.52
470.7462	470.7514	2	225	C ₆₆ H ₆₀ N ₆	M+2	11.01
745.4031			1283110			

--- End Of Report ---

Figure 4.22 High resolution mass data of **1**.

4.4.4 Additional Figures

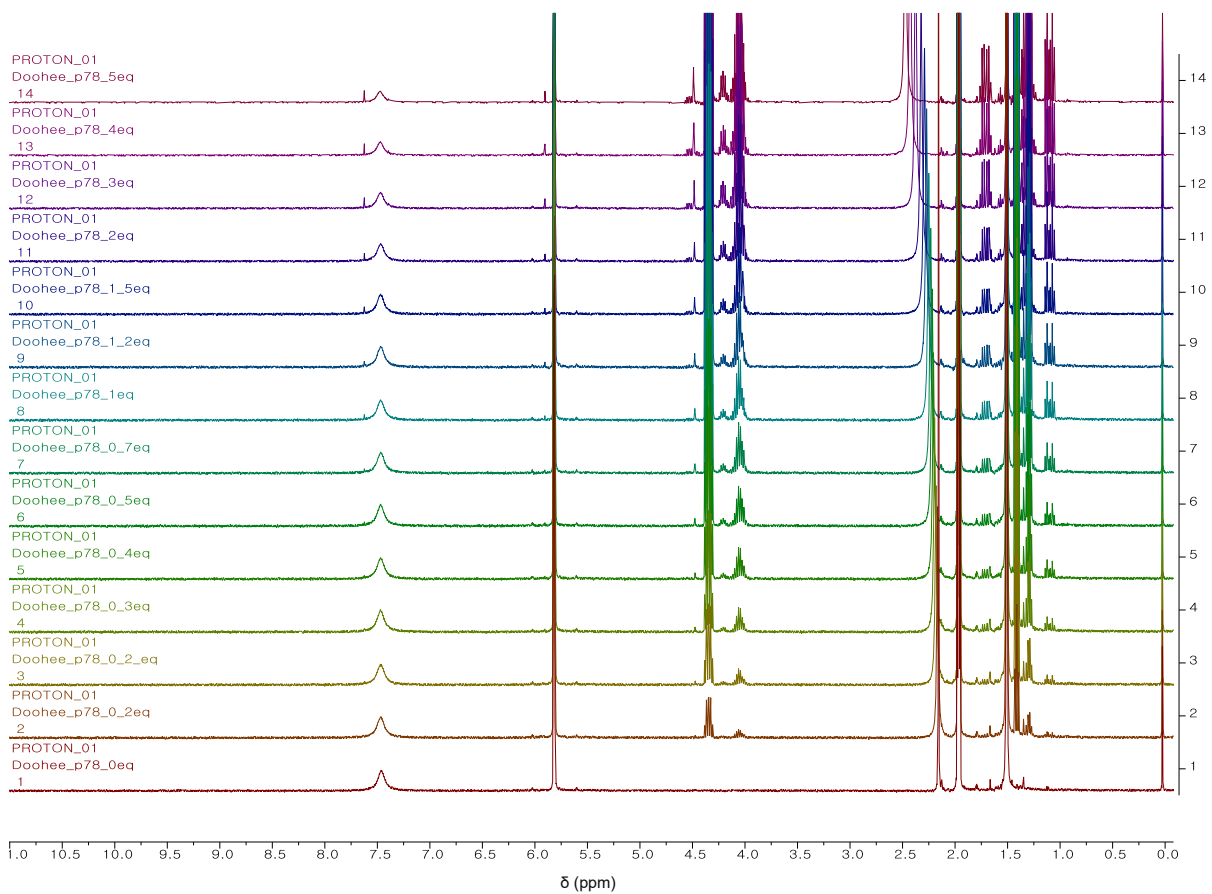


Figure 4.23 ¹H NMR studies between DCNP and **2**. DCNP (0 equivalent (bottom) to 5 equivalent (top)) was gradually added to the solution of CD₃CN in the presence of **2** (6 mM).

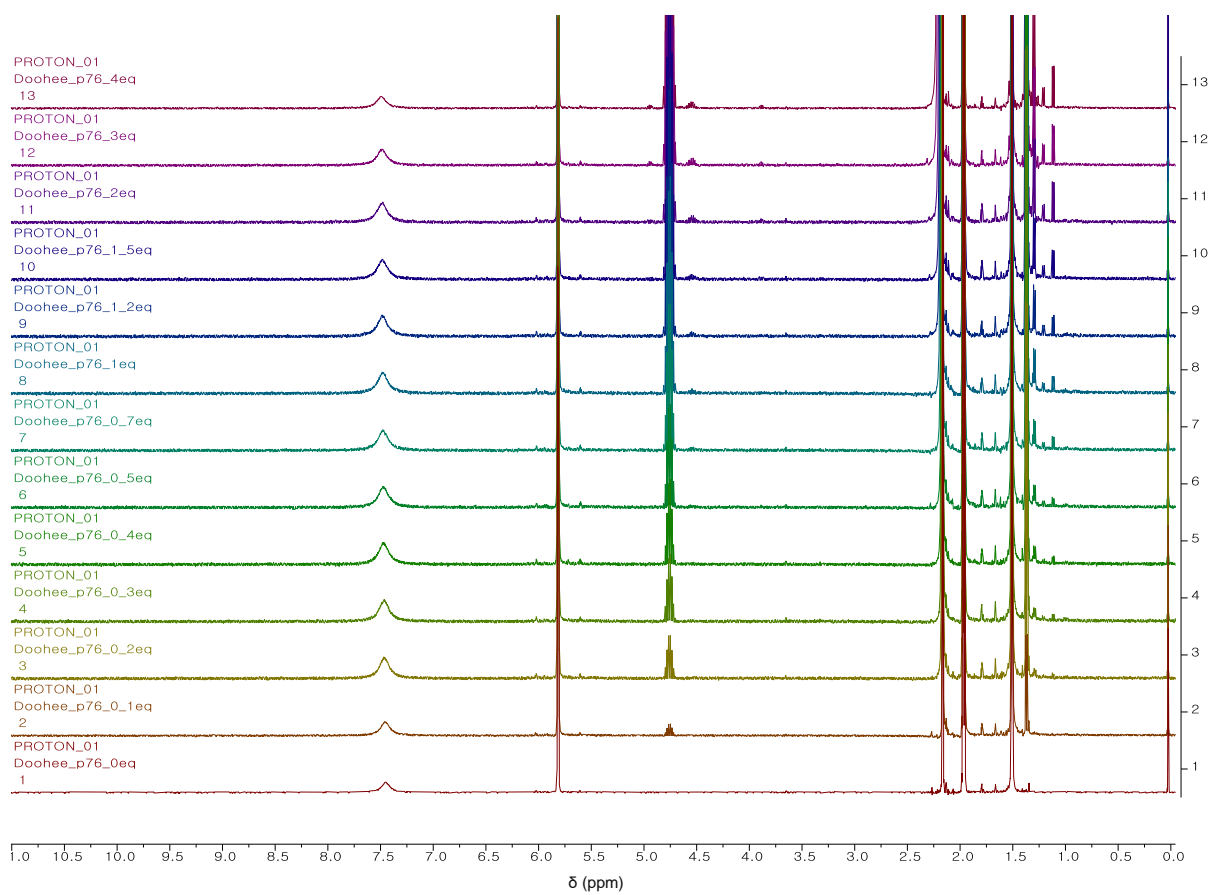


Figure 4.24 ^1H NMR studies between DFP and **2**. DFP (0 equivalent (bottom) to 4 equivalent (top)) was gradually added to the solution of CD_3CN in the presence of **2** (6 mM).

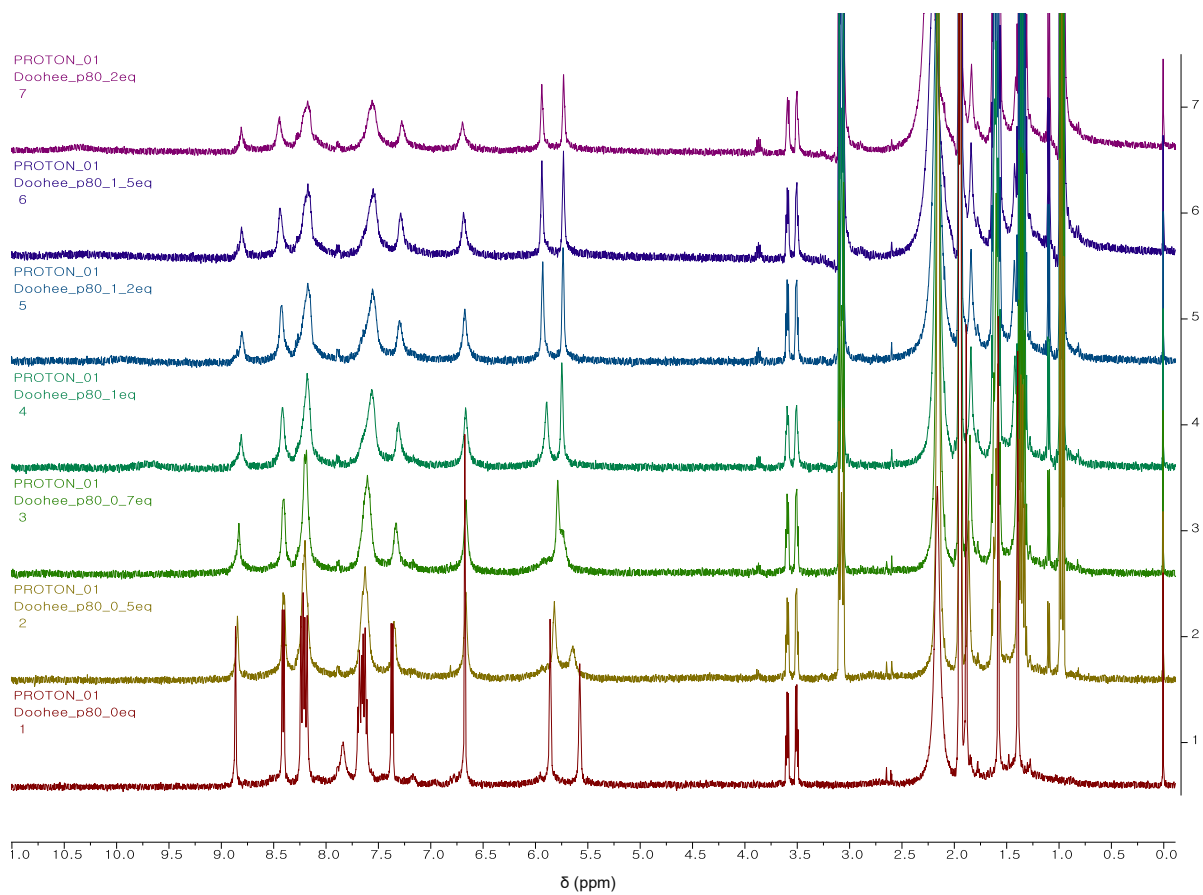


Figure 4.25 ^1H NMR studies between TBACN and **1**. TBACN (0 equivalent (bottom) to 2 equivalent (top)) was gradually added to the solution of CD_3CN in the presence of **1** (6 mM).

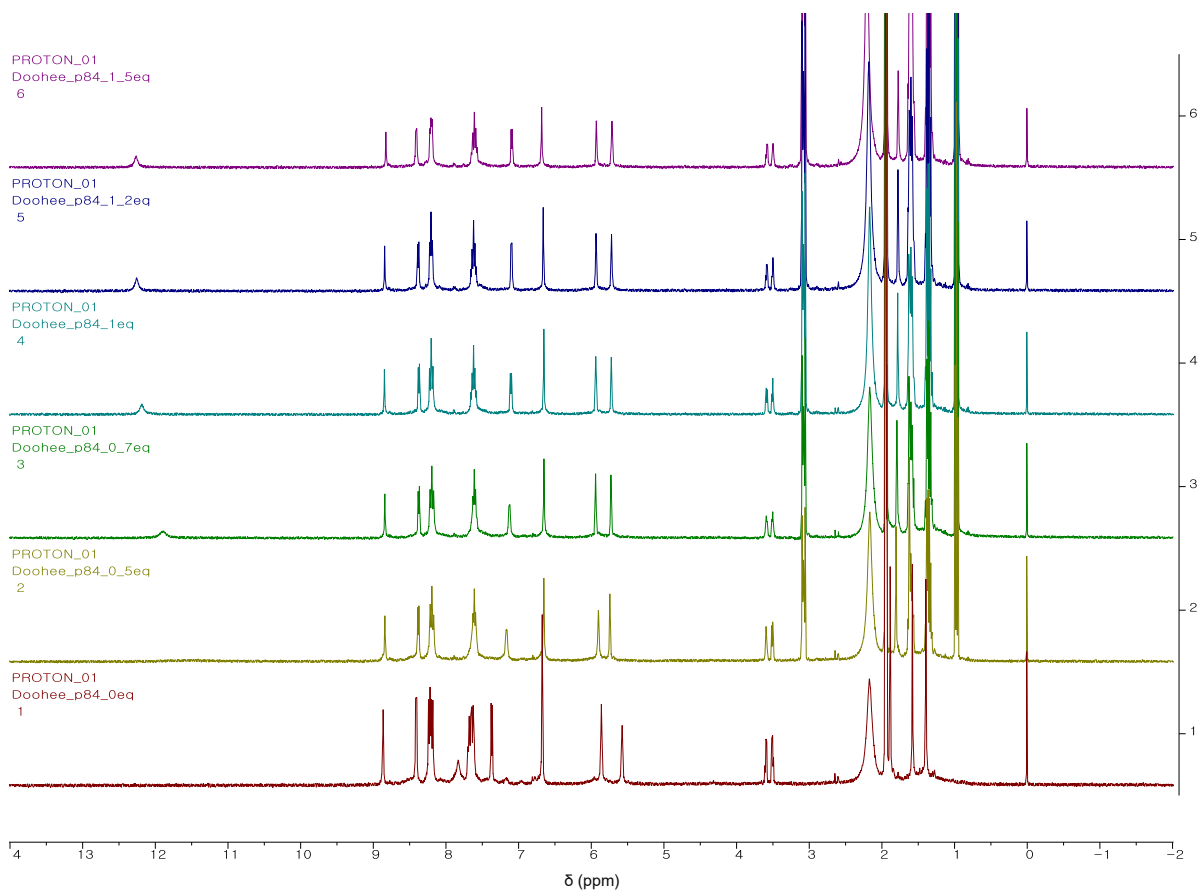


Figure 4.26 ^1H NMR studies between TBAF and **1**. TBAF (0 equivalent (bottom) to 1.5 equivalent (top)) was gradually added to the solution of CD_3CN in the presence of **1** (6 mM).

4.5 REFERENCES

1. Organisation for the Prohibition of Chemical Weapons Home Page. <https://www.opcw.org> (accessed June 01, 2021).
2. Kim, S. W.; Bae, Y. H.; Okano, T., Hydrogels: Swelling, Drug Loading, and Release. *Pharmaceut. Res.* **1992**, *9*, 283-290.
3. Sogorb, M. A.; Vilanova, E., Enzymes Involved in the Detoxification of Organophosphorus, Carbamate and Pyrethroid Insecticides through Hydrolysis. *Toxicol. Lett.* **2002**, *128*, 215-228.
4. Blum, M.-M.; Timperley, C. M.; Williams, G. R.; Thiermann, H.; Worek, F., Inhibitory Potency against Human Acetylcholinesterase and Enzymatic Hydrolysis of Fluorogenic Nerve Agent Mimics by Human Paraoxonase 1 and Squid Diisopropyl Fluorophosphatase. *Biochemistry* **2008**, *47*, 5216-5224.
5. Moon, S.-Y.; Liu, Y.; Hupp, J. T.; Farha, O. K., Instantaneous Hydrolysis of Nerve-Agent Simulants with a Six-Connected Zirconium-Based Metal–Organic Framework. *Angew. Chem. Int. Ed.* **2015**, *54*, 6795-6799.
6. Royuela, S.; Millán, R. G.-S.; Mancheño, M. J.; Ramos, M. M.; Segura, J. L.; Navarro, J. A. R.; Zamora, F., Catalytically Active Imine-based Covalent Organic Frameworks for Detoxification of Nerve Agent Simulants in Aqueous Media. *Materials* **2019**, *12*, 1974.
7. Jabbour, C. R.; Parker, L. A.; Hutter, E. M.; Weckhuysen, B. M., Chemical Targets to Deactivate Biological and Chemical Toxins using Surfaces and Fabrics. *Nat. Rev. Chem.* **2021**, *5*, 370-387.
8. Munro, N. B.; Talmage, S. S.; Griffin, G. D.; Waters, L. C.; Watson, A. P.; King, J. F.; Hauschild, V., The Sources, Fate, and Toxicity of Chemical Warfare Agent Degradation Products. *Environ. Health Perspect.* **1999**, *107*, 933-974.
9. Sambrook, M. R.; Notman, S., Supramolecular Chemistry and Chemical Warfare Agents: From Fundamentals of Recognition to Catalysis and Sensing. *Chem. Soc. Rev.* **2013**, *42*, 9251-9267.
10. Barba-bon, A.; Costero, A. M.; Parra, M.; Gil, S.; Martínez-Máñez, R.; Sancenón, F.; Gale, P. A.; Hiscock, J. R., Neutral 1,3-Diindolylureas for Nerve Agent Remediation. *Chem. Eur. J.* **2013**, *19*, 1586-1590.

11. Hiscock, J. R.; Sambrook, M. R.; Cranwell, P. B.; Watts, P.; Vincent, J. C.; Xuereb, D. J.; Wells, N. J.; Raja, R.; Gale, P. A., Tripodal Molecules for the Promotion of Phosphoester Hydrolysis. *Chem. Commun.* **2014**, *50*, 6217-6220.
12. Kim, S. K.; Sessler, J. L., Calix[4]pyrrole-Based Ion Pair Receptors. *Acc. Chem. Res.* **2014**, *47*, 2525-2536.
13. Peng, S.; He, Q.; Vargas-Zuniga, G. I.; Qin, L.; Hwang, I.; Kim, S. K.; Heo, N. J.; Lee, C.-H.; Dutta, R.; Sessler, J. L., Strapped Calix[4]pyrroles: From Syntheses to Applications. *Chem. Soc. Rev.* **2020**, *49*, 865-907.
14. Kim, D. S.; Sessler, J. L., Calix[4]pyrroles: Versatile Molecular Containers with Ion Transport, Recognition, and Molecular Switching Functions. *Chem. Soc. Rev.* **2015**, *44*, 532-546.
15. Ko, S.-K.; Kim, S. K.; Share, A.; Lynch, V. M.; Park, J.; Namkung, W.; Rossom, W. V.; Busschaert, N.; Gale, P. A.; Sessler, J. L.; Shin, I., Synthetic Ion Transporters can Induce Apoptosis by Facilitating Chloride Anion Transport into Cells. *Nat. Chem.* **2014**, *6*, 885-892.
16. Park, S.-H.; Park, S.-H.; Howe, E. N. W.; Hyun, J. Y.; Chen, L.-J.; Hwang, I.; Vargas-Zuniga, G.; Busschaert, N.; Gale, P. A.; Sessler, J. L.; Shin, I., Article Determinants of Ion-Transporter Cancer Cell Death. *Chem* **2019**, *5*, 2079-2098.
17. Bobbitt, N. S.; Mendonca, M. L.; Howarth, A. J.; Islamoglu, T.; Hupp, J. T.; Farha, O. K.; Snurr, R. Q., Metal–Organic Frameworks for the Removal of Toxic Industrial Chemicals and Chemical Warfare Agents. *Chem. Soc. Rev.* **2017**, *46*, 3357-3385.
18. Climent, E.; Biyikal, M.; Gawlitza, K.; Dropa, T.; Urban, M.; Costero, A. M.; Martinez-Manez, R.; Rurack, K., Determination of the Chemical Warfare Agents Sarin, Soman and Tabun in Natural Waters Employing Fluorescent Hybrid Silica Materials. *Sens. Actuators B Chem.* **2017**, *246*, 1056-1065.
19. Saha, I.; Lee, J. H.; Hwang, H.; Kim, T. S.; Lee, C.-H., Remarkably Selective, Non-Linear Allosteric Regulation of Anion Binding by a Tetracationic Calix[4]pyrrole Homodimer. *Chem. Commun.* **2015**, *51*, 5679-5682.
20. Anslyn, E. V.; Dougherty, D. A. *Modern Physical Organic Chemistry*; University Science Books: Mill Valley, CA, 2006; pp 355-419.
21. Sokkalingam, P.; Kim, D. S.; Hwang, H.; Sessler, J. L.; Lee, C.-H., A Dicationic Calix[4]pyrrole Derivative and its Use for the Selective Recognition and Displacement-Based Sensing of Pyrophosphate. *Chem. Sci.* **2012**, *3*, 1819-1824.

22. Gale, P. A.; Sessler, J. L.; Král, V.; Lynch, V., Calix[4]pyrroles: Old Yet New Anion-Binding Agents. *J. Am. Chem. Soc.* **1996**, *118*, 5140-5141.

Bibliography

- Alexandridis, P.; Lindman, B., *Amphiphilic Block Copolymers: Self-Assembly and Applications*; Elsevier: 2000.
- Ali, M. A.; Tsai, T.-H.; Braun, P. V. Amplified Detection of Chemical Warfare Agents Using Two-Dimensional Chemical Potential Gradients. *ACS Omega* **2018**, *3*, 14665-14670.
- Anslyn, E. V.; Dougherty, D. A. *Modern Physical Organic Chemistry*; University Science Books: Mill Valley, CA, 2006; pp 355-419.
- Arslan, M.; Tasdelen, M. A., Click Chemistry in Macromolecular Design: Complex Architectures from Functional Polymers. *Chemistry Africa* **2018**, *2* (2), 195-214.
- Ashley, G. W.; Henise, J.; Reid, R.; Santi, D. V. Hydrogel Drug Delivery System with Predictable and Tunable Drug Re-release and Degradation Rates. *PNAS* **2013**, *110*, 2318-2323.
- Auilar, M. R.; Roman, J. S., *Smart Polymers and their Applications*, Elsevier, Cambridge, UK, 2014, pp 1-11.
- Bahram, M.; Mohseni, N.; Moghtader M. *An Introduction to Hydrogels and Some Recent Applications, Emerging Concepts in Analysis and Applications of Hydrogels*; IntechOpen, 2016; pp 9-38.
- Balasubramanian, S.; Kulandaisamy, A. J.; Babu, K. J.; Das, A.; Rayappan, J. B. B. Metal Organic Framework Functionalized Textiles as Protective Clothing for the Detection and Detoxification of Chemical Warfare Agents: A review. *Ind. Eng. Chem. Res.* **2021**, *60*, 4218-4239.
- Barba-Bon, A.; Costero, A. M.; Gil, S.; Martínez-Máñez, R.; Sancenón, F. Selective Chromo-Fluorogenic Detection of DFP (a Sarin and Soman Mimic) and DCNP (a Tabun Mimic) with a Unique Probe Based on a Boron Dipyrromethene (BODIPY) Dye. *Org. Biomol. Chem.* **2014**, *12*, 8745-8751.
- Barba-Bon, A.; Costero, A. M.; Gil, S.; Sancenón F.; Martínez-Máñez, R., Chromo-Fluorogenic BODIPY-Complexes for Selective Detection of V-Type Nerve Agent Surrogates. *Chem. Commun.* **2014**, *50*, 13289-13291.
- Barba-bon, A.; Costero, A. M.; Parra, M.; Gil, S.; Martínez-Máñez, R.; Sancenón, F.; Gale, P. A.; Hiscock, J. R., Neutral 1,3-Diindolylureas for Nerve Agent Remediation. *Chem. Eur. J.* **2013**, *19*, 1586-1590.
- Belger, C.; Weis, J. G.; Egap, E.; Swager, T. M. Colorimetric Stimuli-Responsive Hydrogel Polymers for the Detection of Nerve Agent Surrogates. *Macromolecules* **2015**, *48*, 7990-7994.

- Ben Cheikh, A.; Chuche, J.; Manisse, N.; Pommelet, J. C.; Netsch, K. P.; Lorencak, P.; Wentrup, C., Synthesis of Alpha.-Cyano Carbonyl Compounds by Flash Vacuum Thermolysis of (Alkylamino) Methylene Derivatives of Meldrum's Acid. Evidence for Facile 1, 3-Shifts of Alkylamino and Alkylthio Groups in Imidoylketene Intermediates. *J. Org. Chem.* **1991**, *56* (3), 970-975.
- Binauld, S.; Stenzel M. H., Acid-Degradable Polymers for Drug Delivery: A Decade of Innovation. *Chem. Commun.* **2013**, *49*, 2082-2102.
- Binder, W. H.; Sachsenhofer, R., 'Click' Chemistry in Polymer and Material Science: An Update. *Macromol. Rapid Commun.* **2008**, *29* (12-13), 952-981.
- Binder, W. H.; Sachsenhofer, R., 'Click' Chemistry in Polymer and Materials Science. *Macromol. Rapid Commun.* **2007**, *28* (1), 15-54.
- Blanazs, A.; Armes, S. P.; Ryan, A. J., Self-Assembled Block Copolymer Aggregates: From Micelles to Vesicles and their Biological Applications. *Macromol. Rapid Commun.* **2009**, *30*, 267-277.
- Blum, A. P.; Kammeyer, J. K.; Rush, A. M.; Callmann, C. E.; Hahn, M. E.; Gianneschi, N. C., Stimuli-Responsive Nanomaterials for Biomedical Applications. *J. Am. Chem. Soc.* **2015**, *137* (6), 2140-2154.
- Blum, M.-M.; Timperley, C. M.; Williams, G. R.; Thiermann, H.; Worek, F., Inhibitory Potency against Human Acetylcholinesterase and Enzymatic Hydrolysis of Fluorogenic Nerve Agent Mimics by Human Paraoxonase 1 and Squid Diisopropyl Fluorophosphatase. *Biochemistry* **2008**, *47*, 5216-5224.
- Bobbitt, N. S.; Mendonca, M. L.; Howarth, A. J.; Islamoglu, T.; Hupp, J. T.; Farha, O. K.; Snurr, R. Q., Metal–Organic Frameworks for the Removal of Toxic Industrial Chemicals and Chemical Warfare Agents. *Chem. Soc. Rev.* **2017**, *46*, 3357-3385.
- Boles, M.; Ling, D.; Hyeon, T.; Talapin, D. V. The Surface Science of Nanocrystals. *Nature Mater.* **2016**, *15*, 141-153.
- Bräse, S.; Banert, K., *Organic Azides: Syntheses and Applications*; Wiley: Chichester, U.K., 2010.
- Caló, E.; Khutoryanskiy, V. V. Biomedical Applications of Hydrogels: A Review of Patents and Commercial Products. *Eur. Polym.* **2015**, *65*, 252-267.
- Castro, A. T.; Figueroa-Villar, J. D., Molecular Structure, Conformational Analysis and Charge Distribution of Pralidoxime: Ab Initio and DFT Studies. *Int. J. Quantum Chem.* **2002**, *89*, 135-146.
- Cavalcante, S. F. D.; Simas, A. B. C.; Kuca, K. Nerve Agents' Surrogates: Invaluable Tools for Development of Acetylcholinesterase Reactivators. *Curr. Org. Chem.* **2019**, *23*, 1539-1559.
- Chai, P. R.; Hayes, B. D.; Erickson, T. B.; Boyer, E. W. Novichok Agents: A Historical, Current, and Toxicological Perspective. *Toxicol. Commun.* **2018**, *2*, 45-48.

- Chawla, K. K.; Meyers, M., *Mechanical Behavior of Materials*; Prentice Hall: 1999.
- Christensen, P. R.; Scheuermann, A. M.; Loeffler, K. E.; Helms, B. A., Closed-loop Recycling of Plastics Enabled by Dynamic Covalent Diketoenamine Bonds. *Nat. Chem.* **2019**, *11* (5), 442-448.
- Climent, E.; Biyikal, M.; Gawlitza, K.; Dropa, T.; Urban, M.; Costero, A. M.; Martinez-Manez, R.; Rurack, K., Determination of the Chemical Warfare Agents Sarin, Soman and Tabun in Natural Waters Employing Fluorescent Hybrid Silica Materials. *Sens. Actuators B Chem.* **2017**, *246*, 1056-1065.
- Colović, M B.; Kristić, D. Z.; Lazarević-Pašti, T. D.; Bondžić, A. M.; Vasić, V. M., Acetylcholinesterase Inhibitors: Pharmacology and Toxicology. *Curr. Neuropharmacol.* **2013**, *11*, 315-335.
- Cudjoe, E.; Herbert, K. M.; Rowan, S. J., Strong, Rebondable, Dynamic Cross-Linked Cellulose Nanocrystal Polymer Nanocomposite Adhesives. *ACS Appl. Mater. Interfaces* **2018**, *10* (36), 30723-30731.
- DeCollo, T. V.; Lees, W. J. Effects of Aromatic Thiols on Thiol-Disulfide Interchange Reactions that Occur during Protein Folding. *J. Org. Chem.* **2001**, *66*, 4244-4249.
- Delfino, R. T.; Ribeiro, T. S.; Figueroa-Villar, J. D., Organophosphorus Compounds as Chemical Warfare Agents: A Review. *J. Braz. Chem. Soc.* **2009**, *20* (3), 407-428.
- Delplace, V.; Nicolas, J., Degradable Vinyl Polymers for Biomedical Applications. *Nat. Chem.* **2015**, *7* (10), 771-784.
- Dennison, G. H.; Sambrook, M. R.; Johnston, M. R., VX and VG Chemical Warfare Agents Bidentate Complexation with Lanthanide Ions. *Chem. Commun.* **2014**, *50*, 195-197.
- Diehl, K. L.; Kolesnichenko, I. V.; Robotham, S. A.; Bachman, J. L.; Zhong, Y.; Brodbelt, J. S.; Anslyn, E. V. Click and Chemically Triggered Declick Reactions through Reversible Amine and Thiol Coupling via a Conjugate Acceptor. *Nat. Chem.* **2016**, *8*, 968-973.
- Dominguez, M. N.; Howard, M. P.; Maier, J. M.; Valenzuela, S. A.; Sherman, Z. M.; Reuther, J. F.; Reimnitz, L. C.; Kang, J.; Cho, S. H.; Gibbs, S. L.; Menta, A. K.; Zhuang, D. L.; Van der Stok, A.; Kline, S. J.; Anslyn, E. V.; Truskett, T. M.; Milliron, D. J. Assembly of Linked Nanocrystal Colloids by Reversible Covalent Bonds. *Chem. Mater.* **2020**, *32*, 10235-10245.
- Dong, A.; Ye, X.; Chen, J.; Kang, Y.; Gordon, T.; Kikka-wa, J. M.; Murray, C. B. A Generalized Ligand-Exchange Strategy Enabling Sequential Surface Functionalization of Colloidal Nanocrystals. *J. Am. Chem. Soc.* **2011**, *133*, 998-1006.
- Ellison, D. H., *Handbook of Chemical and Biological Warfare Agents*; CRC Press: Boca Raton, FL, 2000; pp 220-239.

- Fenglian Q.; Chunxiao Y.; Zihui M.; Shuguang L.; Jiayu X.; Xiaochun H.; Min X. Acetylcholinesterase-Functionalized Two-Dimensional Photonic Crystal for the Sensing of G-Series Nerve Agents. *Anal. Bioanal. Chem.* **2019**, *411*, 2577-2585.
- Förster, S.; Antonietti, M., Amphiphilic Block Copolymers in Structure-Controlled Nanomaterial Hybrids. *Adv. Mater.* **1998**, *10* (3), 195-217.
- Gale, P. A.; Sessler, J. L.; Král, V.; Lynch, V., Calix[4]pyrroles: Old Yet New Anion-Binding Agents. *J. Am. Chem. Soc.* **1996**, *118*, 5140-5141.
- Ganesan, K.; Raza, S. K.; Vijayaraghavan, R. Chemical Warfare Agents. *J. Pharm. Bioallied Sci.* **2010**, *2*, 166-178.
- Gregory, M. J.; Bruice, T. C. Nucleophilic Displacement Reactions at the Thiol Ester Bond. V. Reactions of 2,2,2-Trifluoroethyl Thiolacetate. *J. Am. Chem. Soc.* **1967**, *89*, 2121-2127.
- Hayoun, M. A.; Smith, M. E.; Ausman, C.; Yarrarapu, S. N. S.; Swoboda, H. D., Toxicology, V-Series Nerve Agents. In *StatPearls [Internet]*; StatPearls Publishg: Treasure Island, FL, 2021.
- Hirsch, A.; Hauke, F., Post-Graphene 2D Chemistry: The Emerging Field of Molybdenum Disulfide and Black Phosphorus Functionalization. *Angew. Chem. Int. Ed.* **2018**, *57*, 4338-4354.
- Hiscock, J. R.; Piana, F.; Sambrook, M. R.; Wells, N. J.; Clark, A. J.; Vincent, J. C.; Busschaert, N.; Brown, R. C. D.; Gale, P. A., Detection of Nerve Agent via Perturbation of Supramolecular Gel Formation. *Chem. Commun*, **2013**, *49*, 9119-9121.
- Hiscock, J. R.; Sambrook, M. R.; Cranwell, P. B.; Watts, P.; Vincent, J. C.; Xuereb, D. J.; Wells, N. J.; Raja, R.; Gale, P. A., Tripodal Molecules for the Promotion of Phosphoester Hydrolysis. *Chem. Commun.* **2014**, *50*, 6217-6220.
- Ishibashi, J. S. A.; Kalow, J. A., Vitrimeric Silicone Elastomers Enabled by Dynamic Meldrum's Acid-Derived Cross-Links. *ACS Macro Lett.* **2018**, *7* (4), 482-486.
- Jabbour, C. R.; Parker, L. A.; Hutter, E. M.; Weckhuysen, B. M., Chemical Targets to Deactivate Biological and Chemical Toxins using Surfaces and Fabrics. *Nat. Rev. Chem.* **2021**, *5*, 370-387.
- Jansons, A. W.; Hutchison, J. E. Continuous Growth of Metal Oxide Nanocrystals: Enhanced Control of Nanocrystal Size and Radial Dopant Distribution. *ACS Nano* **2016**, *10*, 6942-6951.
- Jeremy, P. W.; Sanford A. A. Acetylcholinesterase-Based Organophosphate Nerve Agent Sensing Photonic Crystal. *Anal. Chem.* **2005**, *77*, 1596-1600.
- Jiang, W.; Cao, Y.; Liu, Y.; Wang, W. Rational Design of a Highly Selective and Sensitive Fluorescent PET Probe for Discrimination of Thiophenols and Aliphatic Thiols. *Chem. Commun.* **2010**, *46*, 1944-1946.

- Johnson, A. M.; Anslyn, E. V., Reversible Macrocyclization of Peptides with a Conjugate Acceptor. *Org. Lett.* **2017**, *19* (7), 1654-1657.
- Kaszeta, D., *Toxic: A History of Nerve Agents, from Nazi Germany to Putin's Russia*; C. Hurst & Co.: London, 2020.
- Kim, D. S.; Sessler, J. L., Calix[4]pyrroles: Versatile Molecular Containers with Ion Transport, Recognition, and Molecular Switching Functions. *Chem. Soc. Rev.* **2015**, *44*, 532-546.
- Kim, K.; Tsay, O. G.; Atwood, D. A.; Churchill, D. G. Destruction and Detection of Chemical Warfare Agents. *Chem. Rev.* **2011**, *111*, 5345-5403.
- Kim, S. K.; Sessler, J. L., Calix[4]pyrrole-Based Ion Pair Receptors. *Acc. Chem. Res.* **2014**, *47*, 2525-2536.
- Kim, S. W.; Bae, Y. H.; Okano, T., Hydrogels: Swelling, Drug Loading, and Release. *Pharmaceut. Res.* **1992**, *9*, 283-290.
- Ko, S.-K.; Kim, S. K.; Share, A.; Lynch, V. M.; Park, J.; Namkung, W.; Rossom, W. V.; Busschaert, N.; Gale, P. A.; Sessler, J. L.; Shin, I., Synthetic Ion Transporters can Induce Apoptosis by Facilitating Chloride Anion Transport into Cells. *Nat. Chem.* **2014**, *6*, 885-892.
- Kolb, H. C.; Finn, M.; Sharpless, K. B., Click Chemistry: Diverse Chemical Function from a Few Good Reactions. *Angew. Chem. Int. Ed.* **2001**, *40* (11), 2004-2021.
- Kolb, H. C.; Sharpless, K. B., The Growing Impact of Click Chemistry on Drug Discovery. *Drug. Discov. Today* **2003**, *8* (24), 1128-1137.
- Kucernak, A. R. J.; Fahy, K. F.; Sundaram, V. N. N. Facile Synthesis of Palladium Phosphide Electrocatalysts and Their Activity for the Hydrogen Oxidation, Hydrogen Evolutions, Oxygen Reduction and Formic Acid Oxidation Reactions. *Catalysis Today* **2016**, *262*, 48-56.
- Kumar, V.; Kaushik, M. P.; Srivastava, A. K.; Pratap, A.; Thiruvenkatam, V.; Row, T. N. G., Thiourea Based Novel Chromogenic Sensor for Selective Detection of Fluoride and Cyanide Anions in Organic and Aqueous Media. *Anal. Chim. Acta* **2010**, *663*, 77-84.
- Kumar, V.; Rana, H. Chromogenic and Fluorogenic De-tection and Discrimination of Nerve Agents Tabun and Vx. *Chem. Commun.* **2015**, *51*, 16490-16493.
- Kumar, V.; Rana, H.; Raviraju, G.; Garg, P.; Baghel, A.; Gupta, A. K. Chromogenic and Fluorogenic Multianalyte Detec-tion with a Tuned Receptor: Refining Selectivity for Toxic Ani-ons and Nerve Agents. *RSC Adv.* **2016**, *6*, 59648-59656.
- Kumar, V.; Raviraju, G.; Rana, H.; Rao, V. K.; Gupta, A. K. Highly Selective and Sensitive Chromogenic Detection of Nerve Agents (sarin, tabun and VX): A Multianalyte Detection Approach. *Chem. Commun.* **2017**, *53*, 12954-12957.

- Lamb, J. B.; Willis, B. L.; Fiorenza, E. A.; Couch, C. S.; Howard, R.; Rader, D. N.; True, J. D.; Kelly, L. A.; Ahmad, A.; Jompa, J., Plastic Waste Associated with Disease on Coral Reefs. *Science* **2018**, *359* (6374), 460-462.
- Lee, S.; Yang, I.; Lee, N.; Jeong, W.; Kye, Y.; Kim, S.; Kim, S., *Military Chemistry*; Bongmyeong: Seoul, 2004.
- Malkoch, M.; Vestberg, R.; Gupta, N.; Mespouille, L.; Dubois, P.; Mason, A. F.; Hedrick, J. L.; Liao, Q.; Frank, C. W.; Kingsbury, K.; Hawker, C. J., Synthesis of Well-Defined Hydrogel Networks using Click Chemistry. *Chem. Commun.* **2006**, *26*, 2774-2776.
- Markoski, L.; Thompson, J.; Moore, J., Indirect Method for Determining Degree of Branching in Hyperbranched Polymers. *Macromolecules* **2002**, *35* (5), 1599-1603.
- McCorry, L. K., Physiology of the Autonomic Nervous System. *Am. J. Pharm. Educ.* **2007**, *71* (4), 78.
- Meadows, M. K.; Sun, X.; Kolesnichenko, I. V.; Hinson, C. M.; Johnson, K. A.; Anslyn, E. V., Mechanistic Studies of a “Declick” Reaction. *Chem. Sci.* **2019**, *10* (38), 8817-8824.
- Mohapatra, H.; Phillips, S. T., Using Smell To Triage Samples in Point-of-Care Assays. *Angew. Chem. Int. Ed.* **2012**, *51* (44), 11145-11148.
- Montero de Espinosa, L.; Meesorn, W.; Moatsou, D.; Weder, C., Bioinspired Polymer Systems with Stimuli-Responsive Mechanical Properties. *Chem. Rev.* **2017**, *117* (20), 12851-12892.
- Moon, S.-Y.; Liu, Y.; Hupp, J. T.; Farha, O. K., Instantaneous Hydrolysis of Nerve-Agent Simulants with a Six-Connected Zirconium-Based Metal–Organic Framework. *Angew. Chem. Int. Ed.* **2015**, *54*, 6795-6799.
- Morimoto, N.; Qiu, X. P.; Winnik, F. M.; Akiyoshi, K., Dual Stimuli-Responsive Nanogels by Self-Assembly of Polysaccharides Lightly Grafted with Thiol-Terminated Poly(N-isopropylacrylamide) Chains. *Macromolecules* **2008**, *41*, 5985-5987.
- Motornov, M.; Zhou, J.; Pita, M.; Gopishetty, V.; Tokarev, I.; Katz, E.; Minko, S., “Chemical Transformers” from Nanoparticle Ensembles Operated with Logic. *Nano Lett.* **2008**, *8*, 2993-2997.
- Munro, N. B.; Talmage, S. S.; Griffin, G. D.; Waters, L. C.; Watson, A. P.; King, J. F.; Hauschild, V., The Sources, Fate, and Toxicity of Chemical Warfare Agent Degradation Products. *Environ. Health Perspect.* **1999**, *107*, 933-974.
- Musil, K.; Florianova, V.; Bucek, P.; Dohnal, V.; Kuca, K.; Musilek, K., Development and Validation of a FIA/UV–Vis Method for pKa Determination of Oxime Based Acetylcholinesterase Reactivators. *J. Pharm. Biomed. Anal.* **2016**, *117*, 240-246.

- Nachmansohn, D.; Wilson, I. B., The Enzymic Hydrolysis and Synthesis of Acetylcholine. In *Advances in Enzymology and Related Subjects of Biochemistry Volume XII*; Nord, F. F., Ed.; Interscience Publishers, Inc.: New York, 1951; pp 259-340.
- Oliva, N.; Conde, J.; Wang, K.; Artzi, N., Designing Hydrogels for On-Demand Therapy. *Acc. Chem. Res.* **2017**, *50* (4), 669-679.
- Organisation for the Prohibition of Chemical Weapons Home Page. <https://www.opcw.org> (accessed June 01, 2021).
- Ozcelik, B. *Degradable Hydrogel Systems for Biomedical Applications. Biosynthetic Polymers for Medical Applications*; Elsevier, Australia, 2016; pp 173-188.
- Park, S.-H.; Park, S.-H.; Howe, E. N. W.; Hyun, J. Y.; Chen, L.-J.; Hwang, I.; Vargas-Zuniga, G.; Busschaert, N.; Gale, P. A.; Sessler, J. L.; Shin, I., Article Determinants of Ion-Transporter Cancer Cell Death. *Chem* **2019**, *5*, 2079-2098.
- Peng, S.; He, Q.; Vargas-Zuniga, G. I.; Qin, L.; Hwang, I.; Kim, S. K.; Heo, N. J.; Lee, C.-H.; Dutta, R.; Sessler, J. L., Strapped Calix[4]pyrroles: From Syntheses to Applications. *Chem. Soc. Rev.* **2020**, *49*, 865-907.
- Poisson, T.; Dalla, V.; Marsais, F.; Dupas, G.; Oudeyer, S.; Levacher, V., Organocatalytic Enantioselective Protonation of Silyl Enolates Mediated by Cinchona Alkaloids and a Latent Source of HF. *Angew. Chem. Int. Ed.* **2007**, *46*, 7090-7093.
- Puglisi, R.; Pappalardo, A.; Gulino, A.; Sfrassetto, G. T., Multitopic Supramolecular Detection of Chemical Warfare Agents by Fluorescent Sensors. *ACS Omega* **2019**, *4*, 7550-7555.
- Qin, A.; Lam, J. W. Y.; Tang, B. Z., Click Polymerization. *Chem. Soc. Rev.* **2010**, *39* (7), 2522-2544.
- Quinn, D. M.; Topczewski, J.; Yasapala, N.; Lodge, A., Why is Aged Acetylcholinesterase so Difficult to Reactivate?. *Molecules* **2017**, *22* (9), 1464.
- Reuther, J. F.; Dahlhauser, S. D.; Anslyn, E. V., Tunable Orthogonal Reversible Covalent (TORC) Bonds: Dynamic Chemical Control over Molecular Assembly. *Angew. Chem. Int. Ed.* **2019**, *58* (1), 74-85.
- Rösler, A.; Vandermeulen, G. W.; Klok, H.-A., Advanced Drug Delivery Devices via Self-Assembly of Amphiphilic Block Copolymers. *Adv. Drug Deliv. Rev.* **2001**, *53* (1), 95-108.
- Rowan, S. J.; Cantrill, S. J.; Cousins, G. R.; Sanders, J. K.; Stoddart, J. F., Dynamic Covalent Chemistry. *Angew. Chem. Int. Ed.* **2002**, *41* (6), 898-952.
- Royuela, S.; Millán, R. G.-S.; Mancheño, M. J.; Ramos, M. M.; Segura, J. L.; Navarro, J. A. R.; Zamora, F., Catalytically Active Imine-based Covalent Organic

- Frameworks for Detoxification of Nerve Agent Simulants in Aqueous Media. *Materials* **2019**, *12*, 1974.
- Saha, I.; Lee, J. H.; Hwang, H.; Kim, T. S.; Lee, C.-H., Remarkably Selective, Non-Linear Allosteric Regulation of Anion Binding by a Tetracationic Calix[4]pyrrole Homodimer. *Chem. Commun.* **2015**, *51*, 5679-5682.
- Sambrook, M. R.; Hiscock, J. R.; Cook, A.; Green, A. C.; Holden, I.; Vincent, J. C.; Gale, P. A., Hydrogen Bond-Mediated Recognition of the Chemical Warfare Agent Soman (GD). *Chem. Commun.* **2012**, *48*, 5605-6507.
- Sambrook, M. R.; Notman, S., Supramolecular Chemistry and Chemical Warfare Agents: From Fundamentals of Recognition to Catalysis and Sensing. *Chem. Soc. Rev.* **2013**, *42*, 9251-9267.
- Scheutz, G. M.; Lessard, J. J.; Sims, M. B.; Sumerlin, B. S., Adaptable Crosslinks in Polymeric Materials: Resolving the Intersection of Thermoplastics and Thermosets. *J. Am. Chem. Soc.* **2019**, *141* (41), 16181-16196.
- Schneider, C. A.; Rasband, W. S.; Eliceiri, K. W. NIH Image to ImageJ: 25 Years of Image Analysis. *Nat. Methods* **2012**, *9*, 671-675.
- Shafranek, R. T.; Millik, S. C.; Smith, P. T.; Lee, C.-U.; Boydston, A. J.; Nelson, A., Stimuli-Responsive Materials in Additive Manufacturing. *Prog. Polym. Sci.* **2019**, *93*, 36-67.
- Sidell, F. R., Nerve Agents. In *Textbook of Military Medicine: Medical Aspects of Chemical and Biological Warfare*; Sidell, F. R.; Takafuji, T. E.; Franz, D. R., Eds.; Office of the Surgeon General, U.S. Army: Falls Church, VA, 1997; pp 129-179.
- Silva, G. R.; Borges Jr., I.; Figueroa-Villar, J. D., DFT Conformational Studies of the HI-6 Molecule. *Int. J. Quantum Chem.* **2005**, *105*, 260-269.
- Sogorb, M. A.; Vilanova, E., Enzymes Involved in the Detoxification of Organophosphorus, Carbamate and Pyrethroid Insecticides through Hydrolysis. *Toxicol. Lett.* **2002**, *128*, 215-228.
- Sokkalingam, P.; Kim, D. S.; Hwang, H.; Sessler, J. L.; Lee, C.-H., A Dicationic Calix[4]pyrrole Derivative and its Use for the Selective Recognition and Displacement-Based Sensing of Pyrophosphate. *Chem. Sci.* **2012**, *3*, 1819-1824.
- Stuart, J. A.; Ursano, R. J.; Fullerton, C. S.; Norwood, A. E.; Murray, K. Belief in Exposure to Terrorist Agents: Reported Exposure to Nerve or Mustard Gas by Gulf War Veterans. *J. Nerv. Ment. Dis.* **2003**, *191*, 431-436.
- Stuart, M. A. C.; Huck, W. T. S.; Genzer, J.; Muller, M.; Ober, C.; Stamm, M.; Sukhorukov, G. B.; Szleifer, I.; Tsukruk, V. V.; Urban, M.; Winnik, F.; Zauscher, S.; Luzinov, I.; Minko, S., Emerging Applications of Stimuli-Responsive polymer Materials. *Nat. Mater.* **2010**, *9*, 101-113.

- Su, W.-F., Chemical and Physical Properties of Polymers. In *Principles of Polymer Design and Synthesis*; Springer Berlin Heidelberg: Berlin, Heidelberg, 2013; pp 61-88.
- Sun, H.; Kabb, C. P.; Dai, Y.; Hill, M. R.; Ghiviriga, I.; Bapat, A. P.; Sumerlin, B. S., Macromolecular Metamorphosis via Stimulus-Induced Transformations of Polymer Architecture. *Nat. Chem.* **2017**, *9*, 817-823.
- Sun, H.; Kabb, C. P.; Sims, M. B.; Sumerlin, B. S., Architecture-Transformable Polymers: Reshaping the Future of Stimuli-Responsive Polymers. *Prog. Polym. Sci.* **2019**, *89*, 61-75.
- Sun, X.; Anslyn, E. V., An Auto-Inductive Cascade for the Optical Sensing of Thiols in Aqueous Media: Application in the Detection of a VX Nerve Agent Mimic. *Angew. Chem. Int. Ed.* **2017**, *129* (32), 9650-9654.
- Sun, X.; Boulgakov, A. A.; Smith, L. N.; Metola, P.; Marcotte, E. M.; Anslyn, E. V., Photography Coupled with Self-Propagating Chemical Cascades: Differentiation and Quantitation of G- and V-Nerve Agent Mimics via Chromaticity. *ACS Cent. Sci.* **2018**, *4* (7), 854-861.
- Sun, X.; Chwatko, M.; Lee, D.-H.; Bachman, J. L.; Reuther, J. F.; Lynd, N. A.; Anslyn, E. V. Chemically Triggered Synthesis, Remodeling, and Degradation of Soft Materials. *J. Am. Chem. Soc.* **2020**, *142*, 3913-3922.
- Sun, X.; Shabat, D.; Phillips, S. T.; Anslyn E. V., Self-Propagating Amplification Reactions for Molecular Detection and Signal Amplification: Advantages, Pitfalls, and Challenges. *J. Phys. Org. Chem.* **2018**, *31*, e3827.
- Sun, X.; Dahlhauser, S. D.; Anslyn, E. V., New Autoinductive Cascade for the Optical Sensing of Fluoride: Application in the Detection of Phosphoryl Fluoride Nerve Agents. *J. Am. Chem. Soc.* **2017**, *139* (13), 4635-4638.
- Thakur, S.; Thakur, V. K.; Arotiba, O. A. *History, Classification, Properties and Application of Hydrogels: An Overview. Hydrogels. Gels Horizons: From Science to Smart Materials*; Springer, Singapore, 2018; pp 29-50.
- Trumpener, U., The Road to Ypres: The Beginnings of Gas Warfare in World War I. *J. Mod. Hist.* **1975**, *47*, 460-480.
- Von Delius, M.; Geertsema, E. M.; Leigh, D. A., A Synthetic Small Molecule that can Walk Down a Track. *Nat. Chem.* **2010**, *2*, 96-101.
- Whitaker, C. M.; Derouin, E. E.; O'connor, M. B.; Whitaker, C. K.; Whitaker, J. A.; Snyder, J. J.; Kaufmann, N. R.; Gilliard, A. N.; Reitmayer, A. K. Smart Hydrogel Sensor for Detection of Organophosphorus Chemical Warfare Nerve Agents. *J. Macromol. Sci., Part A* **2017**, *54*, 40-46.
- Wiener, S. W.; Hoffman, R. S., Nerve Agents: A Comprehensive Review. *J. Intensive Care Med.* **2004**, *19*, 22-37.

- Zheng, Y.; Li, S.; Weng, Z.; Gao, C., Hyperbranched Polymers: Advances from Synthesis to Applications. *Chem. Soc. Rev.* **2015**, *44* (12), 4091-4130.
- Zhu, Z.; Yang, C. J., Hydrogel Droplet Microfluidics for High-Throughput Single Molecule/Cell Analysis. *Acc. Chem. Res.* **2017**, *50* (1), 22-31.